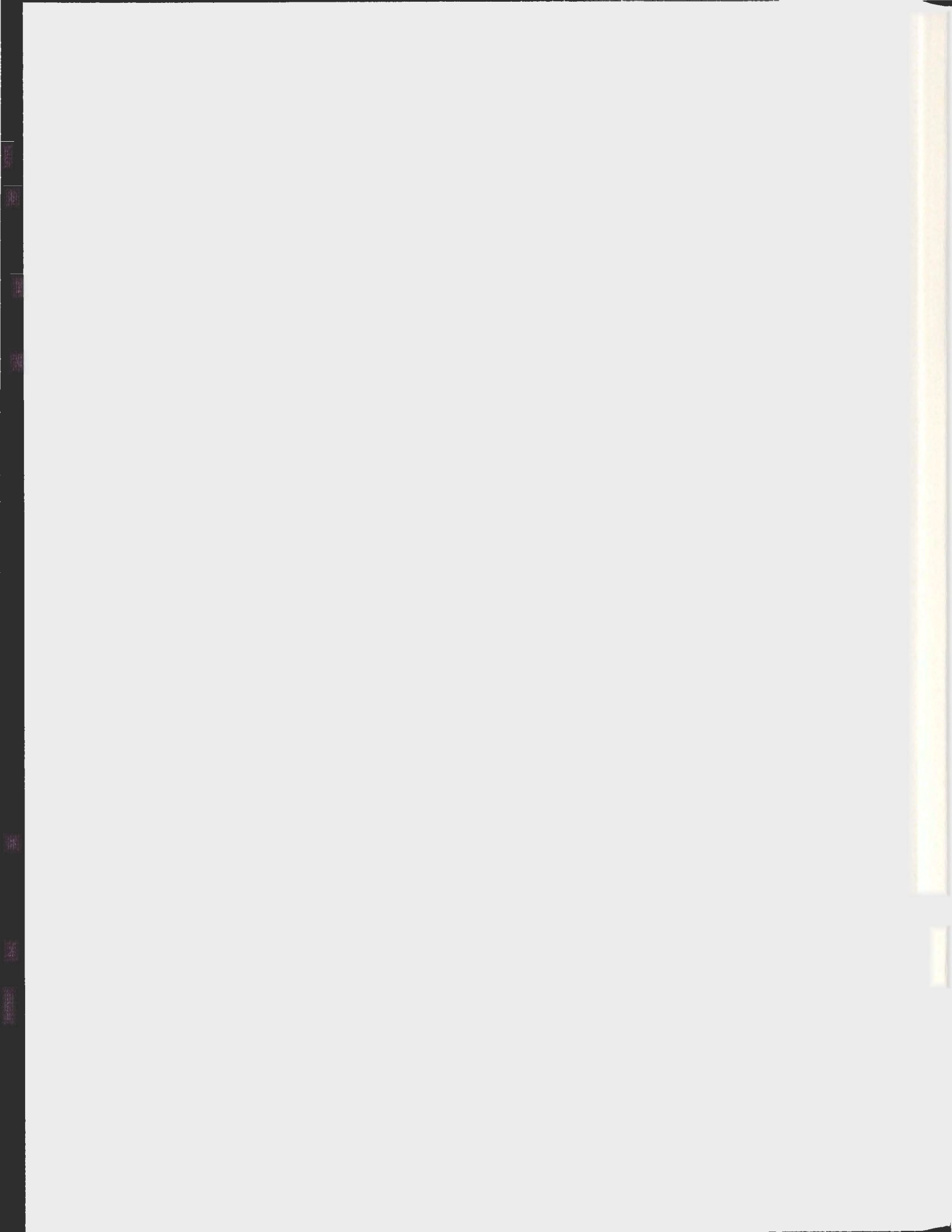


A DETAILED PETROGRAPHIC, GEOCHEMICAL AND  
GEOCHRONOLOGICAL STUDY OF THE HARE BAY  
GNEISS, NORTHEASTERN NEWFOUNDLAND

AMANDA E. LANGILLE







**A DETAILED PETROGRAPHIC, GEOCHEMICAL AND  
GEOCHRONOLOGICAL STUDY OF THE HARE BAY GNEISS,  
NORTHEASTERN NEWFOUNDLAND**

By

© Amanda E. Langille B. Sc. (Hons.)

A Thesis submitted to the School of Graduate Studies in partial fulfillment of the  
requirements for the degree of

**Master of Science**

**Department of Earth Sciences**

Memorial University of Newfoundland

**September 2012**

St. John's

Newfoundland

## ABSTRACT

The Hare Bay Gneiss occurs as three discontinuous northeast-trending belts along the northeastern margin of the Gander Zone and has been described briefly in previous literature as a highly deformed assemblage of paragneiss, orthogneiss and migmatite. Past interpretations of the Hare Bay Gneiss include that it is a highly deformed equivalent of the adjacent Square Pond Gneiss (Blackwood, 1978) and some studies (Blackwood and Kennedy, 1975) proposed it as potential basement to the Gander Zone. Lack of modern documentation and analyses of the rock types that constitute the Hare Bay Gneiss impede definitive interpretations from being made. In an effort to better understand the Hare Bay Gneiss and its importance to the Gander Zone as a whole; this study combines field observations with petrological, geochemical and geochronological data from well-exposed sections from Wind Mill Bight Provincial Park Reserve in the north and the town of Hare Bay, in the south.

Through detailed field mapping and petrographic analysis it is evident that a diverse assemblage of rocks constitutes the studied exposures of the Hare Bay Gneiss. Based on the seven selected study localities the northern belts of the Hare Bay Gneiss predominantly consist of greenschist-facies orthogneiss ranging from granitic to tonalitic in composition, and also includes locally abundant, variably deformed granitic intrusions. The mapped area of the Hare Bay Gneiss contains several minor rock types including tonalite, paragneiss, pegmatite, mafic intrusions, and quartz veins. Nearly all of the orthogneissic and granitic rocks have peraluminous geochemical signatures and REE patterns diagnostic of crustal melts.

Nine main lithologic units yield concordant ages using the CA-TIMS U-Pb zircon technique. In the Windmill Bight map area four dated units constrain magmatism, ranging from  $428 \pm 2$  Ma for foliated leucogranite to  $387 \pm 2$  Ma for late pegmatite. Leucogranite and Al-silicate-bearing orthogneiss in the Greenspond Road section yielded ages of  $460 \pm 2$  Ma and  $510 \pm 4$  Ma, respectively, making the orthogneiss the oldest dated unit so far in the Hare Bay Gneiss. Although lithologically similar, the granitic Valleyfield orthogneiss and the Hare Bay orthogneiss have contrasting concordant U-Pb zircon ages of  $465 \pm 2$  Ma and  $491 \pm 4$  Ma, respectively. Finally a tonalite intrusion cutting an orthogneiss in the "I Love You" section yielded a zircon age of  $415 \pm 1$  Ma.

The new data demonstrates the complexity of the Hare Bay Gneiss, which contains intrusive rocks ranging in age from Series 2 of the Cambrian to mid- Devonian (Givetian). Based on these data, it is unlikely that these rocks are metamorphic equivalents of adjacent gneisses, or basement rocks to the Gander Zone. Rather they may be partial melts of Gander Group sedimentary rocks and mainly represent pulses of magmatism into crust of the Gander Zone. Many magmatic events recorded in this study are observed elsewhere in the Gander Zone in Newfoundland; specifically Ordovician, Silurian and Devonian ages can be correlated in time with Penobscot, Salinic and Acadian orogenic events recognized elsewhere in the Gander Zone in Newfoundland.

## ACKNOWLEDGEMENTS

Several people deserve acknowledgement for their contributions to this thesis project. First, I would like to thank my supervisor, Dr. Greg Dunning for giving me the opportunity to work on this project and providing constant advice and encouragement during the completion of this thesis. I would also like to acknowledge Dr. Aphrodite Indares and Dr. George Jenner for numerous helpful discussions, as well as constructive criticism in many aspects of this project.

Thanks is extended to Sherri Strong for providing explanations and instructions during geochronological processing and analysis, Pam King for providing laboratory assistance and geochemical data, and Susan Strowbridge for help with petrographic analysis. I would like to thank, Brian O'Brien for his sharing of knowledge and guidance during an introductory field trip, as well as Monica Barrington for her assistance in the field. The technical support provided by Dr. Mark Wilson, Peter Bruce and Pauline Honovar while working with MapInfo and ArcGIS was invaluable and I am extremely grateful for their assistance.

Finally I would like to thank my family and friends for their continual encouragement and support throughout this project.

## TABLE OF CONTENTS

ABSTRACT .....	ii
ACKNOWLEDGEMENTS .....	iv
LIST OF APPENDICES .....	xiii
1. CHAPTER 1: INTRODUCTION .....	1
1.1 Introduction .....	1
1.2 Regional Geology .....	4
1.2.1 The Gander Zone .....	4
1.3 Previous Work .....	8
1.3.1 The Hare Bay Gneiss .....	8
1.4 Location of Study Area .....	14
1.5 Purpose and Scope .....	15
2. CHAPTER 2: Rock Units: Field Observations and Petrographic Analysis.....	17
2.1. Introduction .....	17
2.2 Field Observations and Petrographic Analysis .....	18
2.2.1. The Windmill Bight Map Area .....	18
2.2.2. The Greenspond Road Section (A-A').....	44
2.2.3. The Trinity Section (B-B').....	52
2.2.4. The "I Love You" Road Section (C-C') .....	56

2.2.5. North of Cape Freels .....	61
2.2.6. Valleyfield Road .....	63
2.2.7. Town of Hare Bay .....	70
2.3 Interpretation/Summary of Field and Petrographic Observations .....	73
3. CHAPTER 3: GEOCHEMICAL ANALYSIS .....	78
3.1 Preparation .....	78
3.2 Data Analysis .....	79
3.2.1 Windmill Bight Map Area .....	80
3.2.2. The Greenspond Road Section.....	90
3.2.3. The Trinity Road Section.....	95
3.2.4. The “I Love You” Road Section .....	98
3.2.5. North of Cape Freels.....	101
3.2.6. Valleyfield Road .....	102
3.2.7. Town of Hare Bay.....	105
3.3. Interpretation/Summary of Geochemical Data .....	106
4. CHAPTER 4: GEOCHRONOLOGY .....	110
4.1 Sample Selection.....	110
4.2 Results.....	111
4.2.1. WMB Map Area .....	111

4.2.2. Greenspond Road Section.....	119
4.2.2. "I Love You" Road Section .....	122
4.2.3. North of Cape Freels.....	125
4.2.4. Valleyfield Road .....	127
4.2.5. Town of Hare Bay.....	130
4.3 Discussion .....	131
4.3.1. Ages within the Hare Bay Gneiss .....	131
4.3.2. Age Correlations .....	135
5. CHAPTER 5: DISCUSSION AND CONCLUSIONS .....	142
5.1 Importance of the Hare Bay Gneiss .....	142
5.2 Summary of Findings.....	143
5.2.1. Lithologic Units .....	143
5.2.2. Geochemical Signatures.....	145
5.2.3. U-Pb Age Relationships.....	147
5.3. New Interpretation of the Hare Bay Gneiss .....	148
5.4. Key Points.....	149
References.....	151

## LIST OF FIGURES

Figure 1-1: Geology of the Canadian and adjacent New England Appalachians with the geographical distribution of the major tectonic elements. ....	3
Figure 1-2: Geological map showing predominant rock types in the northeastern Gander Zone. Generalized study localities are signified with a star (modified from CanVec). ....	6
Figure 1-3: Legend for the map of the northeastern Gander Zone in Figure 1-2. ....	7
Figure 2-1: Field photos and photomicrographs showing the two foliated leucogranite units in the WMB map area.. ....	23
Figure 2-2: Photomicrograph and field photograph of a feldspar-tourmaline vein in the strongly sheared foliated leucogranite. ....	24
Figure 2-3: Field photographs and photomicrographs showing the variably sheared megacrystic granite of WMB map area.. ....	28
Figure 2-4: Field photographs and photomicrographs showing the foliated granodiorite in WMB map area.. ....	30
Figure 2-5: Field photographs and photomicrographs of intermediate dyke in the WMB map area.. ....	32
Figure 2-6: Field photographs and photomicrographs depicting pegmatite intrusions within the WMB map area.. ....	34
Figure 2-7: Field photograph depicting the highly sheared interlayered unit in the WMB map area.. ....	35
Figure 2-8: Field photographs and photomicrographs showing the aluminous, mica-rich intermediate rock from the WMB map area .....	37
Figure 2-9: Field photographs and photomicrographs showing the actinolite-bearing mafic unit in the WMB map area. ....	39
Figure 2-10: Field photograph and photomicrographs depicting the carbonate-biotite-rich mafic rock in the WMB map area. ....	41
Figure 2-11: A field photograph (left) and photomicrograph (right) showing the layered quartzite unit in the WMB map area. ....	43
Figure 2-12: Field photographs of quartz veins in the WMB map area.. ....	44
Figure 2-13: Field photographs from the Greenspond Road section. ....	46
Figure 2-14: Photomicrographs showing characteristic features of units in the Greenspond Road section. ....	47
Figure 2-15: Field photographs and photomicrographs showing the units in the Trinity Road Section. ....	55

Figure 2-16: Field photographs and photomicrographs showing some characteristic features of units in the “I Love You” Road Section. ....	60
Figure 2-17: Field photographs and photomicrographs showing the Cape Freels Gneiss. ....	63
Figure 2-18: Field photographs and photomicrographs of the Valleyfield orthogneiss. ....	65
Figure 2-19: Field photo and photomicrographs depicting the Valleyfield paragneiss. ....	68
Figure 2-20: Photomicrographs showing sample 10AL076 of a highly migmatized and deformed section of the Valleyfield paragneiss. ....	69
Figure 2-21: Field photograph and photomicrograph showing the Valleyfield mylonite. ....	70
Figure 2-22: Field photographs showing the Hare Bay orthogneiss. ....	71
Figure 2-23: Photomicrographs of the Hare Bay orthogneiss. ....	73
Figure 3-1: Modal and geochemical plots for the foliated granite of WMB map area. ....	82
Figure 3-2: Modal and geochemical plots for the megacrystic granite of WMB map area. ....	84
Figure 3-3: Modal and geochemical plots for the granodiorite and tonalitic dyke of WMB map area. ....	86
Figure 3-4: Modal and geochemical plots for the pegmatite intrusions of WMB map area. ....	88
Figure 3-5: Geochemical plots for the mafic units of WMB map area. ....	89
Figure 3-6: Geochemical plots for the Al-silicate bearing orthogneiss of the Greenspond Section. ....	91
Figure 3-7: Modal and geochemical plots for several units of the Greenspond section. ....	94
Figure 3-8: Modal and geochemical plots for the sampled units of the Trinity section. ....	97
Figure 3-9: Geochemical plots for the mafic unit of the Trinity section. ....	98
Figure 3-10: Modal and geochemical plots for the sampled units of the “I Love You” section. ....	100
Figure 3-11: Two samples of the Cape Freels gneiss plotted on an extended REE diagram normalized to primitive mantle. ....	101
Figure 3-12: Geochemical plots for the Cape Freels diabase dyke. ....	102
Figure 3-13: Geochemical plots for several units occurring along Valleyfield Road. ....	104
Figure 3-14: Two samples of the Valleyfield paragneiss plotted on a REE diagram normalized to upper continental crust (Taylor and McLennan, 1985). ....	105
Figure 3-15: Geochemical plots for the Hare Bay orthogneiss. ....	106

Figure 4-1: Plane polarized light photomicrographs of zircon populations from dated samples in the WMB map: Sample 10AL087 from the megacrystic granite, 10AL088 from the granodiorite, 10AL089 from the pegmatite and 10AL090 from the foliated granite. .... 117

Figure 4-2: Cathodoluminescence images of zircon grains from the four samples dated in the WMB map area: Sample 10AL087 from the megacrystic granite, 10AL088 from the granodiorite, 10AL089 from the pegmatite and 10AL090 from the foliated granite. .... 118

Figure 4-3: Concordia diagrams for the four geochronology samples from WMB map area.  $^{206}\text{Pb}/^{238}\text{U}$  ages and uncertainties are reported at the 95% confidence interval. .... 119

Figure 4-4: On top, photomicrographs taken in plane polarized light of zircon populations from the two dated samples from the Greenspond road section. On bottom, cathodoluminescence images of zircon grains from the same samples: Sample 10AL078 is from the foliated leucogranite and 10AL079 is from the Al-silicate bearing orthogneiss. .... 121

Figure 4-5: Concordia diagrams for the two geochronology samples from the Greenspond road section.  $^{206}\text{Pb}/^{238}\text{U}$  ages and uncertainties are reported at the 95% confidence interval. .... 122

Figure 4-6: On top, photomicrographs taken in plane polarized light of zircon populations from the two dated samples from the “I Love You” road section. On bottom, cathodoluminescence images of zircon grains from the same samples: Sample 10AL096 is from the tonalite and 10AL097 is from the orthogneiss. .... 124

Figure 4-7: Concordia diagrams for the two geochronology samples from the “I Love You” road section.  $^{206}\text{Pb}/^{238}\text{U}$  ages and uncertainties are reported at the 95% confidence interval. .... 125

Figure 4-8: Top, a photomicrograph taken in plane polarized light of the zircon population from the dated sample of the Cape Freels gneiss. Bottom, cathodoluminescence images of zircon grains from the same sample (10AL093)..... 126

Figure 4-9: Concordia diagrams for the U-Pb geochronology samples from Cape Freels, Valleyfield and Hare Bay.  $^{206}\text{Pb}/^{238}\text{U}$  ages and uncertainties are reported at the 95% confidence interval. .... 127

Figure 4-10: Left, photomicrographs taken in plane polarized light of the zircon population from dated orthogneiss and paragneiss units in Valleyfield. Right, cathodoluminescence images of zircon grains from the same samples: Sample 10AL076 from the Valleyfield paragneiss and 10AL077 from the Valleyfield orthogneiss. .... 129

Figure 4-11: Left, a photomicrograph taken in plane polarized light of the zircon population from the dated Hare Bay orthogneiss sample. Right, cathodoluminescence images of zircon grains from the same sample (10AL094). .... 131

Figure 4-12: Age correlation chart with U-Pb ages of igneous and metamorphic rocks of the Gander Zone in NL. Grey shaded areas represent the Devonian Acadian, Silurian Salinic and Ordovician Penobscot Orogenies..... 140

## LIST OF TABLES

Table 1-1: Summary of relevant unit ages and references previously recognized in the northeast Gander Zone. ....	13
Table 4-1: U-Pb isotopic data from lithologic units of the Hare Bay Gneiss, northeast Newfoundland.....	113
Table 4-2: Age and reference guide for the age correlation chart (Figure 4-12). ....	141

## LIST OF APPENDICES

Appendix A: Field Methods.....	158
Appendix B: Sample Guide .....	162
Appendix C: Petrography .....	166
Appendix D: Lithogeochemical Data .....	184
Appendix E: U-Pb Geochronological Analytical Methods.....	206

# 1. CHAPTER 1: INTRODUCTION

## 1.1 Introduction

The northeast-trending Appalachian Orogen is a Paleozoic mountain belt extending from Newfoundland southward to Alabama (Figure 1-1). The formation of the Appalachian mountain belt is thought to be a result of the closure of two early oceans, the Iapetus (Cambrian to Early Devonian) and the Rheic (Devonian to Carboniferous) Oceans (van Staal, 2005).

Geologist Harold Williams first mapped the Canadian Appalachians in Newfoundland in 1964. Over the next decade Williams and others modified the initial subdivisions of the orogen before deciding, in 1978, on the five most useful divisions the essentials of which are still widely accepted today. These divisions from west to east include: the Humber, Dunnage, Gander, Avalon and Meguma Zones (Figure 1-1). Williams (1978) defined these five zones based on contrasts in structure, lithology, geophysical data, reported fauna, plutonism and metallogeny (van Staal, 2005). The most westerly Humber Zone is thought to represent the leading peripheral edge of the Laurentian margin. To the east, the Dunnage Zone consists of an assemblage of oceanic arc terranes that accreted during the closure of the Iapetus Ocean. The Dunnage Zone is internally divided into two subzones: the peri-Laurentian Notre Dame Subzone and the peri-Gondwanan Exploits Subzone. The Gander, Avalon and Meguma Zones have been interpreted to represent peri-Gondwanan microcontinents known as Ganderia, Avalonia and Meguma, respectively.

Remnants of the peri-Gondwanan microcontinent known as Ganderia underlie much of the core of the northern Appalachians, constituting the Gander Zone (van Staal, 2009). Views regarding the Gander Zone have evolved over time, with only relatively recent studies allowing the recognition and greater understanding of its tectonic history before, during and after accretion onto the Laurentian margin. Despite this progress, many features of the Gander Zone remain ambiguous, including the ages of several rock units, the depositional setting of the metasedimentary Gander Group, contrasts in modeling regarding Ganderian tectonic history and the lack of recognized basement.

This thesis was undertaken to better understand the nature of the Hare Bay Gneiss, located along the northeastern margin of the Gander Zone in Newfoundland. This heterogeneous highly deformed package of rocks has not been studied in modern times and is enigmatic, having been previously suggested as possible basement to the Gander Zone (Blackwood and Kennedy, 1975). Through field mapping, petrographic, geochemical and geochronological analysis this project aims to document the nature of the Hare Bay Gneiss, making lithologic and event correlations where possible and ultimately attaining a better understanding of the geological and tectonic significance of the Hare Bay Gneiss to the Gander Zone as a whole.



## **1.2 Regional Geology**

### **1.2.1 The Gander Zone**

The Gander Zone can be traced from northeastern Newfoundland southward into New England. This fault-bound zone was interpreted to represent remnants of a peri-Gondwanan, late Precambrian to early Paleozoic passive margin by Williams (1964). In the northwest the Gander River Ultrabasic Belt (GRUB) and the volcanic and sedimentary rocks that make up the Exploits subzone of the adjacent Dunnage Zone, define the limits of the Gander Zone (Williams, 1978). The southeastern boundary is in contact with the Avalon Zone and the boundary between the zones is marked by the Dover-Hermitage Bay-Caledonian Fault system (Blackwood and Kennedy, 1975). In northeast Newfoundland, the surficial expression of this contact is known as the Dover fault. A 1-2 km wide deformation zone displaying early sinistral ductile deformation as well as later brittle faulting marks this Gander-Avalon contact (Blackwood and Kennedy, 1975). The Dover fault clearly separates Gander Zone rocks in the west from the less deformed, greenschist-facies, Precambrian sedimentary and volcanic rocks of the Avalon Zone to the east. In New Brunswick, the younger Silurian rocks of the Fredericton Trough and Carboniferous strata overlie much of the Gander-Avalon boundary (Williams, 1978).

The predominant rock type of the Gander Zone is the pre-Middle Ordovician arenite-shale sequence of the Gander Group in Newfoundland, and the equivalent Lower Tetagouche Group of New Brunswick. These rocks have undergone significant metamorphism and multiple stages of deformation (O'Neil and Blackwood, 1989). The

eastern Gander Zone contains granitic gneiss, migmatite and foliated megacrystic granite (Figure 1-2). An abundance of Paleozoic megacrystic biotite granite, garnetiferous muscovite leucogranite, as well as late pegmatites are also present throughout (Williams, 1978).

In the past, some of the Upper Neoproterozoic to Lower Cambrian arc plutonic and volcanic rocks in Newfoundland, Nova Scotia and New Brunswick have been inferred to represent basement rocks to the clastic arenite-shale sequence based on Nd-isotope data, geophysical data and inherited zircon populations (Williams, 1978, 1995). However to date, no definite basement to the Gander Zone has been successfully identified.

## Northeastern Gander Zone: Study Locations

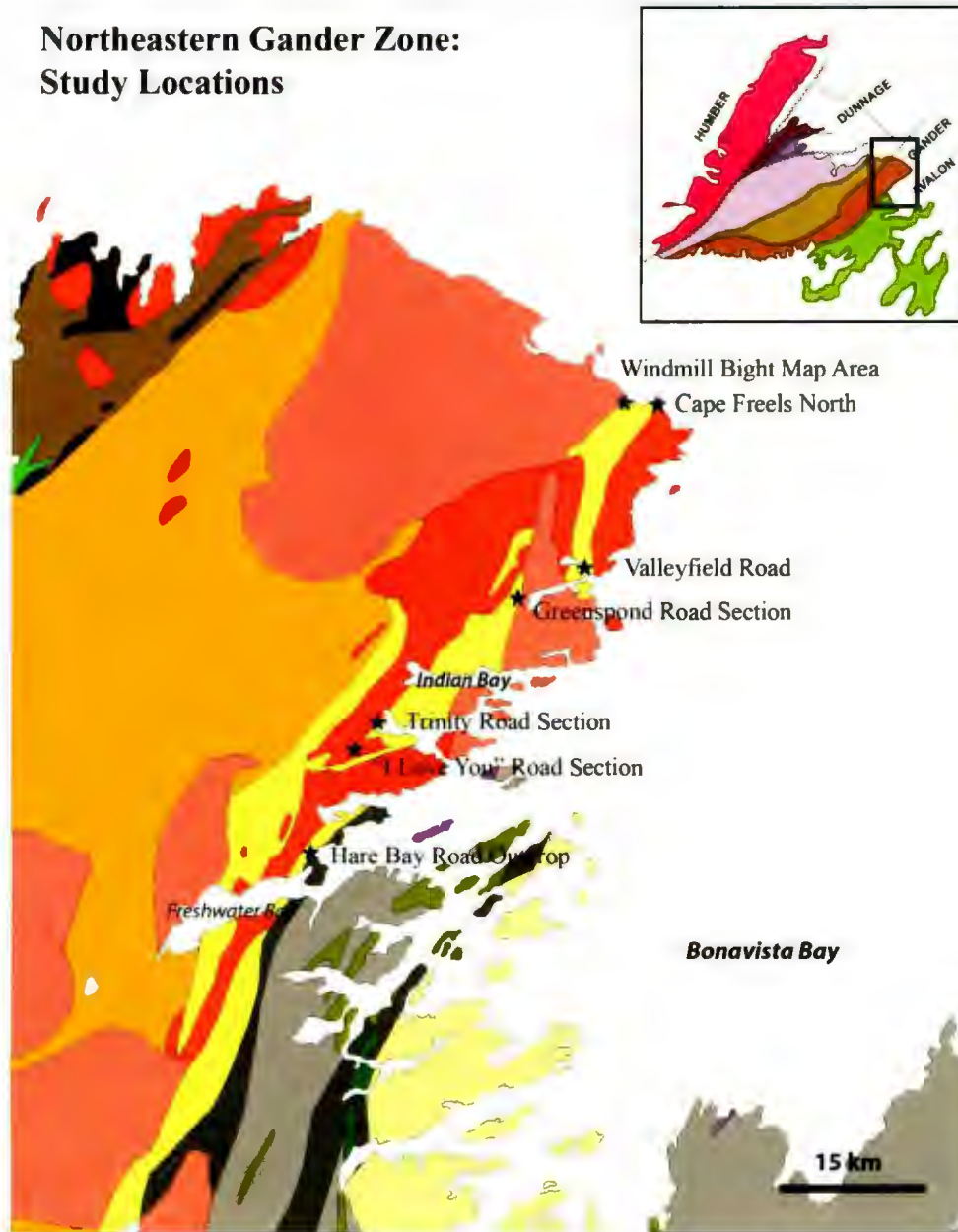


**Figure 1-2: Geological map showing predominant rock types in the northeastern Gander Zone. Generalized study localities are signified with a star (modified from CanVec).**

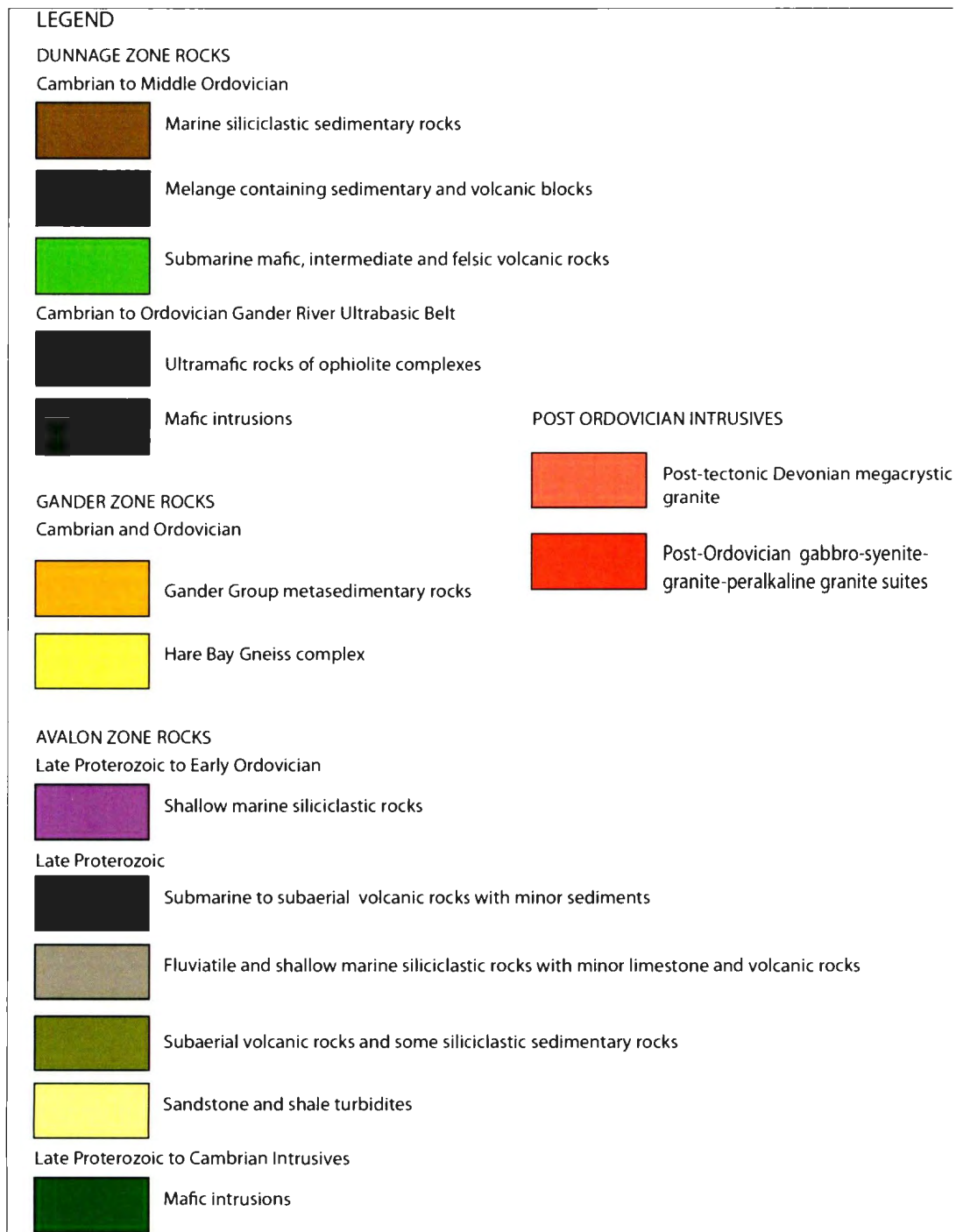


**Figure 1-3: Legend for the map of the northeastern Gander Zone in Figure 1-2.**

## **1.3 Previous Work**

### **1.3.1 The Hare Bay Gneiss**

Blackwood and Kennedy (1975) first referred to the gneissic terrane of the eastern Gander Zone as the Bonavista Gneiss Complex. Blackwood (1977) used inferred protoliths to subdivide these gneissic rocks into a western belt of paragneiss called the Square Pond Gneiss and an eastern belt of granitic gneiss and migmatite called the Hare Bay Gneiss. The two gneissic units are separated by a gradational “migmatite front” approximately 1 km wide in which paragneiss gradually transitions into migmatite.

Blackwood (1977) originally recognized the Hare Bay Gneiss as a distinct unit, defining the unit in the town of Hare Bay. He described the unit as a “complexly folded, banded, tonalitic orthogneiss and migmatite”, and his specific observations are summarized in the following: The gneissic banding is generally less than one centimeter wide and is defined by alternating bands of quartzofeldspathic (leucosome) bands and biotite rich bands (melanosome). The Hare Bay Gneiss is dominantly tonalitic in composition but locally has the composition of granodiorite. Mineral constituents of the Hare Bay Gneiss include quartz, feldspar, biotite, chlorite (minor), muscovite, as well as small euhedral grains of garnet that are observed locally. Blackwood also mentioned the presence of semipelitic, psammitic and amphibolitic gneiss occurring as xenoliths floating in a tonalitic host.

The first interpretations of the Hare Bay Gneiss describe that it is a highly deformed equivalent of the adjacent Square Pond Gneiss (Blackwood, 1978), lying to the

south of the study area, and Blackwood and Kennedy (1975) proposed it as potential basement to the Gander Zone. These interpretations were based largely on outcrops of tonalitic orthogneiss and migmatite described above that are observed around and within the town of Hare Bay.

In 1979, as part of a PhD thesis at Memorial University of Newfoundland, N.R. Jaysinghe studied nine granitoid bodies in the northeastern Gander Zone. The Square Pond Gneiss and the Hare Bay Gneiss were introduced in this study as country rocks to the intrusive rocks of focus, and their structure, petrology, metamorphic grade and geochemistry were briefly summarized. Jaysinghe (1979) documented the spatial extent of the Hare Bay Gneiss, which occurs as 3 discontinuous northeast trending belts within the map area (Figure 1-2). The Hare Bay Gneiss was described as a predominantly migmatic unit with numerous inclusions of Square Pond Gneiss and metamorphosed to amphibolite facies. Jaysinghe (1979) recognized three planar structural features in the gneiss as 1.) a gneissic banding 2.) an axial plane schistosity defined by silicate layers and 3.) a foliation defined by mylonite related to local shearing. The geochemical study conducted was very brief, involving only 10 samples of the Hare Bay Gneiss from various locations, and results are considered outdated. Jaysinghe (1979) interpreted migmatite formation in the Hare Bay Gneiss to be a result of the collective process of partial melting (anatexis), metasomatism, and metamorphic differentiation of an already existing gneissic terrane.

Dallmeyer et al. (1983) determined  $^{40}\text{Ar}$ - $^{39}\text{Ar}$  plateau ages for biotite in the Hare Bay Gneiss. Ages ranged from 365-383 Ma and were suggested to record regional post-

metamorphic cooling and thereby provided a minimum age for initial tectonism along the Dover Fault.

In the 1990's, two British geologists, D'Lemos and Holdsworth studied several granitoid bodies and structural elements within the northeast Gander Zone, with a focus on the Dover Fault. Although neither D'Lemos nor Holdsworth directly focused on the Hare Bay Gneiss, Holdsworth (1991) provided a more recent description of this gneissic unit. Based on relative age Holdsworth identified 3 components within the Hare Bay Gneiss: metasedimentary rocks and amphibolites, mobilized gneisses and orthogneisses. Owing to broad gradational boundaries and intermingled units, Holdsworth (1991) recognized the difficulty in mapping the various components of the Hare Bay Gneiss.

The metasedimentary rocks and amphibolite were documented as enclaves and rafts ranging in size from millimeters to kilometers. The metasedimentary rocks were described as migmatized psammite, semipelite and pelite and are lithologically identical to the rocks of the Gander Group. Next the mobilized gneisses are inferred to be derived from a greater degree of melting of the same metasediments comprising the enclaves and rafts. They range from "relatively coherent soaked migmatites" to "thoroughly mobilized xenolithic granite" (Holdsworth, 1991). Finally the orthogneiss was described as a tonalitic to granitic unit that generally does not possess a large number of the metasedimentary enclaves and is not an obvious product of further melting of these same metasedimentary rocks. The orthogneiss displays the same deformation as the surrounding metasedimentary country rock and rarely preserve original igneous textures. Holdsworth (1991) recognized that the orthogneiss commonly has gradational boundaries

with the intrusive granite, but based on field relationships alone the possibility that these gneisses represent much older phases of intrusion cannot be discounted.

Studies by D`Lemos and Holdsworth not only provided a more in depth description of the Hare Bay Gneiss, but also documented relative ages of units and timing of magmatic events in the area. Based on detailed analysis of structural features and contact relationships between large granitic intrusive bodies some important conclusions were made. Fabrics and contacts of several megacrystic granitic units, including the Cape Freels Granite, Dover Fault Granite and Lockers Bay Granite, were mapped in detail relating them in time with the regional sinistral Silurian deformation event (Salinic Orogeny). The same megacrystic granitic units were dated using TIMS U-Pb zircon analysis and recorded ages between 417-428 Ma (Dunning, pers. comm., 2012). D`Lemos et al. (1995) determined that, although the late Lumsden/Dead Man`s Bay and Newport plutons were post-tectonic with respect to the regional ductile Silurian deformation, they were syntectonic with a later brittle Devonian deformation event. The recognition that emplacement of these granitic bodies correlated in time with Acadian (Devonian) deformation was confirmed with calculated U-Pb ages ranging from 385-384 Ma (Dunning, pers. comm., 2012).

In 1991, Patrick O`Neil published a GSNL report focusing on the Weir`s Pond area, including rocks of the Gander Group along the northwestern margin of the Gander Zone, as well as rocks belonging to the Gander River Complex and Davidsville Group of the adjacent Dunnage Zone. Although the area covered in the report lies west of the present study area, some key findings prove relevant. O`Neil (1991) identified and

mapped a high strain zone known as the Wing Pond shear zone, with relict kyanite-silimanite-staurolite overprinted by andalusite. This shear zone is thought to be a result of a Silurian deformation event. O'Neil and Knight (1988) mapped much of the Gander Group along the northwest margin, identifying the Indian Bay Big Pond and Jonathan's Pond formations. Single detrital zircon ages from a psammite within the Jonathan's Pond Formation yielded ages between 2700-560 Ma, constraining the maximum age of the Gander Group (O'Neil, 1991). A U-Pb zircon age of at 385 Ma was reported for the Lumsden/Deadman's Bay Granite, observed cross cutting the Gander Group. In addition,  $^{40}\text{Ar}$ - $^{39}\text{Ar}$  ages of biotite and muscovite from metasedimentary rocks in the contact aureole surrounding this granite suggest that cooling that through lower greenschist facies conditions occurred between 400-385 Ma (O'Neil and Lux, 1989).

The most recent research in the study area includes the PhD work of both Tanya King (1995) (reference not available) and Chris Buchanan. Tanya King's research focused on the connection between the structural evolution of the Dover Fault and granite emplacement. Chris Buchanan's PhD project (incomplete) is focused on the structural elements of a gold deposit near Gander. Buchannan and Bennett (2009) presented a poster recording metamorphic events at ca. 420 and 460 Ma, through U-Pb electron microprobe dating of monazite within the Gander Group.

Unpublished U-Pb ages of several units within the Hare Bay Gneiss in the northeastern Gander Zone have been provided by Dunning (per. comm., 2012). These units were not mapped as a part of this project but provide the only modern U-Pb data for the Hare Bay Gneiss prior to this study. A sample of dioritic orthogneiss within the Hare

Bay Gneiss, collected from a nearby island, gave a U-Pb TIMS age of  $478 \pm 5$  Ma. A sheet of  $465 \pm 5$  Ma granitic orthogneiss was also dated and is observed southeast of the Windmill Bight (WMB) map area described in this study. A migmatite near Schooner Cove yielded a U-Pb TIMS zircon age of  $416 \pm 2$  Ma recording a melting event at this time. Finally, monazite and titanite ages from several units within the Hare Bay Gneiss documented evidence of metamorphism at  $\sim 420$  Ma (Dunning pers. comm., 2012). Many of these previously determined ages (**Error! Reference source not found.**) prove crucial in interpreting ages obtained in this study, allowing further age correlation between units of the Hare Bay Gneiss.

**Table 1-1: Summary of relevant unit ages and references previously recognized in the northeast Gander Zone.**

Previous Age Data in the NE Gander Zone	
Devonian Rocks	
	<i>New Port Granite</i> ( $384 \pm 3$ Ma) <a href="#">Dunning pers. comm.</a>
	<i>Lumsden/ Deadman's Bay Granite</i> ( $386 \pm 3$ Ma) <a href="#">Dunning pers. comm.</a>
Silurian Magmatism and Metamorphism	
	<i>Dover Fault Granite</i> ( $428 \pm 3$ Ma) <a href="#">Dunning pers. comm.</a>
	<i>Middle Brook Granite</i> ( $427 \pm 3 / -2$ Ma) <a href="#">Dunning pers. comm.</a>
	<i>HBG: Tonalitic Orthogneiss (Monazite)</i> ( $425 \pm 5$ Ma) <a href="#">Dunning pers. comm.</a>
	<i>Gander Group (Monazite)</i> ( $\sim 425$ Ma) <a href="#">Buchanan and Bennett, 2009</a>
	<i>Lockers Bay Granite</i> ( $418 \pm 2$ Ma) <a href="#">Dunning pers. comm.</a>
	<i>Cape Freels Granite</i> ( $417 \pm 2$ Ma) <a href="#">Dunning pers. comm.</a>
	<i>Schooner Cove Migmatite</i> ( $416 \pm 2$ Ma) <a href="#">Dunning pers. comm.</a>
Ordovician Magmatism and Metamorphism	
	<i>HBG: Dioritic Orthogneiss</i> ( $478 \pm 5$ Ma) <a href="#">Dunning pers. comm.</a>
	<i>HBG: Granitic Orthogneiss Sheet</i> ( $465 \pm 5$ Ma) <a href="#">Dunning pers. comm.</a>
	<i>Gander Group (Monazite)</i> ( $\sim 460$ Ma) <a href="#">Buchanan and Bennett, 2009</a>
Precambrian Rocks	
	<i>Gander Group Metasediment</i> ( $< 560$ Ma) <a href="#">O'Neil, 1991</a>

#### **1.4 Location of Study Area**

The thesis area is located in northeastern Newfoundland focusing on exposures of the Hare Bay Gneiss from Windmill Bight Provincial Park south as far as the town of Hare Bay (Figure 1-2). Areas of focus include the detailed “Windmill Bight Map” (Map 1) and the “Greenspond” (Section A-A’), “Trinity”(Section B-B’), and “I Love You”(Section C-C’) road sections. Additional roadside and coastal exposures north of Cape Freels, along Valleyfield road and in the town of Hare Bay were visited and mapped briefly. Both Route 320 (Gambo) and Route 330 (Gander) can be accessed from the Trans-Canada Highway and lead to several of the localities.

Areas for the study were chosen based on accessibility, quality of exposure and potential for enabling an interpretation of the complexity of the Hare Bay Gneiss. The most detailed map work was conducted at Windmill Bight (WMB), where a representative part of the gneiss was mapped on a grid. The map area is 950 m<sup>2</sup>, covering a 65 m strip of coast lying east of the beach at Windmill Bight Provincial Park and can be accessed through the park entrance. Exposure is excellent with minimal cover including small boulder patches and tidal pools.

The “Greenspond” road cut is approximately 36 m long and 6 m in height. It is located ca. 3 km off Route 320 on Greenspond Road. The “Trinity” outcrop is a small, short standing exposure on Main Road near the post office in the town of Trinity. The “I Love You” outcrop is located just south of Trinity on route 320. This section is approximately 78 m long and 14 m in height.

Additional areas in which the Hare Bay Gneiss was examined include the northern shore of Cape Freels, that can also be accessed walking southeast from the WMB map area, roadside and coastal exposures in Valleyfield, as well as roadside outcrops in Hare Bay, the “type area”. Star symbols in Figure 1-2, signify the general location of the studied outcrops.

### **1.5 Purpose and Scope**

Rocks classified as the Hare Bay Gneiss of the northeastern Gander Zone have not yet been studied in detail as previous studies in this area focused on the granitic intrusions and structural history. Although the extent of the Hare Bay Gneiss has been well documented, lack of detailed work leaves the rock types, ages and origin of this unit poorly understood. Past interpretations of the Hare Bay Gneiss include that is a highly deformed equivalent of the adjacent Square Pond Gneiss (Blackwood, 1978) and some studies (Blackwood and Kennedy, 1975) proposed it as potential basement to the Gander Zone. In an effort to better understand the Hare Bay Gneiss and its importance to the Gander Zone as a whole, this study combines field observations with petrological, geochemical and geochronological data from seven selected localities of the Hare Bay Gneiss from Wind Mill Bight Provincial Park in the north, south to Hare Bay.

Careful examination and documentation of field relationships along with extensive petrologic, geochemical and geochronological analysis of a wide diversity of units in these selected areas reveal the complexity in the Hare Bay Gneiss. The

compilation of analytical data with field relationships is crucial in this case as lithologic and event correlations cannot be made based on field observations alone.

## **2. CHAPTER 2: Rock Units: Field Observations and Petrographic Analysis**

### **2.1. Introduction**

A wide diversity of rock types were identified in the Hare Bay Gneiss based on field and petrographic observations. Here units are divided based on geographic location and a detailed description of defining field and petrographic characteristics is provided. Geographic divisions include: 1) the WMB Map Area; road sections including 2) the Greenspond Road Section, 3) the Trinity Road Section, 4) the "I Love You" Road Section and; less detailed traverses along 5) the coast north of Cape Freels, 6) roadside and coastal exposure on and surrounding Valleyfield Road, as well as 7) outcrops along the road in the town of Hare Bay (Figure 1-2). Occurrence and distribution of units from the WMB map area and the three road sections can be observed on Map 1 and the cross sections A-A', B-B' and C-C' in the back cover pocket.

In total, one hundred and seven samples were collected for petrography. The goals of petrographic analysis included: (1) recording petrographic unit diversity and similarity; (2) recognizing mineralogic and textural features to aid in determining genetic relationships and rock type, and; (3) to aid in selecting a subset of representative samples with relatively minor alteration for geochemical analysis.

It should also be noted that many of the highly sheared units exhibit S-C fabrics, recording a strong deformation history. Mapping out these micro- structures was not a

goal of this project and, therefore, although they are present in multiple units, they are not described in detail.

## **2.2 Field Observations and Petrographic Analysis**

A detailed description of field and petrographic methodology is provided in Appendices A and C, respectively. Table C-1 provides a summary of mineralogical and petrographic observations. A list of mineral abbreviations used in figures can be found in Appendix C.

### **2.2.1. The Windmill Bight Map Area**

The WMB map area is relatively small but contains a wide variety of rocks representative of those seen along the coast in this area. It consists of a strongly sheared assemblage of sheet intrusions, all striking roughly north/northeast-south/southwest. Rock units possess a weak to very strong foliation, oriented sub-parallel with the overall strike of the intrusive bodies. Both contacts and foliations are steeply dipping, appearing sub-vertical in places. Contact relationships between units are commonly complex and some are obscured owing to intense shearing. Although shearing commonly makes original contact relationships difficult to identify, in some less deformed areas the nature of the contact and age relationships between units can be determined.

Distinct rock types identified in the WMB map area include locally abundant garnetiferous two-mica leucogranite, megacrystic granite, granodiorite, proto-mylonite, as well as minor cross-cutting garnetiferous pegmatite, tonalitic dykes, mafic intrusions and tourmaline-bearing quartz veins. Both proto-mylonite and mafic intrusions are confined to the west side of the map area. In total 15 separate rock units have been identified and are described in detail below.

#### **2.2.1.1. Foliated Leucogranite**

Field observations define this unit as a muscovite-and garnet-bearing, medium-grained leucogranite. This foliated granite shows orange-white weathering and has a light pink to grey fresh surface (Figure 2-1A). Foliation and fracturing of this granite varies throughout the field area, but typical outcrops have blocky fractures with more shearing along contacts. Crenulation cleavages indicate complex deformation histories in some localities. Generally the foliated leucogranite appears to be one of the oldest rock units in the WMB map area. It cannot be ruled out that individual sheets mapped as part of this unit represent multiple phases of intrusion, despite mineralogical and textural similarities.

Petrographic analyses reveal that the major mineral composition is as follows: quartz 35-50%; K-feldspar 25-50%; plagioclase 10-25%; muscovite 5-15% and; chlorite/biotite <6%. Minor phases, present in some but not all thin sections, include garnet, and oxides, all of which generally make up less than 2% of the rock. Accessory phases include apatite, zircon, titanite and monazite. Secondary alteration minerals are

chlorite, sericite and ( $\pm$ ) epidote. Chlorite replacement ranges from minor to significant and most commonly occurs in biotite, but also affects muscovite. Sericitization of feldspars also ranges from minor to significant, whereas epidote is a minor alteration product.

K-feldspar and plagioclase most commonly occur as coarse grains (up to 5 mm) and host inclusions of muscovite, quartz, biotite/chlorite and apatite. K-feldspar exhibits microcline twinning and exsolution features, and plagioclase displays albite twinning. In some thin sections sericitization is so strong as to obscure these defining features and in such cases feldspar modal percentages are combined. Quartz most commonly occurs as polycrystalline, recrystallized lenses or layers approximately 1-2mm thick. Individual layers vary in thickness across the thin section. Quartz also occurs in combination with muscovite, biotite and chlorite in fine-grained, wispy, discontinuous layers (<0.5mm thick). These fine-grained Al-rich layers define the foliation that varies in intensity and may not be apparent in some thin sections. In places these layers pass into coarser grained (up to 2mm), lens-shaped muscovite grains (Figure 2-1B and C). More randomly oriented, undeformed, euhedral muscovite grains also occur in the quartz-and feldspar-rich layers, indicating multiple phases of growth of the mineral. Numerous muscovite grains are partly broken down to a fine-grained acicular phase along grain boundaries. Garnet appears as an igneous phase and is not confined to Al-rich layers. It is typically seen as sub-euhedral grains less than 1mm in size. Late micro-fractures and turbid quartz and feldspar veins cut across sections and break up the larger feldspar grains.

### **2.2.1.2. Foliated Leucogranite with Layers**

A similar foliated granite identified in the field exhibits grey to white weathering and a grey-pink fresh surface. This strongly sheared granite contains consistent bands that are either quartz-or feldspar-tourmaline-rich, and are approximately 0.5- 4 cm thick (Figure 2-1D). This unit is mineralogically and texturally similar to the foliated leucogranite unit and classification relies solely on the presence or absence of these layers/veins. Intensity of the foliation is variable throughout the field area and in some localities crenulation cleavage is present.

The major mineralogy is very similar to that of non-layered foliated leucogranite described above. A notable difference is the absence of garnet in the foliated granite with layers. Also the layered granite is more strongly foliated than the foliated leucogranite, hence complex microstructures are observed. Muscovite-rich layers create an anastomosing network around augen-shaped feldspars and patches of recrystallized quartz. Titanite and apatite are the most abundant accessory minerals, present in amounts up to 2%.

Two samples were collected from the distinctive bands of this unit. Sample 10AL025B is from a feldspar band with a tourmaline core (Figure 2-2). This thin section reveals that the homogeneous pink material is made up of strongly sericitized feldspar megacrysts in a finer grained matrix of quartz and feldspar. Several continuous, recrystallized layers (<0.5 mm thick) of quartz and feldspar with sutured boundaries also occur. The core of the layer is composed predominantly of tourmaline and plagioclase with minor amounts of chlorite and epidote. The second sample, 10AL032, is from a

quartz-rich layer, composed of 97% quartz, 2% tourmaline and 1% feldspar. The sample predominantly consists of polycrystalline quartz (grain size: ~1 mm) with sutured grain boundaries. Several microfractures separate the quartz into bands with fine-grained feldspar, chlorite and tourmaline along these fractures. A cluster of coarser grained tourmaline was also observed in the thin section.

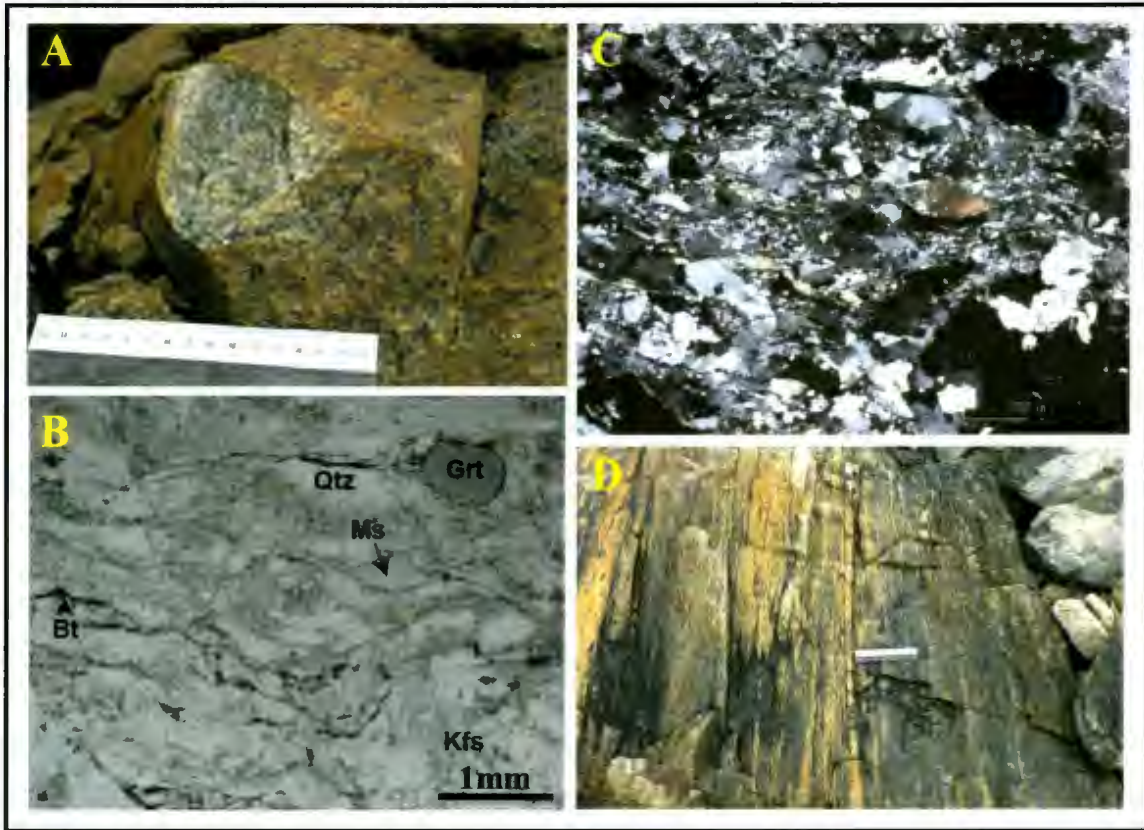


**Figure 2-1: Field photos and photomicrographs showing the two foliated leucogranite units in the WMB map area. (A) Massive blocky exposure of very weakly foliated leucogranite with tiny pinhead garnets. (B) Foliated leucogranite in PPL showing wavy, fine-grained layers of Ms, passing into coarser lenticular Ms grains. Qtz is seen in recrystallized patches with sutured boundaries and as fine grains in groundmass. Coarser feldspars appear turbid due to sericitization. (C) Same view under XPL. (D) Foliated leucogranite with layers consisting of quartz or feldspar-tourmaline.**



**Figure 2-2: Photomicrograph and field photograph of a feldspar-tourmaline vein in the strongly sheared foliated leucogranite. Fsp is interstitial to tourmaline grains. On the left, a vein has a tourmaline-rich core and feldspar-rich outer boundary. On the right clusters of Tourm and Chl , both appear green in PPL.**

### **2.2.1.3. Sheared Megacrystic Granite**

This unit has large feldspars (<1 mm-5 cm) variably aligned in a fine-grained chlorite/biotite/quartz groundmass (Figure 2-3A and B). Some feldspar crystals are euhedral whereas others are rounded, with no remaining crystal faces. Crystal/groundmass ratios are variable throughout the field area, ranging from 30-70% crystals. Several small areas have a significant component of leucocratic lenses and layers throughout. Weathering of this unit is variable depending on proximity to the water, but in many places is dark in appearance. The megacrystic granite commonly has an ambiguous, interfingering relationship with the adjacent foliated leucogranite units,

having parallel foliation and no evidence of intrusive contacts. However, some contacts show the megacrystic granite cutting the foliation of the bordering leucogranite, implying that the megacrystic granite postdated the foliated leucogranite in at least some localities.

In thin section (Figure 2-3C), the composition of this unit is seen to be, 30-50% quartz, 30% K-feldspar, <15% plagioclase, and 10-15% biotite and chlorite combined. Muscovite is present in minor amounts ranging from <1-10% and oxides make up less than 5% of the mode. Myrmekite is also common in minor amounts (<2%) but is absent in several thin sections. The most common accessory phase in this unit is apatite, with other accessory minerals including zircon, monazite and rutile.

Secondary alteration minerals include chlorite, sericite and epidote. Chlorite most commonly occurs as the replacement of biotite. The extent of this alteration is extremely variable within this unit. In some slides chlorite is very minor only affecting a few biotite grains and comprising <1% of the rock. In some samples biotite is significantly, if not completely, replaced by chlorite. Sericitization of both plagioclase and K-feldspar is also variable ranging from minor to extensive. The original twinning and exsolution features may be obscured making it difficult to distinguish feldspars.

Foliation varies from weak to strong and is defined by alignment of biotite, muscovite and chlorite. These fine-to medium-grained minerals form thin (generally <1 mm), wavy, discontinuous bands that comprise an anastomosing network. These layers wrap around larger K-feldspar and plagioclase grains that range from <0.5 mm-2 cm in size. The mica also wraps around recrystallized quartz lenses/layers. Micas are not restricted to the layers and also form more randomly oriented clusters and isolated

subhedral to euhedral grains included in the feldspars. Quartz occurs in various forms in this unit. It ranges from fine (<0.1 mm) to coarse (>2 mm) and occurs in the groundmass, in recrystallized lenses/layers as well as in late veins. The lenses and layers of polycrystalline quartz with sutured grain boundaries are oriented parallel with the foliation, and range in thickness from 0.2-2 mm with variable lengths difficult to determine in thin section. Lastly, late quartz veins and microfractures commonly cut the larger feldspar grains.

#### **2.2.1.4. Highly Sheared Megacrystic Granite (proto-mylonite)**

This unit appears to be a higher strain equivalent of the sheared megacrystic granite. It contains 5-10% feldspar megacrysts, typically less than 1 cm in size. It has planar leucosome layers and lenses (1-5 cm thick) throughout and coarser grained, less deformed slivers are also present. It is dominant on the western side of the map area, where it exhibits highly sheared contact relationships with surrounding units.

In thin section (Figure 2-3D) this unit is seen to contain 30-40% quartz, 30% feldspar and 25% biotite and/or chlorite, depending on the degree of chloritization. Oxides, zircon and titanite were identified as accessory phases, totaling less than 3% of the rock. Muscovite appears in very minor quantities in sample 10AL020. Epidote is a common alteration mineral and in sample 10AL040 appears as grains up to 1 cm in size, growing along feldspar boundaries. Sample 10AL040 also contains 10% of iron-poor

amphibole. The presence of multiple hydrous minerals such as biotite, amphibole and epidote in this sample suggests the possible influx of hydrous fluids.

In general, this unit appears petrologically similar to the sheared megacrystic granite, with a foliation defined by a fine-grained network of biotite and chlorite. The key differences are the amount and size of feldspar megacrysts as well as the overall grain size of the rocks being finer in the highly sheared samples.

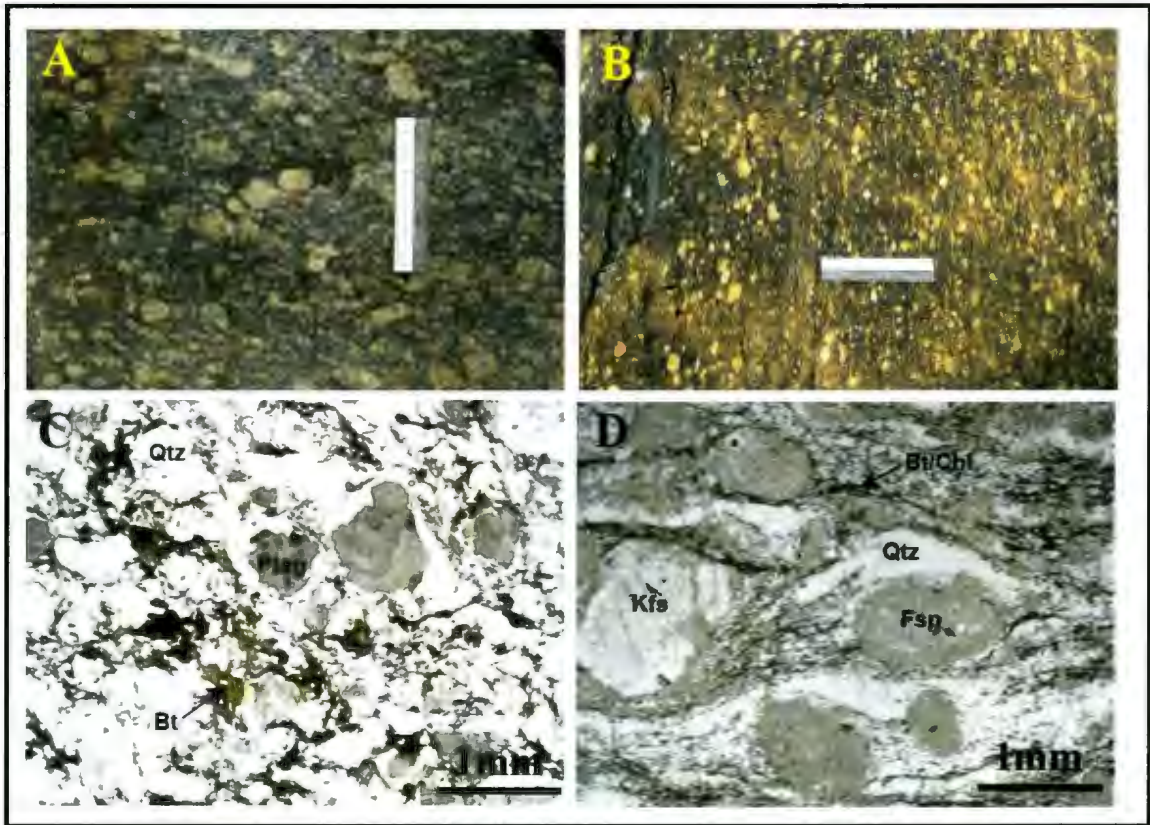


**Figure 2-3: Field photographs and photomicrographs showing the variably sheared megacrystic granite of WMB map area. (A) Less deformed sheared megacrystic granite showing feldspar megacrysts up to 3-4 cm in size. (B) Highly sheared megacrystic granite with a lower ratio of megacrysts to groundmass and megacrysts appear smaller on average (~1-2 cm). (C) Less deformed sample of the sheared megacrystic granite. Patches of recrystallized quartz are more irregularly shaped and feldspar augen are less pronounced. (D) Strongly foliated (protomylonitic) megacrystic granite (PPL). Coarser feldspar augen and lenticular patches of recrystallized quartz are strung out in a matrix of finely ground quartz, biotite and chlorite.**

### **2.2.1.5. Foliated Granodiorite**

The foliated granodiorite is a fine-to medium-grained rock with small (<5 mm) feldspar phenocrysts throughout (Figure 2-4A). Thin pegmatite layers (<2 cm) as well as layers and lenses of foliated, coarse-grained granite are common (Figure 2-4B). Fresh surfaces appear dark grey and weathered surfaces are white to light grey. This unit displays conjugate sets of fractures and many show fluid alteration of the adjacent granodiorite, as orange to red weathering. This unit clearly cross-cuts the adjacent granite, as it encloses slivers and lenses of these granite units.

Based on petrographic observations the major mineralogy of this rock includes 40-52% quartz, 20-25% plagioclase, 5-15% K-feldspar, and variable amounts of biotite and chlorite totaling less than 20% (Figure 2-4C and D). Minor and accessory phases include epidote, oxides, apatite, titanite, zircon and rutile. Titanite and apatite are the most abundant accessories with titanite grains up to 0.5 mm and totaling up to 2% of modal mineralogy.

The matrix is predominantly composed of finer grained quartz, biotite and chlorite, generally less than 0.5mm. Quartz forms equant grains with well-defined boundaries. Anhedral feldspars are highly sericitized, obscuring twinning. Sericitization is locally concentrated in grain cores, with relatively unaltered rims. A fine-grained web-like network of biotite and chlorite defines the foliation. Minor late quartz veins are commonly offset by microshear zones and microfaults.

Sample 10AL035 is from one of the coarser grained granitic lenses that occur throughout this unit. The feldspars are up to 1 cm in size and are set in a finer grained matrix of quartz, biotite and chlorite. Biotite and chlorite are confined to thin wavy bands less than 0.1mm thick. In addition, this sample has abundant irregular patches of recrystallized quartz with sutured boundaries.

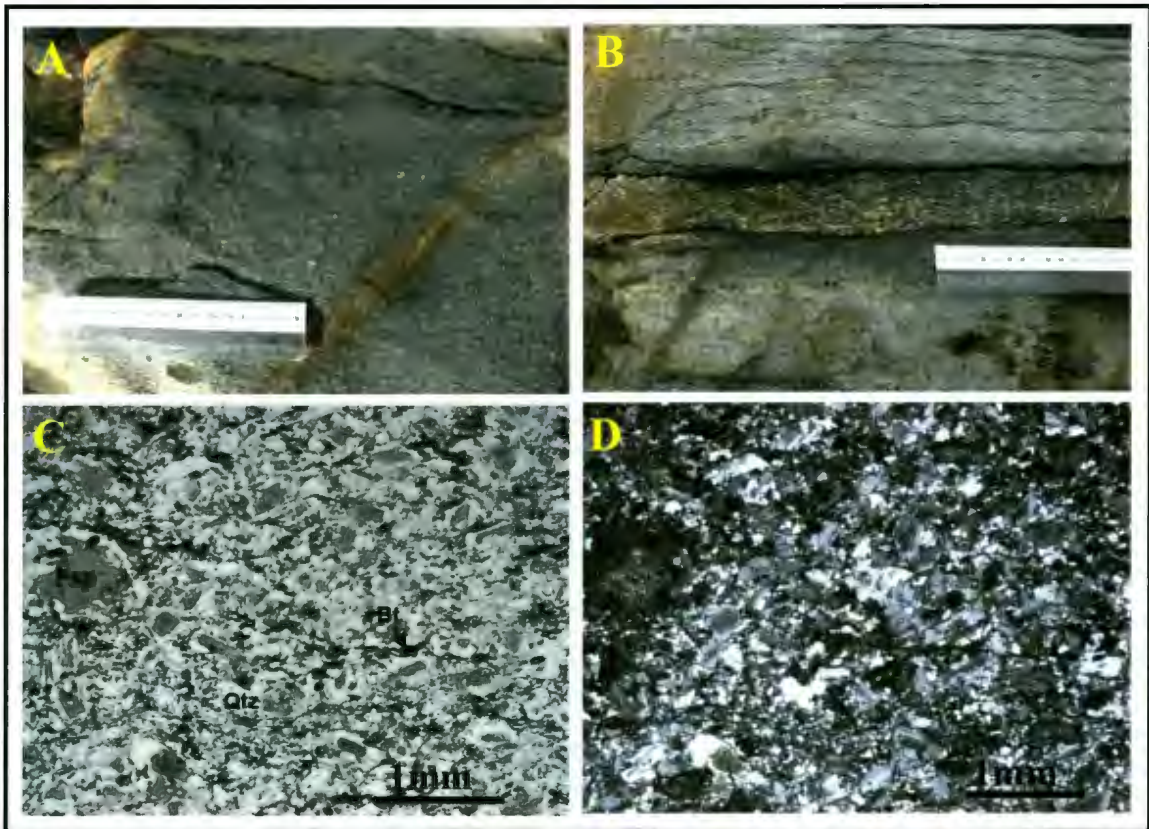


**Figure 2-4: Field photographs and photomicrographs showing the foliated granodiorite in WMB map area. (A) A distinctive fracture cuts unit with red fluid staining. Here the foliated granodiorite appears relatively fine-grained in comparison to the previously mentioned granitic units with coarser feldspars (1-2 mm) throughout. (B) A lens of medium-grained granite within the foliated granodiorite. (C) In PPL the weak foliation of granodiorite is defined by alignment of biotite grains. Visible sericitization targets the core of feldspar grains with relatively unaltered rims. (D) Same view in XPL showing twinning in plagioclase grains and sutured grain boundaries of some quartz.**

#### **2.2.1.6. Intermediate Dyke**

In the field this unit appears as a fine-grained cross-cutting body. The dyke has a blue-grey fresh surface and a dark brown weathered surface (Figure 2-5A and B). Several faults cause minor offsets of this steeply dipping dyke, which represents a late magmatic event as it cuts the foliation of the megacrystic granite. It is in faulted contact with the adjacent pegmatite so the age relationship between the two units remains uncertain.

Both the mineralogy and microstructures of the dyke are strikingly similar to that of the granodiorite of the WMB map area. This unit is slightly more tonalitic in composition with little to no K-feldspar, and slightly more plagioclase (Figure 2-5C). Otherwise the description of the granodiorite above may be applied to both units.

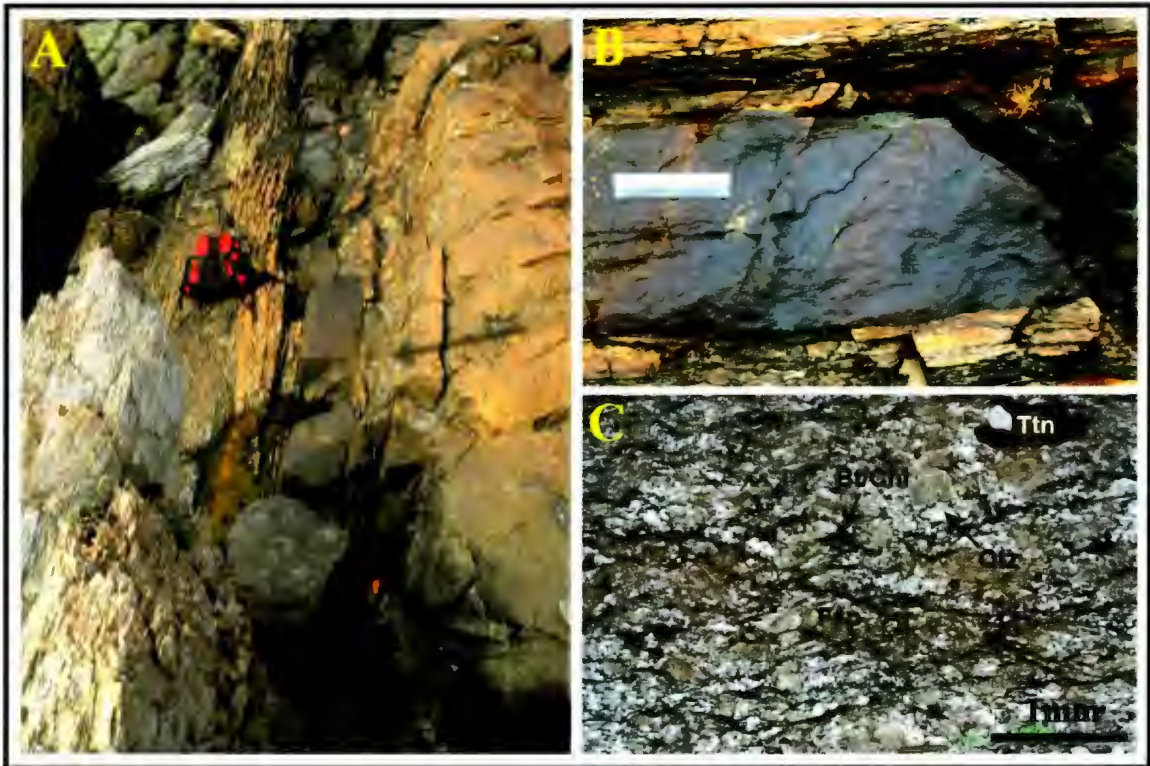


**Figure 2-5: Field photographs and photomicrographs of intermediate dyke in the WMB map area. (A) and (B) show the steeply dipping intrusive body oriented parallel with fabric in surrounding units. It is a massive, dark, fine grained unit. (C) In thin section the foliation is defined by a weaving network of fine-grained biotite and chlorite. Feldspar and quartz occur as irregular lenticular polycrystalline patches. Also in this micrograph is a coarse titanite grain in the top right.**

### **2.2.1.7 Late Pegmatite Intrusions and Pegmatite/Aplite Veins**

Pegmatite intrusions with irregular contacts are common throughout the WMB map area (Figure 2-6A and B). Commonly the mineral assemblage consists of K-feldspar, quartz, plagioclase, muscovite and garnet. These bodies are oriented approximately parallel with the overall foliation in the older units and commonly occur as large sheet-

like bodies. The dip of these intrusions is typically ambiguous, changing substantially along strike. Pegmatite and aplite veins are also common throughout the map area, and range from thin (<1 cm) to thick (~30 cm) linear bodies. Veins with pegmatitic margins and aplitic cores have been identified and several pegmatite veins have been boudinaged. The composition of mapped veins is similar with the addition of some localized minor phases, locally. Minerals observed in veins include quartz, K-feldspar, plagioclase, ( $\pm$ ) muscovite, ( $\pm$ ) garnet, ( $\pm$ ) tourmaline and ( $\pm$ ) pyrite. Contact relationships with other units show that pegmatite intrusions and veins represent one of the youngest magmatic events within the WMB map area. These intrusive bodies commonly cross-cut fabrics of older units at low angles and commonly finger into granitic units.

Petrographic work shows that between 85-95% of the mode of the collected samples composition is K-feldspar, quartz and plagioclase. Muscovite content is variable ranging from 5-10% and, garnet and oxides content is less 5% (Figure 2-6C and D). Tourmaline was identified in sample 10AL027 and pyrite was identified in the field. Minor chloritization of the muscovite is observed in some samples.

K-feldspar occurs as megacrysts up to 2 cm in size. These megacrysts are poikilitic with inclusions of quartz, plagioclase, muscovite and chlorite. Micro-shear zones that are filled with quartz commonly fracture the coarser grains (Figure 2-6D). The groundmass consists of ground quartz and muscovite with variable garnet (0.2-1 mm in size) content. Irregular patches as well as oriented ribbons of medium-grained recrystallized quartz are present. Larger flakes of randomly oriented euhedral muscovite were also observed.

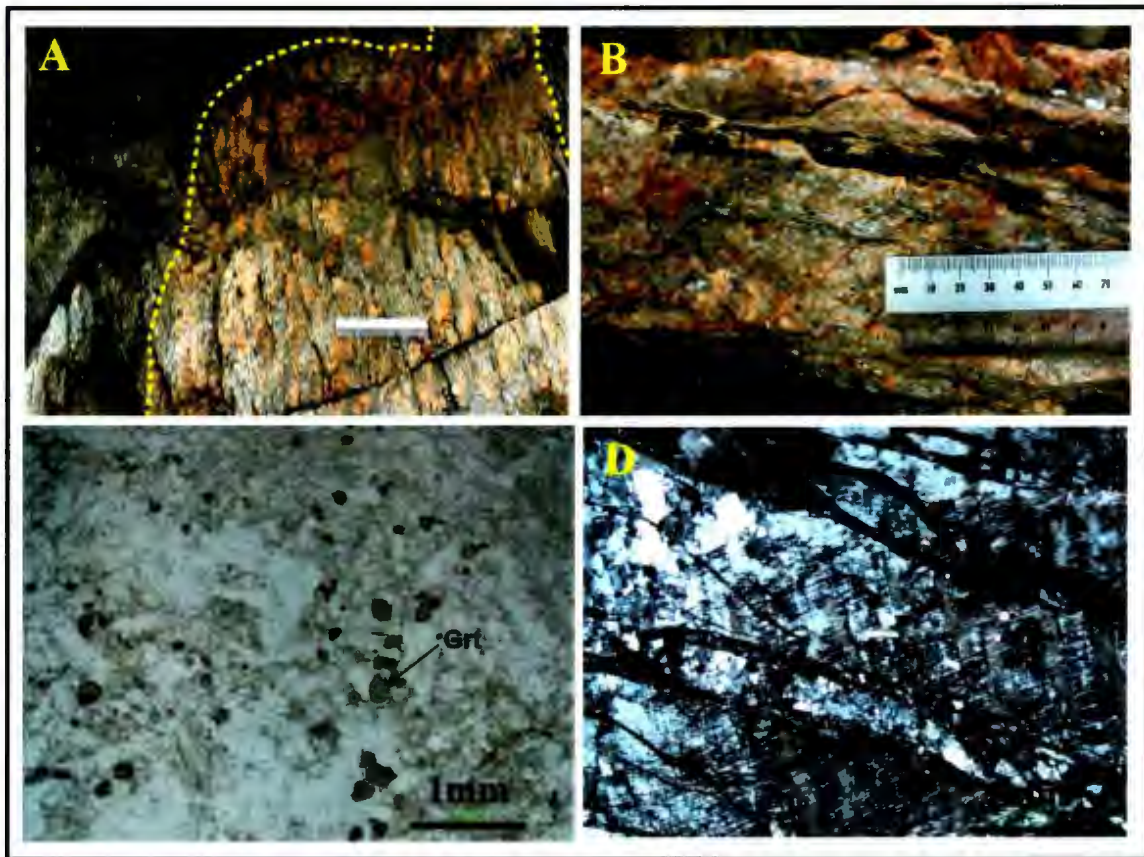


**Figure 2-6: Field photographs and photomicrographs depicting pegmatite intrusions within the WMB map area. (A) A pegmatite (right) intrudes a sheared megacrystic granite (left). (B) Pegmatite intrusion in which large fractured feldspars and elongate quartz ribbons are visible. (C) View of pegmatite with pinhead garnet in PPL. (D) XPL view of a coarse K-feldspar grain exhibiting microcline twinning and with multiple fractures, commonly filled with quartz.**

### **2.2.1.8 Interlayered Mylonite Unit**

Generally this is a fine-to medium-grained dull grey unit possessing layers, <1-2 cm thick, of pegmatite, medium-grained granite, and the highly sheared megacrystic granitic unit (Figure 2-7). Layering occurs at too fine a scale to accurately depict on the map, and although these rocks do not represent a unique lithology within the map area it

has been combined into a single undifferentiated unit. Because of the heterogeneity of this unit, thin section analysis is not effective in describing the unit as a whole. Samples 10AL053, 10AL081 and 10AL052 collected from this unit vary from medium-grained granite to a fine-grained biotite-muscovite schist.



**Figure 2-7: Field photograph depicting the highly sheared interlayered unit in the WMB map area. The unit has multiple components including fine-grained, dark layers, coarser granitic layers as well as very coarse pegmatitic layers.**

#### **2.2.1.9. Aluminous Mica-rich Intermediate Unit**

In the field the fine-grained mica-rich rock is dark in appearance with grey to black fresh and weathered surfaces. It is highly sheared and has thin (<1 cm)

discontinuous layers and lenses of slightly coarser grained material. The abundance of fine-grained mica flakes in this unit cause surface exposure to be highly reflective or shimmery in appearance (Figure 2-8A and B).

This fine-grained unit is composed of approximately 30-40% biotite and muscovite, 40-50% quartz and less than 15% feldspar (Figure 2-8C and D). Accessory and secondary phases include oxides, chlorite, epidote, garnet, zircon and rutile. Grains of major phases are typically anhedral and less than 1 mm, with some coarser (1 mm) subhedral muscovite grains throughout. Garnet and zircon are euhedral, with garnet being very minor and absent from some thin sections. Aggregates of elongated micas produce a foliation in places forming thin (<0.5 mm) discontinuous layers that pinch and swell along their length. Quartz is commonly recrystallized with sutured grain boundaries.

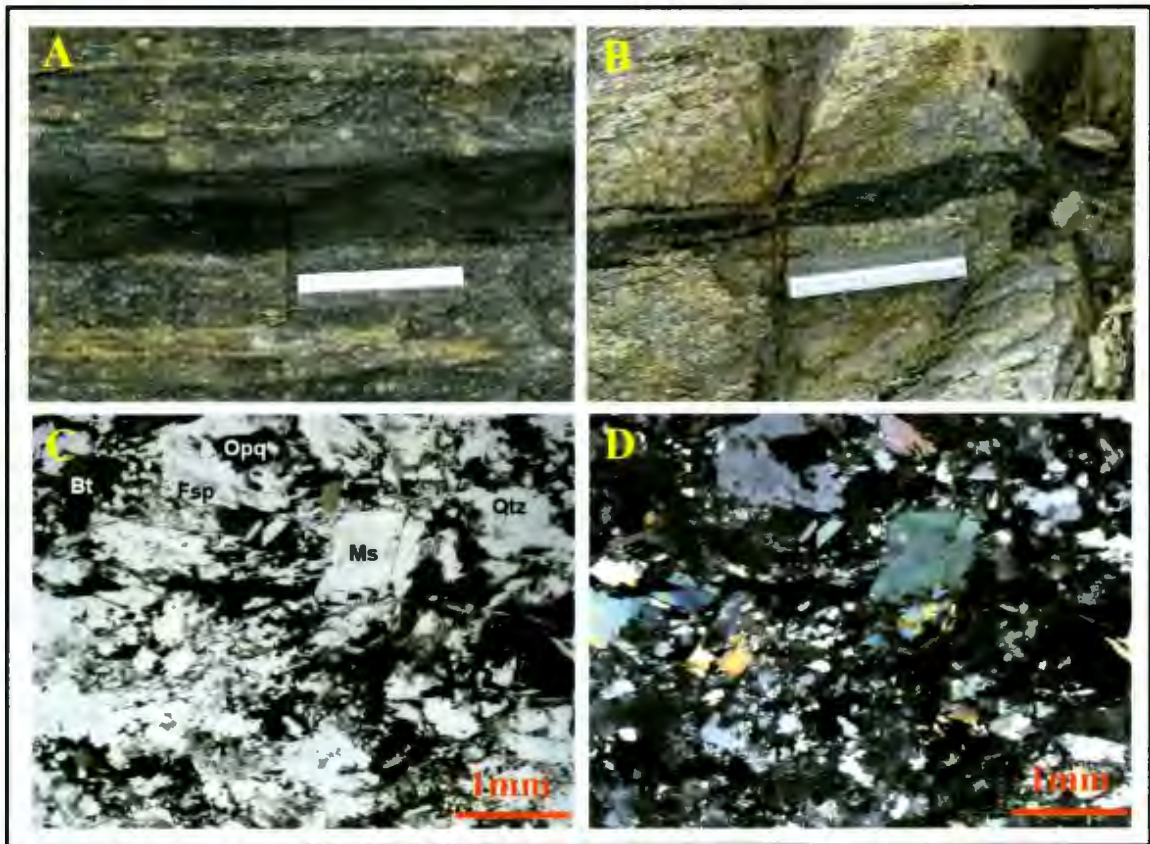


**Figure 2-8: Field photographs and photomicrographs showing the aluminous, mica-rich intermediate rock from the WMB map area. (A) and (B) The unit appears fine-grained and dark. In (A) it is contact with a highly sheared megacrystic granite and in (B) it is seen as a finger into a much more leucocratic foliated granite. (C) and (D) show PPL and XPL views of this unit, with large flakes of biotite and muscovite as well as coarser feldspar and patches of recrystallized quartz. It is evident that some mica is randomly oriented whereas other grains show a faint alignment, defining the foliation.**

#### **2.2.1.10. Actinolite-Biotite Mafic Unit**

In the field this unit is recognized as a fine-grained mafic rock with coarser (<0.5 cm) feldspar grains present throughout (Figure 2-9A and B). A small number of thin, coarse-grained granitic layers and lenses (<2 cm thick) are also present. This unit

occurs in the western side of the WMB map area within a highly sheared assemblage of rock units. It is inferred to represent a later phase of mafic intrusion, postdating megacrystic granite emplacement and at least some pegmatite intrusions.

The major minerals include biotite, actinolite, quartz and feldspar (Figure 2-9C and D). Titanite is the most abundant accessory mineral making up 3-4% of whole rock composition. Apatite, epidote and rutile are also present in minor quantities (<1%). Elongated biotite and actinolite grains as well as recrystallized polycrystalline quartz ribbons define a strong fabric. Coarser, strongly sericitized, anhedral feldspar is present throughout. Titanite is commonly associated with the mafic minerals, occurring as high relief sub-to euhedral grains approximately 200  $\mu\text{m}$  in size (Figure 2-9D).

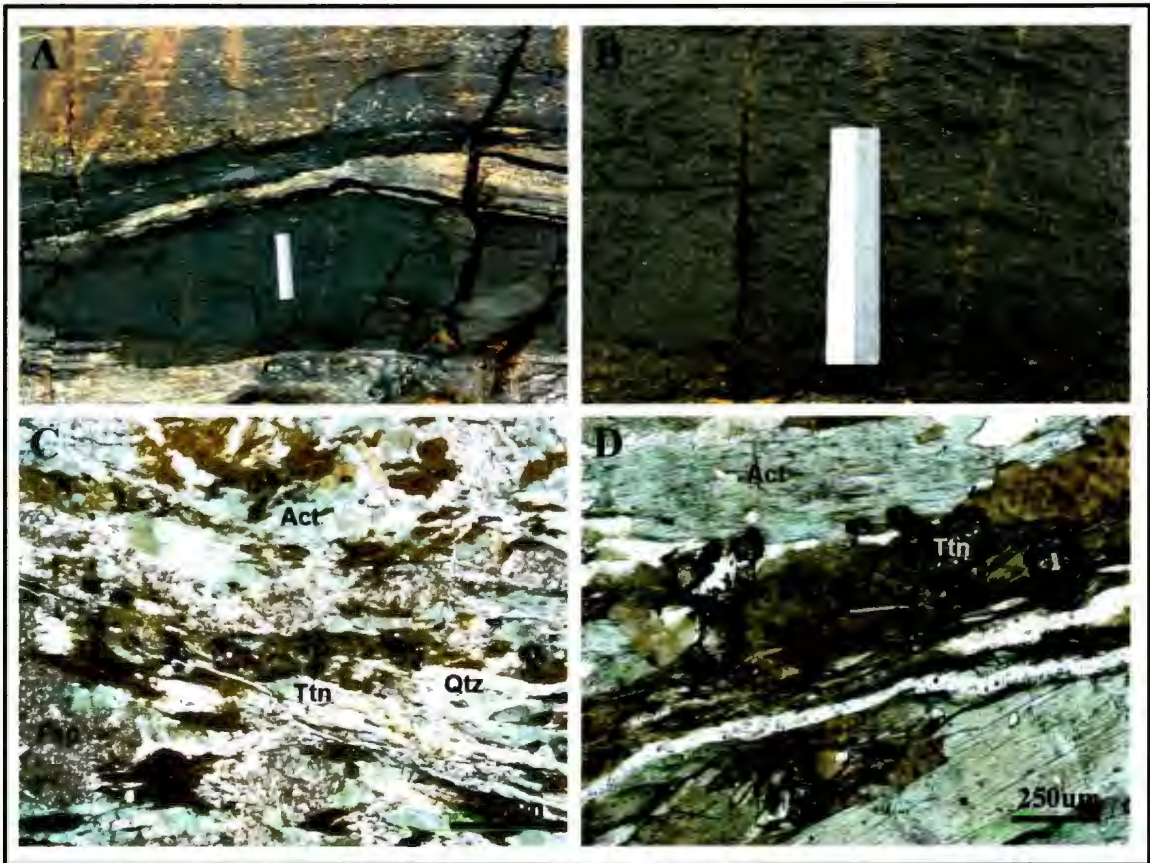


**Figure 2-9: Field photographs and photomicrographs showing the actinolite-bearing mafic unit in the WMB map area. (A) This unit appears in a shear zone and therefore contacts are commonly sheared. (B) The unit appears fine-grained with tiny feldspar grains (<1 mm) floating in a finer matrix. (C) A PPL view showing strongly oriented biotite, actinolite and layers of recrystallized quartz. Feldspar grains are slightly coarser with irregular grain boundaries. (D) A closer PPL view of titanite grains, up to 250  $\mu\text{m}$  in size, commonly occurring with biotite.**

#### **2.2.1.11. Biotite-Carbonate Mafic Unit**

A biotite-carbonate-bearing mafic schist occurs as a unique lens in the northwestern corner of the map area. It is very fine-grained with a dull grey to black fresh and weathered surface (Figure 2-10A). Contact relationships with surrounding units are

obscured as the lens occurs in an area of intense shearing with faulted contacts between surrounding units.

This rock consists of approximately 70% biotite, 10% carbonate, 10% quartz, 5% epidote 3% feldspar and 2% chlorite (Figure 2-10B,C and D). Fine-grained, elongate biotite grains show a strong alignment and quartz and feldspar form thin layers, 0.1-1 mm thick aligned parallel with the foliation. Feldspars show weak to moderate sericite alteration. Carbonate occurs as elongated porphyroblasts dispersed evenly throughout biotite layers and in aggregated clusters (<1 mm) (Figure 2-10B). Carbonate grains commonly cut across the principle fabric of the unit. Epidote occurs as slightly coarser grains and some exhibit zoning, with possible clinozoisite cores.

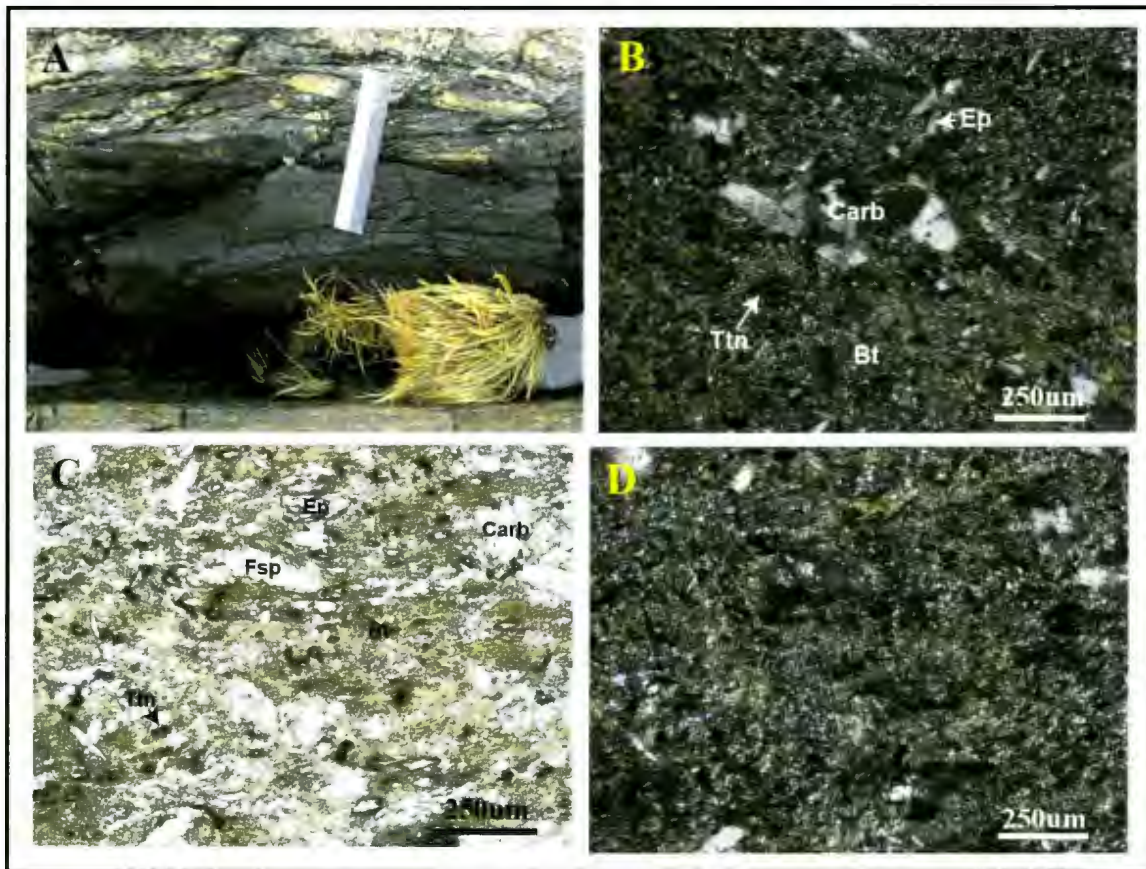


**Figure 2-10: Field photograph and photomicrographs depicting the carbonate-biotite-rich mafic rock in the WMB map area. (A) A single lenticular section of this unit is found in the area. It is very fine-grained and dark in appearance, and contacts with surrounding units are obscure due to shearing. (B) XPL view of a patch of elongate carbonate grains surrounding by fine-grained mass consisting dominantly of biotite with tiny (~100  $\mu\text{m}$ ) epidote and titanite grains throughout. (C) PPL view showing overall composition of rock with biotite, carbonate, feldspar, titanite and epidote. (D) Same as previous view but in XPL.**

#### 2.2.1.12. Layered Quartzite Unit

Layered quartzite (Figure 2-11) occurs in one locality on the western side of the map as a lens just under 0.5 m thick and approximately 8 m in length. This layered unit is composed almost entirely of quartz. Fine-grained tourmaline, as well as garnet and minor

epidote pods occur along layer boundaries. Contacts with surrounding units are highly sheared and because of the unique lithology of this unit with respect to other units in the map area, it has likely undergone vertical or horizontal displacement, now juxtaposed against multiple intrusive bodies or represents a raft within the granitoid assemblage.

Petrographic examination revealed the rock is comprised of upwards of 90% quartz, occurring as elongate, oriented grains with sutured boundaries. These quartz-rich layers have minor amounts of sericitized feldspar and some coarse andalusite grains ~1 mm in size. Alumina-rich horizons separate individual layers and are comprised of fine-grained micas and tourmaline (<100  $\mu\text{m}$ ), as well as coarser garnet (500  $\mu\text{m}$ ) and apatite (250 $\mu\text{m}$ ) grains (Figure 2-11). This unit contrasts with the surrounding rock types and may represent a mylonitized sedimentary rock.

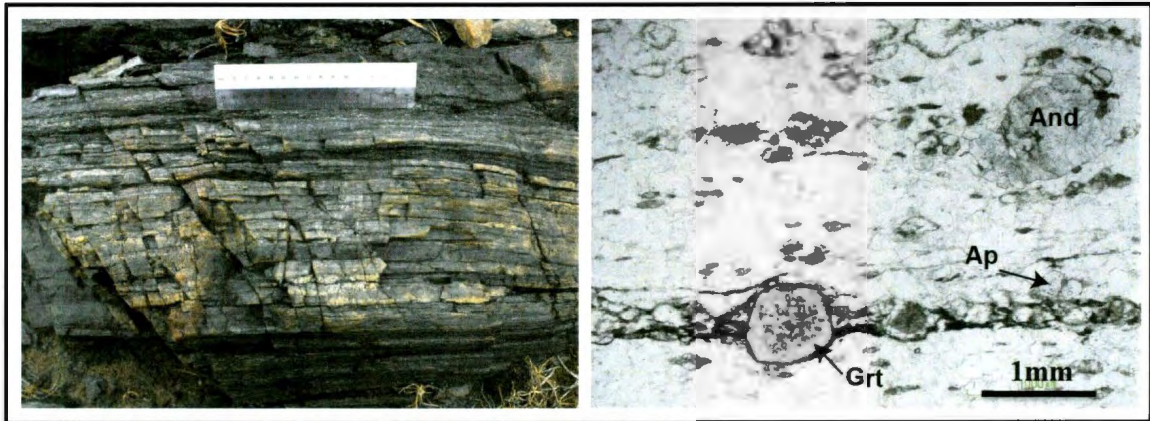


**Figure 2-11: A field photograph (left) and photomicrograph (right) showing the layered quartzite unit in the WMB map area. On the left the unit is approximately 30 cm thick. Contacts with surrounding units are sheared and difficult to interpret. Uniform layers ~1 cm thick of almost pure quartz are separated by fine-grained black material and some garnet and epidote pods also occur along these boundaries. On the right, a PPL view of sample 10AL005. Here the unit is dominated by quartz with some feldspar and very minor coarse andalusite grains throughout. A layer boundary can also be observed and is abundant in alumina-rich minerals. Euhedral garnet porphyroblasts and euhedral apatite grains occur in a thin layer of fine-grained biotite and chlorite.**

### 2.2.1.13. Quartz Veins

Late quartz veins and lenses are found throughout the map area with thickness varying from less than a centimeter to approximately 30 cm (Figure 2-12). Some quartz veins are uniform in both thickness and continuity and are parallel to the dominant foliation whereas others are randomly oriented, oblique to foliation and may pinch or thicken along their length. Quartz veins contain minor amounts of tourmaline and pyrite in some places. As they are observed cutting most granitic intrusions as well as pegmatite veins, they are inferred to postdate most other units within the map area.



**Figure 2-12: Field photographs of quartz veins in the WMB map area. On the far left, a quartz vein cuts perpendicular to the foliation of a sheared megacrystic granite. In the middle a thick (~25 cm) quartz vein cuts parallel to the foliation of a sheared megacrystic granite. On the far right, a small quartz vein has an abundance of tourmaline clusters throughout.**

### **2.2.2. The Greenspond Road Section (A-A')**

The Greenspond Road section consists of a heterogeneous assemblage of Al-silicate-bearing granitic orthogneiss cut by foliated two-mica leucogranite, late pegmatite veins and undeformed medium-grained granite intrusions. The orthogneiss locally contains tonalitic enclaves, ranging from a few millimeters to several meters in size. The foliation in granite and the banding in the gneiss have the same general orientation, striking at roughly  $220^{\circ}$  and dipping steeply, between  $60$  to  $70^{\circ}$  (RH). Eight separate rock units were identified in the section and detailed descriptions are provided below.

### **2.2.2.1 Al-Silicate-Bt-Ms-bearing Orthogneiss**

The orthogneiss is a relatively homogeneous and banded. The layering ranges from continuous to irregular and the ratio of mafic to felsic layers is variable along the road section. In general, the dark-colored layers are thin (<1 cm) and are composed primarily of fine-grained biotite and chlorite. The light-colored layers appear granitic in composition with a pink/grey color and are on average 3-5 cm thick. Grain size in the felsic layers range from medium- to coarse (Figure 2-13A).

Petrographic analysis identified the complete mineral composition of this unit as quartz, plagioclase, K-feldspar, biotite, muscovite, sillimanite, cordierite, ( $\pm$ ) andalusite, myrmekite and oxides. The accessory mineral assemblage includes zircon, apatite and monazite. Replacement of micas by chlorite and feldspars by sericite is common and the majority of cordierite exhibits pinite alteration (Figure 2-14A). Chloritization of the micas commonly creates a striped pattern as the cleavage planes are primarily altered.

A network of Al-rich minerals including muscovite, biotite, sillimanite and cordierite defines the foliation. Sample 10AL003 contains nodules of Al-rich minerals including andalusite (Figure 2-14B and C). Bundles of acicular sillimanite cut across these clusters in places. The andalusite is poikilitic with blebs of quartz and biotite, and andalusite grains grow over sillimanite bundles. Cordierite appears interstitial in these clusters and contains bleb-like biotite grains. In places where the foliation is not strong, randomly oriented, irregular clusters of biotite, muscovite, sillimanite and cordierite are present. Sample 10AL071 contains a wispy lens (1x10 mm)



**Figure 2-13: Field photographs from the Greenspond Road section. (A) Contact between the tonalitic enclave and the Al-silicate-bearing orthogneiss. (B) Granitic orthogneiss with lenses of a mafic component defining the foliation (marked with arrows). (C) Foliated leucogranite that cuts the Al-silicate orthogneiss in the middle of the section. An arrow highlights the alignment of thin layers and lenses of biotite and chlorite. (D) Contact between foliated leucogranite and orthogneiss, where the leucogranite clearly cuts the banding defined in the orthogneiss. (E) Al-silicate-bearing orthogneiss with an abundance of tonalitic enclaves.**

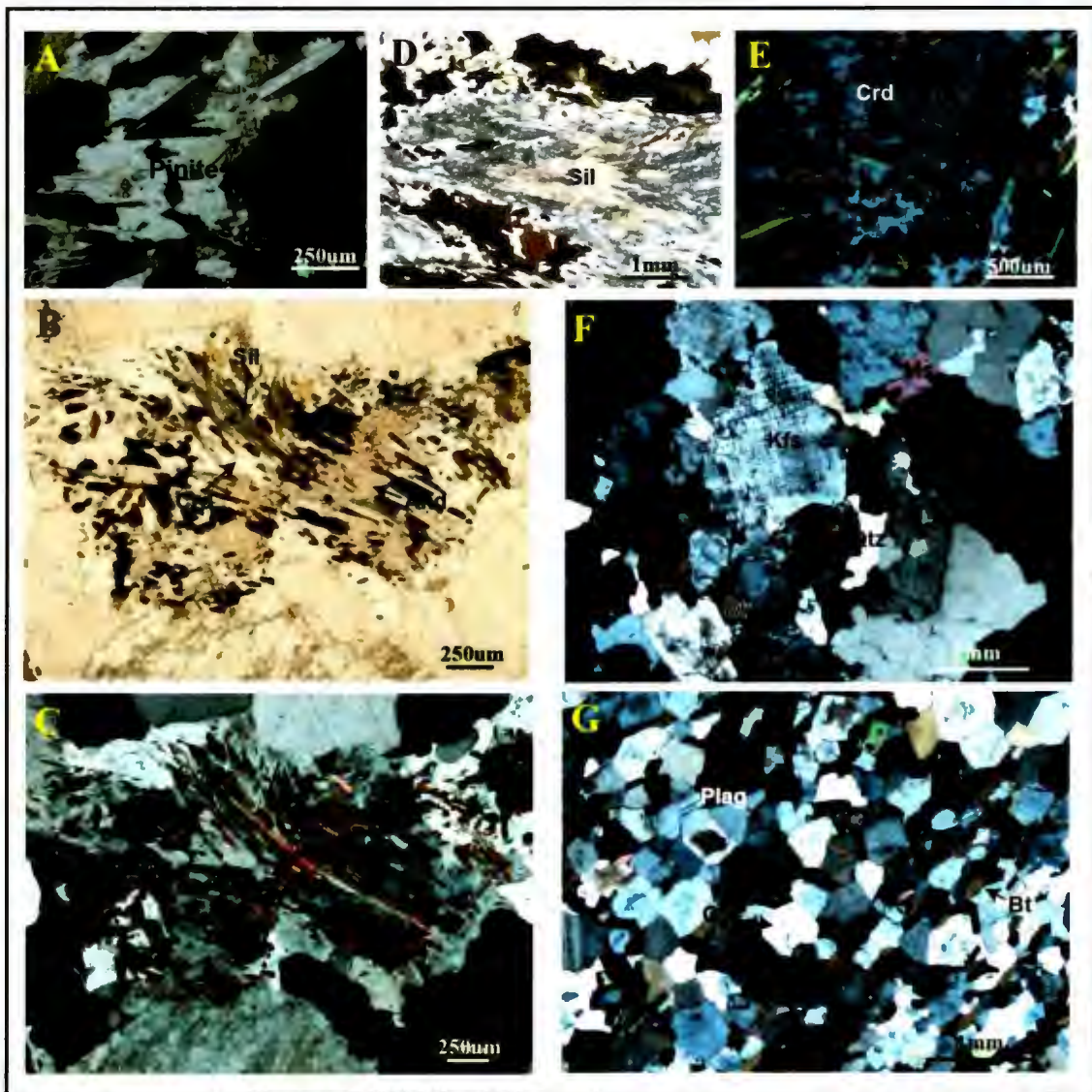


**Figure 2-14: Photomicrographs showing characteristic features of units in the Greenspond Road section. (A) PPL view of cordierite partially altered to pinitite. (B) A cluster of Al-rich phases in PPL including andalusite, cordierite, sillimanite and biotite from sample 10AL003 of the Al-silicate bearing orthogneiss. (C) Same view in XPL. (D) A fibrous bundle of fine grained sillimanite needles in PPL. (E) Large patch of cordierite in XPL with blebs of biotite and oxides as well as some sillimanite needles throughout. (F) XPL view of sample of the foliated leucogranite. Foliation is not apparent in this photo. K-feldspar has irregular grain boundaries and exhibits tartan twinning. (G) A XPL view of a tonalitic enclave. Triple junction grain boundaries are obvious and biotite grains show alignment.**

of fine-grained sillimanite (Figure 2-14D). Large feldspar grains, up to 5 mm in size, have broken down to a fine-grained phase and have irregular corroded grain boundaries. Muscovite and biotite appear unstable as they are commonly skeletal and needle-like at the edge of grains.

Sample 10AL073 is from a more siliceous sample of the same orthogneiss. The contact between the orthogneiss and this more siliceous unit is gradational and difficult to define. Petrographic similarities are apparent between this rock and the Al-silicate, Bt-Ms orthogneiss with the exception of one unique cordierite lens. The lens contains irregular blebs of biotite and oxides, elongate blades of muscovite and fine-grained bundles of sillimanite (Figure 2-14E).

#### **2.2.2.2. Bt-Ms-Sil-bearing Orthogneiss**

This unit appears as a leucogranite with thin mafic lenses and slivers throughout (Figure 2-13B). The mafic component appears biotite rich and the lenses are approximately 5-15 cm long and 1-5 cm in width. The mafic component is minor compared to the previous unit, making up 10-15% of the mode. This unit postdated the Al-silicate bearing orthogneiss because it cuts the fabric of this unit. Contacts are not easy to identify and are in many places obscured by weathering and fracturing. Late pegmatite veins cut this unit locally.

In thin section (10AL074) this unit contains K-feldspar, plagioclase, quartz, biotite, muscovite and very minor amounts of sillimanite and oxides. Feldspar megacrysts

are up to 5 mm in size and have a moderate amount of sericite alteration. Biotite occurs as coarse elongate grains and appears to be disintegrating along grain boundaries. Muscovite occurs as elongate grains as well as anhedral irregular grains. Feldspars commonly exhibit characteristic twinning and have patches of significant sericitization. Sillimanite occurs as rare bundles of fine-grained acicular grains. The distinguishing features of this unit are much more apparent in the field than in thin section.

### **2.2.2.3. Foliated, Two-mica Leucogranite**

In the field this unit is a massive, blocky intrusion of a medium-to coarse-grained leucogranite. The alignment of mafic minerals creates a weak foliation that is variable in intensity (Figure 2-13C). Both weathered and fresh surfaces appear light pink to white. This intrusion cuts across the layering of the orthogneiss and is itself cut by late pegmatite veins (Figure 2-13D).

The leucogranite is comprised of nearly equal parts of K-feldspar, quartz and plagioclase, making up between 85-90% of the rock (Figure 2-14F). Biotite content is variable ranging from 5-10% and muscovite is minor (<5%). Minor chlorite and epidote alteration are observed (<2% content) and oxides and apatite are present as accessories (<1%).

The feldspars reach 4 mm in size and are commonly significantly sericitized. K-feldspar shows exsolution features and microcline twinning, and plagioclase possesses

characteristic lamellar twinning. Irregular patches of polycrystalline recrystallized quartz are seen throughout. The foliation is defined by biotite and is only weakly apparent in thin section. Several late microfractures with fine-grained quartz, cut across the rock and fracture large feldspar grains in places.

#### **2.2.2.4. Enclave-bearing Orthogneiss**

This unit consists of irregularly interfingering coarse-grained granite and intermediate foliated enclaves (Figure 2-13E). Contacts of this unit with the surrounding orthogneiss are gradational as enclaves become less abundant and banding becomes more homogenous. The enclaves range from 1-15 cm wide and length is variable up to approximately 2m.

Sample 10AL070 is from the intermediate biotite rich enclave. The enclave is tonalitic in composition with 47% quartz, 26% plagioclase and 26% biotite. Minor amounts of muscovite, oxides and apatite are also present. This gneiss is equigranular (0.5-2mm grains) and many of the grain boundaries between quartz and feldspar grains are sutured. Biotite possesses pleochroic haloes and forms 2mm thick bands that alternate with quartz+feldspar rich layers. Biotite is subhedral to euhedral in form and feldspars and quartz are anhedral.

Sample 10AL069 was collected adjacent to the enclave bearing gneiss. Because of limited exposure it is difficult to determine whether this unit is a large enclave or an intermediate dyke. A strong foliation is apparent with the same orientation as banding of

the adjacent orthogneiss. Mineralogy of sample 10AL069 includes 40% quartz, 30% plagioclase, 10% Kfeldspar, 15% biotite with minor amounts of muscovite and chlorite. Accessory minerals include zircon, apatite and oxides. In contrast to the neighbouring enclaves this sample has less biotite and Kfeldspar is present. The grain boundaries are well-defined, and triple junctions exist between many grains. This unit is equigranular and the minerals are dispersed evenly within the unit, lacking compositional banding. The lath shaped biotite, however, does create a strong foliation (Figure 2-14G). Alteration of this unit is minor and includes chloritization of biotite and mild sericitization of some feldspar grains.

#### **2.2.2.5. Late Pegmatite and Granitic Intrusions**

Late pegmatite and medium- to coarse-grained granite cut across this section (Section A-A'). These granitic units represent the latest intrusions within the outcrop. Pegmatite mineralogy commonly includes Kfeldspar, quartz, plagioclase and muscovite (not sampled for petrography).

Sample 10AL067 was taken from a late, coarse-grained leucogranite intrusion near the west end of the outcrop section. This rock includes nearly equal parts of K-feldspar, quartz and plagioclase and minor amounts of biotite, muscovite, chlorite and oxides. Feldspar megacrysts are up to 2cm and many of the feldspar crystals show growth zoning and also contain inclusions of muscovite, biotite, quartz and plagioclase. Quartz commonly occurs as bleb-like inclusions in this sample and these blebs are concentrated

along the boundaries of K-feldspar grains. K-feldspar shows excellent microcline twinning and exsolution features, and plagioclase exhibits lamellar twinning.

### **2.2.3. The Trinity Section (B-B')**

This short road cut section contains units striking nearly parallel with the rock face. For this reason the proportion of some units may be over or under represented in the drawing. The predominant unit of the Trinity section is a homogenous granitic orthogneiss (Figure 2-15A). Foliated, fine-grained intermediate blocks are in contact with the orthogneiss but because of limited exposure and the orientation of the unit, the nature of the contact between the two is difficult to interpret. Garnet-bearing leucogranite cuts the orthogneiss and late pegmatite (Figure 2-15B) and tourmaline-bearing quartz veins are common.

#### **2.2.3.1. Two-mica Granitic Orthogneiss**

This gneissic unit has fairly homogenous banding of mafic and felsic layers (Figure 2-15A). The mafic layers consist largely of biotite, muscovite and chlorite and are generally less than 2 cm thick. The felsic layers are 3-4 cm thick and range from K-feldspar-rich to quartz-plagioclase-rich. They display a pink to grey fresh surface, depending on feldspar composition, and white to grey weathered surfaces. A more leucogranitic variety of the orthogneiss with very minor biotite-rich lenses and layers defining a foliation is present in the middle of the section.

In thin section the quartz and feldspar contents are variable, typically making up between 70-85% of the whole rock composition (Figure 2-15C). Mica content is also variable with biotite ranging from 5-20% and muscovite ranging from 3-10%. Chlorite is apparent in some thin sections but is typically minor (<2%). Other minor and accessory phases include myrmekite, oxides, zircon and apatite.

This unit is medium-grained with some coarser feldspar up to 8 mm in size. Feldspar shows minor to significant sericitization and is poikilitic with inclusions of quartz, biotite and muscovite in places. K-feldspar commonly exhibits microcline twins and exsolution features and plagioclase has lamellar twins. The boundaries of the feldspar grains are commonly irregular, suggesting the feldspars were breaking down.

Fine-grained wavy, biotite and muscovite-rich layers, commonly less than 2 mm thick, define the foliation. Biotite and muscovite also occur in coarser grained, randomly oriented clusters and are intergrown in places. Quartz occurs as fine-grained matrix material as well as in medium- grained, irregular patches of recrystallized quartz with sutured boundaries.

#### **2.2.3.2. Bt-Ms-Grt bearing Leucogranite**

This pale pink to white leucogranite has variable grain size ranging from medium- to coarse and intrudes the host granitic orthogneiss (Figure 2-15D). The leucogranite appears massive and undeformed with muscovite, minor biotite and pinhead garnet throughout.

In thin section this peraluminous leucogranite contains equal parts of quartz, plagioclase and K-feldspar, totaling 90% of whole rock composition. Muscovite makes up about 7% of the unit, and biotite, chlorite and garnet combined represent 3% of the rock. Medium-grained (<3 mm), anhedral quartz and feldspar with sutured grain boundaries make up the majority of this unit. Quartz also occurs in finer grained recrystallized patches. Coarser, subhedral muscovite laths are seen throughout and are approximately 3 mm in size. Late microshear zones, consisting of finely ground quartz and mica cut across the section, weaving along grain boundaries.

#### **2.2.3.3. Bt-Hbl Intermediate Blocks**

One sample was collected to represent this unit (10AL099), and was taken from a detached block that appeared not to have been displaced since it broke from the outcrop. In the section this unit has a much darker grey to black weathered and fresh surface compared to the surrounding orthogneiss. It is a fine-to medium-grained intermediate gneiss with alternating thin (<1 cm), mafic and felsic layers.

In thin section (Figure 2-15E), the modal proportion of minerals was determined as 30% biotite, 25% amphibole, 20% feldspar, 20% quartz, 5% oxides and <1% each of zircon and apatite. This unit is relatively equigranular, with most grains <0.5 mm in size, with the exception of some biotite laths up to 2 mm in length. Amphibole occurs as pale

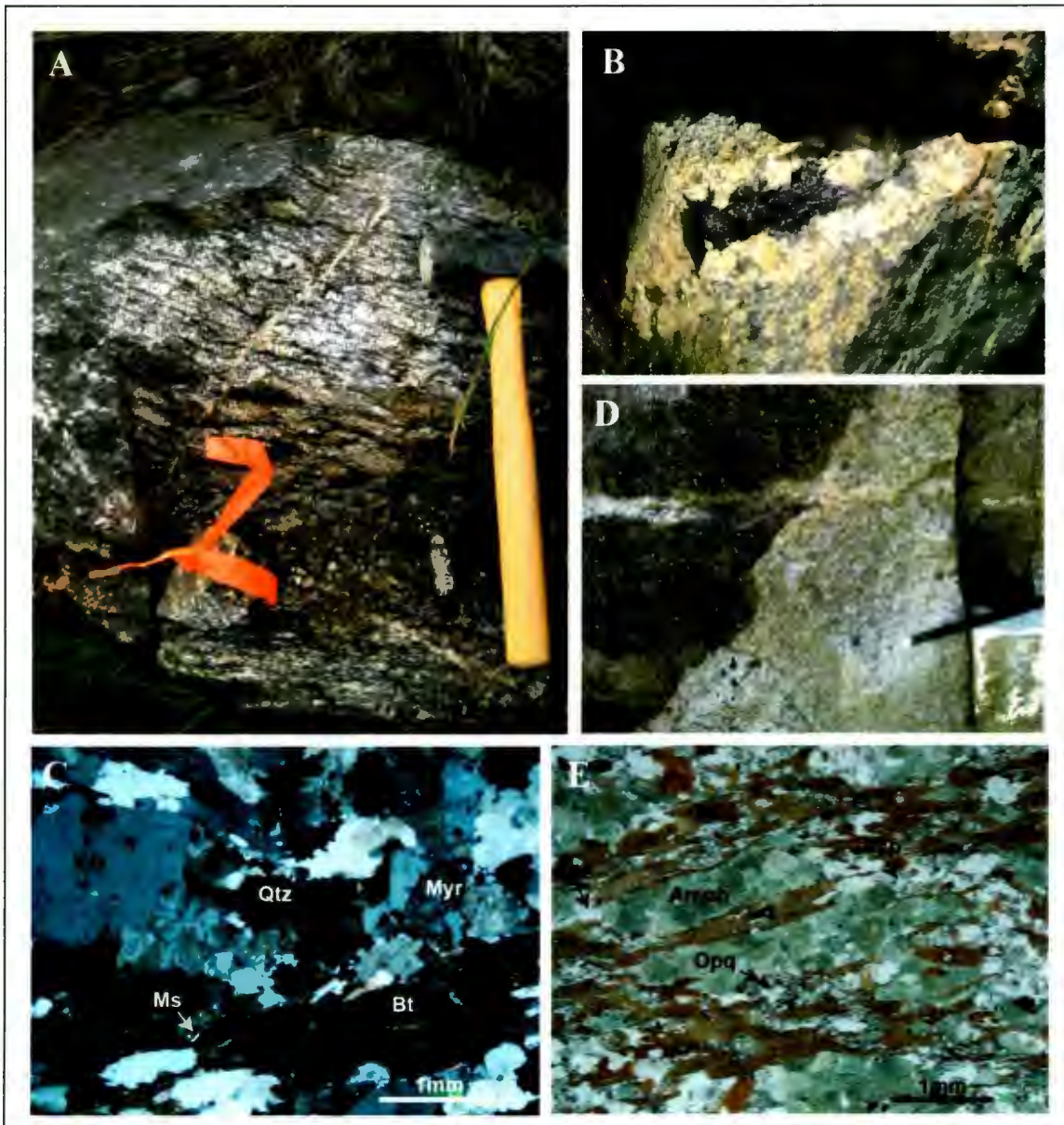


**Figure 2-15: Field photographs and photomicrographs showing the units in the Trinity Road Section. (A) Granitic orthogneiss (B) Tourmaline cluster in a late pegmatitic intrusion. (C) XPL view of the granitic orthogneiss with biotite and minor muscovite showing strong alignment. (D) Leucogranite (right) intruded the orthogneiss (left), where banding of orthogneiss is not apparent due to photo orientation. (E) PPL view of a mafic block with all major minerals strongly aligned.**

green, stubby, subhedral grains with a strongly developed orientation. The amphibole is restricted to polycrystalline layers, up to 1 cm in thickness. Alternating layers rich in quartz, feldspar and biotite are less continuous and vary in thickness; also up to 1 cm. Biotite in this unit is notably orange in color and occurs as elongate, strongly oriented grains. Feldspar grains are highly sericitized, obscuring primary twinning features.

#### **2.2.4. The “I Love You” Road Section (C-C’)**

The “I Love You” (ILY) road section dominantly consists of a homogeneous tonalitic orthogneiss cut by an undeformed tonalite. The tonalite is cut by a large leucogranite intrusion and late pegmatite, aplite and quartz veins are present along the section. Here, contact relationships are clearcut and the three main lithologic units are described in detail.

##### **2.2.4.1. Tonalitic Orthogneiss**

The “I Love You” orthogneiss is fairly homogenous with prominent alternating biotite-muscovite and quartzofeldspathic layers (Figure 2-16A). Fresh surfaces appear black and white, and weathered surfaces range from white-grey to darker orange-brown. Banding occurs on a fine scale with fine-grained mica layers <0.5 cm and quartzofeldspathic layers <1 cm. In comparison to other orthogneiss identified in Hare Bay and Trinity this unit is less granitic with little to no K-feldspar and has a larger mafic

component. The ILY orthogneiss strikes roughly east-west with a shallow dip of 36° northward, and is the oldest unit in the outcrop.

Major mineralogy consists of 35% quartz, 35% plagioclase, 15% biotite, 10% muscovite with minor amounts of chlorite, K-feldspar, myrmekite and oxides (Figure 2-16B). Accessory minerals include monazite, apatite, rutile and zircon, and are present in amounts <1%. Alteration includes both minor chloritization of muscovite and biotite, and moderate to strong sericitization of feldspar. Coarser muscovite grains (~2 mm) appear skeletal and needle-like along grain boundaries, suggesting grains are partially broken down. Muscovite also commonly contains fine-grained oxides along cleavage planes. As is expected because of the identification of both zircon and monazite, biotite has an abundance of pleochroic radiation haloes.

Fine-grained biotite and muscovite-rich layers form semi-continuous, wavy bands approximately 0.5-2 mm thick. The alternating medium grained quartzofeldspathic layers consist of quartz and feldspar grains, ranging from 0.1-4 mm in size with sutured grain boundaries. These bands are slightly thicker than the mica layers and range from 0.5-1 cm thick. Micas are not confined to the fine-grained layers and occur as more randomly oriented subhedral grains within the quartz-feldspar-rich layers.

#### **2.2.4.2. Tonalite**

This undeformed plutonic rock appears white-grey to dark brown-orange on weathered surfaces and exhibits a medium grey fresh surface. This unit possesses unique

corona features, up to 2 cm in size, consisting of tourmaline blades surrounded by a rim of plagioclase grains. Aplite veins cutting the tonalite have a thin (<1 cm), orthoclase-rich layer along the contact (Figure 2-16C). The tonalite has multiple sets of conjugate fractures giving the unit an overall massive blocky appearance. This unit is dominant comprising over 80% of the outcrop and cross-cuts the banding of the orthogneiss on the northern end of the outcrop.

Major mineralogy identified in thin section includes 35-40% plagioclase, 25-30% quartz, 20% biotite and 5% Na-rich amphibole. Titanite, apatite, epidote and oxides occur in minor amounts, between 1-5%. Plagioclase, quartz, biotite and amphibole occur as anhedral grains dispersed evenly throughout, ranging in size from 0.1-2 mm. A prominent feature in this unit is the presence of subhedral titanite oikocrysts approximately 1 mm in size. The titanite grains are subophitic with multiple plagioclase lath inclusions throughout. Several plagioclase grains with excellent lamellar twinning surround the titanite grains, with no evidence of chemical reactions (Figure 2-16D). Prisms of apatite, less than 200  $\mu\text{m}$ , are abundant throughout. Alteration reactions in this unit include mild sericitization of feldspars as well as biotite altering to epidote along grain boundaries. The presence of both biotite and hornblende reflect water availability during crystallization.

### 2.2.4.3 Leucogranite

This massive, medium-grained, leucogranite intrusion has a light pink to white fresh and weathered surface (Figure 2-16E). It cuts the outcrop and is relatively undeformed. The leucogranite contains minor biotite (<5%) that is absent near the boundary with the tonalite, creating a 0.5 cm feldspar-rich contact. This intrusive body has an irregular contact with the surrounding tonalite and is inferred by weathering contrast in inaccessible localities of the outcrop.

The rock is composed of 40% K-feldspar, 22% plagioclase, 20% quartz, 8% muscovite and 6% biotite. Minor and accessory phases include myrmekite, chlorite, epidote and apatite, in amounts totaling <2% of whole rock. Quartz, biotite and muscovite are medium-grained (<0.1-1 mm) and slightly coarser (~2 mm) feldspar grains are seen throughout. Feldspars commonly have significant sericitization of their cores, leaving relatively unaltered rims. K-feldspar grains commonly have irregular grain boundaries and show excellent microcline twins as well as minor exsolution features. Many K-feldspar grains host inclusions of quartz, muscovite and biotite. The mica in this unit is randomly oriented and evenly dispersed throughout the slide. A few clusters of muscovite and biotite intergrowths are present.



**Figure 2-16: Field photographs and photomicrographs showing some characteristic features of units in the “I Love You” Road Section. (A) Tonalitic orthogneiss. (B) XPL view of the tonalitic orthogneiss. (C) Aplite vein with a orthoclase-rich contact with the tonalite. (D) PPL view showing the poikilitic titanite grain surrounded by plagioclase grains in the tonalite unit. (E) Undeformed leucogranite.**

### **2.2.5. North of Cape Freels**

Northwest from the town of Cape Freels a progression of various rock types are encountered. The first outcrops consist largely of the Cape Freels megacrystic granite, this has variable shearing and contains xenoliths and multiple fine-grained sheet-like intrusions throughout. Walking northwestward zones of strongly sheared mylonite becomes prominent and in certain localities ultramylonite is present. Deformation appears to increase continuing along the coast, as the next major identifiable unit is a complexly folded gneiss, mapped as part of the Hare Bay Gneiss complex. Travelling further along the coast several pegmatitic and granitic intrusions cut the gneiss before a large (100's of meters thick) granitic intrusion dominates the coastal exposure. As the Hare Bay Gneiss is the focus of this project the gneissic unit, "the Cape Freels Gneiss", was the target of further sampling and analysis.

#### **2.2.5.1. Cape Freels Gneiss**

This wave-washed, dimpled exposure has an orange-grey weathered surface and a darker grey fresh surface. It is a fine-grained massive unit with an abundance of complexly deformed and folded leucosome layers/lenses (Figure 2-17A and B). The gneiss ranges from leucosome-poor to leucosome-rich (20-70%). Samples were collected from both of these extremes.

On a thin section scale major mineral constituents are generally the same between samples; however the proportion of minerals, grain size and fabrics are heterogeneous.

Major minerals include quartz, feldspar, muscovite, biotite and chlorite with minor and accessory amounts of oxides, epidote, sillimanite, apatite, and zircon. Samples range from strongly foliated (10AL001) to compositionally banded (10AL002 and 10AL093). In banded samples, layers of quartz and feldspar alternate with layers composed of quartz, feldspar, biotite, chlorite, muscovite and oxides (Figure 2-17C). The continuous quartzofeldspathic layers have sutured grain boundaries with several turbid patches throughout (Figure 2-17D). These layers appear with uniform thickness of approximately 2 mm. In contrast, the mica-bearing layers are thicker (up to 2 cm) and mica shows a strong alignment. Banding is absent in sample 10AL001, from a more leucosome-rich section of the gneissic unit (Figure 2-17E and F). Muscovite is predominant, composing approximately 45% of this section. It is present as fine-grained, strongly aligned masses as well as coarser subhedral, cross-cutting flakes. Quartz and feldspar again appear recrystallized but are randomly distributed throughout the section sometimes forming irregularly shaped aggregates as well as isolated anhedral grains.

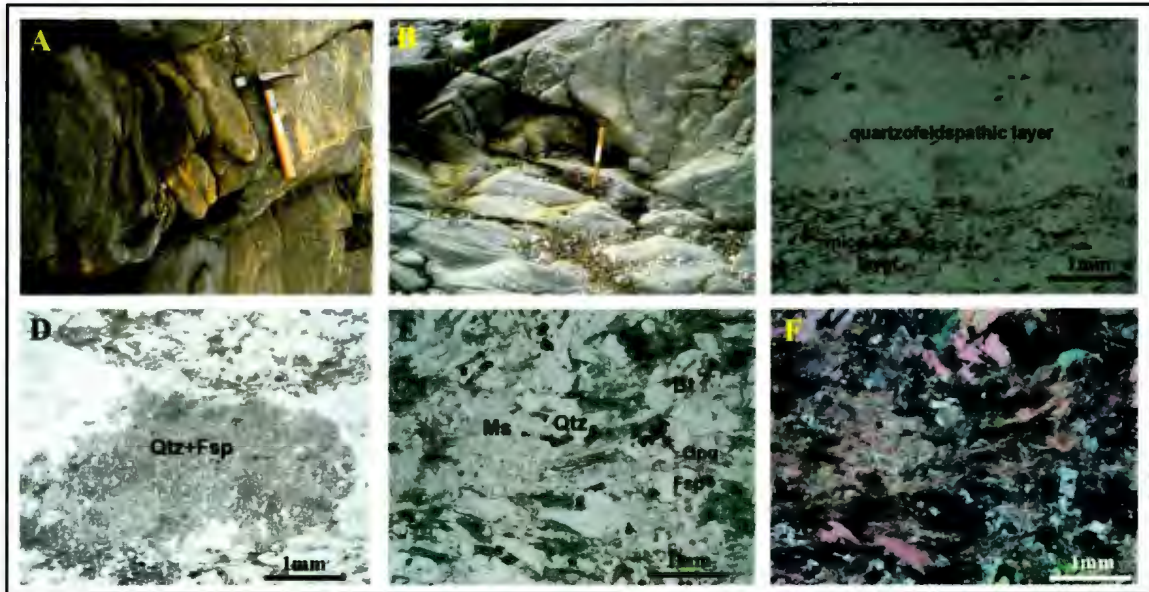


**Figure 2-17: Field photographs and photomicrographs showing the Cape Freels Gneiss. (A) the complex, folded leucosome in a fine-grained, grey, massive unit. (B) the location of sample 10AL093 of the gneiss. (C) PPL view showing contrasting layer compositions in sample 10AL093. (D) A turbid patch within the quartzofeldspathic layer, in PPL. (E) PPL view of sample 10AL001 from more massive section of the gneiss. (F) same view in XPL.**

### 2.2.6. Valleyfield Road

Traversing Valleyfield road allows the recognition of several different rock types, belonging to the Hare Bay Gneiss Complex. The dominant unit is a homogeneous, two-mica granitic orthogneiss (Figure 2-18A). The composition of this unit appears fairly consistent for several hundred meters across strike along the road with only slight variations in mineralogy. Locally, late phases of leucogranitic intrusions as well as pegmatite were observed cutting the orthogneiss. Another notable unit identified is a granitic mylonite with well developed, augen-shaped feldspar grains. The exposure was

limited and only a few 10's of meters in size and contacts with the orthogneiss were not observed. The last noteworthy unit was located along the coast across the road from Mercer's Marine Equipment store. Here a complexly folded and deformed paragneiss contrasts with the surrounding lithologies (Figure 2-19A). Again the extent of this unit and the nature of contact with the orthogneiss is difficult to infer due to cover (lichen, shrubs, ocean, grass, etc.) and accessibility (private property, cliff-sides, etc.). The surficial limit of the Valleyfield orthogneiss is found near the Blue Mist Motel where sheared megacrystic granite becomes predominant.

#### **2.2.6.1. Valleyfield Orthogneiss**

In thin section this unit is granitic with major phases including quartz, plagioclase, K-feldspar, biotite, chlorite and muscovite. Less abundant, secondary and accessory phases include oxides, epidote, zircon, apatite, monazite and myrmekite. Average grain size is 0.5-2 mm with some fine-grained, sheared and recrystallized patches throughout.

Discontinuous to semi-continuous, anastomosing, biotite-rich layers, less than 0.5 mm thick, outline augen-shaped patches of feldspar and quartz (Figure 2-18B and C). In some sections, quartz and feldspar have irregular sutured boundaries (i.e. 10AL077), whereas in others quartz occurs as equant grains with clearcut grain boundaries (i.e. 10AL006). Intergrown biotite and muscovite have significant oxides and alteration along their cleavage planes (Figure 2-18D). Elongate grains of quartz are also present along

mica cleavage planes. Plagioclase and K-feldspar show minor to significant sericitization and are slightly coarser (up to 4 mm) than surrounding grains.



**Figure 2-18: Field photographs and photomicrographs of the Valleyfield orthogneiss. (A) Regularly banded orthogneiss with alternating leucosome and melanosome layers from the roadside outcrop in Valleyfield. (B) and (C) PPL view showing thin, wispy layers of biotite, chlorite and muscovite, wavy around lenticular patches of feldspar and quartz. (D) Complex intergrowth of biotite and muscovite.**

### **2.2.6.2. Valleyfield Paragneiss**

Multiple distinct samples were collected for petrographic analysis representing different degrees of migmatization within the paragneiss unit. Sample 10AL008 was collected from the most massive, relatively undeformed component. Sample 10AL007 showed a moderate degree of migmatization and sample 10AL076 represents the most significantly deformed, leucosome-rich portion of this unit.

Sample 10AL008 is fairly equigranular with grain size averaging about 0.5 mm. Major minerals identified include quartz, plagioclase, K-feldspar, biotite and muscovite. Minor amounts of oxides epidote, chlorite and a few zircon grains are also present. Sericitization of feldspar ranges from moderate to significant, making it difficult to determine type and proportion. Quartz is present as equant grains, and quartz and feldspar frequently show triple junction grain boundaries. This sample lacks foliation and mineral components are distributed somewhat evenly (Figure 2-19B and C).

Sample 10AL007 is similar to 10AL008 in mineral composition. Micas are seen in a greater proportion and the combined percentage of biotite and muscovite almost doubles, making up 20% of this sample. Very minor (<1%) sillimanite is present as fine-grained bundles of acicular grains. On average grain size ranges between 0.25-2 mm. Mica defines the foliation in this unit occurring as wavy, discontinuous layers, less than 1 mm thick (Figure 2-19D and E). Coarser muscovite grains, up to 2 mm in size appear skeletal. Quartz occurs in irregularly shaped recrystallized patches with coarser feldspar (up to 2 mm) throughout.

Sample 10AL076 has distinct layers (Figure 2-20A and B). Muscovite is seen as a major phase comprising up to 35% of the rock. Additional aluminous phases such as garnet and sillimanite are seen in abundances up to 5%. Here distinct bands (~1 cm thick) alternate in composition between quartzofeldspathic and aluminous, muscovite, biotite and garnet-rich layers. In the quartzofeldspathic layers quartz, feldspar and a network of fine-grained mica separate lenticular patches of recrystallized quartz with sutured grain boundaries. Alumina-rich layers have complex grain orientations, commonly exhibiting micro-folding. Sillimanite occurs as fine-grained needles in muscovite grains and record deformation through wavy alignment of grains (Figure 2-20C). Garnet occurs as sub-euhedral grains up to 300  $\mu\text{m}$  in size and is generally confined to the aluminous layers (Figure 2-20D).

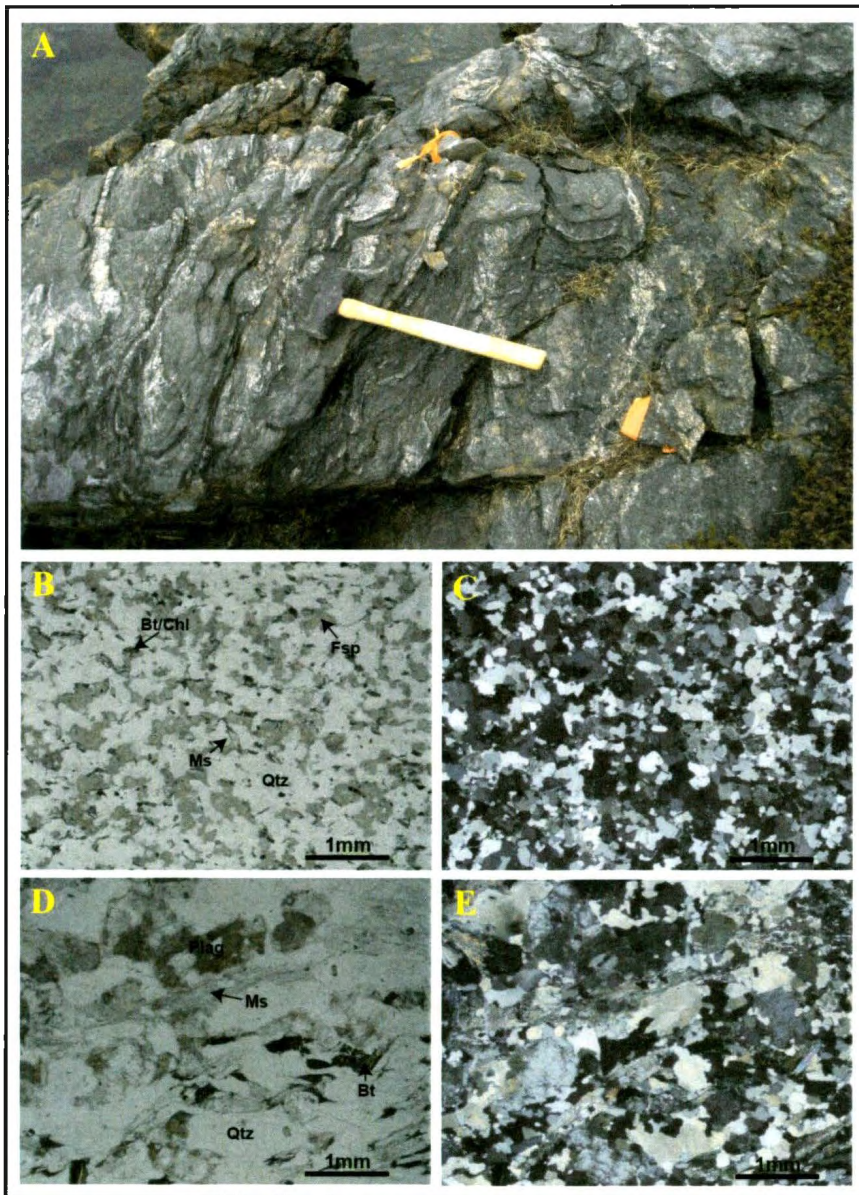


**Figure 2-19: Field photo and photomicrographs depicting the Valleyfield paragneiss. (A) Complexly folded and deformed leucosomes in a fine-grained, more massive appearing rock. (B) and (C) show sample 10AL008 of a relatively undeformed, massive section of this unit in PPL and XPL, respectively. This unit appears fairly equigranular, dominantly consisting of quartz and feldspar with minor mica. (D) and (E) shows sample 10AL007 from a section of moderate migmatization in PPL and XPL, respectively. Here micas become a more major phase and their alignment defines a strong foliation. It is also notable that the muscovite appears in needle-like or skeletal form.**

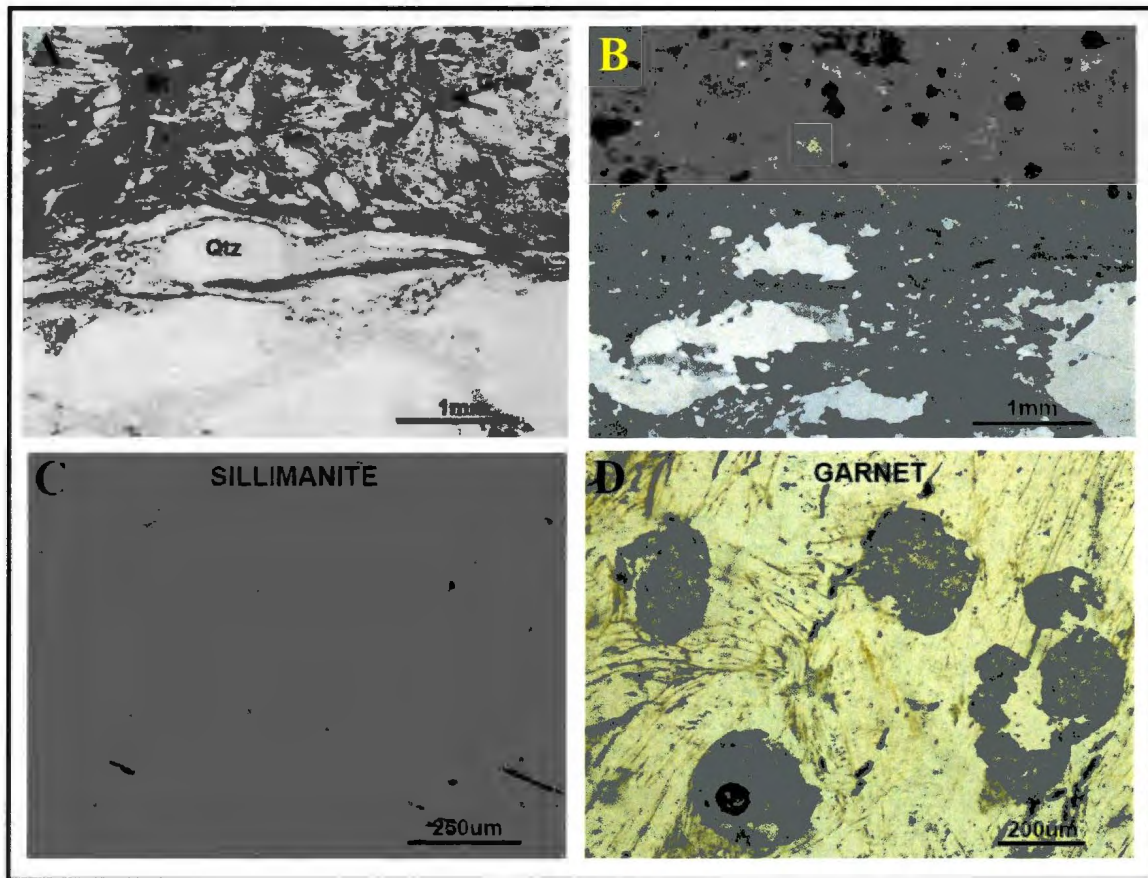


**Figure 2-20: Photomicrographs showing sample 10AL076 of a highly migmatized and deformed section of the Valleyfield paragneiss. (A) A PPL view of the boundary between a mica-rich, aluminous layer (top) and a quartz rich layer (bottom). In the aluminous layers pinhead garnet and large flakes (up to 2 mm) of biotite and muscovite are the dominant components. The micas show a complex alignment, sometimes appearing random and other times define intricate micro-folding and deformation. The quartz-rich layers show lenticular patches of recrystallized quartz separated by a finely ground network of quartz and mica. (B) the same view in XPL. (C) Fine sillimanite needles record deformation through folding and crenulations. (D) pinhead garnet up to 250  $\mu\text{m}$ .**

### 2.2.6.3. Valleyfield Mylonite

The Valleyfield mylonite is a highly deformed granite with augen-shaped aggregates of quartz and feldspar separated by finely ground shear zones containing quartz, muscovite and biotite (Figure 2-21). Coarse feldspars commonly exhibit multiple fractures that are filled with fine-grained quartz. A small number of coarse lenticular muscovite grains (<2 mm) with kinked and folded cleavage were also identified.

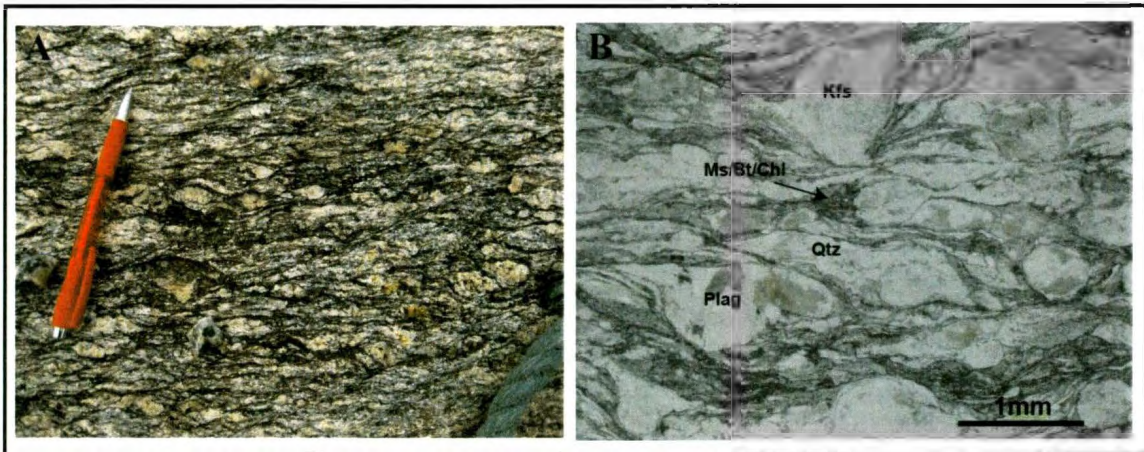


**Figure 2-21: Field photograph and photomicrograph showing the Valleyfield mylonite. (A) Feldspar augen strung out in a fine-grained matrix of biotite and chlorite. (B) PPL view of a mylonite taken across the road from the location of the field photo. This mylonite is finer grained than the unit shown in the previous photo with lenses of quartz and feldspar.**

### 2.2.7. Town of Hare Bay

Limited outcrop exposure as well as lichen cover and staining made proper examination of many of the visited outcrops difficult and therefore, only one outcrop at the north end of Hare Bay was sampled. This outcrop was tall standing with significant

lichen coverage and water staining giving a dark brown to black weathered surface (Figure 2-22A). Fresh surfaces showed a pink/white and black well-banded two-mica granitic orthogneiss (Figure 2-22B).

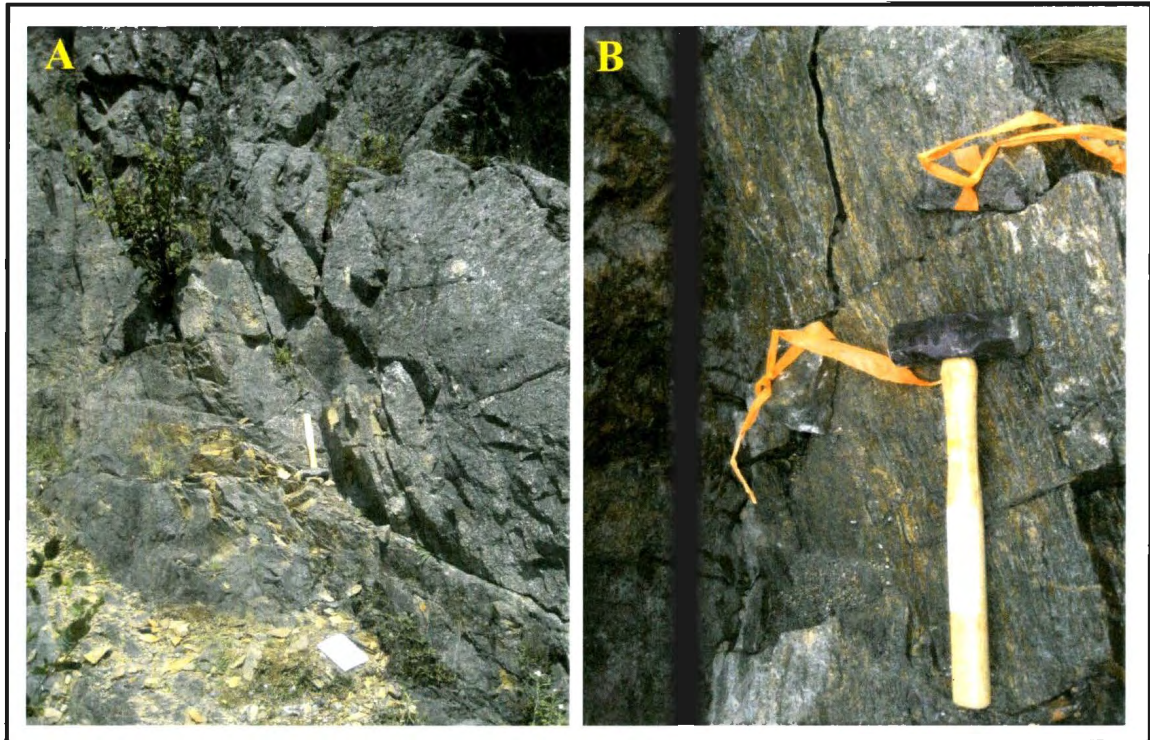


**Figure 2-22: Field photographs showing the Hare Bay orthogneiss. (A) The roadside outcrop from which the geochron sample (10AL094) of this unit was collected. Lichen on the surface obscures any features of this unit. (B) shows a less weathered surface of the same outcrop. Here leucosome and melanosome layers are evident.**

Petrographic examination reveals this unit is variable in composition ranging from granitic to granodioritic. Major mineral phases include quartz, plagioclase, K-feldspar, biotite, muscovite and chlorite. Minor and accessory phases include apatite, zircon, epidote, myrmekite and oxides, generally totaling less than 5% of the rock.

Plagioclase is more abundant than K-feldspar, but strong sericitization makes exact amounts difficult to estimate. Feldspars are generally slightly coarser than surrounding minerals and are up to 4 mm in size. Biotite with variable chloritization is more abundant than muscovite and generally constitutes less than 15%. Coarse muscovite grains are partially broken down appearing skeletal or need-like along grain boundaries. Biotite, chlorite, muscovite and oxides are commonly, but not exclusively, found in thin, semi-continuous layers, less than 0.5 mm thick (Figure 2-23A and B). Clusters of these minerals up to 8 mm in diameter are present, yet less common (Figure 2-23C and D). Grain orientations in these clusters vary from strongly aligned with the general fabric to randomly oriented. Some individual mica grains have kinked cleavage planes recording internal deformation. Patches of fine-grained (~0.1 mm) equant quartz grains are common. In these recrystallized patches, triple junction grain boundaries are commonly observed.

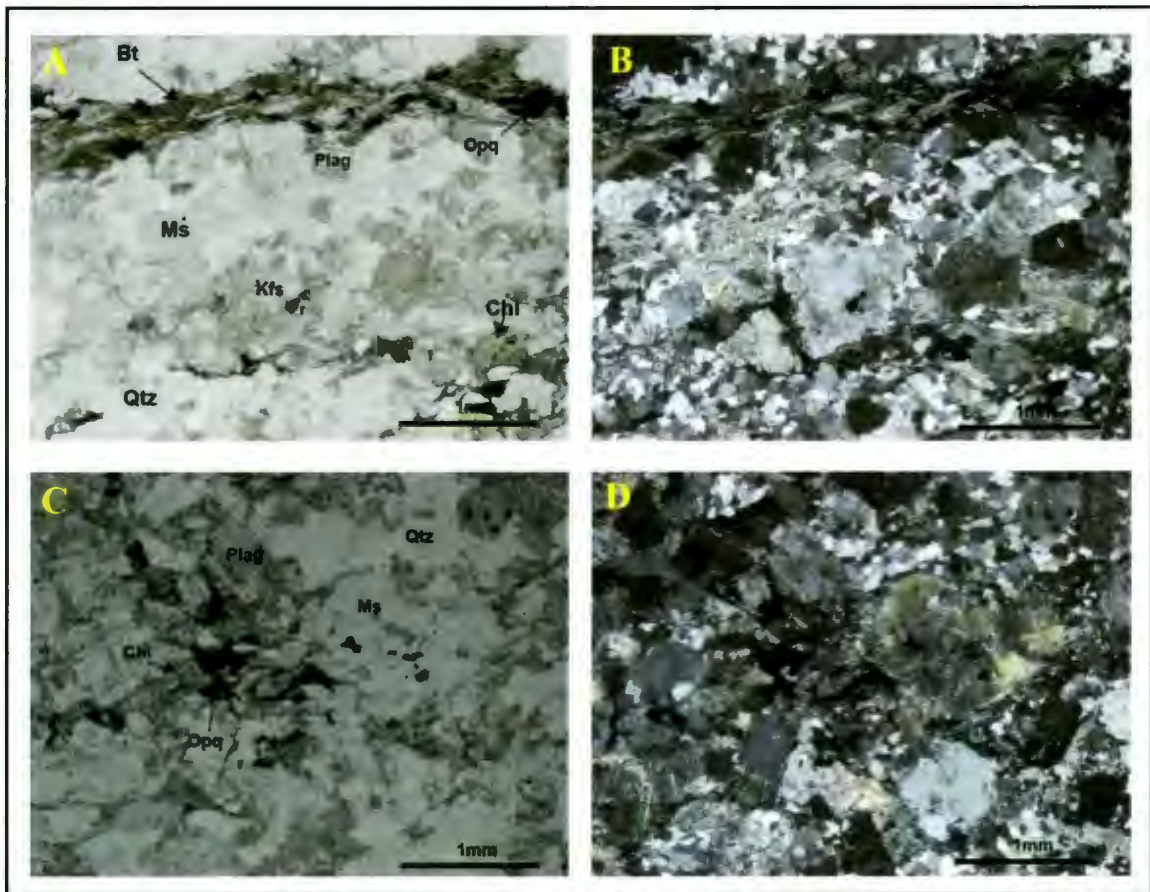


**Figure 2-23: Photomicrographs of the Hare Bay orthogneiss. (A) and (C) show PPL views of the orthogneiss. (A) shows a band rich in biotite and oxides running across the section. (C) shows a more randomly oriented cluster of biotite and oxides. In both views large muscovite flakes (up to ~1.5 mm) are visible. (B) and (D) show XPL of the same views in (A) and (C), respectively. Here grain boundaries and twinning features in feldspar are obvious.**

### 2.3 Interpretation/Summary of Field and Petrographic Observations

Field observations and petrographic analysis provide the primary means for identifying and correlating rock units between the studied geographic localities. Although it is possible to make lithologic and event correlations within a single outcrop it is

difficult to project these correlations to geographic locations several 10's of km away. Based on field observation, the Hare Bay Gneiss is heterogeneous on a large-scale although both similar and contrasting rock units have been identified within and between localities. It is clear that components of Hare Bay Gneiss represent multiple phases of magmatism and deformation, however, correlations between outcrop areas are not obvious. Below some general conclusions are made for each locality and the remaining ambiguity is highlighted.

The units mapped in the WMB map area appear as multiple sheet intrusions that have undergone varying degrees of deformation. The units have evidence of greenschist facies metamorphism commonly having both chlorite and epidote alteration. The oldest units are inferred to be the foliated leucogranite and the sheared megacrystic granite. The nature of the contact between the two units is typically unclear as shearing and contradictory evidence for timing of the intrusions prevents any conclusive relationship from being determined. Also, it cannot be discounted that each separate, but lithologically similar, granitic sheet may not correlate in time with a single intrusive event. These two units are clearly cross-cut by the granodiorite as well as the tonalitic dyke. Pegmatite is observed cutting most of the main lithologic units in the map area and these intrusions are commonly oriented oblique to the main foliation and the orientation of surrounding units. Quartz veins are locally observed cutting across pegmatite intrusions, showing that, at least in some instances, they are the youngest unit of the map area. Mafic units on the western side of the map area are interpreted to represent a later phase of intrusion; however the exact timing remains unclear. Locally they are observed fingering into the

early granite sheets but most contacts are faulted or sheared and contact with later units (granodiorite, pegmatite, quartz veins) is limited or nonexistent. Overall it is obvious that multiple phases of intrusion with variable compositions formed this rock assemblage yet the exact timing between events remains unknown.

The Greenspond Road Section appears different from other outcrops of the Hare Bay Gneiss. The presence of Al-silicates as well as tonalitic enclaves sets it apart from the other orthogneiss units observed. The Al-silicates do not appear to be a function of metamorphic grade of the entire rock unit as they are contained in Al-rich clusters, rather than more evenly throughout. The shape of the clusters suggests they may be replacing earlier grains, possibly feldspar. Al-silicate formation appears to be a function of composition and magmatic temperatures rather than later fluid related reactions. The greenschist grade of the unit is indicated by chlorite replacing micas throughout. Many of the contacts observed in this section are gradational, however it is clear that the foliated leucogranite cuts the Al-silicate-bearing orthogneiss near the middle of the section. Late pegmatite and undeformed granite intrusions represent the latest phases of magmatism having cut all other units. A potential source for the late undeformed granitic intrusions has been interpreted to be the young Newport granite, which outcrops several hundred meters east along the road. The granitic orthogneiss observed in the Greenspond section is petrologically unique in comparison with all other orthogneiss observed in this study.

The Cape Freels Gneiss contains at least two distinct types of muscovite. Minor sillimanite indicates high grade metamorphism and the chloritization of muscovite is retrograde. In the field, the Cape Freels Gneiss bears a similar appearance to the

Valleyfield Paragneiss, as both appear as highly deformed rock packages with multiple complexly folded leucosome throughout. However, whereas the protolith of the Cape Freels Gneiss remains unclear, the Valleyfield Paragneiss appears to have a sedimentary origin. The Valleyfield Paragneiss also shows sillimanite grade metamorphism with retrograde chlorite and epidote alteration. Both units are potentially paragneiss, having undefined relationships with surrounding units.

Both the Trinity and "I Love You" sections, and outcrops in Valleyfield and Hare Bay contain orthogneiss units. The orthogneiss are granitic to granodioritic in composition and are Al-rich, containing both muscovite and biotite, although muscovite is typically very minor. Greenschist grade metamorphism is evident throughout as chlorite and epidote replacement. Biotite and muscovite commonly occur as two distinct morphologies including fine-grained aligned laths and coarse subhedral cross-cutting flakes. In most sections biotite and muscovite occur in intergrown clusters indicating they crystallized concurrently from a peraluminous melt. Mica, specifically muscovite occurs as partially broken down needle-like or skeletal grains. The presence of late fluids is evident through alteration and oxide formation along mica cleavage planes. Based on field and petrological examination, no clear indication of the age relationships between these separate orthogneiss units is observable.

Nearly all of the granitic orthogneiss units are cut by later leucogranite intrusions, with the exception of the Hare Bay outcrop where leucogranite was not identified. Overall the composition of these leucogranite units are homogeneous, but some minor phases such as garnet in the Trinity section and slight variation in major mineral proportions are

recorded. The leucogranite in all outcrops is peraluminous containing both biotite and muscovite. Igneous garnet occurs in some localities, reflecting high alumina content of the melt. Feldspar grains are typically anhedral and coarser than surrounding minerals indicating early crystallization. In all cases leucogranite units with a similar composition postdate orthogneissic rocks however, the timing of these magmatic events with respect to those observed in other study areas cannot be inferred.

### 3. CHAPTER 3: GEOCHEMICAL ANALYSIS

#### 3.1 Preparation

Forty-eight samples from the various study locations were selected for major and trace element geochemical analysis. Table A-1 in appendix A provides a summary of the distribution of samples collected for geochemical analysis from each locality. A detailed description of sample processing and analytical techniques is found in appendix C. All forty eight samples were submitted for XRF-pressed pellet and ICP-MS trace element analysis at Memorial University. Additional XRF-fusion analysis was carried out at Actlabs to acquire higher quality major element data.

Several steps were taken to convert raw geochemical data provided by the analytical facilities into a more useful format, prior to plotting and interpretation. First values lower than the detection including erroneous negative values were omitted. Since raw data does not differentiate between ferrous and ferric Fe, laboratory values are converted from  $\text{Fe}_2\text{O}_3$  to  $\text{FeO}^*$ , where  $\text{FeO}^*$  is the total Fe as FeO. This is done using the equation  $\text{FeO}^* = (\text{Fe}_2\text{O}_3)(0.8998)$ . Each analysis was then recalculated volatile-free, to a total of 100% by multiplying laboratory values of both major and trace elements by a recalculation factor  $(100/(100-\text{LOI}))$ .

A comparison was made between elements that were determined using both XRF and ICP-MS techniques. First, results from light rare earth elements (LREE), Ba, Rb and Sr are compared. When compared, the elemental values had acceptable variation. Next, Nb, Y and Zr values from both analytical techniques are compared. When XRF and ICP-MS data agreed within acceptable error an average value is used. When technique results did not agree XRF

(solid state) data is used, as possible incomplete dissolution of accessory minerals rich in Nb, Y or Zr may be an issue with ICP-MS analysis.

### 3.2 Data Analysis

Below, geochemical signatures of rock types selected for analysis are described and interpreted. They are presented based on their geographic locations and the lithology previously defined in Chapter 2. Select diagrams are used to display geochemical trends for each lithologic unit. They include a QAP plot based on normalized modal mineralogy percentages observed in thin section. QAP diagrams are mainly presented for deformed igneous plutonic rocks rather than gneisses, therefore this plot is absent from the analysis of several units. Shand's index is used to classify the units based on the ratio of alkalis to alumina. The fields shown in this plot include peralkaline, peraluminous and metaluminous, defined based on the molar alkali-alumina ratio, called the peralkalinity index. Trace elements patterns are shown through an XY plot of  $(La/Sm)_N$  against  $(Gd/Yb)_N$ , that effectively compares the slope of the LREE and heavy rare earth elements (HREE), where the N subscript denotes normalization to the primitive mantle values of Sun & McDonough (1989). Like the complementing multi-element rare earth element (REE) plots, these values are normalized to primitive mantle values. Finally, primitive mantle normalized extended REE diagrams are used to show patterns in the trace element concentration of the samples.

Mafic units are present as minor intrusions or inclusions at several of the studied localities. These units are plotted on the Pearce (1996) revision of Winchester and Floyd's

(1977) plot with Nb/Y on the x-axis against Zr/TiO<sub>2</sub> on the y-axis, and an extended REE diagram is used to define chemical signatures of these mafic units.

The Valleyfield paragneiss is the only unit that was confidently identified as a metasedimentary rock that was also selected for geochemical analysis. The geochemical data was used to plot trace element concentrations on a REE diagram normalized to average upper continental crust after Taylor and McLennan (1985).

### **3.2.1 Windmill Bight Map Area**

Below, the lithologic divisions of the WMB map area are simplified and the geochemical trends of the foliated leucogranite (with and without layers), megacrystic granite (sheared and highly sheared), foliated granodiorite, tonalitic dyke, pegmatite and mafic intrusions are described.

#### **3.2.1.1. WMB Foliated Leucogranite**

Foliated leucogranite samples include those from the foliated leucogranite unit with layers, as well as the unit without. Three representative thin sections with little to no seritization of feldspars were plotted on the QAP diagram (Figure 3-1A). Samples plot in the granite field, in the normative classification, with modest variation in the proportion of the three defining phases. Based on Shand's peralkalinity index, samples are in the peraluminous field with Al/(Na+K) ratios between 1.1 and 1.4, and Al/(Ca+Na +K) ratios between 1.1 and 1.3 (Figure 3-1B).

The XY trace element plot comparing the slope of LREE and HREE shows variation with LREE slopes ( $(La/Sm)_N$ ) between 2.5 and 4.5, and HREE slopes ( $(Gd/Yb)_N$ ) ranging from flat with values of 1, to more steeply inclined with values near 3.5 (Figure 3-1C). These variations in slope are again evident in the extended REE diagram (Figure 3-1D). The geochemical trends of all samples are similar with the LREEs enriched relative to the HREE and prominent negative Nb, Eu and Ti anomalies. LREE enrichment appears variable between samples whereas the concentration of HREEs is more consistent, as the data points for HREE are tightly clustered.

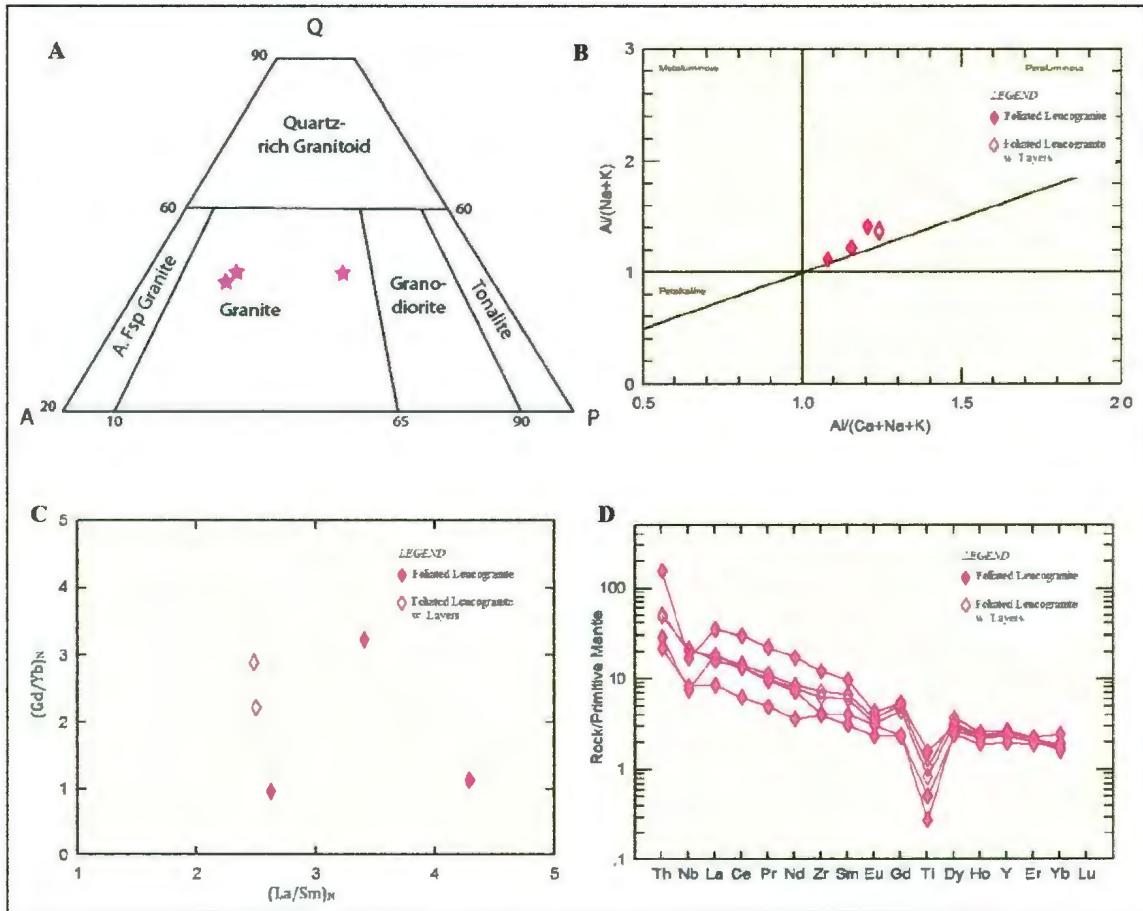


**Figure 3-1: Modal and geochemical plots for the foliated granite of WMB map area. Samples are plotted on (A) a QAP diagram based on normalized modal proportions observed in thin section, (B) Shand's (1927) diagram with fields defined by Al saturation indices, (C) a La/Sm vs. Gd/Yb plot, normalized to primitive mantle, and showing slope of the LREE and HREE, respectively and (D) an extended REE diagram normalized to primitive mantle.**

### 3.2.1.2. WMB Megacrystic Granite

Three representative samples of megacrystic granite were selected to plot on the QAP diagram (Figure 3-2A). Samples plot in the granitic field, near the quartz-rich limit, and show variable alkali feldspar and plagioclase content. Based on Shand's index samples are classified as peraluminous with  $Al/(Na+K)$  ratios between 1.4 and 1.8 and  $Al/(Ca+Na+K)$  ratios between 1.1 and 1.3 (Figure 3-2B).

LREE and HREE slopes are fairly consistent between samples with LREE slope values from 3 to 4, and less steep HREE slopes between 1.5 and 3 (Figure 3-2C). The extended REE plot (Figure 3-2D) shows significant data overlap and LREE are again enriched relative to HREE, with prominent Nb and Ti anomalies. Whereas the concentrations of the LREE show some variation, the HREE show more variable degrees of enrichment.

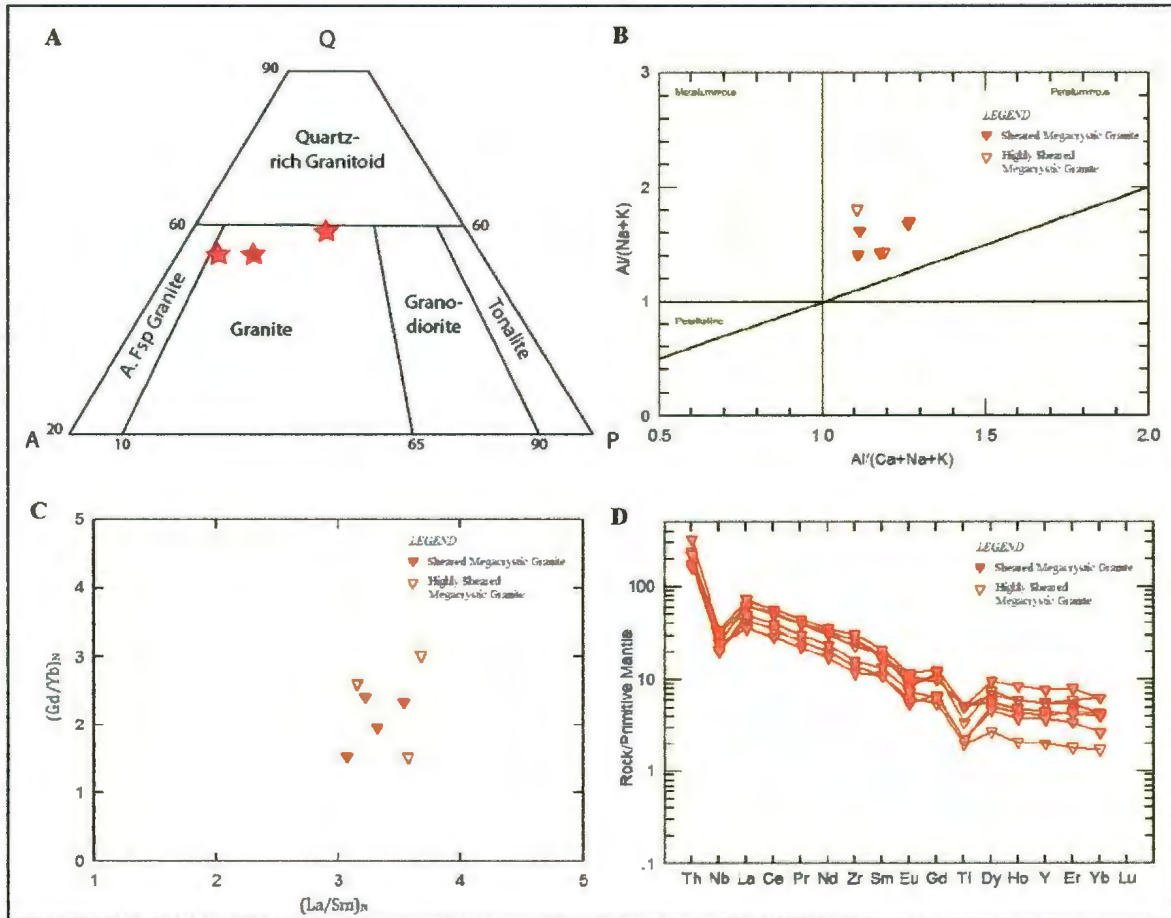


**Figure 3-2: Modal and geochemical plots for the megacrystic granite of WMB map area. Samples are plotted on (A) a QAP diagram based on normalized modal proportions observed in thin section, (B) Shand's (1927) diagram with fields defined by Al saturation indices, (C) an XY plot of trace element ratios La/Sm vs. Gd/Yb, normalized to primitive mantle, and showing slope of the LREE and HREE, respectively and (D) an extended REE diagram normalized to primitive mantle.**

### 3.2.1.3. WMB Foliated Granodiorite and Tonalitic Dyke

Rocks of intermediate composition including the foliated granodiorite and tonalitic dyke of WMB map area, are shown together in modal and geochemical diagrams. Three representative samples of granodiorite and one sample of tonalite are plotted in the QAP diagram. The granodiorite samples plot near the quartz-rich end of the granodiorite field (Figure 3-3A). The sample of the tonalitic dyke contains minor amounts of alkali feldspar and plots near the middle of the tonalite field. Classification based on Shand's index shows that the samples are peraluminous, although one granodiorite sample plots close to the border between peraluminous and metaluminous fields with  $Al/(Ca+Na+K)$  at approximately 1.0 to 1.1. The tonalitic sample has a higher  $Al/(Ca+Na+K)$  ratio of 1.3 and both the granodiorite and the dyke have similar  $Al/(Na+K)$  ratios between 1.6 and 1.7 (Figure 3-3B).

The slopes of the LREE patterns vary from 3 to 4.5, whereas the HREE slopes are more consistent at about 1.5 to 2 (Figure 3-3C). The extended REE plot (Figure 3-3D) shows enrichment of LREE relative to HREE, and the patterns for all samples are tightly clustered. Samples have negative Nb anomalies, with the exception of one granodiorite sample, and positive weak to distinct Zr anomalies (Figure 3-3D).

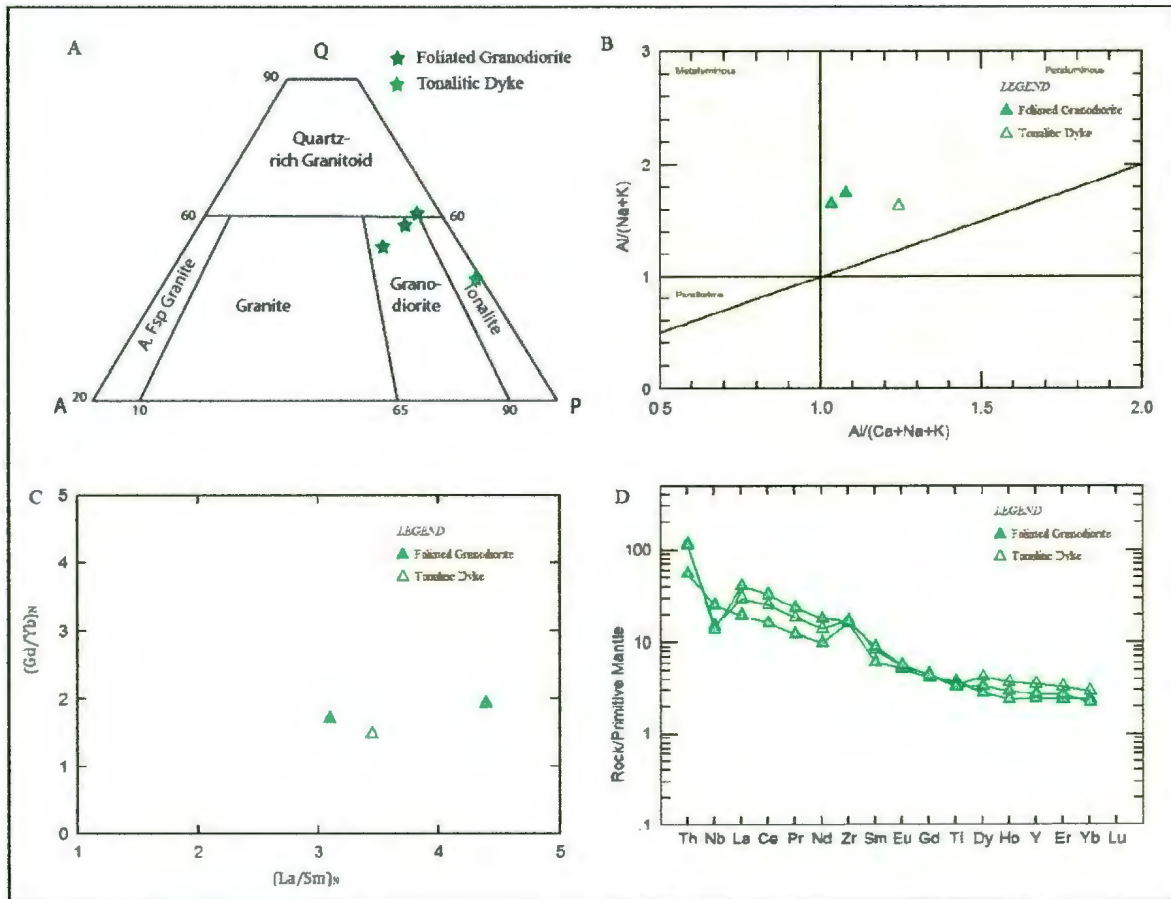


**Figure 3-3: Modal and geochemical plots for the granodiorite and tonalitic dyke of WMB map area. Samples are plotted on (A) a QAP diagram based on normalized modal proportions observed in thin section, (B) Shand's (1927) diagram with fields defined by Al saturation indices, (C) an XY plot of trace element ratios La/Sm vs. Gd/Yb, normalized to primitive mantle, and showing slope of the LREE and HREE, respectively and (D) an extended REE diagram normalized to primitive mantle.**

#### 3.2.1.4 WMB Pegmatite Intrusions

Two samples of pegmatite from WMB map area are plotted on the QAP for normative classification. Samples plot in the granitic field corroborating field observations (Figure 3-4A). It should be noted, however, that the coarse grain size of the pegmatite intrusions allows significant modal proportion variation between thin sections and only a rough estimate can be made.

Pegmatite intrusions are classified as peraluminous based on Shand's index with  $Al/(Na+K)$  and  $Al/(Ca+Na+K)$  values at approximately 1.1 (Figure 3-4B).

Samples have a LREE slope of 1.8 and 2.6 and both have HREE slopes less than 1 (Figure 3-4C). The extended REE plot shows a concave-up pattern with negative Eu and Ti anomalies and positive Nb and Zr anomalies, perhaps reflecting accessory mineral removal or accumulation (Figure 3-4D). Trace element trends of the pegmatite intrusions are unusual which may be a function of the pegmatite forming from late residual melts and/or late fluids redistributing elemental components

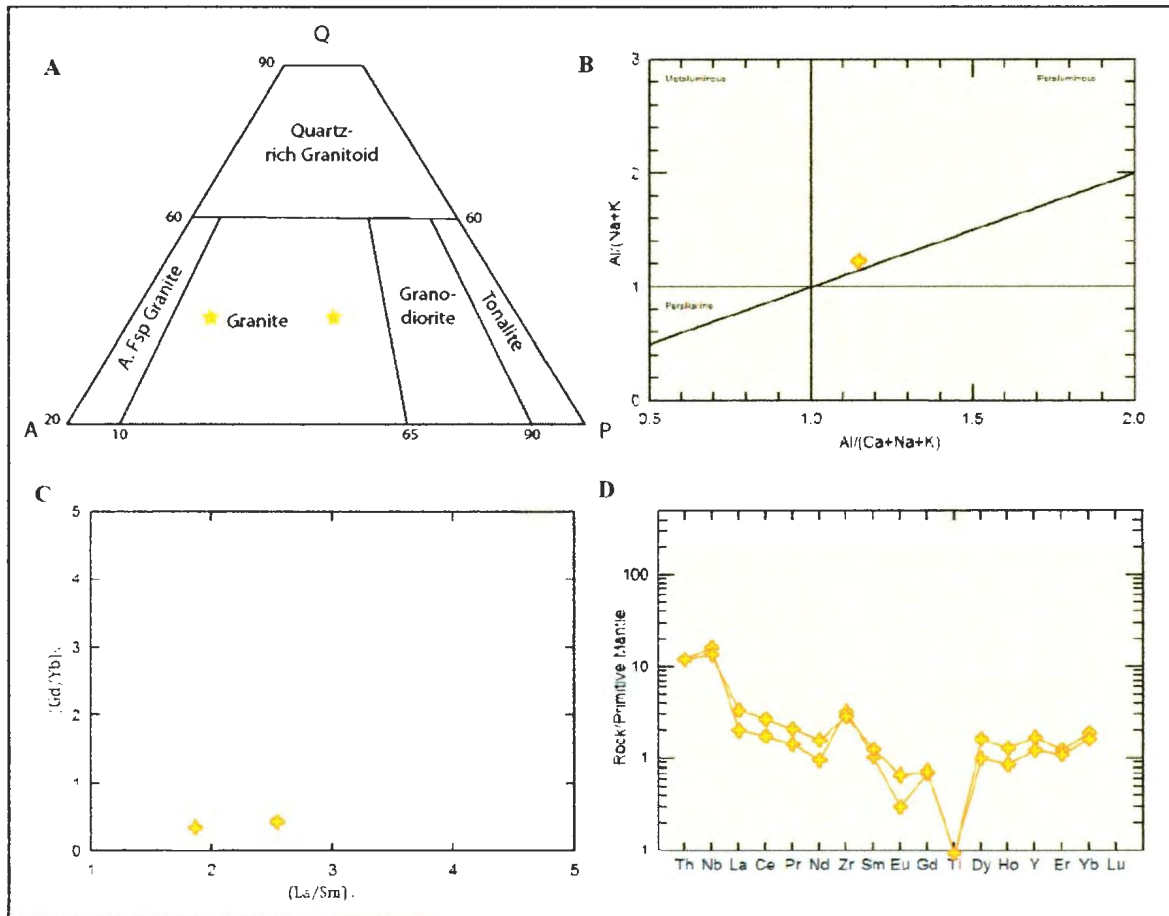


**Figure 3-4: Modal and geochemical plots for the pegmatite intrusions of WMB map area. Samples are plotted on (A) a QAP diagram based on normalized modal proportions observed in thin section, (B) Shand's (1927) diagram with fields defined by Al saturation indices, (C) an XY plot of trace element ratios La/Sm vs. Gd/Yb, normalized to primitive mantle, and showing slope of the LREE and HREE, respectively and (D) an extended REE diagram normalized to primitive mantle.**

### 3.2.1.5. WMB Mafic Units

Samples of both the biotite-carbonate and actinolite-biotite bearing mafic units from WMB map area were selected for geochemical analysis. On the revised Winchester and Floyd plot (Figure 3-5A) the biotite-carbonate-bearing mafic unit plots in the basalt field and the actinolite-biotite bearing mafic unit plots in the alkali basalt field.

The trace element trend for the biotite-carbonate bearing mafic unit is relatively flat with a slight enrichment of LREE relative to HREE and a modest negative Nb anomaly is also present. The actinolite-biotite bearing mafic unit is significantly enriched in the LREE relative to the HREE. The sample has a steep trace element slope and a prominent negative Nb anomaly (Figure 3-5B).

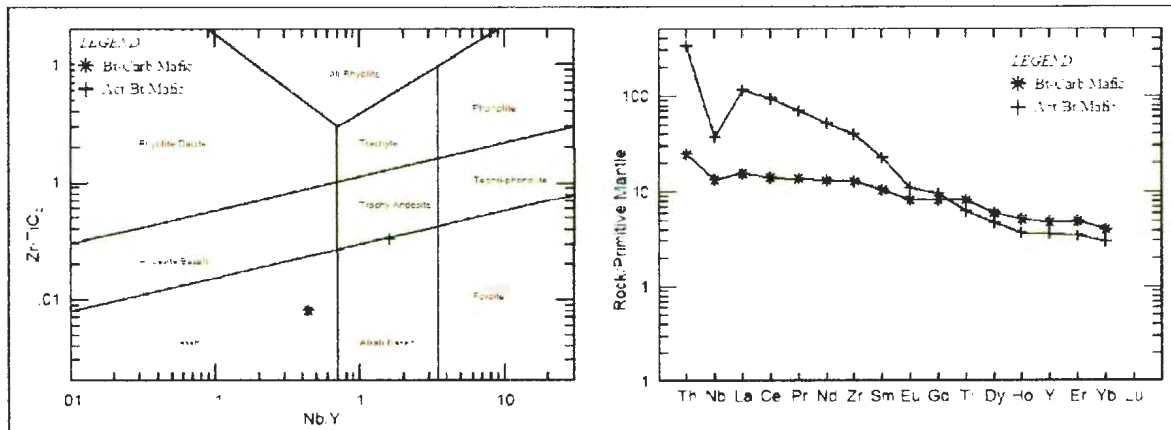


**Figure 3-5: Geochemical plots for the mafic units of WMB map area. Samples are plotted on a revised Winchester and Floyd diagram from Pearce (1996,) on the left, and an extended REE diagram normalized to primitive mantle, on the right.**

### **3.2.2. The Greenspond Road Section**

Samples of the Al-silicate-bearing orthogneiss, Bt-Ms-Sil-bearing granitic orthogneiss, foliated two-mica leucogranite and the tonalitic enclave were analysed. The most densely sampled unit was the Al-silicate orthogneiss, therefore, data collected for this unit is presented separately from the other units.

#### **3.2.2.1. GP Al-silicate Orthogneiss**

Modal proportions were not recorded for the two gneissic units of the Greenspond section. Using Shand's alkali-alumina ratios for classification, this unit consistently plots in the peraluminous field.  $Al/(Na+K)$  values are between 1.4 and 2.0, and  $Al/(Ca+Na+K)$  values are range from 1.2 up to 1.8 (Figure 3-6A). The degree of Al-saturation is variable from sample to sample, a feature also apparent in thin section analysis. It should be noted that if Al-silicate growth is not a function of igneous processes then classification based on Shand's index is not appropriate. However, based on petrographic observations, the presence of biotite and muscovite, and geochemical data it is inferred that the Al-silicates are of igneous origin.

All samples show tight clustering on the La/Sm vs. Gd/Yb plot (Figure 3-6B) with relatively flat HREE slopes (1.0-1.6) and more steeply sloped LREE patterns (3.2-3.8). The extended REE plots show tight clustering of data with significant overlap between samples (Figure 3-6C). All samples have LREE enrichment relative to HREE, as well as negative Nb and Ti anomalies. Here a steeply sloping LREE trend and relatively flat HREE trend is apparent.

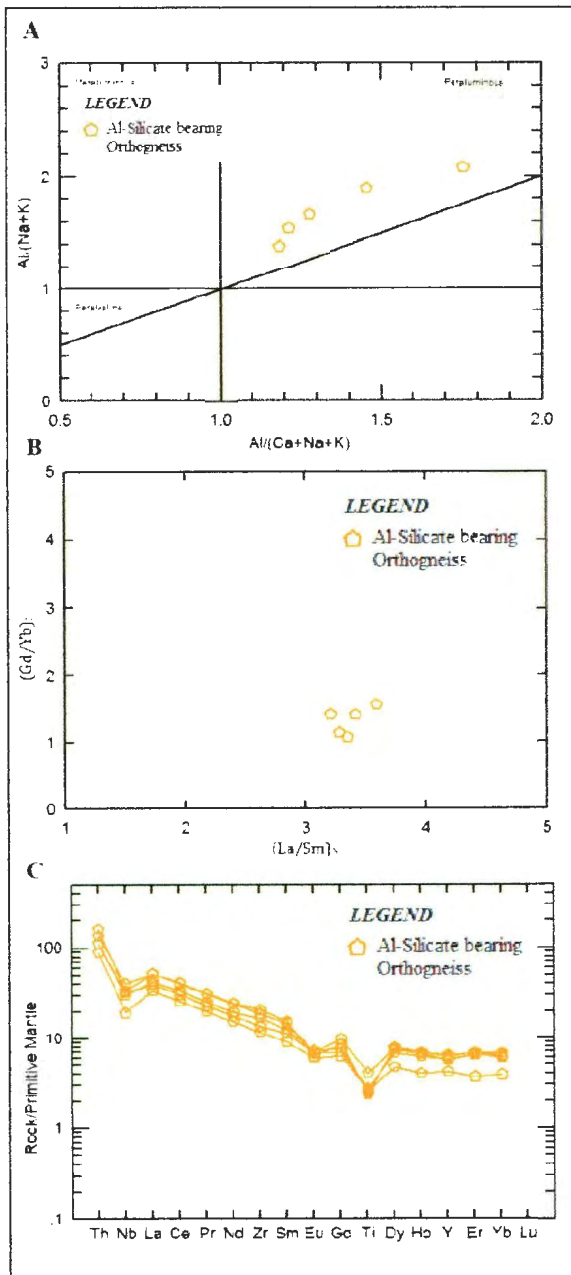


**Figure 3-6: Geochemical plots for the Al-silicate bearing orthogneiss of the Greenspond Section. Samples are plotted on (A) Shand's (1927) diagram with fields defined by Al saturation indices, (B) an XY plot of trace element ratios La/Sm vs. Gd/Yb, normalized to primitive mantle, and showing slope of the LREE and HREE, respectively and (C) an extended REE diagram normalized to primitive mantle.**

#### **3.2.2.2. GP Bt-Ms-Sil bearing Granitic Orthogneiss**

The geochemical pattern shown by one sample of this unit is nearly identical to those observed in some samples of the Al-silicate bearing orthogneiss. This unit is strongly peraluminous, enriched in LREE relative to HREE, and has a negative Nb and Ti anomaly, as well as a sloping LREE pattern and a relatively flat HREE pattern (Figure 3-7).

#### **3.2.2.3. GP Foliated Two-mica Leucogranite**

On the QAP diagram, two samples of the Greenspond leucogranite plot near the center of the granitic field, with very little variation between samples. They show little variation on Shand's index, plotting in the peraluminous field with  $Al/(Na+K)$  values around 1.4 and  $Al/(Ca+Na+K)$  values between 1.1 and 1.2 (Figure 3-7).

These samples have a LREE slope of approximately 3.3 and a HREE slope almost equal to 1, reflecting the flat HREE pattern in the extended REE diagram. LREE are enriched relative to HREE and a negative Nb and Ti anomaly is apparent.

#### **3.2.2.4. GP Tonalitic Enclave**

An average of the two tonalitic samples plotted on the QAP, lies in the quartz-rich end of the tonalitic field. Plotted individually, samples plot at the boundaries of the

defined tonalitic field. Even these enclaves appear oversaturated in Al and plot in the peraluminous field of Shand's plot.

The LREE have a more gentle slope than the surrounding units in this road section with a  $(La/Sm)_N$  value of 2.6. The HREE pattern is flat with a slope of approximately 1, but at higher concentration than the other units. Extended REE plots have negative Nb, Eu and Ti anomalies (Figure 3-7).

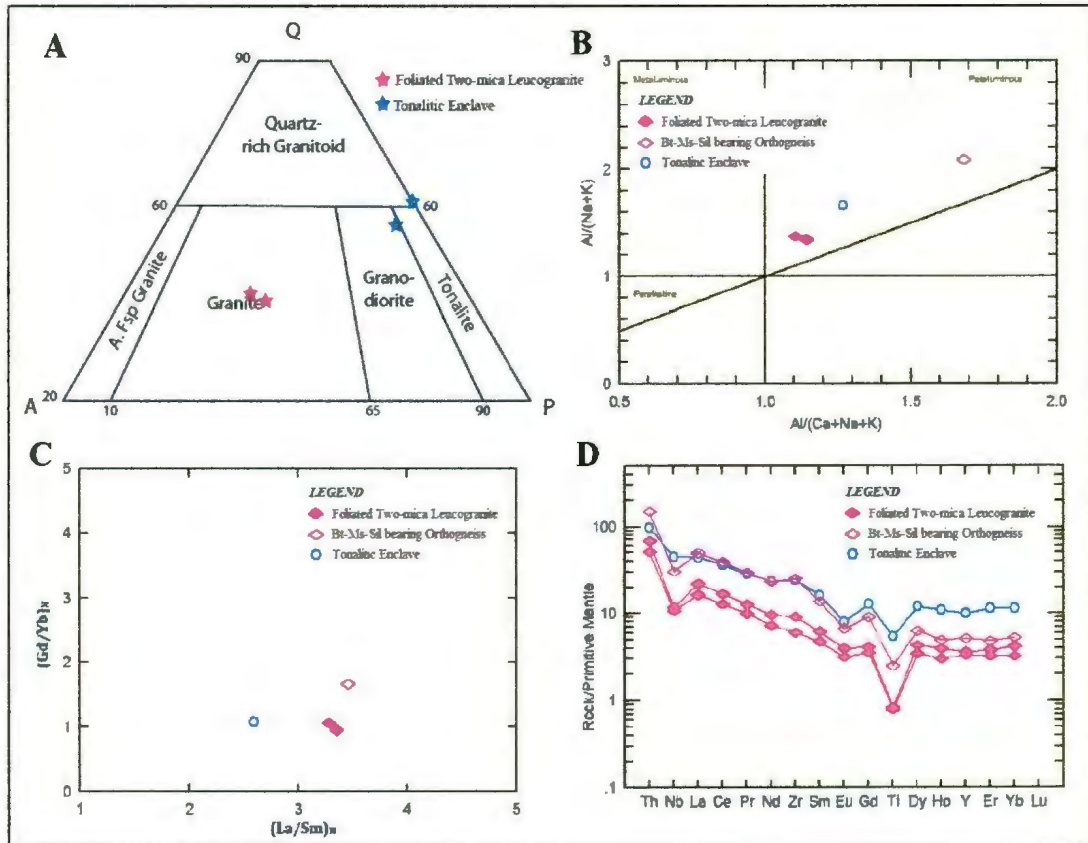


**Figure 3-7: Modal and geochemical plots for several units of the Greenspond section. Samples are plotted on (A) a QAP diagram based on normalized modal proportions observed in thin section, (B) Shand's (1927) diagram with fields defined by Al saturation indices, (C) a La/Sm vs. Gd/Yb plot, normalized to primitive mantle, and showing slope of the LREE and HREE, respectively and, (D) an extended REE diagram normalized to primitive mantle.**

### **3.2.3. The Trinity Road Section**

Units sampled for geochemical analysis from the Trinity section include the two-mica granitic orthogneiss, the Bt-Ms-Grt bearing leucogranite and the Bt-Hbl intermediate blocks.

#### **3.2.3.1. Trinity Two-mica Granitic Orthogneiss**

Based on Shand's index these samples are classified as peraluminous, with Al/(Na+K) ratios of 1.2 and 1.5, and Al/(Ca+Na+K) of approximately 1.1 to 1.2. LREE (La/Sm) and HREE (Gd/Yb) slopes are fairly high, between 3 and 4 for the LREE, and 2 and 4 for the HREE. This is reflected in the extended REE plot where both samples show steep slopes in both LREE and HREE patterns, and have negative Nb and Ti anomalies (Figure 3-8).

#### **3.2.3.2 Trinity Bt-Ms-Grt Leucogranite**

This unit has near equal amounts of quartz, alkali feldspar and plagioclase putting it in the granitic field on the QAP diagram. On Shand's index this unit is peraluminous with Al/(Na+K) of 1.2 and Al/(Ca+Na+K) of approximately 1.1. The trace element ratio plot shows the slope of the LREE is 3.5 and the HREE is also approximately 3.5 and a Nb and Ti anomaly is observed (Figure 3-8).

### **3.2.3.3 Trinity Intermediate Blocks**

On the diagram of Pearce (1996) this unit plots on the boundary between the basalt and alkali basalt field. Trace element patterns show a relatively consistent LREE and HREE slope with significant enrichment of the LREEs with respect to the HREEs. The extended REE pattern shows pronounced negative Nb and Ti anomalies as well as more subtle, negative Zr and Eu anomalies (Figure 3-9).

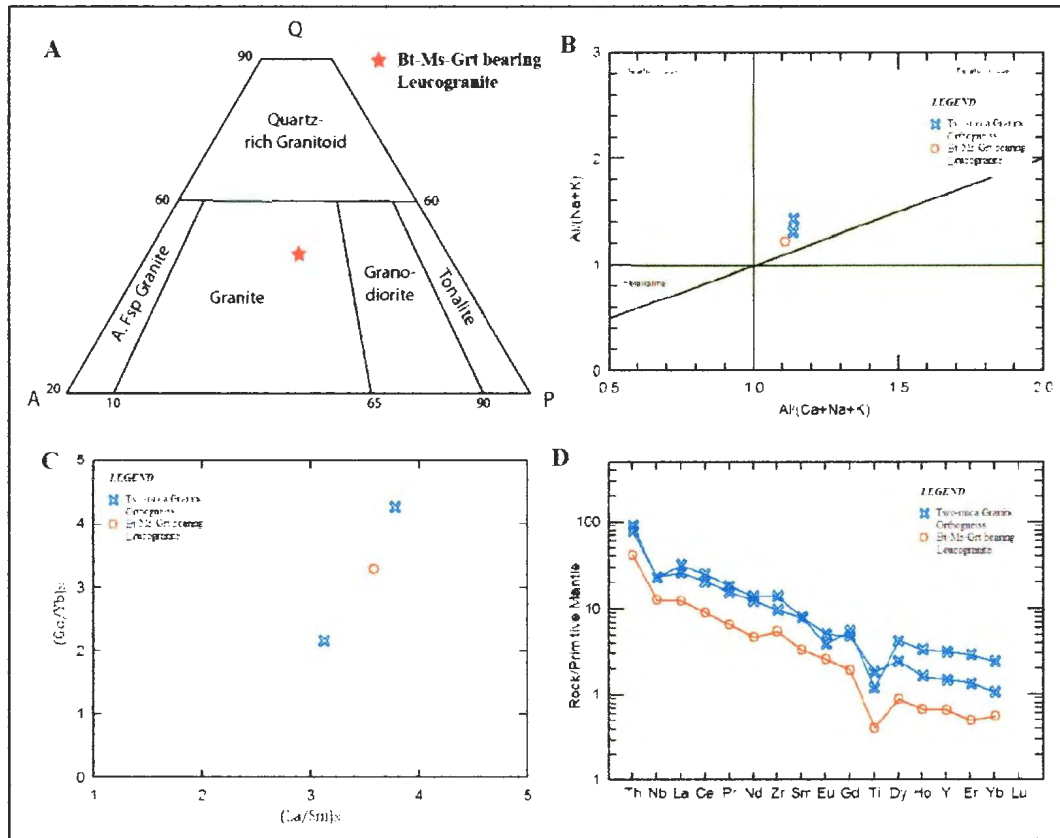


**Figure 3-8: Modal and geochemical plots for the sampled units of the Trinity section. Samples are plotted on (A) a QAP diagram based on normalized modal proportions observed in thin section, (B) Shand's (1927) diagram with fields defined by Al saturation indices, (C) a La/Sm vs. Gd/Yb plot, normalized to primitive mantle, and showing slope of the LREE and HREE, respectively and (D) an extended REE diagram normalized to primitive mantle.**

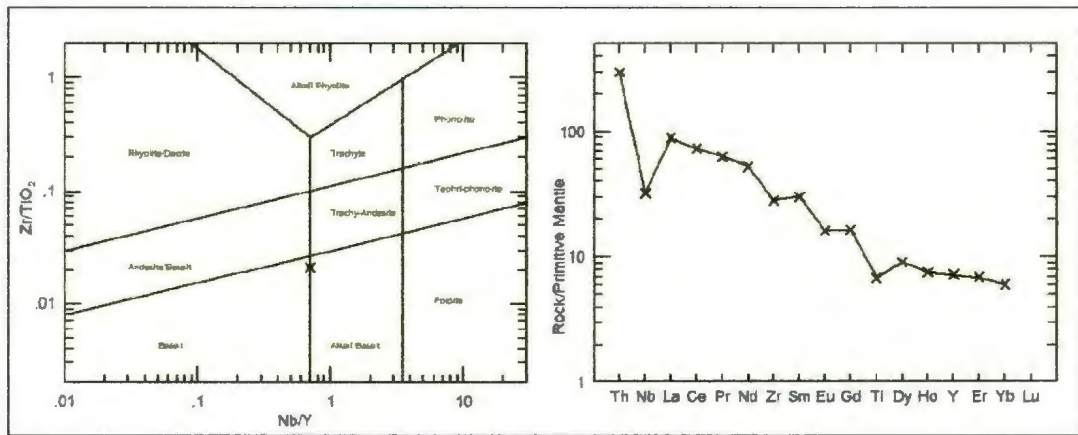


**Figure 3-9: Geochemical plots for the mafic unit of the Trinity section. Sample 10AL099 is plotted on a revised Winchester and Floyd diagram from Pearce (1996,) on the left, and an extended REE diagram normalized to primitive mantle, on the right.**

### 3.2.4. The “I Love You” Road Section

Samples from the tonalitic orthogneiss, the cross cutting tonalite and the late leucogranite intrusion were analyzed.

#### 3.2.4.1. “I Love You” Tonalitic Orthogneiss

This sample is strongly peraluminous plotting well within Shand’s defined peraluminous field, with  $Al/(Na+K)$  of 2.0 and  $Al/(Ca+Na+K)$  of approximately 1.6. Trace elements have a relatively flat HREE slope of 1.5 and a steeper LREE of 3.3. The extended REE plot shows the contrasting slope of LREE and HREE, with LREE enrichment relative to the HREE and also displays a negative Nb and Ti anomaly (Figure 3-10).

#### **3.2.4.2. “I Love You” Tonalite**

Based on the QAP diagram normative classification, this unit is tonalitic with a nearly equal proportion of quartz and plagioclase. Shand's index shows this unit plots on the peraluminous-metaluminous boundary, with a  $Al/(Ca+Na+K)$  value of 1.0. The sample has steep LREE and HREE slopes of approximately 4.5 and 3.2, respectively, and the extended REE plot shows enrichment of LREE relative to HREE as well as negative Nb and Ti anomalies (Figure 3-10).

#### **3.2.4.3. “I Love You” Leucogranite**

On the QAP diagram this sample is near the alkali feldspar-rich end of the defined granitic field. Shand's index of classification shows this sample is peraluminous, with an  $Al/(Na+K)$  ratio of 1.3 and an  $Al/(Ca+Na+K)$  ratio of approximately 1.2. Both the LREE and HREE slope values are approximately 3. Trace element patterns show negative anomalies for Nb, Eu and Ti (Figure 3-10).

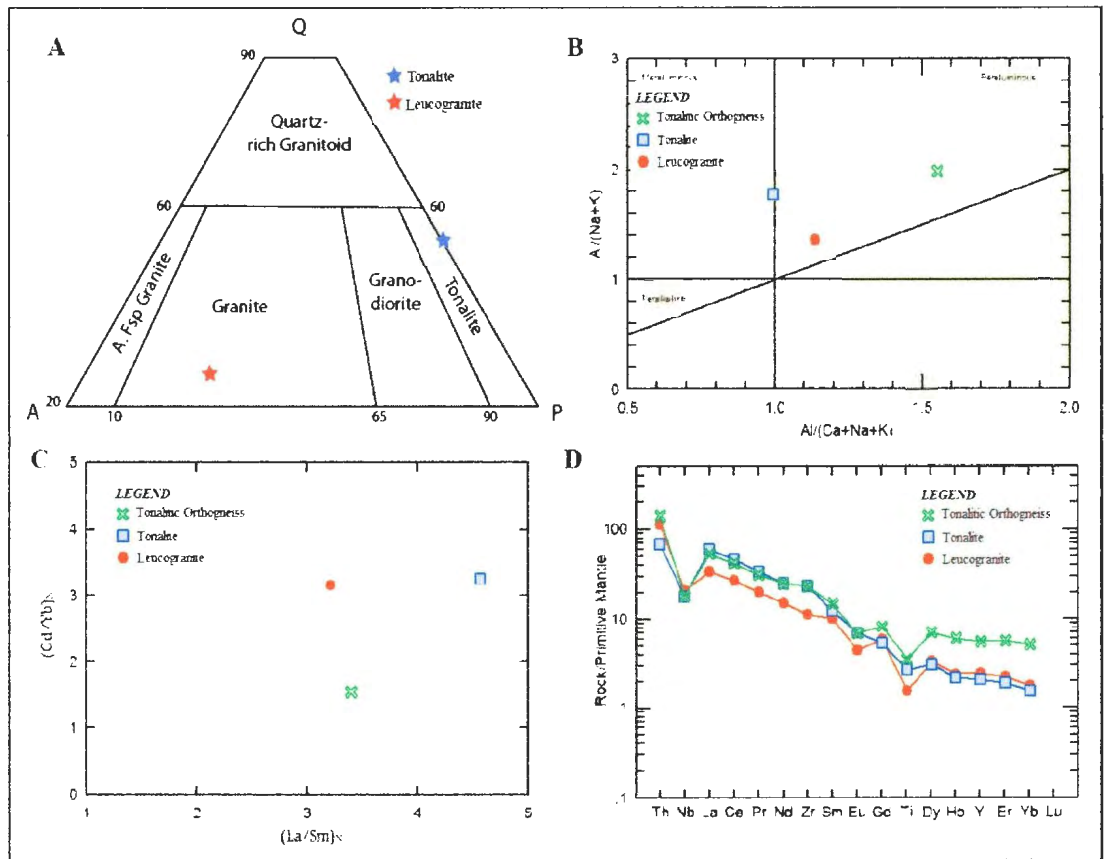


**Figure 3-10: Modal and geochemical plots for the sampled units of the “I Love You” section. Samples are plotted on (A) a QAP diagram based on normalized modal proportions observed in thin section, (B) Shand’s (1927) diagram with fields defined by Al saturation indices, (C) a La/Sm vs. Gd/Yb plot, normalized to primitive mantle, and showing slope of the LREE and HREE, respectively and (D) an extended REE diagram normalized to primitive mantle.**

### 3.2.5. North of Cape Freels

The Cape Freels gneissic unit, as well as a unique diabase dyke identified further north along the Cape Freels coast, were sampled for geochemical analysis.

#### 3.2.5.1. Cape Freels Gneiss

As the origin of this rock remains unclear two samples from the Cape Freels gneissic unit are plotted solely on an extended REE diagram normalized to primitive mantle. The trace element signatures show virtually identical, with LREEs enriched relative to HREEs, a flat HREE segment, negative Nb and Ti anomalies and a positive Zr anomaly (Figure 3-11).

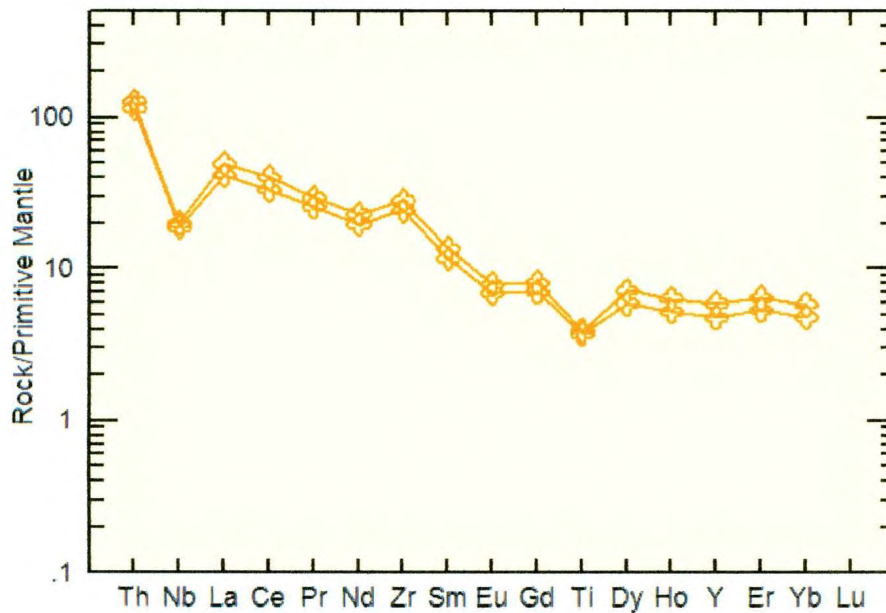


**Figure 3-11: Two samples of the Cape Freels gneiss plotted on an extended REE diagram normalized to primitive mantle.**

### 3.2.5.2. Cape Freels Diabase Dyke

This unit plots in the basalt field of the Pearce (1996) rock-type classification diagram. The extended REE pattern has a gentle slope, and is relatively flat with respect to most other analyzed units. A subtle negative Nb anomaly, as well as slightly positive Zr and Ti anomalies are present (Figure 3-12).

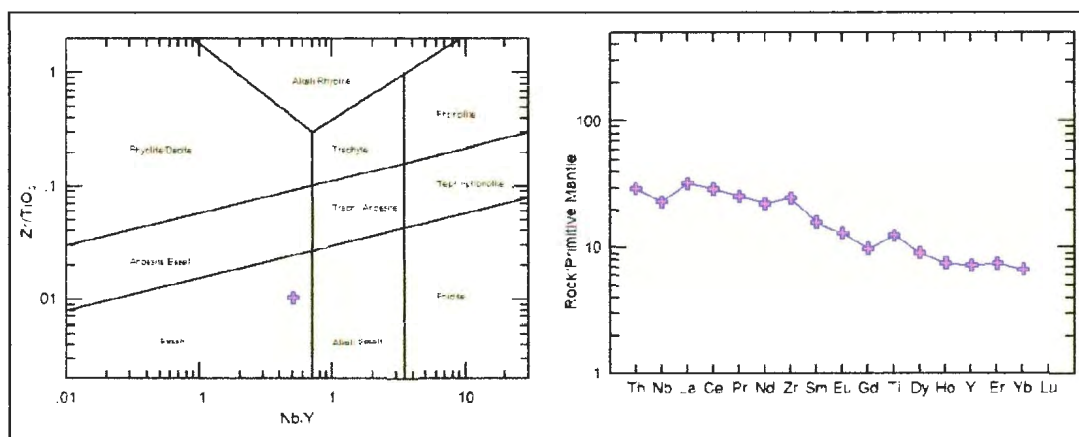


**Figure 3-12: Geochemical plots for the Cape Freels diabase dyke. The sample is plotted on a revised Winchester and Floyd diagram from Pearce (1996,) on the left, and an extended REE diagram normalized to primitive mantle, on the right.**

### 3.2.6. Valleyfield Road

Several samples of the orthogneiss and the mylonite occurring along Valleyfield road were selected for geochemical analysis. A sample of the Valleyfield paragneiss was also submitted for geochemistry but data is displayed on a separate diagram normalized to upper continental crust (Taylor and McLennan, 1985), a composition which is more or less representative of typical sedimentary material.

### **3.2.6.1. Valleyfield Orthogneiss**

Based on Shand's classification index this unit is peraluminous with  $Al/(Na+K)$  values of approximately 1.4 and 1.6, and  $Al/(Ca+Na+K)$  values of approximately 1.2 (Figure 3-13A). On the trace element ratio plot samples are tightly clustered with consistent LREE slopes of approximately 3.3 to 3.6, and gentle sloping HREE patterns with slopes of approximately 1.6 to 1.8 (Figure 3-13B). Extended REE patterns show significant overlap, with slightly variable concentrations of HREEs. All patterns show strong LREE enrichment relative to HREE, and prominent negative Nb, Eu and Ti anomalies. One sample of this unit has a positive Zr anomaly (Figure 3-13C).

### **3.2.6.2. Valleyfield Mylonite**

This unit plots in the peraluminous field of Shand's classification diagram, with  $Al/(Na+K)$  values of 1.3 and 1.4, and  $Al/(Ca+Na+K)$  values of approximately 1.1 and 1.2 (Figure 3-13A). The slope of the LREE is approximately 3.4, and the HREE slopes are more variable, from 1.5 to 2.4 (Figure 3-13B). Extended REE patterns show LREE enrichment relative to HREE, negative Nb, Eu and Ti anomalies and one sample shows a slight positive Zr anomaly. Overall, samples show similar trace element patterns to the adjacent orthogneiss with slight variation in the degree of trace element enrichment (Figure 3-13C).

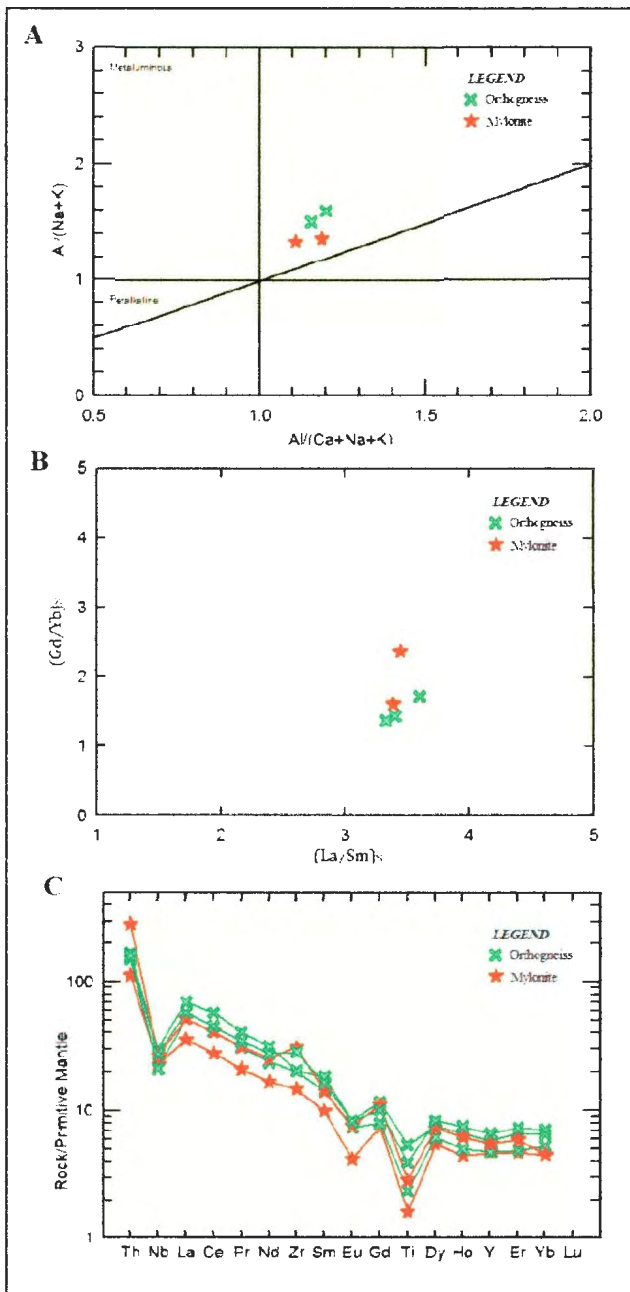


**Figure 3-13: Geochemical plots for several units occurring along Valleyfield Road. Samples are plotted on (A) Shand's (1927) diagram with fields defined by Al saturation indices, (B) a La/Sm vs. Gd/Yb plot, normalized to primitive mantle, and showing slope of the LREE and HREE, respectively and (C) an extended REE diagram normalized to primitive mantle.**

### 3.2.6.3. Valleyfield Paragneiss

The REE diagram is normalized to average upper continental crust (Taylor and McLennan, 1985) and shows two samples of the paragneiss unit plotting as a relatively flat line, at approximately 1 (Figure 3-14). This trend is expected for a metamorphic rock with a sedimentary protolith, further supporting the origin of this unit.

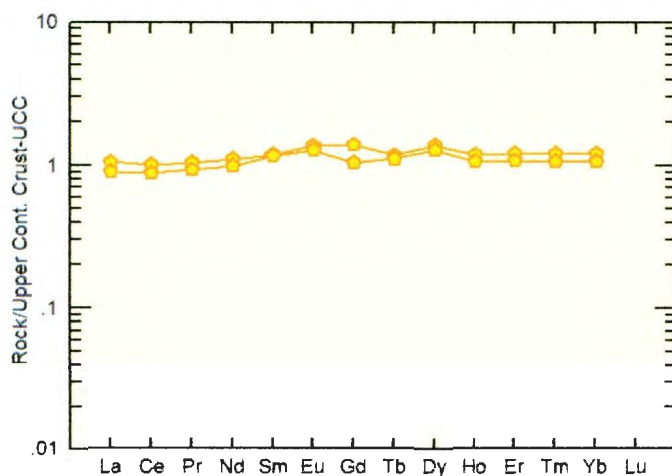


**Figure 3-14: Two samples of the Valleyfield paragneiss plotted on a REE diagram normalized to upper continental crust (Taylor and McLennan, 1985).**

### 3.2.7. Town of Hare Bay

A single sample of the Hare Bay orthogneiss was selected for geochemical analysis.

### 3.2.7.1. Hare Bay Orthogneiss

On Shand's classification diagram this unit plots well into the peraluminous field with an Al/(Na+K) ratio of 2.0 and an Al/(Ca+Na+K) ratio of 1.5 (Figure 3-15A). The LREE have a slope of 3.3 and the HREE have a relatively flat slope of 1.3 (Figure 3-15B). The extended REE pattern shows enrichment of LREE relative to HREE, negative Nb and Ti anomalies as well as a more subtle negative Eu anomaly (Figure 3-15C).

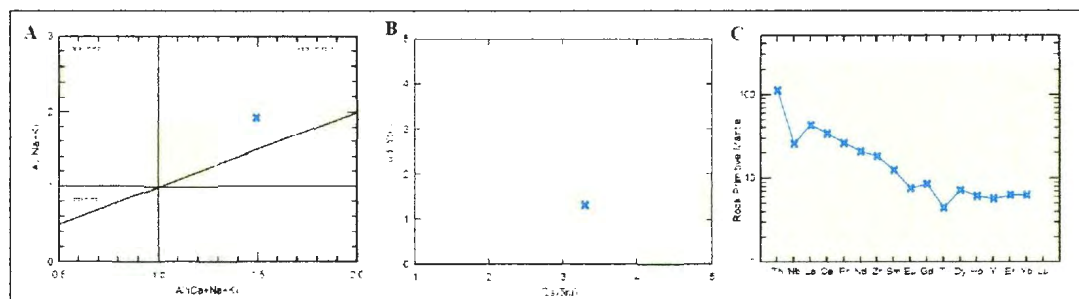


**Figure 3-15: Geochemical plots for the Hare Bay orthogneiss. The sample is plotted on (A) Shand's (1927) diagram with fields defined by Al saturation indices, (B) a La/Sm vs. Gd/Yb plot, normalized to primitive mantle, and showing slope of the LREE and HREE, respectively and (C) an extended REE diagram normalized to primitive mantle.**

### 3.3. Interpretation/Summary of Geochemical Data

According to the QAP normative classification, several units from the WMB map area are granitic, but show slight variation in modal mineralogy. Mapped rock units are classified as granodiorite or tonalite based on the QAP plot, supporting field observations. Most units are peraluminous, based on Shand's index. Alkali-alumina ratios >1.1 along

with mineralogy including muscovite ( $\pm$ )garnet, classify the granitic units as peraluminous or “S-type granite” (Chappell and White, 1974; Chappell and White, 1984), implying melting of a metasedimentary source. Trace element patterns are very similar between units, with only minor variation. The majority of the units show LREE enrichment relative to the HREE and prominent Nb and Ti anomalies. This type of pattern is representative of melts derived from crustal material. Individual granitic samples also show slightly negative Zr and Eu anomalies, likely a function of zircon and feldspar fractionation, respectively. Several samples of the granodiorite unit have positive Zr anomalies possibly a result of accumulation of zircon in the sample. Exceptions to these generalized geochemical trends among granitic rocks are observed in the pegmatitic unit, which may have a more complicated chemical evolution involving gains and losses of accessory phases. This suggestion is supported by the abundance of inherited zircon (Chapter 4).

Samples of the Greenspond orthogneiss show tightly clustered geochemical trends indicating homogeneity. Plotted on Shand’s diagram, samples show some variation but all lie within the peraluminous field, which is likely due to Al-silicate content of a particular sample. The protolith of this gneiss is inferred to be peraluminous. The leucogranite and tonalitic enclaves plot in their respective fields on the QAP confirming field observations, and both plot in the peraluminous field of Shand’s diagram. The trace element geochemical trends of all units from the Greenspond section are very similar, and typical of melted crustal material. The foliated leucogranite appears slightly depleted in REEs in comparison with the other units of this section, possibly a result of fractionation of the

source magma or an alternate source. Homogeneity of the geochemical trends within the Greenspond section prevents geochemical divisions between or within units from being made.

Similarities were identified when comparing the geochemical trends for the orthogneiss units located in the Trinity and "I Love You" road sections, as well as along roads in the towns of Valleyfield and Hare Bay. All samples of the orthogneiss units mapped in these areas have a peraluminous signature with compositions ranging from granitic to tonalitic. Trace element patterns of the units have LREE enrichment relative to the HREE and negative Nb and Ti anomalies. The signatures are again similar to those of major units in WMB and Greenspond, all being typical of crustal melts. Several samples of the orthogneiss units show negative Eu anomalies, likely related to feldspar fractionation. Orthogneiss from the Trinity section appear slightly less enriched in REEs, and both the Trinity and "I Love You" orthogneiss have a gentle HREE slopes in contrast to the flat HREE patterns observed in orthogneiss from other localities. This contrast is likely controlled by accessory phases.

Late granitic intrusions (Greenspond, Trinity, "I Love You") vary slightly in composition but all plot in the granitic field on the QAP and also show a peraluminous signature based on Shand's index. The trace element signatures are similar to those identified in previous units. It is noteworthy that in all occurrences where a late granitic unit postdates host orthogneiss (Greenspond, Trinity, "I Love You"), the REE patterns of the granite are at lower concentrations relative to the orthogneiss. In the Trinity road

section the leucogranite contains garnet, partially explaining depletion of the HREE in this case.

Geochemistry of mafic units including those at WMB, Cape Freels and the Trinity section are also compared. On the rock classification diagram of Pearce (1996) these samples plot in the basalt or alkali basalt field. Two contrasting REE patterns were identified from the mafic units. Both the Act-Bt mafic unit in WMB and the Cape Freels diabase dyke, occurring just south of WMB, have similar flat geochemical signatures. In contrast to other units the LREE enrichment relative to HREE is minor. Both have a minor negative Nb anomaly as well as subtle positive Zr and Ti anomalies. In contrast, the Bt-Carb bearing mafic unit of WMB and the Amph-bearing intermediate unit in the Trinity section, show similar REE patterns with significant enrichment of the LREE relative to the HREE and steeply sloping LREE and HREE segments. These units also have prominent negative Nb anomalies. Other anomalies are observed but are not common to both units.

In summary, litho-geochemistry alone is not enough to differentiate between mapped units or identify groups within units. All granitic and orthogneiss samples have relatively similar peraluminous signatures and REE patterns diagnostic of crustal melts.

## 4. CHAPTER 4: GEOCHRONOLOGY

A key focus of this study is to understand the relationships between rock units mapped as the “Hare Bay Gneiss”, as well as the relationship of these units to the Gander Group. This information will lead to a better overall understanding of the Gander Zone in Newfoundland. Age information is critical for this assessment and therefore much of this study was directed towards obtaining U-Pb ages for important map units.

### 4.1 Sample Selection

Twelve lithologic units from various study locations were selected for U-Pb zircon analysis using the chemical abrasion thermal ionization mass spectrometry (CA-TIMS) technique. In the WMB map area 4 units were selected, including pegmatite, granodiorite, megacrystic granite and foliated leucogranite. In the field it was clear that these units recorded several stages of magmatism, with the granitic units appearing older than the granodiorite and late cross-cutting pegmatite. The samples were collected from the eastern half of the map area and exact localities are signified by stars on Map 1. In the Greenspond section the Al-silicate orthogneiss and the foliated leucogranite were selected for age determination as they clearly represent two separate magmatic events, with the orthogneiss being the oldest unit in the section. Sample locations are marked with a star on Section A-A'. In the “I Love You” road section the orthogneiss and the cross-cutting tonalite were selected with sample locations appearing on Section C-C' as stars. The orthogneiss in Valleyfield as well as Hare Bay were also analyzed, and UTM coordinates

for these samples are shown in Appendix B. These units were selected for analysis as they represent significant magmatic events, yet no reliable correlations between outcrops can be made. Samples of the Cape Freels gneiss and the Valleyfield paragneiss were collected to confirm the nature of origin, as this was not always clear in the field, the UTM coordinates for these samples are reported in Appendix B.

Laboratory procedures and a detailed description of U-Pb zircon analysis using the CA-TIMS technique is provided in Appendix E. The data acquired from CA-TIMS analysis including U and Pb concentrations, determined isotopic ratios and the associated uncertainties and ages are listed in Table 4-1. In each case the  $^{206}\text{Pb}/^{238}\text{U}$  age was calculated using the best, most precise single fraction, or a weighted average of multiple fractions, with each fraction containing between 1 to 4 grains. In several cases Pb-loss, metamorphic overgrowths, or older inherited cores result in discordant analyses, which do not yield a reliable age for the rock.

## **4.2 Results**

### **4.2.1. WMB Map Area**

#### **4.2.1.1 Foliated Leucogranite**

This unit (10AL090) yielded 3 main zircon populations including, large, cracked 3:1 prisms and prism fragments that are stained orange, short, clear, sub-rounded zircon, and small, clear, 3:1 aspect ratio subhedral prisms approximately 100 to 150  $\mu\text{m}$  in length (Figure 4-1). Cathodoluminescence (CL) images show well developed igneous growth

zones, and in contrast one grain lacks zoning and has a rounded inherited core (Figure 4-2). The clearest, well-defined prisms were selected for analysis, but cores were not observable under the binocular microscope and could not be preferentially avoided. Although five fractions were analyzed the  $^{206}\text{Pb}/^{238}\text{U}$  age was calculated using the Z3 fraction (containing 2 prisms) as  $428 \pm 2$  Ma. This fraction shows considerable overlap with the Z2 fraction but is more precise (Figure 4-3). Fractions Z1, Z4 and Z5 show evidence of an older component, that is also visible as inherited cores in CL images. These analyses were, therefore, excluded from the age calculation.

#### **4.2.1.2. Megacrystic Granite**

Megacrystic granite (10AL087) yielded abundant clear prismatic zircon with variable morphology, including clear, 3:1 and 4:1, euhedral to subhedral prisms as well as small, clear, rounded grains (Figure 4-1). CL images reveal clear igneous growth zones, and inclusions are observable in some grains (Figure 4-2). Obvious inclusion-bearing grains, as well as the small rounded zircon population were avoided when selecting grains for analysis. Three analyzed fractions, Z1, Z2 and Z3, plot on concordia showing significant overlap. All fractions were used in determining a weighted average  $^{206}\text{Pb}/^{238}\text{U}$  age of  $420 \pm 1$  Ma (MSWD=0.82) at the 95% confidence interval (Figure 4-3).

**Table 4-1: U-Pb isotopic data from lithologic units of the Hare Bay Gneiss, northeast Newfoundland  
WMB and Greenspond**

Fraction	Concentration		Measured		Corrected Atomic Ratios (°)						Age [Ma]				
	Weight [mg]	Pb total [ppm]	total common Pb [pg]	206Pb 204Pb	206Pb	207Pb	208Pb	235U	238U	207Pb	206Pb	238U	235U	206Pb	
					±	±	±	±	±	±	±	±	±		
<b>WMB: Foliated Leucogranite: 10AL090 (314087, 5461404)</b>															
Z1 1 frag 1 prm	0.008	33	16.4	4.5	8.8	0.1247	0.06734	60	0.0118	50	0.00631	50	413	46	46
Z2 2 sm prm	0.008	111	3.7	2.8	8	0.1109	0.06868	3	0.0557	40	0.05551	34	424	420	423
Z3 3 less defined prm	0.003	393	27.6	3.2	16.1	0.1009	0.06868	3	0.0557	40	0.05551	34	424	420	423
Z4 1 long prm	0.001	355	3.2	12	3.4	0.0508	0.01387	70	0.5707	80	0.00603	80	424	458	454
Z5 2 sm shrt prm	0.002	319	3.7	1	1	0.083	0.07311	4	0.2517	38	0.05009	80	424	469	59
<b>WMB: Megacrystic Granite: 10AL087 (314076, 5461402)</b>															
Z1 3 prm	0.003	456	24.0	1.5	259	0.1533	0.06718	38	0.5129	32	0.05520	24	420	420	420
Z2 4 prm	0.004	984	72.6	1.1	438	0.142	0.06718	38	0.111	18	0.0516	14	419	419	419
Z3 4 prm	0.004	752	29.6	4.9	2621	0.1731	0.06747	34	0.116	20	0.0510	20	421	420	476
<b>WMB: Granodiorite: 10AL088 (314071, 5461407)</b>															
Z1 2 prm r tips	0.002	709	16.7	2.7	667	0.306	0.06614	50	0.014	78	0.0498	68	413	413	411
Z2 2 prm frag	0.002	216	17.1	2.3	896	0.222	0.06533	38	0.496	41	0.0463	46	412	400	397
Z3 3 prm frag	0.003	390	17.1	2.6	1174	0.1788	0.06337	70	0.844	94	0.01333	80	517	622	1103
<b>WMB: Pegmatite: 10AL089 (314090, 5461404)</b>															
Z1 3 prms	0.003	554	38.0	1.2	215	0.1617	0.06547	38	0.4947	28	0.05481	22	419	408	404
Z2 1 lrg, 1 sm prm	0.003	118	21.4	2.0	2186	0.1098	0.06449	30	0.4191	30	0.0500	16	401	404	422
Z3 1 lrg, 2 sm prm	0.004	1015	69.7	2.9	6022	0.1114	0.06722	64	0.112	42	0.0516	28	419	410	417
Z4 1 l frag	0.001	643	47.4	3.0	844	0.1550	0.06184	34	0.4624	26	0.05423	14	387	380	380
Z5 1 rect crck frag	0.001	1394	99.7	1.4	1739	0.1819	0.0628	22	0.5116	26	0.05516	24	420	420	417
Z6 1 shrt cr kd prm	0.001	1028	69.3	1	299	0.1100	0.06112	38	0.118	34	0.0517	14	420	420	431
<b>Greenspond: Orthogneiss: 10AL079 (302249, 5441578)</b>															
Z1 1 lrg prm	0.002	525	47.4	2.1	429	0.2214	0.06206	44	0.6497	14	0.0174	20	508	500	508
Z2 3 sm prm	0.003	30	3.2	3.4	13	0.065	0.01413	50	0.6791	174	0.019	116	526	528	528
Z3 2 sm prm	0.002	302	21.6	2.7	642	0.1134	0.1676	25	1.1798	30	0.0819	10	1000	1100	1159
<b>Greenspond: Leucogranite: 10AL078 (302249, 5441578)</b>															
Z1 1 sm, 1 md prm	0.002	689	47.9	4.7	174	0.0458	0.07331	38	0.745	84	0.05683	74	476	461	475
Z2 1 sm long prm	0.001	689	49.5	2.9	1114	0.038	0.0162	28	0.5608	34	0.0560	26	452	452	453
Z3 1 tiny prm	0.001	31	60.6	4.5	371	0.017	0.01759	4	0.5863	54	0.068	48	467	469	477
Z4 1 crckd prm	0.001	601	24.1	3.7	4568	0.112	0.040	60	0.1738	46	0.05624	22	460	460	462
Z5 2 crckd	0.002	107	77.5	165	8	0.0463	0.07387	47	0.578	24	0.0625	206	470	461	462

**Table 4-1: U-Pb isotopic data from lithologic samples from the Hare Bay Gneiss, northeast Newfoundland  
"I Love You", Cape Freels, Valleyfield and Hare Bay**

FRACTION	Concentration		Measured		Corrected Atomic Ratios (ppm)				Age [Ma]						
	Weight [mg]	U [ppm]	Pb rad [ppm]	Total Common Pb [ppm]	206Pb		207Pb		206Pb / 207Pb						
					206Pb [ppm]	206Pb [ppm]	207Pb [ppm]	207Pb [ppm]	206Pb [ppm]	206Pb [ppm]					
<b>"I Love You": Orthogneiss: 10AL097 (284449, 5426398)</b>															
Z1 4 tiny	0.004	45	4.9	2.1	361	0.1102	0.1086	44	0.9348	84	0.06354	54	673	670	674
Z2 5 tiny prm	0.003	1	4.2	4.1	36	0.1407	0.1243	14	1.1079	474	0.06803	252	747	787	794
Z4 1 clr prm	0.001	1.1	34.6	3.1	334	0.1701	0.1049	39	0.6057	28	0.05865	87	325	341	354
Z5 1 frag, 1 sm clr prm	0.001	38	34.6	3.1	4034	0.2383	0.1536	66	1.1331	90	0.10000	18	81	1161	1241
Z6 1 lr prm	0.002	1133	18.1	5.7	3476	0.844	0.13989	116	1.4376	110	0.17433	31	144	305	306
<b>"I Love You": Tonalite: 10AL096 (284449, 5426398)</b>															
Z1 2 sm	0.002	71	9.0	6.1	344	0.1329	0.06527	47	0.4936	70	0.15488	71	417	417	417
Z2 1 tiny	0.001	14.5	97.4	4.1	3367	0.1346	0.06391	31	0.9001	24	0.05599	22	417	417	413
Z3 1 rnd, 1 sm prm	0.002	64	38.1	4.1	733	0.183	0.06877	34	0.4003	32	0.05417	32	413	416	419
Z4 1 rnd frag, 1 prm	0.002	2394	20.6	3.4	741	0.1119	0.0641	34	0.4803	26	0.05494	14	412	412	410
Z5 1 sm crackd frag	0.001	117	88.4	2.1	180	0.1478	0.06613	316	0.1034	24	0.05804	2	414	414	414
Z6 1 crackd w/ clr rim	0.001	46	200.9	1.4	3403	0.1114	0.06600	41	0.4800	14	0.05596	34	416	415	415
<b>Cape Freels: Gneiss: 10AL093 (317643, 5461369)</b>															
Z1 2 sm clr prm	0.001	17	12.2	2.1	119	0.1078	0.09153	30	0.7505	58	0.05899	41	511	516	566
Z2 4 sm clr prm	0.004	277	31.9	1.1	114	0.1668	0.08299	46	1.0591	26	0.07033	26	563	713	919
Z3 3 sm clr prm	0.003	198	17.3	3.6	907	0.1379	0.08445	54	0.7163	40	0.05974	40	546	549	551
<b>Valleyfield: Paragneiss: 10AL076 (308557, 5445348)</b>															
Z1 1 tiny prm	0.001	11	11.7	5.1	1400	0.1055	0.03668	30	0.7961	72	0.10164	18	517	595	661
Z2 1 sm, 1 frag	0.001	189	9.1	4.1	1008	0.1605	0.04553	234	0.6800	46	0.10551	17	7416	1883	4100
<b>Valleyfield: Orthogneiss: 10AL077 (309400, 5444508)</b>															
Z1 3 euh prm	0.004	35	11.2	2.3	40	0.0991	0.03556	36	0.8996	114	0.06660	94	410	411	416
Z2 4 euh prm	0.006	135	17.9	6.2	1070	0.1307	0.09176	58	0.8667	56	0.16883	31	563	673	894
Z3 3 clr euh prm	0.004	191	14.1	4.7	160	0.1149	0.07499	38	0.8117	35	0.05614	28	466	466	466
Z4 4 clr euh prm	0.006	149	12.2	6.1	181	0.1349	0.07499	68	0.8864	38	0.05999	46	466	462	448
Z5 2 clr euh prm	0.003	34	20.9	1.1	423	0.1001	0.07477	41	0.8799	38	0.05617	24	466	464	419
<b>Hare Bay: Orthogneiss: 10AL094 (719561, 5415836)</b>															
Z1 1 prm	0.001	174	13.2	1.7	513	0.1424	0.07887	116	0.6718	138	0.05671	188	435	411	473
Z2 1 clr prm	0.001	442	11.2	1.1	7193	0.1155	0.03691	41	0.8103	66	0.10834	41	596	600	676
Z3 1 clr prm	0.001	242	11.2	1.1	378	0.1000	0.0791	68	0.6184	208	0.05611	188	411	489	480

Notes: All minerals were chemically abraded (CA-HMS, Mattinson 2005) prior to dissolution. / zircon; 1,2, etc. = number of grains in the analysis; clr = clear, crackd = cracked euh = euhedral, frag = fragment s/lrg = large, md = medium, omg = orange, prm = prism s, rect = rectangular shrt = short, sm = small, mg = milligrams, ppm = parts per million, pg = picograms; (11M's (easting, northing) NAD27 Z22 (10AL093 Z21) after sample number.  
a. weights of grains were estimated, with potential uncertainties of 25-50% for small samples.  
b. radiogenic lead  
c. Atomic ratios corrected for fractionation, spike, laboratory blank of 2 picograms (pg) common lead, and initial common lead at the age of the sample calculated from the model of Stacey and Kramers (1975), and 0.3 pg l blank. Two sigma uncertainties are reported after the ratios and refer to the final digits.

#### 4.2.1.3. Granodiorite

The granodiorite (10AL088) yielded large, cracked, turbid, subhedral grains and grain fragments, smaller, clear prisms typically appearing as prisms without grain tips, as well as small, clear fragments (Figure 4-1). The clearest, best defined prisms and fragments were selected for analysis. CL images for many of the smaller fragments were too bright for quality imaging, however, many appear to have complex growth histories, whereas rectangular prisms show clear longitudinal growth zones (Figure 4-2). Two concordant points, of the three analyzed fractions, yield a weighted average  $^{206}\text{Pb}/^{238}\text{U}$  age of  $412 \pm 2$  Ma, at the 95% confidence interval with a MSWD of 0.37 (Figure 4-3). The excluded fraction, Z3, has inheritance plotting on a line between the determined age and the age of an older component.

#### 4.2.1.4. Pegmatite

Zircon in the pegmatite (10AL089) showed significant variation in morphology and was less abundant than in other units from this area. Grain morphologies included large, extremely crackled, orange-stained grain fragments; cracked, 3:1 prismatic grains, ranging in size from  $<50$ - $250$   $\mu\text{m}$ ; smaller, rounded grains, and clear zircon fragments (Figure 4-1). In some cases, CL imaging shows clear igneous growth zoning and embayed grain boundaries. Some grains have metamorphic overgrowths, sector zoning, and irregular turbid patterns in their interiors (Figure 4-2). Few grains survived annealing and etching, therefore selection for analysis was limited. Fraction Z4, provides a

$^{206}\text{Pb}/^{238}\text{U}$  age of  $387 \pm 2$  Ma (Figure 4-3). This was the youngest concordant age acquired in this sample and agrees with the relatively undeformed and cross-cutting nature of this unit in the field.

The possibility of this late intrusion picking up zircon from older units through which it intrudes, provides an explanation for the older ages of the other analyzed fractions. Fractions Z3, Z5 and Z6 cluster at ca. 420 Ma and correlate temporally with the megacrystic granite that the pegmatite intrudes. Fractions Z1 and Z2, overlap concordia between the age of this unit, 387 Ma, and the cluster of fractions at 420 Ma. These fractions could, therefore, contain inherited grains with younger over-growths, zircon of a different age also picked up during intrusion, or be a result of analyzing zircon of both ages in one fraction.

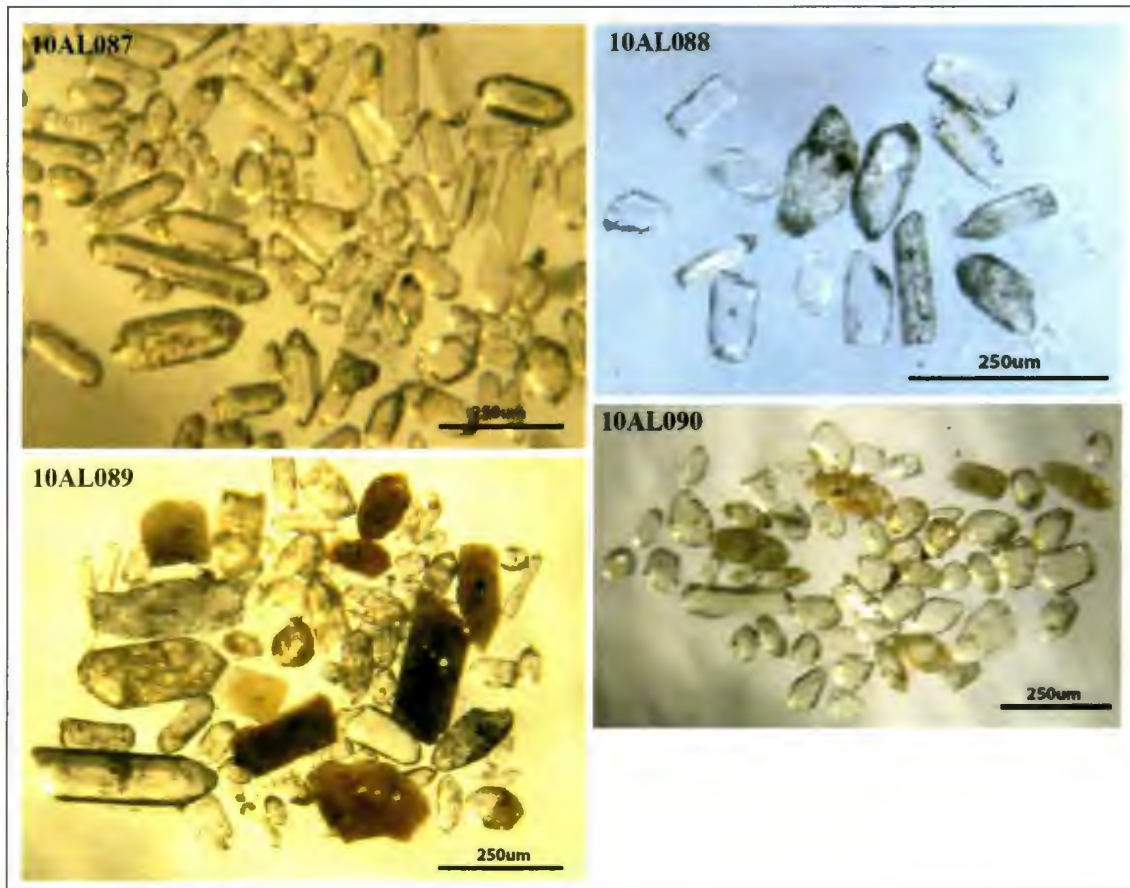


**Figure 4-1: Plane polarized light photomicrographs of zircon populations from dated samples in the WMB map: Sample 10AL087 from the megacrystic granite, 10AL088 from the granodiorite, 10AL089 from the pegmatite and 10AL090 from the foliated granite.**

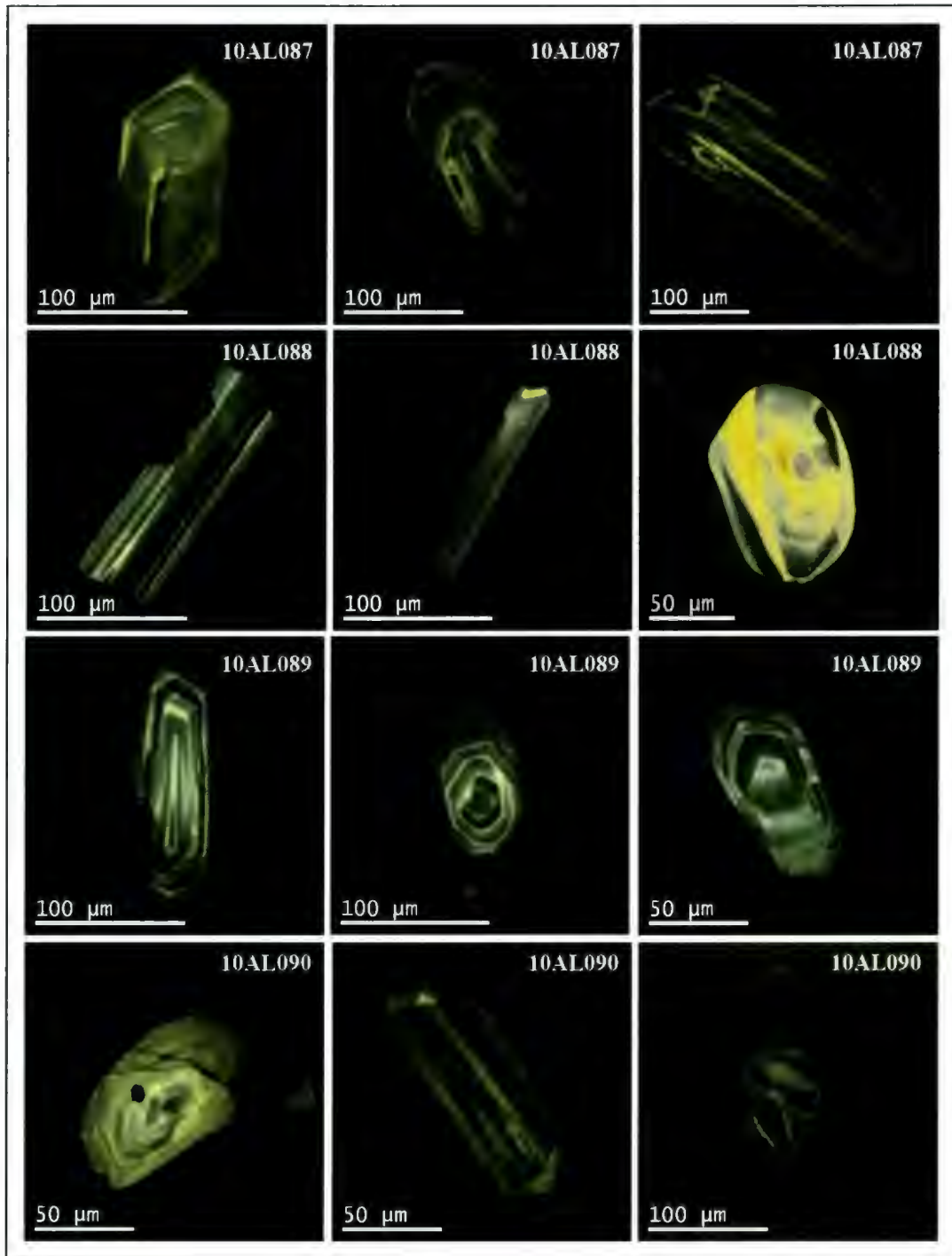


**Figure 4-2: Cathodoluminescence images of zircon grains from the four samples dated in the WMB map area: Sample 10AL087 from the megacrystic granite, 10AL088 from the granodiorite, 10AL089 from the pegmatite and 10AL090 from the foliated granite.**

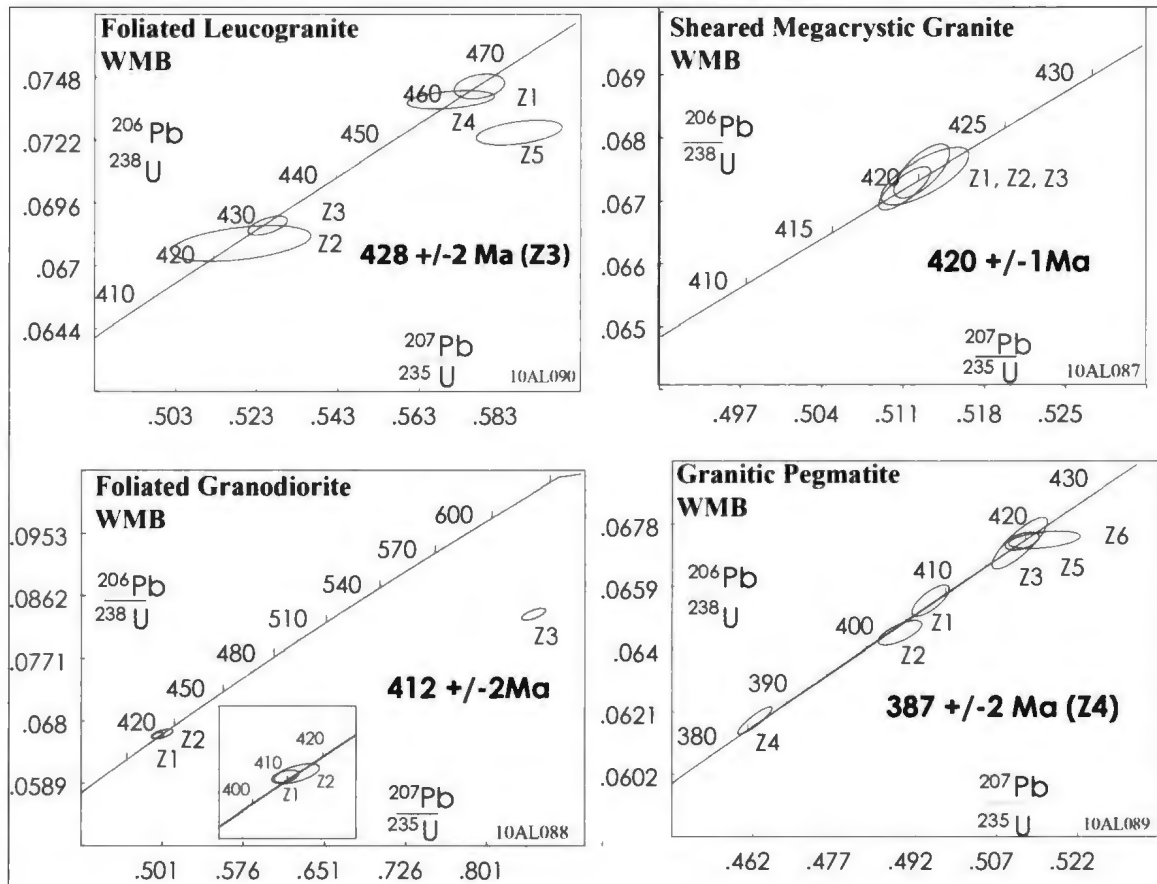


**Figure 4-3: Concordia diagrams for the four geochronology samples from WMB map area.  $^{206}\text{Pb}/^{238}\text{U}$  ages and uncertainties are reported at the 95% confidence interval.**

## 4.2.2. Greenspond Road Section

### 4.2.2.1. Al-silicate Orthogneiss

Two main populations of zircon are present in this orthogneiss sample (10AL079) including clear, euhedral 3:1 prisms and 2:1, clear, euhedral to subhedral grains with a larger proportion of prism tips and poorly developed prism faces (Figure 4-4). In CL, some grains show clear igneous growth zoning whereas others are much more complex

internally, and some grains with metamorphic overgrowths were also identified. The Z1 fraction, of one large single grain along with the lower intercept of the line of best fit (13.1% probability of fit) was used to determine the  $^{206}\text{Pb}/^{238}\text{U}$  age of  $510 \pm 4$  Ma. Fractions, Z2 and Z3, show evidence of an older component and the upper intercept of this line is 1546 Ma (Figure 4-5).

#### **4.2.2.2. Foliated Leucogranite**

Zircon is abundant in this unit (10AL078) and grains selected for analysis are clear, euhedral 4:1 prisms, as well as some shorter 3:1 prisms. CL imaging reveals igneous growth zoning, with one grain showing longitudinal zoning. Grains with dark metamorphic rims are also present, although difficult to see in the images provided (Figure 4-4). Analysed fractions, Z4 and Z5 show significant overlap on concordia and were used to determine a U-Pb age of  $460 \pm 2$  Ma (Figure 4-5). Fractions, Z1 and Z2 show younger ages, which could be a function of metamorphic overgrowths and/or Pb-loss and fraction, Z3 appears to have an older component, resulting in a slightly older age. The measured  $^{208}\text{Pb}/^{206}\text{Pb}$  ratio of this sample (0.03212 to 0.0938) is consistently lower than all other analyzed samples, correlating with a lower Th/U ratio, and implying a different source of melt material for this granite.

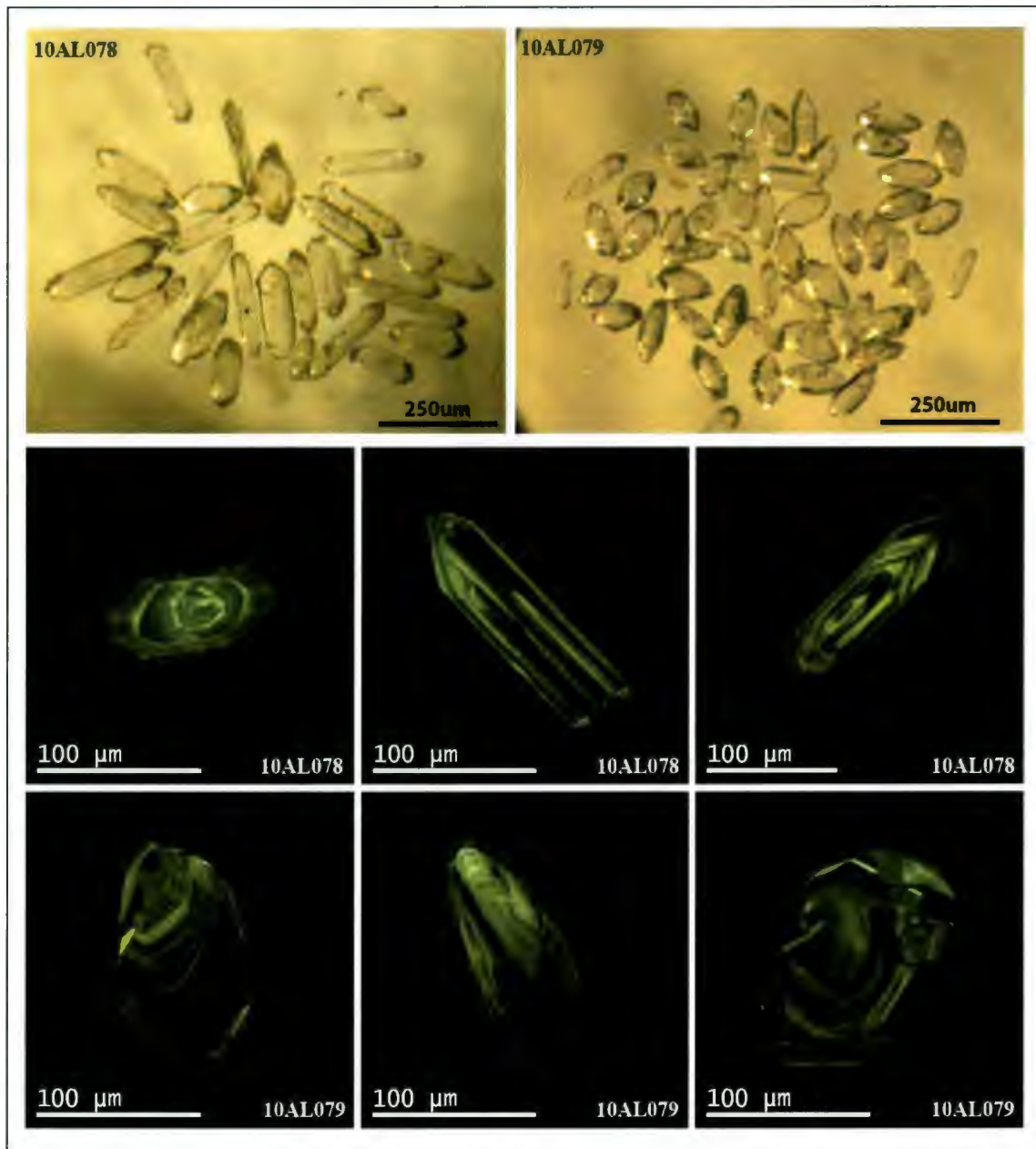


**Figure 4-4: On top, photomicrographs taken in plane polarized light of zircon populations from the two dated samples from the Greenspond road section. On bottom, cathodoluminescence images of zircon grains from the same samples: Sample 10AL078 is from the foliated leucogranite and 10AL079 is from the Al-silicate bearing orthogneiss.**

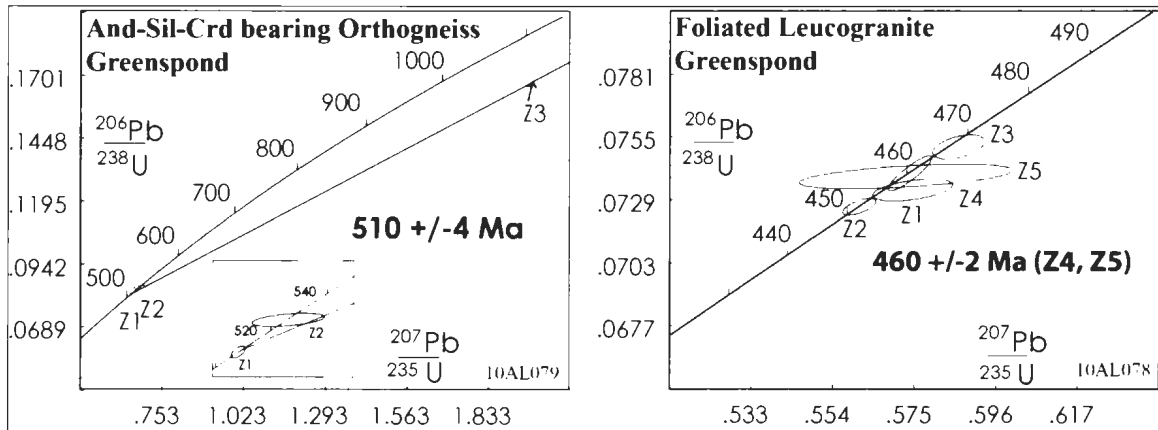


**Figure 4-5: Concordia diagrams for the two geochronology samples from the Greenspond road section.  $^{206}\text{Pb}/^{238}\text{U}$  ages and uncertainties are reported at the 95% confidence interval.**

#### 4.2.2. "I Love You" Road Section

##### 4.2.2.1. Tonalitic Orthogneiss

Tonalitic orthogneiss (10AL097) from the ILU road section contains an abundance of clear zircon grains, ranging from rounded to euhedral (Figure 4-6). Some grains show evidence of separate growth of cores and rims in PPL and CL imaging. These grains, along with rounded grains, were preferentially avoided in analysis. Zircon grains selected for U-Pb geochronology were clear, 2:1, euhedral to subhedral prisms. CL imagery reveals multiple phases of growth within single grains and older cores are commonly identified. Analyzed fractions, Z1, Z2, Z4, Z5 and Z6 are plotted on concordia (Figure 4-7) giving inconclusive, wide spread results and further analysis of single grains from this sample are needed to resolve the age.

#### 4.2.2.2. Tonalite

The zircon population from this unit (10AL096) is predominantly composed of elongate, cracked shards with yellow staining. A small population of clear prisms, prism fragments and tiny rounded grains was also identified. CL imagery reveals shards with complex growth histories commonly containing inclusions, as well as a prism with igneous growth zoning and a dark core, also with inclusions (Figure 4-6). Relatively few grains survived chemical pre-treatment to be used for U-Pb analysis. In total six fractions were analyzed, of which three, Z3, Z5 and Z6, were used to determine a  $^{206}\text{Pb}/^{238}\text{U}$  age of  $415 \pm 1$  Ma, at the 95% confidence interval, with a MSWD of 0.85 (Figure 4-7). These fractions show significant overlap, with Z6 being a single grain analysis. Younger ages, shown by the other analyzed fractions could be a result of Pb-loss and/or the presence of a younger component, such as metamorphic overgrowths.

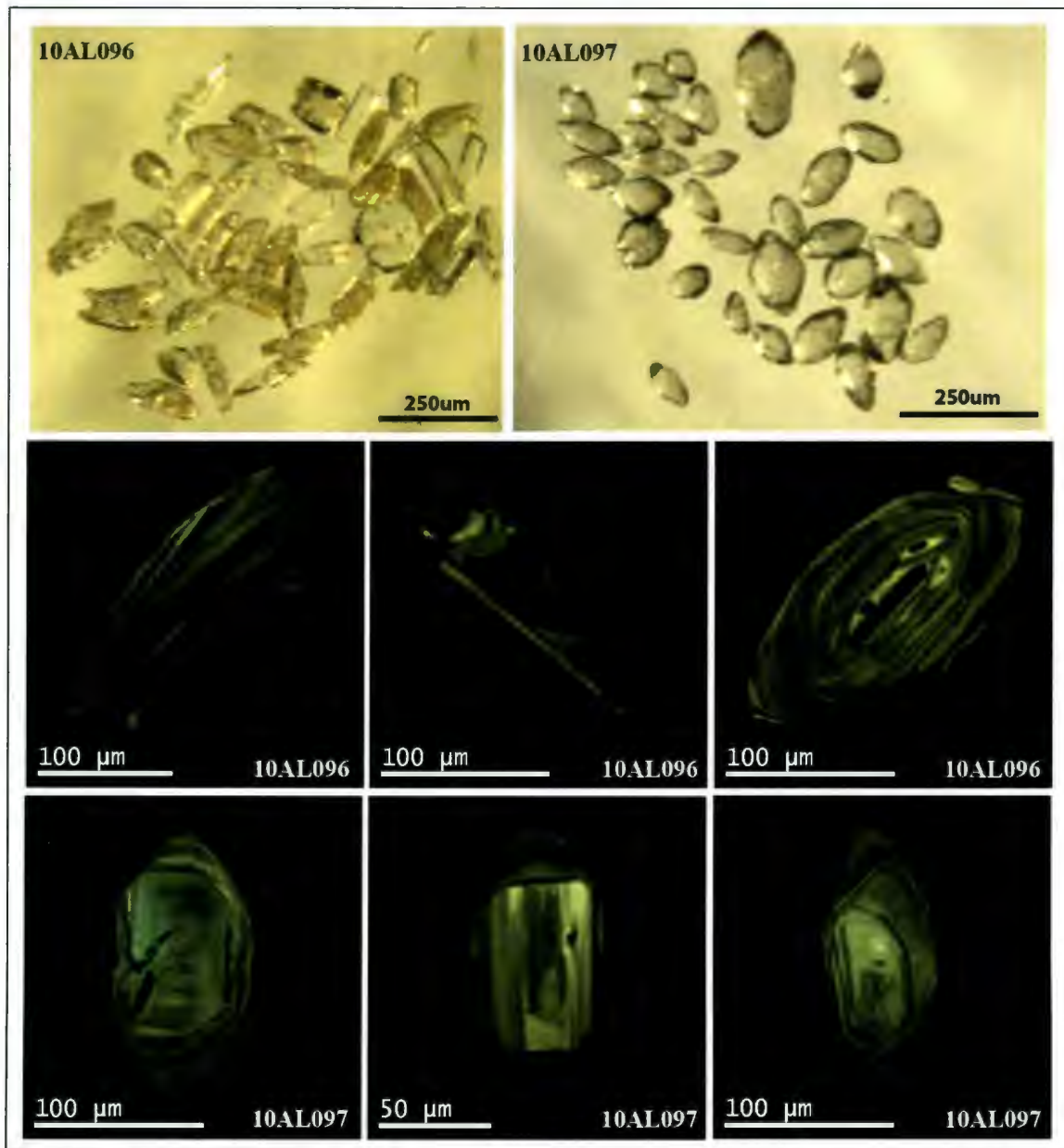


**Figure 4-6: On top, photomicrographs taken in plane polarized light of zircon populations from the two dated samples from the “I Love You” road section. On bottom, cathodoluminescence images of zircon grains from the same samples: Sample 10AL096 is from the tonalite and 10AL097 is from the orthogneiss.**

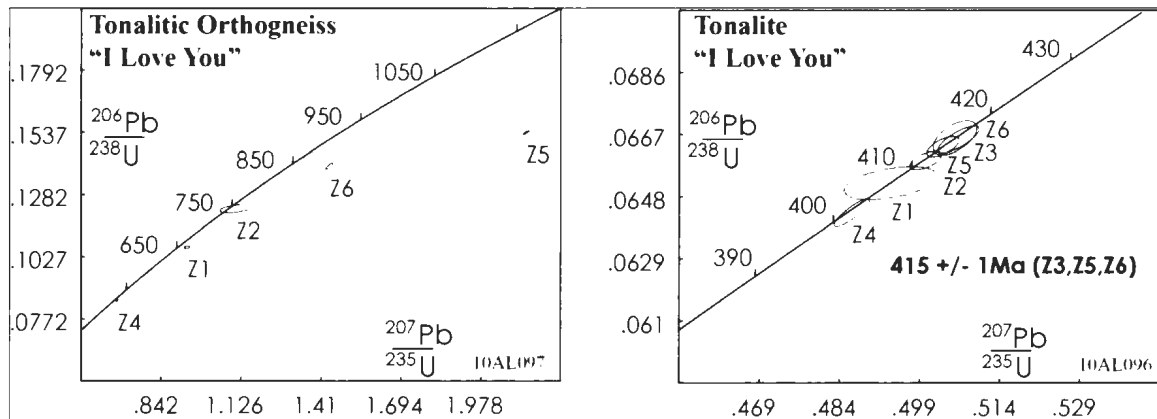


**Figure 4-7: Concordia diagrams for the two geochronology samples from the "I Love You" road section.  $^{206}\text{Pb}/^{238}\text{U}$  ages and uncertainties are reported at the 95% confidence interval.**

### 4.2.3. North of Cape Freels

#### 4.2.3.1. Cape Freels Gneiss

This gneissic unit (10AL093) contained a range of zircon morphologies and sizes, from rounded to prismatic, and from <50 to 250  $\mu\text{m}$  in size. Grains are generally clear and crack and inclusion-free. CL images show cores are present in some grains, but clear igneous growth zoning paired with bright metamorphic overgrowths are the most commonly observed features (Figure 4-8). Three fractions were analyzed from this sample gave variable results. Fractions Z1 and Z3 had concordant results with  $^{206}\text{Pb}/^{238}\text{U}$  ages of 571 and 546 Ma, respectively (Figure 4-9), neither of which can be confidently assigned as an age of the unit. If this unit is not sedimentary in origin it potentially represents the products of an older magmatic event in the northeast Gander zone. However, because of the observed complex cores, diversity within the zircon population,

and thesis time constraints, no further analyses were completed. Further analyses are needed before confidently determining the origin and defining an age for this unit.

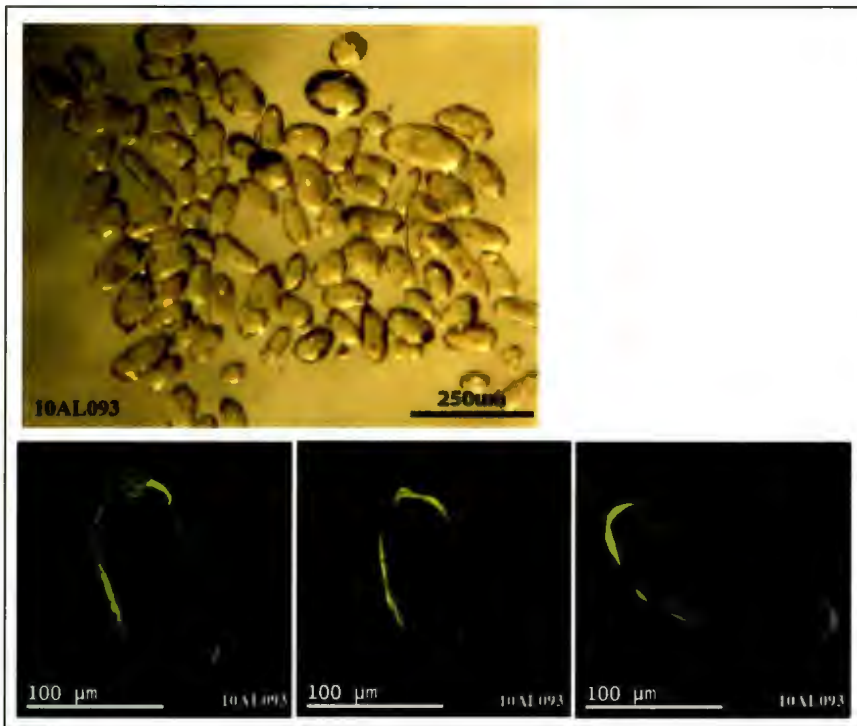


**Figure 4-8: Top, a photomicrograph taken in plane polarized light of the zircon population from the dated sample of the Cape Freels gneiss. Bottom, cathodoluminescence images of zircon grains from the same sample (10AL093).**

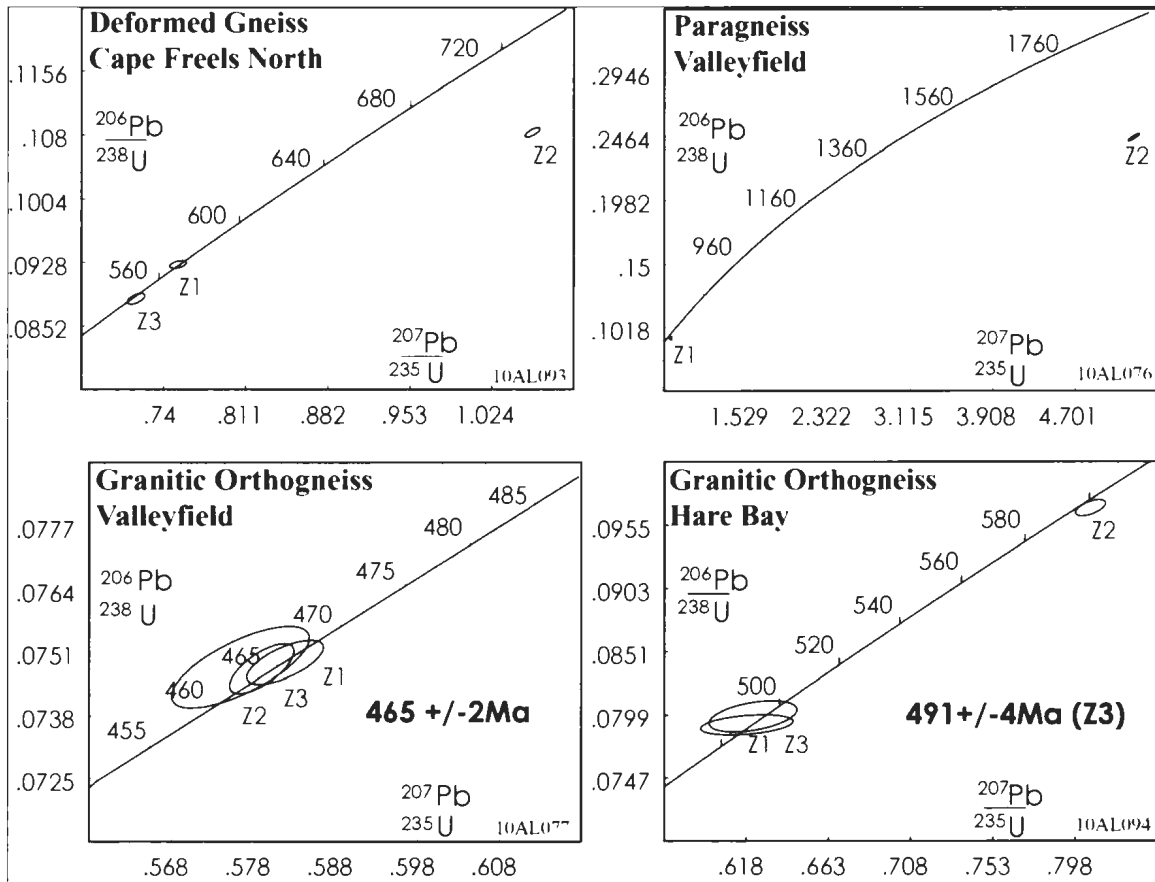


**Figure 4-9: Concordia diagrams for the U-Pb geochronology samples from Cape Freels, Valleyfield and Hare Bay.  $^{206}\text{Pb}/^{238}\text{U}$  ages and uncertainties are reported at the 95% confidence interval.**

#### 4.2.4. Valleyfield Road

##### 4.2.4.1. Valleyfield Paragneiss

To confirm a sedimentary origin, zircon grains from the paragneiss unit in Valleyfield (10AL076) were analyzed. The unit yielded an abundance of clear grains with rounded to euhedral crystal shapes and crystal size ranging from <50-250  $\mu\text{m}$ . CL imaging reveals a predominance of large cores as well as complex growth patterns,

however, some grains contain well-developed igneous growth zones (Figure 4-10). The diversity within the zircon population, support a sedimentary origin for this unit. Two fractions are shown on Figure 4-9, no further analyses were conducted as grains are detrital and, therefore, not useful to this study. The Z1 fraction has a concordant  $^{206}\text{Pb}/^{238}\text{U}$  age of 570 Ma, providing an older age constraint for sedimentation. The Z2 fraction is discordant with evidence of a significantly older component.

#### **4.2.4.2. Valleyfield Orthogneiss**

The orthogneiss sample from Valleyfield (10AL077) yielded three main morphological groups: small (50 $\mu\text{m}$ ), clear, rounded oval-shaped grains, sub-rounded, 2:1, prisms with remnant tips, but lacking defined faces, and clear to turbid 3:1, well-defined prisms with multiple growth zones evident in PPL. The clearest grains of the latter group were targeted for U-Pb geochronology. CL imaging reveals clear igneous growth zones, with inclusions and more complex growth patterns in some grains (Figure 4-10). Analysis of three fractions, Z1, Z2, and Z3 show significant overlap on concordia and gave a  $^{206}\text{Pb}/^{238}\text{U}$  age of  $465 \pm 2$  Ma (95% C.I., MSWD of 0.11) (Figure 4-9).

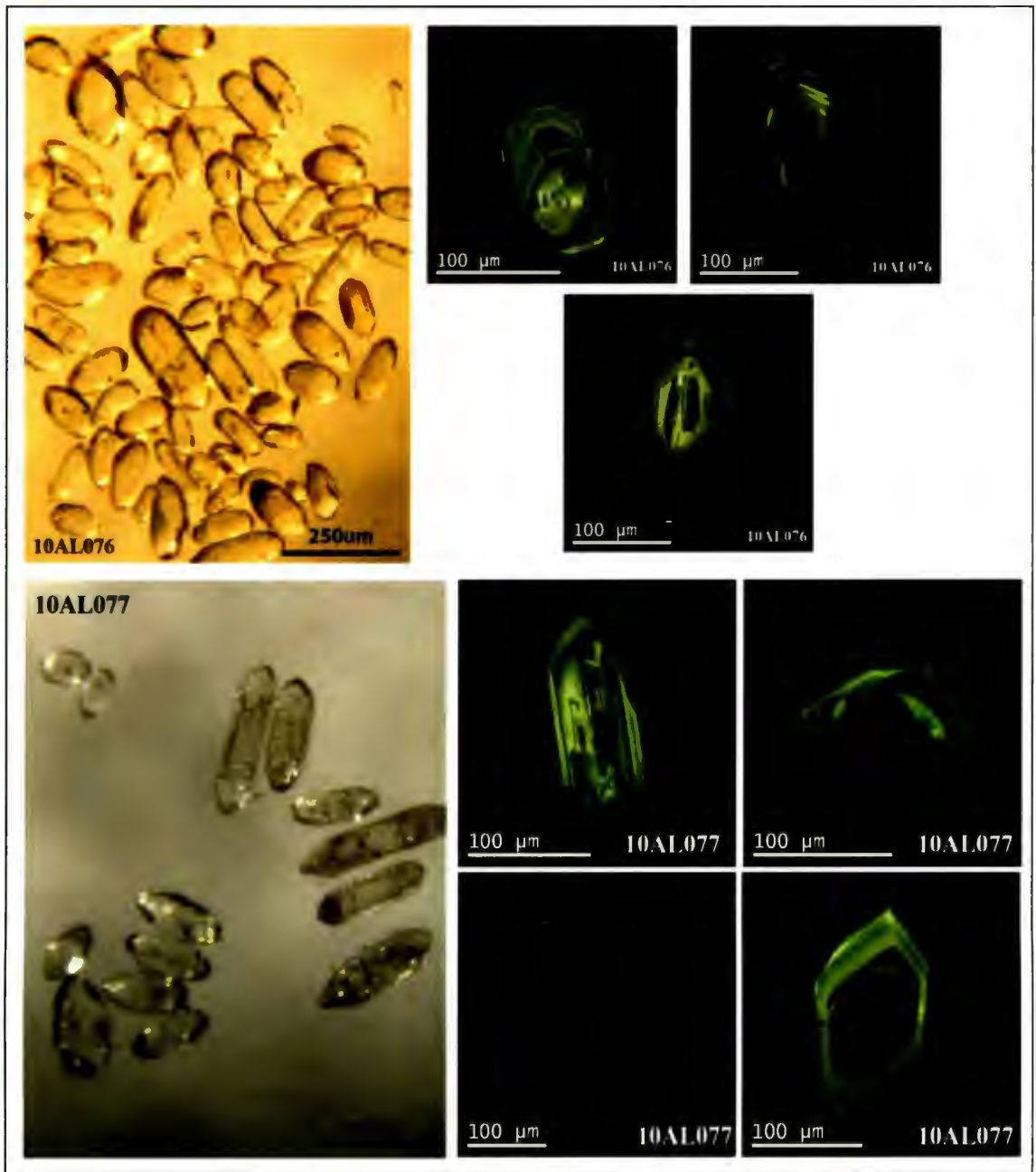


**Figure 4-10: Left, photomicrographs taken in plane polarized light of the zircon population from dated orthogneiss and paragneiss units in Valleyfield. Right, cathodoluminescence images of zircon grains from the same samples: Sample 10AL076 from the Valleyfield paragneiss and 10AL077 from the Valleyfield orthogneiss.**

#### **4.2.5. Town of Hare Bay**

##### **4.2.5.1. Hare Bay Gneiss**

Orthogneiss from Hare Bay (10AL094) contained clear, rounded zircon ranging from 50-100  $\mu\text{m}$  in size and 2:1, clear to turbid, 100 to 200  $\mu\text{m}$  prisms, as well as fragments of both of these types. The best developed clearest prisms were selected for U-Pb analysis. CL imaging shows that many grains possess igneous growth zones and some show an overgrowth rim and/or sector zoning. The rounded grains appear as fragments of larger grains, with zoning truncated by grain boundaries, whereas others appear internally complex (Figure 4-11). Two of three analyzed fractions were used to calculate a  $^{206}\text{Pb}/^{238}\text{U}$  age of  $491 \pm 4$  Ma, at the 95% confidence interval with a MSWD of 1.2. The excluded fraction (Z2) clearly shows evidence of an older component (Figure 4-9).

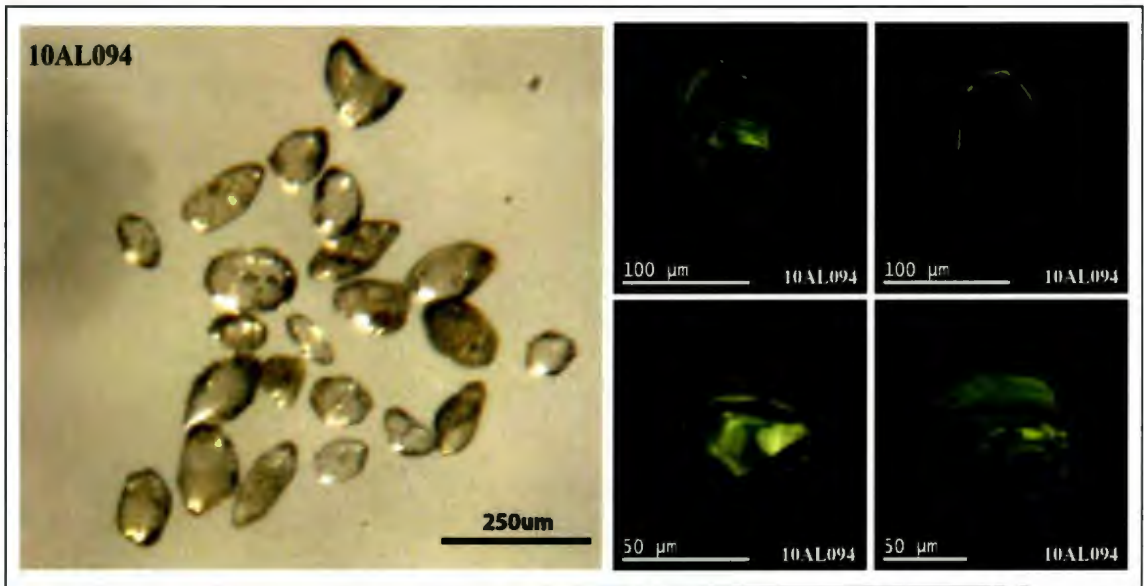


**Figure 4-11: Left, a photomicrograph taken in plane polarized light of the zircon population from the dated Hare Bay orthogneiss sample. Right, cathodoluminescence images of zircon grains from the same sample (10AL094).**

### 4.3 Discussion

#### 4.3.1. Ages within the Hare Bay Gneiss

In the WMB map area the oldest rock unit analyzed using CA-TIMS U-Pb zircon dating is the foliated leucogranite at  $428 \pm 2$  Ma. Although it was clear, based on field relationships that this unit represents one of the earliest phases of magmatism in the area, the relationship between the foliated leucogranite and the adjacent megacrystic granite is ambiguous, as contrasting evidence was observed along the WMB headlands. The megacrystic granite gave a  $^{206}\text{Pb}/^{238}\text{U}$  age of  $420 \pm 1$  Ma, making this intrusion roughly 8 Ma younger than the foliated leucogranite. Both of these rock units represent major phases of magmatism in the field area, occurring as separate nearly parallel sheets.

However, it cannot be discounted that separate sheets of granitic rock grouped into these lithologic units represent different additional ages of magmatism having similar compositions.

The sheet of foliated granodiorite in the WMB map area clearly cuts the foliated leucogranite and the megacrystic granite, representing a younger magmatic event. This was confirmed by the U-Pb age of  $412 \pm 2$  Ma. This unit may correlate in time with the tonalitic dyke (not-dated) of similar composition, but this cannot be confirmed.

The youngest dated unit in WMB is the pegmatite at  $387 \pm 2$  Ma. This supports field evidence as this unit lacks the foliation of adjacent units and commonly obliquely cuts surrounding lithologies. The pegmatite appears as the only unit lacking the predominant foliation observed in the three other units, suggesting that the deformation event responsible for foliation development predated 387 Ma pegmatite emplacement. At least some quartz veins formed post 387 Ma, as they are locally observed cutting across pegmatitic intrusions.

Units occurring exclusively on the western side of the map area, such as mafic units and the layered quartzite unit cannot be placed in time relative to those dated to the east. The contacts with surrounding units are typically highly sheared, or are faults. It is reasonable however to assume units such as the highly sheared megacrystic granite, foliated leucogranite and pegmatite mapped on the western side of the map have the same age relationships as observed in the east, now obscured by intense shearing.

Units dated from the WMB area range from 428 to 387 Ma, indicating a 41 My age gap between the emplacement of the foliated leucogranite and the late pegmatite. The four dated units represent four distinct magmatic events separated in time by 8 to 25 Ma.

The oldest unit dated in the Greenspond Road section is the Al-silicate bearing orthogneiss, at  $510 \pm 4$  Ma, which also makes it the oldest currently recorded magmatic age in the northeast Gander Zone. It was cut, 50 My later, by the emplacement of the foliated leucogranite, dated at  $460 \pm 2$  Ma. Based on a significantly lower Th/U ratio in zircon it is inferred that this leucogranite has a different melt source than other units in the study, perhaps a pooled melt of Gander Group sedimentary rocks. Pegmatite intrusions are mapped cutting the foliated leucogranite, making them younger than 460 Ma and the undeformed granite intrusions lack mineral orientation, therefore they too are younger than 460 Ma. The host orthogneiss is not itself old enough to be considered as potential basement to the Gander Zone, however it may cut a unit that is, as it must intrude older rocks. Such a relationship may not be observable in surface outcrops and it is also possible that this orthogneiss simply cuts the Gander Group sedimentary rocks, which have a maximum age of 560 Ma (O'Neil, 1991). If so, the orthogneiss provides a minimum age for the Gander Group.

Based on field relationships, it is clear that the orthogneiss is the oldest unit in the I Love You road section, however, analysis of several fractions did not yield conclusive results. The tonalite, observed cutting the layered fabric of the orthogneiss, has a U-Pb age of  $415 \pm 1$  Ma. This unit is cut by a leucogranite that is itself cut by late pegmatite,

recording two magmatic events in this section that postdate the 415Ma tonalite emplacement.

The Valleyfield orthogneiss and the Hare Bay orthogneiss both had concordant zircon giving U-Pb ages of  $465 \pm 2$  Ma and  $491 \pm 4$  Ma, respectively. Although lithologically similar, these orthogneiss units represent magmatic events separated by a ca. 26 My age gap. The orthogneiss in Valleyfield is cut by late leucogranite that must postdate 465 Ma.

After analysis of fractions from the Cape Freels gneiss and the Valleyfield paragneiss, some conclusions can be made. Zircon grains from the Valleyfield paragneiss were clearly detrital, supporting field observations and the inferred sedimentary origin of this unit. The youngest “subcordant” detrital zircon age in this unit was ~570 Ma. The origin of the Cape Freels gneissic unit remains unclear, and more analyses are necessary. If this unit is igneous in origin, it may represent an older magmatic event based on data collected thus far.

To summarize, rock units classified as the Hare Bay Gneiss, and dated in this study record multiple magmatic events. The oldest unit dated is the 510 Ma Al-silicate-bearing orthogneiss of the Greenspond Road section, and the youngest dated unit is the 387 Ma pegmatite of the WMB map area. These record over 120 My of magmatism in the northeast Gander Zone. In most cases, U-Pb ages from the various study locations do not correlate with one another and >10 My age differences exist between dated orthogneiss units from different localities.

### 4.3.2. Age Correlations

The new age data provided in this study allows temporal correlations to be made with previously dated units in the northeast Gander Zone, as well as with rocks elsewhere in the Gander Zone, specifically in central and southwest Newfoundland. Figure 4-12 provides a summary of relevant U-Pb ages in the Gander Zone divided based on geographic location and presented along side the new age data from this study.

The occurrence of Cambrian magmatism in the northeast Gander Zone is newly documented through the dating of the  $510 \pm 4$  Ma Greenspond orthogneiss and the  $491 \pm 4$  Ma Hare Bay orthogneiss. The U-Pb zircon age of  $491 \pm 4$  Ma for the Hare Bay orthogneiss roughly correlates in time with the emplacement of gabbro and granite intrusions in southwest Newfoundland. Specifically crystallization ages of the  $495 \pm 2$  Ma Ernie Pond Gabbro dated by O'Brien et al. (1991), and the  $499 +3/-2$  Ma Wild Cove Granite pluton dated by Dunning and O'Brien (1989). The intrusions are both observed to have intruded into Precambrian rocks in southwest Newfoundland, recording Cambrian magmatism within rocks of the Gander Zone. As well, in southwest Newfoundland, Precambrian magmatism is recorded in the Roti Intrusive Suite (578-563 Ma) (Dunning and O'Brien, 1989; O'Brien et al., 1991; Dubé et al., 1995), as well as other intrusive units that cut the Cinq-Cerf Gneiss ( $675 +12/-11$  Ma) (Valverde-Vaquero et al., 2006), however, Precambrian magmatism was not recorded in the units dated in this study.

Middle Ordovician magmatism is recognized in the northeast Gander Zone in the  $460 \pm 2$  Ma Greenspond leucogranite and the  $465 \pm 2$  Ma Valleyfield orthogneiss. These ages correlate approximately in time with each other, and coincide with the timing of the

widely recognized Penobscot Orogeny. The Penobscot Orogeny involved the obduction of the Upper Cambrian (494 Ma) back-arc ophiolites, known as the Coy Pond and Pipestone Pond complexes onto the Gander margin in the Tremadoc to Early Arenig (Colman-Sadd et al., 1992). In the northeast Gander Zone, monazite in the Gander Group was dated at ~460 Ma (Buchanan and Bennett, 2009) and an unpublished age of  $465 \pm 5$  Ma for a granitic orthogneiss sheet in the Hare Bay Gneiss (Dunning, pers comm.), located southeast of the WMB map area, recorded metamorphism and magmatism during the Ordovician. This, along with the new data from this study, confirms that the Penobscot Orogeny affected the study area and the enclosing host lithologies.

In southwest Newfoundland, the Penobscot event is evident through the formation of the Margaree orthogneiss. Various components of the Margaree orthogneiss (474-465 Ma) were dated by Valverde-Vaquero et al. (2000), including a biotite-bearing, granitic orthogneiss (Grandys Brook) with a U-Pb age of  $465 \pm 3$  Ma. In central Newfoundland, Penobscot age granite and related metamorphism mark this event. Colman-Sadd et al. (1992) determined crystallization ages of the Thorough Hill and the Great Burnt Lake granites at  $464 \pm 3$  Ma and  $464 \pm 2$  Ma, respectively. They also dated  $465 \pm 2$  Ma monazite from tonalite and migmatite of the Mount Cormack Subzone, documenting Ordovician metamorphism. Valverde-Vaquero et al. (2006) further documented the Mid-Ordovician tectonic event in the Mount Cormack Subzone in central Newfoundland, with U-Pb metamorphic ages for amphibolite at  $460 \pm 3$  Ma (titanite) and migmatite at  $462 \pm 1$  Ma (monazite).

The U-Pb zircon ages for the WMB foliated leucogranite and megacrystic granite, of  $428 \pm 2$  Ma and  $420 \pm 1$  Ma, respectively, correlate in time with the Silurian Salinic Orogeny (Dunning et al., 1990). The Salinic Orogeny is arguably the most important tectonic event recognized in the Gander Zone marking the Late Ordovician to Silurian closure of the Tetagouche-Exploits back arc basin (van Staal, 1994), and ultimately represents the sinistral collision of Ganderia and Avalonia onto the Laurentian margin. Magmatism associated in time with this event was also studied in detail by D'Lemos and Holdsworth who identified a number of Silurian intrusions of megacrystic granite (Cape Freels Granite, Middle Brook Granite, Dover Fault Granite, etc.). Unpublished U-Pb crystallization ages between 417 and 429 Ma (Dunning, pers. comm.) provide additional time constraints for this Silurian orogenic event. An unpublished migmatite age of  $416 \pm 2$  Ma in the northeast Gander Zone marks a synchronous (within error) anatectic event (Dunning pers. comm.), overlapping with the youngest Silurian granites including the Cape Freels Granite and Lockers Bay Granite. It should be noted that this melting event overlaps in time the Silurian-Devonian boundary and could also be roughly correlated with Devonian magmatism marked by the  $415 \pm 1$  Ma tonalite and  $412 \pm 2$  Ma granodiorite dated in this study. Metamorphism in the northeast Gander Zone during the Silurian is documented by an unpublished monazite age of  $425 \pm 5$  Ma in a tonalitic orthogneiss unit of the Hare Bay Gneiss (Dunning, pers. comm.). The new crystallization ages for granite from this study, together with unpublished granite, migmatite and tonalitic orthogneiss (monazite) ages, document magmatism, metamorphism and melting in the northeast Gander Zone during the Silurian (Figure 4.12).

In southwest Newfoundland, intrusions mapped as part of the Western Head Granite, including a  $432 \pm 1$  Ma mylonitic granite (Valverde-Vaquero et al., 2006), a  $429 \pm 2$  Ma biotite-hornblende granodiorite and a  $430 \pm 2$  Ma quartz-feldspar porphyry (O'Brien et al., 1991), together with the Hawks Nest Pond Porphyry and the Otter Point Granite with identical ages of  $418 \pm 2$  Ma (O'Brien et al., 1991), have also been linked to this Salinic orogenic event. In addition, Valverde-Vaquero et al. (2006) dated titanite from a cross-cutting hornblende porphyritic dyke at  $420 \pm 3$  Ma, which was interpreted to represent a Silurian greenschist facies event in southwest Newfoundland.

The  $412 \pm 2$  Ma, granodiorite from the WMB map area and the  $415 \pm 1$  Ma I Love You tonalite correlate in time with metamorphism recognized elsewhere in the Gander Zone in Newfoundland. In southwest Newfoundland, Dunning (1990) and Valverde-Vaquero et al. (2000) determined the metamorphic age of several units, determining multiple U-Pb titanite ages, all at approximately 410 Ma. Although no major metamorphic event is recognized at this time, previously recognized metamorphism along with the newly dated granodiorite, suggest the possibility that tectono-metamorphic activity documented at ~410 Ma, is widespread. By this time, all of the tectonostratigraphic zones are connected and Devonian magmatism is widely distributed across the Newfoundland Appalachians.

The youngest unit dated unit in the study is the  $387 \pm 2$  Ma pegmatite in the WMB area. This unit correlates in time with another widely recognized event in the history of the Gander Zone, the Acadian Orogeny. The resulting deformation and magmatism is pervasive in rocks of the Gander Zone and commonly overprints earlier fabrics. The

390±3 Ma Chetwynd Granite (O'Brien et al., 1991) in southwest Newfoundland, and the Devonian Lumsden/Dead Man`s Bay and Newport plutons in the northeast Gander Zone are major plutons emplaced during the Acadian Orogeny and these correlate in time with the new pegmatite age in this study. The pegmatite may be an offshoot of the Lumsden granite, whose eastern contact is less than one kilometer from the dated pegmatite.

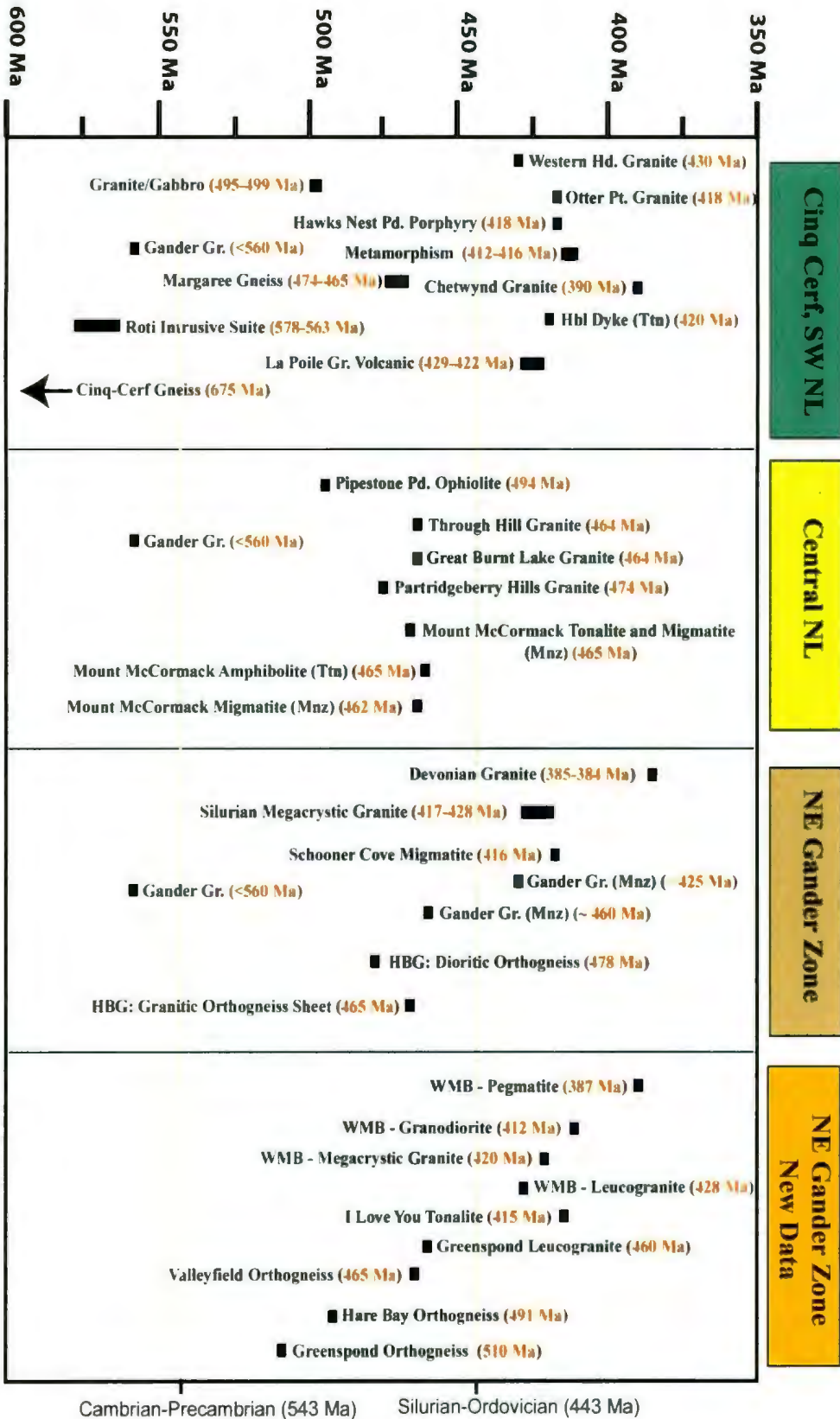


Figure 4-12: Age correlation chart with U-Pb ages of igneous and metamorphic rocks of the Gander Zone in NL. Grey shaded areas represent the Devonian Acadian, Silurian Salinic and Ordovician Penobscot Orogenies.

Cambrian-Precambrian (543 Ma)      Silurian-Ordovician (443 Ma)

**Table 4-2: Age and reference guide for the age correlation chart (Figure 4-12).**

**NORTHEAST GANDER ZONE**

Devonian Rocks

- New Port Granite* (384±3 Ma) Dunning pers. comm.
- Lumsden/ Deadman's Bay Granite* (386±3 Ma) Dunning pers. comm.

Silurian Magmatism and Metamorphism

- Dover Fault Granite* (428±3 Ma) Dunning pers. comm.
- Middle Brook Granite* (427+3/-2 Ma) Dunning pers. comm.
- HBG: Tonalitic Orthogneiss (Monazite)* (425±5 Ma) Dunning pers. comm.
- Gander Group (Monazite)* (-425 Ma) Buchanan and Bennett, 2009
- Lockers Bay Granite* (418±2 Ma) Dunning pers. comm.
- Cape Freels Granite* (417±2 Ma) Dunning pers. comm.
- Schooner Cove Migmatite* (416±2 Ma) Dunning pers. comm.

Ordovician Magmatism and Metamorphism

- HBG: Dioritic Orthogneiss* (478±5 Ma) Dunning pers. comm.
- HBG: Granitic Orthogneiss Sheet* (465±5 Ma) Dunning pers. comm.
- Gander Group (Monazite)* (-460 Ma) Buchanan and Bennett, 2009

Precambrian Rocks

- Gander Group Metasediment* (<560 Ma) O'Neil, 1991

**CENTRAL NEWFOUNDLAND**

Ordovician Magmatism and Metamorphism

- Mount Cormack Amphibolite (Titanite)* (460±3 Ma) Valverde-Vaquero et al., 2006
- Mount Cormack Migmatite (Monazite)* (462±1 Ma) Valverde-Vaquero et al., 2006
- Through Hill Granite* (464+4/-3 Ma) Colman-Sadd et al., 1992
- Great Burnt Lake Granite* (464±2 Ma) Colman-Sadd et al., 1992
- Mount Cormack Tonalite and Migmatite (Monazite)* (465±2 Ma) Colman-Sadd et al., 1992
- Partridgeberry Hills Granite* (474+6/-3 Ma) Colman-Sadd et al., 1992

Cambrian Rocks

- Pipestone Pond Complex* (494+3/-2 Ma) Dunning and Krogh, 1985

Precambrian Rocks

- Gander Group Metasediment* (<560 Ma) O'Neil, 1991

**SOUTHWEST NEWFOUNDLAND**

Devonian Magmatism and Metamorphism

- Chetwynd Granite* (390±3 Ma) O'Brien et al., 1991
- Margaree Orthogneiss (Titanite in several units)* (-410-415 Ma) Dunning et al., 1990, Valverde-Vaquero et al., 2000

Silurian Magmatism and Metamorphism

- Hawks Nest Pond Porphyry* (418±2 Ma) O'Brien et al., 1991
- Otter Point Granite* (418±2 Ma) O'Brien et al., 1991
- Hornblende Dyke (Titanite)* (420±3 Ma) Valverde-Vaquero et al., 2006
- La Poile Group Volcanic Units* (429-422 Ma) O'Brien et al., 1991
- Western Head Granite* (-430 Ma) O'Brien et al., 1991 and Valverde-Vaquero et al., 2006

Ordovician Magmatism

- Margaree Orthogneiss* (-474-465 Ma) Valverde-Vaquero et al., 2000

Cambrian Magmatism

- Ernie Pond Gabbro* (495±2 Ma) O'Brien et al., 1991
- Wild Cove Granite* (499+3/-2 Ma) Dunning and O'Brien, 1989

Precambrian Rocks

- Roti Intrusive Suite* (578-566 Ma) Dunning and O'Brien, 1989, O'Brien et al., 1991, Dubé et al., 1995
- Whittle Hill Sandstone* (585 Ma) Dubé et al., 1995
- Cinq-Cerf Gneiss* (675+12/-11 Ma) Valverde-Vaquero et al., 2006

## 5. CHAPTER 5: DISCUSSION AND CONCLUSIONS

### 5.1 Importance of the Hare Bay Gneiss

Previous literature describes the Hare Bay Gneiss as three discontinuous northeast trending belts comprised of a highly deformed assemblage of paragneiss, orthogneiss and migmatite. Past interpretations of the Hare Bay Gneiss include that it is a highly deformed equivalent of the adjacent Square Pond Gneiss (Blackwood, 1978), and some studies (Blackwood and Kennedy, 1975) proposed it as potential basement to the Gander Zone. The diversity of rock types, complexity of relationships and degree of deformation in the Hare Bay Gneiss has been documented in previous studies and Holdsworth (1991) provided a brief description of distinct lithologic units within the Hare Bay Gneiss based on field observations. However, no modern analytical work had focused on the Hare Bay Gneiss prior to the present study and therefore little petrographic and geochemical data were previously available. No published geochronology data has been reported other than outdated  $^{40}\text{Ar}/^{39}\text{Ar}$  cooling ages for mica, which in any case would not represent protolith ages. This study has combined detailed mapping and new geochemical and age data using modern analytical techniques in an effort to further characterize the Hare Bay Gneiss and to reinterpret the importance of this unit.

## **5.2 Summary of Findings**

### **5.2.1. Lithologic Units**

Prior to this study the most detailed description of the varying lithologies comprising the Hare Bay Gneiss were those documented by Holdsworth (1991), describing three distinct divisions, including metasedimentary rocks and amphibolite, mobilized gneiss and orthogneiss. During reconnaissance work for this study, outcrops of the described metasedimentary rocks and mobilized gneiss (migmatite) were identified in specific locations including east of the WMB map area, along Greenspond Road and south of the town of Hare Bay, however, these areas were not further mapped in detail. The selected study areas generally focus on the igneous and meta-igneous rocks mapped as part of the Hare Bay Gneiss.

Through detailed field mapping and petrographic analysis it is evident that a diverse assemblage of rocks constitutes northern exposures of the Hare Bay Gneiss. Based on the selected study localities the northern belt of the Hare Bay Gneiss predominantly consists of greenschist-facies orthogneiss ranging from granitic to tonalitic composition, and the unit includes locally abundant, variably deformed granitic intrusions. The mapped area of the Hare Bay Gneiss contains several minor units including tonalite, paragneiss, pegmatite, mafic intrusions, and quartz veins. Although unit relationships were documented within a single outcrop, correlations between lithologically similar units, and correspondence of sequences of magmatic events between study locations, was not possible in the field.

Rocks belonging to the Hare Bay Gneiss in the WMB map area appear to constitute a sheeted intrusive complex rather than "gneiss". Based on mineralogy this complex experienced greenschist-facies metamorphism; it is highly sheared, and although the contact relationships are typically obscured, some original relationships were observed. Eleven lithologic units were defined in the map area and of these, sheets of foliated leucogranite and megacrystic granite are predominant. These units are clearly cut by a granodiorite sheet and a tonalitic dyke. Late pegmatite intrusions and quartz veins are observed locally cutting the fabrics defined by older units showing they are the youngest discernible units in the area. Rocks observed in minor abundance, such as the mafic and layered quartz units, are confined to the western side of the map area where intense shearing has obscured relationships between adjacent units; therefore, their relative ages are undetermined.

The dominant unit of the Greenspond Road section is an Al-silicate-bearing orthogneiss that is granitic in composition, is oversaturated in alumina, and contains biotite and muscovite in addition to the Al-silicates. Based on petrographic observations the Al-silicates are inferred to be products of magmatic crystallization processes, rather than being fluid-derived or a function of metamorphic grade. The host orthogneiss, cross-cutting foliated leucogranite, as well as late pegmatite and undeformed granite intrusions clearly represent separate magmatic events, with obvious relative ages. The abundance of Al-silicates, gradational contacts, and tonalitic enclaves differentiate this section from other mapped areas.

Road sections and brief traverses (Trinity, "I Love You", Valleyfield and Hare Bay locations) documented the predominance of orthogneiss hosts were documented, some of which are cut by granitic intrusions and late pegmatite (Trinity, "I Love You" and Valleyfield). Mapped orthogneiss and granite all have greenschist-facies mineral assemblages and are alumina-rich, containing variable amounts of biotite and muscovite, with some granite intrusions containing igneous garnet. Pegmatite intrusions are also Al-rich and are observed to locally contain igneous muscovite, garnet, tourmaline and pyrite. The "I Love You" road section is unique in that it contains a host orthogneiss cut by a tonalite that is cut by later leucogranite. The tonalite is unique to this outcrop, is relatively undeformed, and exhibits orthoclase-rich contacts with aplite veins, as well as orthoclase-rich rims surrounding titanite oikocrysts.

The presence of paragneiss is documented in Valleyfield but the relationship with the surrounding orthogneiss is not clear. The complexly folded Cape Freels gneiss is unique to its location and its origin is not obvious. It is Al-rich, containing an abundance of biotite and muscovite, and has minor sillimanite documenting high grade metamorphism.

### **5.2.2. Geochemical Signatures**

Field observations and QAP modal mineral plots were used to classify the majority of sampled units: these range from granitic to tonalitic in composition. Based on Shand's (1927) classification diagram, all sampled granite and orthogneiss units in this

study have similar peraluminous compositions, agreeing with the commonly observed mineralogy of biotite, muscovite and  $\pm$ garnet. The same samples show multi element patterns diagnostic of crustal melts, with LREE enrichment relative to HREE and negative Nb and Ti anomalies. The geochemical signatures, along with observed mineralogy, implies that melting of a sedimentary source is needed to generate the granite and orthogneiss in the Hare Bay Gneiss. An exception to these geochemical attributes is in the pegmatite from WMB map area that has an unusual concave-up REE pattern, likely due to accessory phase gains and losses.

Mafic units from the WMB, Cape Freels and Trinity areas plot as basalt or alkali basalt on the classification diagram of Pearce (1996). The actinolite-biotite mafic unit and a diabase dyke sampled north of Cape Freels show similar flat REE trends with a subtle negative Nb anomaly and minor positive Zr and Ti anomalies. In contrast, the biotite-carbonate-bearing mafic unit from WMB and the amphibole-bearing intermediate unit in the Trinity section have REE trends with significant enrichment of the LREE relative to the HREE, steeply sloping LREE and HREE patterns, as well as prominent negative Nb anomalies.

Although slight variations exist between individual samples, they are not consistently distinct; therefore geochemical trends alone are not enough to differentiate mapped lithologic units or groups within units. However, it was noted that in all instances where both a host orthogneiss and a cross-cutting leucogranite were analyzed (Greenspond, Trinity, "I Love You") the incompatible trace elements of the younger granite are relatively depleted, with respect to the orthogneiss.

### 5.2.3. U-Pb Age Relationships

The oldest unit dated in the study was the  $510 \pm 4$  Ma Al-silicate-bearing orthogneiss from the Greenspond Road Section. This unit is interpreted to be too young to represent basement to the Gander Zone, however, it is currently the oldest granitoid intrusion dated in the northeast Gander Zone. Cambrian magmatism is also documented through dating of the  $491 \pm 4$  Ma Hare Bay orthogneiss, which also is older than previously dated intrusive units in the area.

Ordovician units dated in this study include the  $465 \pm 2$  Ma Valleyfield orthogneiss and the  $460 \pm 2$  Ma Greenspond foliated leucogranite. These units are granitic, contain two micas, are peraluminous based on Shand's index and have trace element patterns typical of crustal melts. These units further document intrusive events into the Gander Group sedimentary rocks throughout the Ordovician, although contrasting Th/U ratios imply that the two units have different melt sources.

Units dated in the WMB map area are Silurian to Middle Devonian in age and clearly represent intrusive sheets as opposed to "gneiss". The oldest units mapped in WMB are the Silurian  $428 \pm 2$  Ma and  $420 \pm 1$  Ma foliated and megacrystic granite, respectively. The youngest unit dated is the  $387 \pm 2$  Ma pegmatite, appearing relatively undeformed and post-deformation. This unit is likely an offshoot of the nearby Lumsden/Deadman's Bay Granite dated at  $386 \pm 3$  Ma (Dunning, pers. comm., 2012). It may also be speculated that the undeformed granite in the Greenspond section to the south, which was not dated in this study, also represents a post deformation intrusion and is an offshoot of the nearby Newport Granite of similar Devonian age.

The ages determined in this study show little mutual overlap, rather they record multiple magmatic events that span over 120 Myr. The new ages of magmatism determined in this study can be correlated with previously determined U-Pb ages in the surrounding northeast Gander Zone, as well other areas in which the Gander Zone was studied including central and southwest Newfoundland. Notably the ages can be correlated with magmatism associated with the Middle Ordovician Penobscot Orogeny, Silurian Salinic Orogeny and Devonian Acadian Orogeny, all of which are recognized in other areas of the Gander Zone.

### **5.3. New Interpretation of the Hare Bay Gneiss**

The presence of migmatitic and metasedimentary rocks mapped as part of the Hare Bay Gneiss near Greenspond Island and south of Hare Bay has been well documented in previous work. It has been speculated that these units represent high-grade metamorphic equivalents of the Gander Group metasedimentary rocks. These units were not studied as a part of this thesis; rather the focus is on igneous and meta-igneous rocks in selected locations that have been included previously as part of the Hare Bay Gneiss in the northeastern Gander Zone.

It is clear that the units mapped in this study are not simply highly deformed and metamorphosed equivalents of the adjacent Gander Group metasedimentary rocks. All orthogneiss and granitic samples show mineralogical and geochemical characteristics that classify them as “S-type”, peraluminous igneous rocks. The abundance of Al-rich

magmatism in the area requires a sedimentary source that may involve melting of the adjacent Gander Group, although the exact sedimentary source cannot be determined based on data collected in this study.

No rocks dated in this study are old enough to be interpreted as basement to the Gander Zone, however the possibility that an as-yet undated unit in the area may represent basement cannot be discounted. Dated units cover a wide range spanning Cambrian to Devonian periods, revealing distinct magmatic events that have produced magmas of very similar composition. These rocks, in many cases, cannot be distinguished in the field. The ages determined in this study are consistent with ages of units dated in previous work in the northeast Gander Zone as well as in central and southwest Newfoundland. Importantly, the ages of dated units correlate in time with the widely recognized Ordovician Penobscot, Silurian Salinic, and Devonian Acadian Orogenies.

The mapped Hare Bay Gneiss is therefore ripe for re-definition, as many of the rocks included in it are not gneissic and are essentially further examples of plutons related to orogenic events that are already well documented in the Newfoundland Appalachians.

#### **5.4. Key Points**

► In the studied localities, the Hare Bay Gneiss can be described as tonalitic to granitic intrusive and gneissic units, locally with minor metasedimentary, mafic and pegmatitic components.

- ▶ Dated Hare Bay Gneiss units show ca. 120 Myrs of magmatism from mid-Cambrian to mid-Devonian.
- ▶ Granitic and orthogneiss units dated at ca. 460 and 465 Ma correlate in time with the Penobscot Orogeny, whereas granitic units dated at ca. 428 and 420 Ma correlate with events of the Salinic Orogeny, and the 387 Ma pegmatitic unit correlates in time with the Acadian Orogeny, all events are well documented elsewhere in the Gander Zone in Newfoundland.
- ▶ Many of the units have very similar geochemistry, typical of melts of sedimentary crustal material, with nearly all samples having peraluminous compositions and negative Nb anomalies.
- ▶ None of the dated units are old enough to be basement to the Gander Zone.
- ▶ The Hare Bay Gneiss is not simply a high-grade metamorphic equivalent to the adjacent Square Pond Gneiss or Gander Group.

## References

- Andrews, P. W., 1985, Structural Analysis of the Cape Freels Shear Zone northeastern Gander Zone Newfoundland, Bachelor of Science (Hons.) Thesis, Memorial University of Newfoundland, St. John's NL, p. 108.
- Blackwood, R. F., and Kennedy, M. J., 1975, The Dover Fault: western boundary of the Avalon Zone in northeastern Newfoundland. *Canadian Journal of Earth Sciences*, vol. 12, p. 320-325.
- Blackwood, R. F., 1997, Geology of the east half of the Gambo (2D/16) map area and the northwest portion of the St. Brendan's (2C/13) map area, Newfoundland, Geological Survey Branch Department of Mines and Energy Government of Newfoundland and Labrador, Report 77-5, p. 20.
- Buchanan, C. and Bennett, V. 2009. Implications of new geochronology for the tectonometamorphic history of the northern Gander Zone. CIM/GSNL Open House, Poster Session.
- Chappell, B. W., and White, A.J.R., 1974, Two contrasting granite types. *Pacific Geol.* 8, p. 173-174.
- Chappell, B.W., and White, A.J.R., 1984, I- and S-type granites in the Lachlan Fold Belt, southeastern Australia. In: Keqin, X., Guangchi, T. (Eds.), *Geology of Granites and Their Metallogenic Relations*. Science Press, Beijing, p. 87-101.
- Colman-Sadd, S. P., Dunning, G. R., and Dec, T., 1992, Dunnage-Gander relationships and Ordovician Orogeny in central Newfoundland: a sediment provenance and U-Pb age study. *American Journal of Science*, 292, p. 317-355.
- Corfu, F., Hanchar, J.M., Hoskin, P.W.O., Kinny, P., 2003, Atlas of Zircon Textures, *In* Hanchar, J.M., Hoskin, P.W.O. (Eds), *Zircon, Review in Mineralogy and Geochemistry*, Vol. 53, p. 469-500.
- Dallmeyer, R. D., Blackwood, R. F. and Odom, A. L., 1981, Age and origin of the Dover Fault: tectonic boundary between the Gander and Avalon Zones of the northeastern Newfoundland Appalachians. *Canadian Journal of Earth Sciences*, v.18, p. 1431-1442.
- Dimitrov, I., 2007, The Silurian Salinic Disturbance — newly discovered orogenic event in the northern Appalachians, *Geologica Balcanica*, 36, 3-4, p. 97-102.

- D'Lemos, R. S., and Holdsworth, R. E., 1995, Samarium–neodymium isotopic characteristics of the northeastern Gander zone, Newfoundland Appalachians. *Current perspectives in the Appalachian–Caledonian Orogen: Geological Association of Canada, Special Paper 41*, p. 239-252.
- D'Lemos, R. S., Tribe, I. R., and Pembroke, J. W., 1995, Emplacement and construction of Devonian 'postectonic' granites northeast Newfoundland Appalachians. Newfoundland Department of Natural Resources, *Current Research, Report 95-1*, p. 221-235.
- D'Lemos, R. S., Schofield, D. I., Holdsworth, R. E., and King, T. R., 1997, Deep Crustal and Local Rheological Controls on the Siting and Reactivation of Fault and Shear Zones, Northeastern Newfoundland. *Journal of the Geological Society, London*, vol. 154, p. 117-121.
- Dubé, B., Dunning, G. R., Lauzière, K., 1995, Geology of the Hope Brook Mine, Newfoundland, Canada: A preserved Late Proterozoic high-sulphidation epithermal gold deposit and its implications for exploration. *Economic Geology*, v. 93, p. 405-436.
- Dubé, B., Dunning, G. R., Lauzière, K., and Roddick, J. C., 1996, New insights into the Appalachian Orogen from geology and geochronology along the Cape Ray fault zone, southwest Newfoundland. *Geological Association of America Bulletin*, 108, p. 101-116.
- Dunning, G. R., and O'Brien, S. J., 1989, Late Proterozoic–early Paleozoic crust in the Hermitage flexure, Newfoundland Appalachians: U-Pb ages and tectonic significance. *Geology*, v. 17, no. 6, p. 548–551.
- Dunning, G. R., O'Brien, S. J., Colman-Sadd, S. P., Blakewood, R. F., Dickson, W. L., O'Neil, P. P., and Krough, T. E., 1990, Silurian orogen in the Newfoundland Appalachians. *Journal of Geology*, vol. 98, p. 895-913.
- Goodwin, L. B. and O'Neil, P. P., 1991, The structural evolution of the northern segment of the Dunnage Zone-Gander Zone boundary, Newfoundland. *Current Research, Report 91-1*, p. 97-107.
- Gradstein, F. M., Ogg, J. G., Ogg, G., and Schmitz, M., 2012, *The geological time scale 2012*. Elsevier Publishing.
- Hanchar, J. M., Miller, C. F., 1993, Zircon zonation patterns as revealed by cathodoluminescence and backscattered electron images: Implications for interpretation of complex crustal histories, *Chemical Geology*, vol. 110, p. 1-13.

- Hibbard, J. P., van Staal, C. R., Rankin, D. W., 2007, A comparative analysis of pre-Silurian crustal building blocks of the northern and the southern Appalachian Orogen. *American Journal of Science*, vol. 307, pp. 23-45.
- Holdsworth, R. E., 1991, The geology and structure of the Gander-Avalon boundary zone in northeastern Newfoundland. Newfoundland Department of Mines and Energy, Current Research, Report 91-1, pp. 109-126.
- Holdsworth, R. E., D'Lemos, R. S., McErlean, M. A. and O'Brien, S. J., 1993, Deformation of the Cape Freels Granite related to dextral displacements along the Dover Fault, northeast Newfoundland. Current Research, Report 93-1, p. 221-228.
- Jaffey, A. H., Flynn, K. F., Glendenin, L. E., Bentley, W. C. and Essling, A. M., 1971, Precision measurement of half-lives and specific activities of  $^{235}\text{U}$  and  $^{238}\text{U}$ . *Phys. Rev.*, v.4, p. 1889.
- Jayasinghe, N. R., 1979, Granitoids of the Wesleyville area in northeastern Newfoundland: A study of their evolution and geological setting, PhD Thesis, Memorial University of Newfoundland, St. John's NL, p. 350.
- Jenner, G. A., 1996, Trace element geochemistry of igneous rocks: geochemical nomenclature and analytical geochemistry, in Wyman, D., ed., Trace element geochemistry of volcanic rocks: applications for massive-sulphide exploration: Geological Association of Canada, Short Course Notes, v. 12, p. 51-77.
- Kennedy, M. J., 1976, Southeastern margin of the northeastern Appalachians: Late Precambrian orogeny on a continental margin. *Geological Society of America Bulletin*, v.87, p. 1317-1325.
- Krogh, T. E., 1973, A low-contamination method of hydrothermal decomposition of zircon and extraction of U and Pb for isotopic age determinations. *Geochimica et Cosmochimica Acta*, v.37, no.3, p. 485-494.
- Krogh, T. E., Davis, G. L., 1975, The production and preparation of  $^{205}\text{Pb}$  for use as a tracer isotope dilution analyses. *Carnegie Inst. Washington Yearbook*, vol. 74, p. 416-417.
- Mattinson, J. M., 2005, Zircon U-Pb chemical abrasion (CA-TIMS) method; combined annealing and multi-step partial dissolution analysis for improved precision and accuracy of zircon ages. *Chemical Geology*, v. 220, p. 47-66.
- Murphy, J. B., Gutierrez-Alonso, G., Nance, R. D., Fernandez-Suarez, J., Keppie, J. D., Quesada, C., Strachan, R. A., Dostal, J., 2006, Origin of the Rheic Ocean.: Rifting along a Neoproterozoic suture? *Geology*, v. 34, p. 325-328.

- Murphy, J. B., Keppie, J. D., Nance, R. D., Dostal, J., 2010, Comparative evolution of the Iapetus and Rheic oceans: A North America perspective. *Gondwana Research*, v. 17, p. 482-499.
- Nance, R. D., Gutierrez-Alonso, J., Keppie, D. J., Linnemann, U., Murphy, J. D., Quesada, C., Strachan, R. A., Woodcock, N.H., 2009, Evolution of the Rheic Ocean. *Gondwana Research*, vol. 17, p. 194-222.
- O'Brien, B. H., O'Brien, S. J., and Dunning, G. R., 1991, Silurian cover, Late Precambria-Early Ordovician basement, and the chronology of Silurian orogenesis in the Hermitage Flexure (Newfoundland Appalachians). *American Journal of Science*, v. 291, p. 760-799.
- Ohnenstetter, D., Cesbron, F., Remond, G., Caruba, R., Claude, J.M., 1991, Emissions de cathodoluminescence de deux populations de zircons naturels: tentative d'interprétation: *Comptes Rendues de Academie des Sciences Serie II Fascicule A: Sciences de la Terre et des planets*, v. 313, p. 641-647.
- O'Neil, P. P. and Blackwood, R. F., 1989, A proposal for the revised stratigraphic nomenclature of the Gander and Davidsville Groups and the Gander River Ultramafic Belt, of northeastern Newfoundland. Newfoundland Department of Natural Resources, Current Research, Report 89-1, p. 127-130.
- O'Neil, P. P. and Lux, D., 1989, Tectonothermal history and  $^{40}\text{Ar}/^{39}\text{Ar}$  geochronology of northeastern Gander Zone, Weir's Pond area (2E/1). Newfoundland Department of Natural Resources, Current Research, Report 89-1, p.131-139.
- O'Neil, P. P., 1991, Geology of the southeastern part of the Gander Lake map area (NTS 2D/15) and the southwestern part of the Gambo map area (NTS 2D/16). Newfoundland Department of Natural Resources, Current Research, Report 91-1, p. 167-174.
- O'Neil, P. P., 1991, Geology of the Weir's Pond area, Newfoundland (NTS 2E/1), Geological Survey Branch Department of Mines and Energy Government of Newfoundland and Labrador, Report 91-3.
- O'Neil, P. P., Colman-Sadd, S. P., 1993, Geology of the Eastern Part of the Gander (NTS 2D/15) and Western Part of the Gambo (NTS 2D/16) Map Areas, Newfoundland, Geological Survey Branch Department of Mines and Energy Government of Newfoundland and Labrador, Report 93-2.
- Parrish, R. R., Noble, S. R., 2003, Zircon U-Th-Pb geochronology by isotope dilution-thermal ionization mass spectrometry (ID-TIMS), *In* Hanchar, J.M., Hoskin,

- P.W.O. (Eds), Zircon, , Review in Mineralogy and Geochemistry, Vol. 53, p. 183-213.
- Pearce, J. A., 1996, A users guide to basalt discrimination diagrams. In:Wyman, D. A. (eds) Trace Element Geochemistry of Volcanic Rocks: Applications for Massive Sulphide Exploration. Geological Association of Canada, Short Course Notes 12, p. 79-113.
- Potts, P. J., 1987, A Handbook of Silicate Rock Analysis, Chapman & Hall, p. 622.
- Sanchez-Garcia, T., Bellido, F., Quesada, C., 2003, Geodynamic setting and geochemical signatures of Cambrian-Ordovician rift-related igneous rocks. Tectonophysics, v. 365, p. 233-255.
- Shand, S. J., 1927, On the relations between silica, alumina, and the bases in eruptive rocks, considered as a means of classification. Geological Magazine, v. 64, p. 446-449.
- Stacey, J. S. and Kramers, J. D., 1975, Approximation of terrestrial lead isotope evolution by a two-stage model. Earth and Planetary Science Letters, v. 26, no. 2, p. 207-221.
- Sun, S. S. and McDonough, W. F., 1989, Chemical and isotopic systematics of oceanic basalts; implications for mantle composition processes. Geological Special Publications, v. 42, p. 313-345.
- Swinden, H. S, and Jenner, G. A., 1992, Volcanic stratigraphy northwest of New Bay Pong, central Newfoundland, and the strike-extent of the Point Leamington massive sulfide horizon: Newfoundland geology Branch, Current Research, Report 92-1, p. 315-345.
- Taylor, S. R. and McLennan, S. M., 1985, The continental crust: Its composition and evolution. Blackwell, Oxford.
- Valverde-Vaquero, P., Dunning, G. R., van Staal, C. R., 2000, The Margaree orthogneiss: an Ordovician, peri-Gondwanan, mafic-felsic igneous complex in southwestern Newfoundland. Canadian Journal of Earth Science, 37, p. 1691-1710.
- Valverde-Vaquero, P., Dunning, G. R., O'Brien, S. J., 2006a, Polycyclic evolution of the Late Neoproterozoic basement in the Hermitage Flexure region (southwest Newfoundland Appalachians): New evidence from Cinq-Cerf gneiss. Precambrian Research 148, p. 1-18.

- Valverde-Vaquero, P., van Staal, C. R., McNicoll, V., and Dunning, G. R., 2006b, Mid-Late Ordovician magmatism and metamorphism along the Gander margin in central Newfoundland: *Journal of the Geological Society of London*, v. 163, no. 2, p. 347-362,
- van Staal, C. R., 1994, Brunswick subduction complex in the Canadian Appalachians: Record of the Late Ordovician to Late Silurian collision between Laurentia and the Gander margin of Avalon. *Tectonics*, v. 13, p. 946-962.
- van Staal, C. R., 2005, The Northern Appalachians. *In Encyclopedia of geology. Edited by R.C. Selley, L. Robin, M. Cocks, and I.R. Plimer. Elsevier, Oxford, UK., vol. 4, pp. 81-91.*
- van Staal, C. R., 2007, Pre-Carboniferous tectonic evolution and metallogeny of the Canadian Appalachians. *Mineral Deposits of Canada: A Synthesis of Major Deposit-Types, District Metallogeny, the Evolution of Geological Provinces, and Exploration Methods: Geological Association of Canada, Mineral Deposits Division, Special Publication No. 5, p. 793-818.*
- van Staal, C. R., Dewey, J. F., Mac Niocaill, C., and McKerrow, W. S., 1998, The Cambrian-Silurian tectonic evolution of the northern Appalachians: history of a complex southwest Pacific-type segment of Iapetus. *Geological Society, London, Special Publication*, v. 143, p. 197-242.
- van Staal, C. R., Sullivan, R. W., and Whalen, J. B., 1996, Provenance of the tectonic history of the Gander Zone in the Caledonian / Appalachian Orogen; implications for the origin and assembly of Avalon. *Geological Society of America Special Paper*, v. 304, p. 347-367.
- van Staal, C. R., Whalen, J. B., Valverde-Vaquero, P., Zagorevski, A., Rogers, N., 2009, Pre-Carboniferous, episodic accretion-related, orogenesis along the Laurentian margin of the northern Appalachians. *Geological Society of London*, vol. 327 pp.271-316.
- Williams, H., 1964, The Appalachians in northeastern Newfoundland; a two-sided symmetrical system. *American Journal of Science*, vol. 262, p. 1137-1158.
- Williams, H., 1978, Appalachian Orogen in Canada. *Canadian Journal of Earth Sciences*, vol. 16, pp. 792-807.
- Williams, H., 1978, Tectonic Lithofacies Map of the Appalachian Orogen. Memorial University of Newfoundland, Map 1.

- Williams, H., 1995, Chapter: 2: Temporal and spatial divisions, *in* Williams, H., editor, *Geology of the Appalachian-Caledonian Orogen in Canada and Greenland: Geological Survey of Canada, Geology of Canada, no. 6, pp. 23-42.*
- Williams, H., Currie, K. L., and Liasecki, M. A. J., 1993, The Dog Bay Line: A major Silurian tectonic boundary in northeast Newfoundland. *Canadian Journal of Earth Sciences, v. 30, p. 2481-2494.*
- Winchester, J. A. & Floyd, P. A., 1977, Geochemical discrimination of different magma series and their differentiation products using immobile elements. *Chemical Geology v. 20, p. 325-343.*
- Zagorevski, A., van Staal, C. R., McNicoll, V., Rogers, N., 2007, Upper Cambrian to Upper Ordovician Peri-Gondwana island arc activity in the Victoria Lake Supergroup, central Newfoundland: tectonic development of the northern Ganderian margin. *American Journal of Science, v. 307, p. 339-370.*

## **Appendix A: Field Methods**

### **A-1: Sample Collection and Mapping**

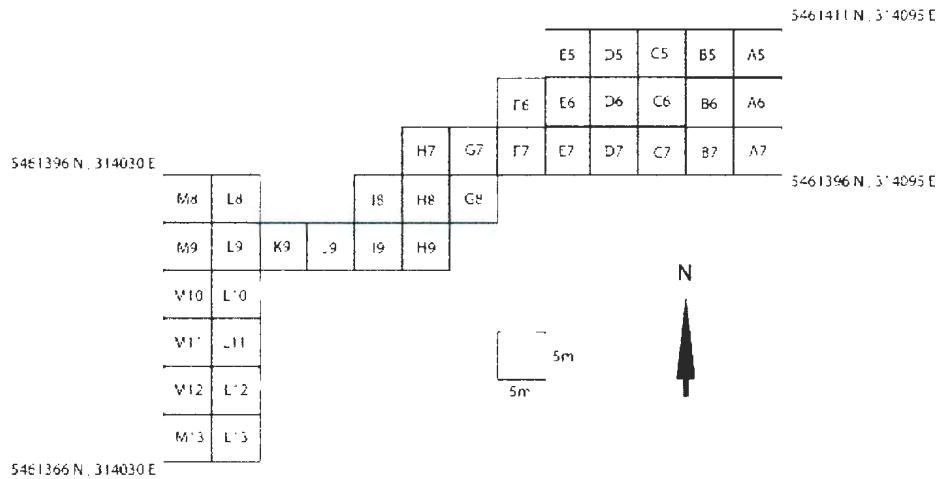
Fieldwork for the project was completed in the summer of 2010. The basis of the field study was in detailed, fine-scale mapping of select areas within the Hare Bay Gneiss. Geological reconnaissance was conducted on easily accessed road cuts and coastal exposures in order to select a set of localities that displayed both unit diversity and contact relationships as a target for more extensive mapping and sampling. The final selections were based on exposure and accessibility, visibility of geologic units and their relationships, as well as adequate spacing and coverage of the Hare Bay Gneiss as a whole. More brief large-scale traverses gave further insight to the complexity and diversity existing within the Hare Bay Gneiss. These areas were less extensively sampled for petrographic, geochemical and geochronological analysis, but expanded project coverage and overall understanding of the Hare Bay Gneiss.

Table A-1 summarizes sample distribution for this project. Samples are divided into geographic areas and the total number of samples collected for each analytical method is displayed at the bottom. In total 107 samples were collected from various localities, the most heavily sampled area being the WMB map area. A subset of 48 samples was selected for geochemical analysis and 12 for age determinations using the CA-TIMS U-Pb zircon method.

<b>Location</b>	<b>No. of Samples for Petrography</b>	<b>No. of Samples for Geochemistry</b>	<b>No. of Samples for Geochronology</b>
<b>Wind Mill Bight Map Area</b>	56	20	4
<b>Greenspond Road</b>	15	10	2
<b>I Love You Section</b>	6	3	2
<b>Trinity Section</b>	5	4	0
<b>Valleyfield Road</b>	13	7	2
<b>North of Cape Freels</b>	10	3	1
<b>Hare Bay</b>	2	1	1
<b>Total:</b>	107	48	12

**Table A-1:** Samples collected for various analyses arranged according to geographic location.

The Windmill Bight map area was gridded using flagging tape to mark the corners of 38 5x5 meter grid blocks (Figure A-1). Each block was drawn, measured and described in detail on oversized sheets of grid paper. The grid blocks were later scanned, stitched and digitized to produce a comprehensive geologic map of the area.



**Figure A-1:** Schematic of WMB grid area showing 5x5m blocks mapped separately on oversized grid sheets and stitched together to produce a final map.

The three road cuts were photographed to produce a panoramic image of each exposure. These images were printed and overlain with mylar paper in order to accurately map geological units, contact relationships, and specific sample localities within each road section. The mylar was later used to produce digital copies, more clearly displaying the significant geologic features.

A Global Positioning System (GPS) was used to acquire UTM coordinates for road and coastal traverses. However, due to the scale of mapping in the grid and road

sections the GPS was only used to determine UTM coordinates for the outer corners of the grid, or ends of road sections. Once digitized specific WMB map coordinates were extracted and/or calculated from the geo-referenced map.

The majority of samples were collected during the 2010 summer field season with the exception of six (11AL001-11AL006) that were sampled in September 2011. Samples were typically taken from areas showing minimal effects of physical and chemical weathering. Samples were also selected as a representative portion of the entire geological unit. Care was taken to avoid areas with significant veining or other unrepresentative features.

Sample Number	Location	UTM Coordinates		Rock Type/Unit	Analytical Method		
		Northing	Easting		Petrography	Geochemistry	Geochronology
10AL001	N of Cape Freels	5461119	317517	Gneiss	X		
10AL002	N of Cape Freels	5461130	317517	Gneiss	X		
10AL003	GP Road Section	5441540	302262	Al-silicate Orthogneiss	X		
10AL004	GP Road Section	5441556	302259	Tonalitic Enclave	X		
10AL005	GP Road Section	5441545	302259	Foliated Leucogranite	X		
10AL006	Valleyfield Road	5444593	309349	Orthogneiss	X		
10AL007	Valleyfield Road	5445348	308557	Paragneiss	X		
10AL008	Valleyfield Road	5445348	308557	Paragneiss	X		
10AL009	Hare Bay	5415751	719428	Orthogneiss	X		
10AL010	ILU Road Section	5426419	284516	Orthogneiss	X		
10AL011	ILU Road Section	5426409	284492	Tonalite	X		
10AL012	Trinity Road Section	5429094	287030	Orthogneiss	X		
10AL013	Valleyfield Road	5444903	308873	Augen Mylonite	X		
10AL014	Valleyfield Road	5444866	308932	Mylonite	X	X	
10AL015	GP Road Section	5441555	302258	Al-silicate Orthogneiss	X		
10AL016	WMB Map Area	N/A	N/A	Megaacrystic Granite	X	X	
10AL017	WMB Map Area	N/A	N/A	Foliated Leucogranite	X	X	
10AL018	WMB Map Area	N/A	N/A	Megaacrystic Granite	X		
10AL019	WMB Map Area	N/A	N/A	Foliated Leucogranite	X		
10AL020	WMB Map Area	N/A	N/A	Mylonite	X		
10AL021	WMB Map Area	N/A	N/A	Contact: Peg and MG	X		
10AL022	WMB Map Area	N/A	N/A	Pegmatite	X		
10AL023	WMB Map Area	N/A	N/A	Foliated Leucogranite	X		
10AL024	WMB Map Area	N/A	N/A	Megaacrystic Granite	X		
10AL025(a)	WMB Map Area	N/A	N/A	Foliated Granite w. Layers	X	X	
10AL025(b)	WMB Map Area	N/A	N/A	Esp. Tourm Layer in FGwL	X		

\* BMI: Bt-Ms Intermediate, FG: Foliated Granite, FGw L: Foliated Granite with Layers, FGd: Foliated Granodiorite, MG: Megaacrystic Granite, Peg: Pegmatite

\*Sample 10AL062 was omitted and samples SF of WMB are not described

## Appendix B: Sample Guide

Sample Number	Location	UTM Coordinates		Rock Type/Unit	Analytical Method		
		Northing	Easting		Petrography	Geochemistry	Geochronology
10AL026	WMB Map Area	N/A	N/A	Mega-crystic Granite	X		
10AL027	WMB Map Area	N/A	N/A	Pegmatite	X		
10AL028	WMB Map Area	N/A	N/A	Foliated Granite w/ Layers	X		
10AL029	WMB Map Area	N/A	N/A	Mega-crystic Granite	X		
10AL030	WMB Map Area	N/A	N/A	Foliated Leucogranite	X		
10AL031	WMB Map Area	N/A	N/A	Foliated Granite w/ Layers	X	X	
10AL032	WMB Map Area	N/A	N/A	Qtz Layer in FGw-L	X		
10AL033	WMB Map Area	N/A	N/A	Pegmatite	X		
10AL034	WMB Map Area	N/A	N/A	Foliated Granodiorite	X		
10AL035	WMB Map Area	N/A	N/A	Granitic Layer in FGD	X		
10AL036	WMB Map Area	N/A	N/A	Foliated Granodiorite	X	X	
10AL037	WMB Map Area	N/A	N/A	Foliated Leucogranite	X		
10AL038	WMB Map Area	N/A	N/A	Foliated Leucogranite	X		
10AL039	WMB Map Area	N/A	N/A	Foliated Leucogranite	X		
10AL040	WMB Map Area	N/A	N/A	Highly Sheared MG	X		
10AL041	WMB Map Area	N/A	N/A	Foliated Leucogranite	X	X	
10AL042	WMB Map Area	N/A	N/A	Tonalitic Dyke	X	X	
10AL043	WMB Map Area	N/A	N/A	Pegmatite	X	X	
10AL044	WMB Map Area	N/A	N/A	Foliated Leucogranite	X		
10AL045	WMB Map Area	N/A	N/A	Foliated Granite w/ Layers	X		
10AL046	WMB Map Area	N/A	N/A	Mega-crystic Granite	X	X	
10AL047	WMB Map Area	N/A	N/A	Mega-crystic Granite	X		
10AL048	WMB Map Area	N/A	N/A	Mega-crystic Granite	X		
10AL049	WMB Map Area	N/A	N/A	Pegmatite	X		
10AL050	WMB Map Area	N/A	N/A	Contact: FG and MG	X		
10AL051	WMB Map Area	N/A	N/A	Mega-crystic Granite	X	X	
10AL052	WMB Map Area	N/A	N/A	Contact: BMI and Peg	X		
10AL053	WMB Map Area	N/A	N/A	Interlayered Unit	X		
10AL054	WMB Map Area	N/A	N/A	Highly Sheared MG	X	X	
10AL055	SE of WMB	5461496	314418	Contact: FG and Orthogneiss	X		
10AL056(a&b)	SE of WMB	5461484	314598	Gneiss	X		
10AL057	N of Cape Freels	5461443	314705	Diabase Dyke	X	X	
10AL058	SE of WMB	5461316	314841	Gneiss	X		

\* BMI: Bt-Ms Intermediate, FG: Foliated Granite, FGw-L: Foliated Granite with Layers, FGD: Foliated Granodiorite, MG: Mega-crystic Granite, Peg: Pegmatite

\*Sample 10AL062 was omitted and samples SE of WMB are not described.

## Appendix B: Sample Guide

Sample Number	Location	UTM Coordinates		Rock Type/Unit	Analytical Method		
		Northing	Easting		Petrography	Geochemistry	Geochronology
10AL059	N of Cape Freels	5461577	317476	Gneiss	X	X	
10AL060	Valleyfield Road	5445345	308646	Orthogneiss	X	X	
10AL061	Valleyfield Road	5445423	308630	Paragneiss	X	X	
10AL063	Valleyfield Road	5444508	309400	Orthogneiss	X		
10AL064	Valleyfield Road	5444470	309414	Leucogranite	X		
10AL065	Valleyfield Road	5444333	309514	Orthogneiss	X	X	
10AL066	Valleyfield Road	5444140	310007	Mylonite	X	X	
10AL067	GP Road Section	N/A	N/A	Undeformed Granite	X		
10AL068	GP Road Section	N/A	N/A	Al-silicate Orthogneiss	X	X	
10AL069	GP Road Section	N/A	N/A	Tonalitic Enclave	X	X	
10AL070	GP Road Section	N/A	N/A	Tonalitic Enclave	X	X	
10AL071	GP Road Section	N/A	N/A	Al-silicate Orthogneiss	X	X	
10AL072	GP Road Section	N/A	N/A	Foliated Leucogranite	X	X	
10AL073	GP Road Section	N/A	N/A	Al-silicate Orthogneiss	X	X	
10AL074	GP Road Section	N/A	N/A	Orthogneiss	X	X	
10AL075	GP Road Section	N/A	N/A	Al-silicate Orthogneiss	X	X	
10AL076	Valleyfield Road	5445348	308557	Paragneiss	X	X	X
10AL077	Valleyfield Road	5444508	309400	Orthogneiss	X	X	X
10AL078	GP Road Section	5441545	302259	Foliated Leucogranite	X	X	X
10AL079	GP Road Section	5441545	302259	Al-silicate Orthogneiss	X	X	X
10AL080	WMB Map Area	N/A	N/A	Highly Sheared MG	X		
10AL081	WMB Map Area	N/A	N/A	Interlayered Unit	X		
10AL082	WMB Map Area	N/A	N/A	Highly Sheared MG	X	X	
10AL083	WMB Map Area	N/A	N/A	Foliated Leucogranite	X		
10AL084	WMB Map Area	N/A	N/A	Bt-Ms Intermediate	X		
10AL085	WMB Map Area	N/A	N/A	Act-Bt Mafic	X	X	
10AL086	WMB Map Area	N/A	N/A	Carb-Bt Mafic	X	X	
10AL087	WMB Map Area	N/A	N/A	Megacrystic Granite	X	X	X
10AL088	WMB Map Area	N/A	N/A	Foliated Granodiorite	X	X	X
10AL089	WMB Map Area	N/A	N/A	Pegmatite	X	X	X
10AL090	WMB Map Area	N/A	N/A	Foliated Leucogranite	X	X	X
10AL091	SE of WMB	5460933	315637	Pssamite	X		
10AL092	SE of WMB	5460977	315390	Gneiss	X		
10AL093	N of Cape Freels	5461369	317643	Gneiss	X	X	X
10AL094	Hare Bay	5415836	719561	Orthogneiss	X	X	X

\* BMI: Bt-Ms Intermediate, FG: Foliated Granite, FGw/L: Foliated Granite with Layers, FGD: Foliated Granodiorite, MG: Megacrystic Granite., Peg: Pegmatite  
 \*Sample 10AL062 was omitted and samples SE of WMB are not described.

## Appendix B: Sample Guide

Sample Number	Location	UTM Coordinates		Rock Type/Unit	Analytical Method		
		<i>Northing</i>	<i>Easting</i>		<i>Petrography</i>	<i>Geochemistry</i>	<i>Geochronology</i>
10AL095	ILU Road Section	N/A	N/A	Leucogranite	X	X	
10AL096	ILU Road Section	N/A	N/A	Tonalite	X	X	X
10AL097	ILU Road Section	N/A	N/A	Orthogneiss	X	X	X
10AL098	Trinity Road Section	N/A	N/A	Orthogneiss	X	X	
10AL099	Trinity Road Section	N/A	N/A	Intermediate Block	X	X	
10AL100	Trinity Road Section	N/A	N/A	Leucogranite	X	X	
10AL101	Trinity Road Section	N/A	N/A	Orthogneiss	X	X	
11AL001	WMB Map Area	N/A	N/A	Bt-Ms Intermediate	X	X	
11AL002	WMB Map Area	N/A	N/A	Interlayered Unit	X		
11AL003	WMB Map Area	N/A	N/A	Highly Sheared MG	X	X	
11AL004	WMB Map Area	N/A	N/A	Carb-Bt Mafic	X		
11AL005	WMB Map Area	N/A	N/A	Layered Quartz Unit	X		
11AL006	ILU Road Section	N/A	N/A	Aplite Vein	X		

\* BMI: Bt-Ms Intermediate. FG: Foliated Granite. FGwL: Foliated Granite with Layers. FGD: Foliated Granodiorite. MG: Megacrystic Granite. Peg: Pegmatite

\*Sample 10AL062 was omitted and samples SE of WMB are not described.

## Appendix B: Sample Guide

## Appendix C: Petrography

A total of 107 samples were collected for petrographic observation and a brief description of each section was recorded. The goals of petrographic analysis include: (1) recording petrographic unit diversity and similarity; (2) recognizing mineral components and textural features to aid in determining genetic relationships and rock origin, and; (3) to aid in selecting a subset of representative samples with relatively minor alteration for geochemical analysis.

Table C-1 summarizes observations made in thin section, where samples are divided based on location and lithology. The listed modal percentages are estimated from petrographic examination. It should be noted that not all samples analysed are included in this table. Abbreviations used include: Plag – plagioclase, Kfs – alkali feldspar, Fsp – feldspar, Qtz – quartz, Bt – biotite, Ms – muscovite, Chl – chlorite, Carb – carbonate, Act – actinolite, Hbl – hornblende, Amph – amphibole, Grt – garnet, And – andalusite, Sil – sillimanite, Crd – cordierite, Ep – epidote, Tourm – tourmaline, Ap – apatite, Mnz – monazite, Rt – rutile, Ttn – titanite, Zrc – zircon, fg – fine-grained, mg – medium-grained, cg – coarse-grained, TS – thin section, PL – plane polarized light, WMB – Windmill Bight.

<b>WMB Map</b>				
<b>Unit/Sample No.</b>	<b>Mineralogy</b>	<b>Grain Size</b>	<b>Crystal Habit</b>	<b>Additional Notes (Textures, fabrics, etc.)</b>
<i>Foliated Leucogranite</i>				
10AL017	Qtz (45%), Plag/Kfs (35%), Ms (15%), Chl/Bt (5%), Ap (<1%), Oxides (<1%)	Fine to Medium Qtz (<0.1-1mm), Ksp/Plag (<0.5-4mm), Ms (<0.1-2mm), Chl/Bt (<0.5mm), Ap (up to 0.3mm)	Qtz/Chl (anhedral), Kfs/Plag (an-subhedral), Ms (anhedral), Ap (euhedral)	<ul style="list-style-type: none"> <li>• minor-significant seritization of Fsp</li> <li>• fg, wavy, discontinuous, mica-rich bands (&lt;0.5mm thick)</li> <li>• Ms occurs fg in thin, wavy bands but also as larger, randomly oriented flakes throughout</li> <li>• myrmekite present</li> <li>• Qtz, Ap and Chl inclusions in Fsp</li> </ul>
10AL019	Qtz (40%), Kfs (35%), Plag (10%), Ms (8%), Bt (2%), Chl (2%), Grt (1%), Oxides (1%), Ap (1%), Zrc (<1%)	Fine to Medium Qtz (<0.1-1mm), Kfs/Plag (0.5-3mm), Ms (<0.1-3mm), Grt (0.5-1.5mm), Bt/Chl (<0.5mm)	Qtz/Kfs/Plag/Bt/Chl (anhedral), Ms (anhedral), Grt (sub-euhedral), Ap (euhedral)	<ul style="list-style-type: none"> <li>• patches, layers and lenses of recrystallized Qtz (~1mm thick)</li> <li>• Kfs with inclusions of Ap, Chl and Ms</li> <li>• minor to significant seritization of Fsp</li> <li>• Ms breaking down into needles</li> <li>• Ms occurs fg as well as larger euhedral flakes</li> <li>• orange staining along micro-fractures</li> <li>• microcline twinning in Kfs</li> </ul>
10AL023	Kfs+Plag (55%), Qtz (36%), Ms (5%), Bt (1%), Chl (1%), Ap (1%), Rt/Zrc (<1%)	Fine-Medium Kfs/Plag (<0.1-3mm), Qtz (<0.1-1mm), Ms (<0.1-2mm), Bt/Chl (<0.2mm)	Kfs/Plag/Qtz (anhedral), Ms (an-subhedral), Bt/Chl (anhedral), Ap/Zrc (euhedral)	<ul style="list-style-type: none"> <li>• Fsp with inclusions of Ms and Qtz</li> <li>• thin (&lt;0.5mm), discontinuous Ms-rich layers</li> <li>• layers of recrystallized Qtz pinching and bulging (~1-2mm thick)</li> <li>• turbid veins</li> <li>• minor seritization of Fsp</li> <li>• twinning in Plag</li> </ul>
10AL030	Kfs (47%), Qtz (40%), Plag (10%), Ms (3%), Chl (<1%), Oxides (<1%)	Qtz (<0.1-2mm), Kfs (<0.5-8mm), Plag (<0.1-3mm), Ms (<0.1-1mm), Chl (<0.1mm)	Qtz/Kfs/Plag/Ms/Chl (anhedral)	<ul style="list-style-type: none"> <li>• Kfs with inclusions of Qtz, Ms and Plag</li> <li>• Kfs with microcline and exsolution features</li> <li>• minor seritization of Fsp</li> <li>• very thin (&lt;0.2mm), fg Chl-Ms layers define a foliation</li> <li>• Qtz filled micro-fractures cut across coarse Fsp grains</li> </ul>
10AL037	Qtz (40%), Kfs (30%), Plag (18%), Ms (10%), Chl/Bt (2%), Oxides/Ttn/Zrc/Ap (<1%)	Fine to Medium Qtz/Plag (<0.1-3mm), Kfs (<0.1-8mm), Chl/Bt (<0.5mm), Ms (<0.1-2mm), Oxides/Ttn/Zrc/Ap (<0.1mm)	Qtz/Kfs/Plag/Chl/Bt (anhedral), Ms (an-subhedral), Zrc/Ap/Ttn (euhedral)	<ul style="list-style-type: none"> <li>• lenses and layers of recrystallized Qtz, pinching and thickening (up to 1-2mm)</li> <li>• Kfs with exsolution and microcline</li> <li>• significant seritization of Fsp</li> <li>• minor myrmekite</li> <li>• thin (&lt;0.5mm), fg bands of Ms</li> </ul>

**Table C-1:** Summary of mineralogy and petrography of thin sections. Not all samples are included here.

10AL038	Qtz (50%), Kfs+Plag (34%), Ms (12%), Chl/Bt (2%), Ap (1%), Oxides (1%), Rt (<1%)	Fine to Medium Qtz (<0.1-1mm), Kfs/Plag (0.1-3mm), Ms (<0.1-2mm), Bt/Chl (<0.5mm), Ap/Oxides (<0.5mm)	Qtz/Kfs/Plag (anhedral), Ms (anhedral), Chl/Bt (anhedral), Oxides (anhedral), Ap (euhedral)	<ul style="list-style-type: none"> <li>• lens-shaped Ms grains</li> <li>• Ap with inclusions</li> <li>• Bt and Ap inclusions in Ms</li> <li>• minor to significant seritization of Fsp</li> <li>• Qtz and euhedral Ms inclusions in Kfs</li> <li>• wavy, recrystallized Qtz lenses (1-2mm thick)</li> </ul>
10AL039	Qtz (40%), Kfs+Plag (40%), Ms (15%), Bt/Chl (3%), Grt (1%), Oxides (1%)	Fine to Medium Qtz (<0.1-1mm), Kfs/Plag (0.1-3mm), Ms (<0.1-2mm), Bt/Chl (<0.5mm), Oxides/Grt (up to 1mm)	Qtz/Plag/Kfs/Bt/Chl (anhedral), Ms (anhedral), Oxides (anhedral), Grt (euhedral)	<ul style="list-style-type: none"> <li>• Kfs with inclusions of Qtz, Bt and Ms</li> <li>• Kfs with microcline and exsolution</li> <li>• Plag with lamellar twinning</li> <li>• some Ms is lens-shaped but also occurs as euhedral flakes</li> <li>• turbid veining</li> <li>• Qtz micro-fractures cutting across coarse Kfs grains</li> <li>• irregular patches of recrystallized Qtz</li> <li>• Grt occurs in Qtz patches, not in Al-rich mineral layers</li> </ul>
10AL041	Qtz (50%), Kfs+Plag (30%), Ms (12%), Bt/Chl (2%), Grt (1%), Rt/Zrc/Oxides/Ep/Ap/Mnz (<1%)	Fine to Medium Qtz (0.2-2mm), Kfs/Plag/Ms (0.2-4mm), Bt/Chl (<0.5mm), Grt (~1mm)	Qtz/Kfs/Plag/Bt/Chl (anhedral), Grt (euhedral), Ms (anhedral), Mnz/Zrc/Ap (euhedral)	<ul style="list-style-type: none"> <li>• almost all Bt altered to Chl, and minor chloritization of Ms</li> <li>• late turbid Fsp veins</li> <li>• Kfs with microcline twins</li> <li>• foliation weakly apparent in thin section</li> <li>• less fg material than other TS of this unit</li> <li>• Ms breaking down to needles at edges</li> <li>• Kfs with inclusions of Qtz and Ms</li> </ul>
10AL044	Qtz (40%), Kfs/Plag (40%), Ms (16%), Bt/Chl (3%), Ap (1%), Zrc/Rt (<1%)	Fine to Medium Qtz/Ms (<0.1-2mm), Kfs/Plag (0.1-3mm), Chl/Bt (<0.1-1mm), Ap/Zrc/Rt (<0.2mm)	Qtz/Kfs/Plag (anhedral), Ms (anhedral), Bt/Chl (anhedral), Zrc/Ap (euhedral)	<ul style="list-style-type: none"> <li>• in PL rainbow tint to Ms</li> <li>• turbid veining cutting perpendicular to foliation</li> <li>• Ms as cg lenses and fg, thin (&lt;0.5mm), wavy bands</li> <li>• banding ~1-2mm thick plucked from slide</li> <li>• Ms breakdown to needles along edges</li> <li>• Kfs with exsolution</li> </ul>
10AL083	Qtz (50%), Kfs/Plag (28%), Ms (12%), Bt/Chl (6%), Ep (2%), Oxides (1%), Grt (1%), Ap/Zrc/Rt (<1%)	Fine to Medium Qtz/Ms (<0.1-4mm), Kfs/Plag (0.1-5mm), Grt (~0.5mm), Bt/Chl (<0.5mm)	Qtz/Kfs/Plag/Bt/Ep (anhedral), Ms (anhedral), Grt (euhedral)	<ul style="list-style-type: none"> <li>• majority of Qtz has sutured boundaries</li> <li>• moderate to significant seritization of Fsp</li> <li>• mica forms thin (&lt;0.5mm) wavy, discontinuous bands</li> <li>• few coarser lens-shaped Ms grains</li> <li>• significant chloritization of Bt</li> </ul>

**Table C-1:** Summary of mineralogy and petrography of thin sections. Not all samples are included here.

10AL090	Kfs (40%), Qtz (35%), Plag (10%), Ms (10%), Ap (1%), Chl (1%), Bt (1%), Grt (1%), Oxides (1%)	Fine to Medium Qtz (<0.1-1mm), Kfs/Plag/Ms (<0.1-2mm), Chl/Bt (<0.2mm), Grt (~0.2mm), Ap (0.2mm)	Qtz/Plag/Kfs/Chl/Bt /Oxides (anhedral), Ms (an-subhedral), Grt/Ap (euhedral)	<ul style="list-style-type: none"> <li>• thin, fg Ms bands, waving along grain boundaries</li> <li>• some coarser grained Ms implying two growth phases</li> <li>• fg Qtz and Ms with large Fsp grains and patches of recrystallized Qtz throughout</li> </ul>
<b>Foliated Leucogranite w/ Layers</b>				
10AL025A	Qtz (60%), Kfs (8%), Plag (8%), Ms (17%), Bt (3%), Chl (2%), Ap (2%), Oxides (<1%)	Fine -Medium Qtz (0.1-1mm), Kfs/Plag (0.1-2mm), Ms (0.1-1mm), Bt/Chl (<0.2mm), Ap (0.2mm)	Qtz/Kfs/Plag (anhedral), Ms (an-euhedral), Ap (subhedral), Oxides (sub-euhedral)	<ul style="list-style-type: none"> <li>• moderate seritization of Fsp</li> <li>• recrystallized Qtz layers and lenses (&lt;0.5mm thick)</li> <li>• thin(0.1mm), wavy bands of fg Ms around Fsp augens</li> <li>• coarse (1mm) euhedral grain on Ms</li> <li>• waves are pronounced. Micro-folds (?)</li> </ul>
10AL025B(vein)	<b>Outer boundary:</b> (Kfs+Plag (80%), Qtz (20%) <b>Core of layer:</b> Tourm (55%), Plag (30%), Chl (10%), Ep (5%)	Kfs/Plag (0.1-4mm), Qtz (0.1-1mm), Tourm (0.5-3mm), Ep (<0.5mm)	Kfs/Plag/Qtz/Chl/Ep (anhedral), Tourm (sub-euhedral)	<ul style="list-style-type: none"> <li>• late fluid alteration veins perpendicular to foliation</li> <li>• continuous layers of recrystallized Qtz and Fsp in outer layer</li> <li>• outer layer dominantly fg strongly seritized Fsp</li> <li>• Tourm fills center of layer and is included in Plag</li> <li>• minor Chl and Ep also in center of layer</li> </ul>
10AL028	Qtz (50%), Kfs+Plag (30%), Ms (12%), Bt (5%), Ap (3%)	Fine and Medium (bimodal) Kfs/Plag (0.1-5mm), Qtz (0.1-2mm), Ms (0.1-1mm), Bt (<0.1mm), Ap (0.2mm)	Qtz/Kfs/Plag/Bt (anhedral), Ms (an-subhedral), Ap (sub-euhedral)	<ul style="list-style-type: none"> <li>• fg with mg lenses of recrystallized Qtz and mg Fsp</li> <li>• augen-shaped Fsp up to 4mm with inclusions of Qtz and Ms</li> <li>• thin (0.1mm) layers and lenses of recrystallized Qtz</li> <li>• strong, wavy foliation defined by Ms</li> <li>• Kfs megacryst with blebs of Qtz along grain boundaries</li> </ul>
10AL031	Qtz (50%), Kfs+Plag (35%), Ms (12%), Bt (2%), Chl (1%), Ap (<1%)	Fine to Medium Qtz (0.1-1mm), Kfs/Plag (0.1-3mm), Ms (0.1-2mm), Bt (<0.2mm), Ap (0.2mm)	Qtz/Kfs/Plag/Bt (anhedral), Ms (an-subhedral), Ap (euhedral)	<ul style="list-style-type: none"> <li>• more cg than other samples of this unit</li> <li>• mg Ms laths create criss-cross network and overall foliation</li> <li>• irregular patches of mg recrystallized Qtz</li> <li>• Fsp megacrysts with inclusions of Qtz and Ms</li> <li>• moderate seritization of Fsp</li> </ul>
10AL032(vein)	Qtz (96%), Fsp (1%), Tourm (3%), Chl (<1%)	Medium Qtz (1mm), Tourm (1-3mm), Fsp/Chl (<0.2mm)	Qtz/Fsp/Chl (anhedral), Tourm (sub-euhedral)	<ul style="list-style-type: none"> <li>• mg sutured Qtz, polycrystalline Qtz shows slight elongation</li> <li>• bands of Qtz separated by tiny fractures filled with Chl and fg, strongly seritized Fsp</li> <li>• cluster of coarser Tourm and minor fg Tourm seen along tiny fractures</li> </ul>

**Table C-1:** Summary of mineralogy and petrography of thin sections. Not all samples are included here.

10AL045	Qtz (50%), Kfs+Plag (38%), Ms (11%), Bt/Chl (<1%)	Fine w/ Coarse Fsp Qtz (0.1-1mm), Kfs/Plag (0.1-4mm), Ms (0.1-1mm), Bt/Chl (<0.1mm)	Kfs/Plag/Qtz/Ms/Bt/Chl (anhedral)	<ul style="list-style-type: none"> <li>• continuous layers and lenses of mg recrystallized Qtz pinch and swell (~0.5mm thick)</li> <li>• crenulation cleavage defined by Ms</li> <li>• augen-shaped Fsp up to 4mm</li> <li>• most Ms is fg but some mg lense-shaped grains</li> </ul>
<i>Sheared Megacrystic Granite</i>				
10AL016	Qtz (36%), Kfs (30%), Bt+Chl (16%), Plag (10%), Ep (6%), Oxides (2%), Ap/Rt/Zrc (<1%)	Fine-Coarse Kfs (5mm), Plag (1-3mm), Qtz (<0.1-2mm), Bt/Chl (<0.1-2mm), Ep (<0.5mm), Oxides (<2mm)	Qtz (anhedral), Kfs/Plag (anhedral), Bt/Chl (anhedral), Oxides (an-euhedral), Zrc/Ap (euhedral)	<ul style="list-style-type: none"> <li>• finely ground Qtz, Bt, Chl layers wrapping around larger Fsp and Qtz grains.</li> <li>• some layers and lenses of coarser Qtz</li> <li>• Kfs with microcline twinning and exsolution features.</li> <li>• significant chloritization of Bt</li> <li>• late Qtz veins and micro-shear zones fracture coarse Fsp grains</li> </ul>
10AL018	Qtz (40%), Kfs (30%), Plag (14%), Bt (10%), Chl (2%), Oxides (2%), Ms (1%), Ap (1%), Zrc (<1%)	Fine to Coarse Kfs/Plag (0.5-20mm), Qtz (<0.1-3mm), Bt (<0.1-2mm), Ms/Chl/Oxides (<0.5mm), Ap (~0.2mm)	Qtz/Kfs/Plag/Ms (anhedral), Bt (an-subhedral), Zrc/Ap (euhedral)	<ul style="list-style-type: none"> <li>• moderate to significant seritization of Fsp</li> <li>• myrmekite present</li> <li>• late Qtz veins and micro-shear-zones cutting through Fsp megacrysts</li> <li>• minor chloritization of Bt</li> <li>• lenses of recrystallized Qtz (1-2mm thick)</li> <li>• fg mica-rich layers, wisp along grain boundaries</li> </ul>
10AL024	Qtz (50%), Kfs (30%), Chl (8%), Ms (5%), Plag (3%), Bt (1%), Ap (2%), Oxides (1%), Zrc (<1%)	Fine-Medium Qtz (0.1-2mm), Kfs/Plag (0.5-5mm), Ms/Chl (<0.1-2mm), Ap/Oxides (<0.2mm), Zrc (<0.1mm)	Qtz/Kfs/Plag (anhedral), Ms/Bt/Chl (an-subhedral), Ap/Zrc (euhedral), Oxides (anhedral)	<ul style="list-style-type: none"> <li>• myrmekite present</li> <li>• Kfs with microcline and exsolution</li> <li>• moderate to significant seritization of Fsp</li> <li>• two phases of Ms</li> <li>• Bt and Ms intergrowths</li> <li>• thin, wavy Chl layers along micro-shear-zones</li> <li>• weak foliation defined by mica</li> </ul>
10AL026	Kfs (30%), Qtz (27%), Plag (15%), Chl+Bt (15%), Ms (2%), Ap (8%), Oxides (3%), Rt (<1%)	Fine-Coarse Kfs/Plag (<0.5-15mm), Qtz (<0.1-2mm), Ms/Bt/Chl (<0.5mm), Ap (<0.2mm), Oxides (<0.2mm)	Kfs/Plag/Ms (an-subhedral), Bt (an-euhedral), Ap (euhedral), oxides (an-subhedral)	<ul style="list-style-type: none"> <li>• Qtz filled micro-fractures</li> <li>• moderate seritization of Fsp</li> <li>• thin (~0.1mm), wavy bands of fg Bt and Ms across TS</li> <li>• large masses of fg randomly oriented Fsp, Qtz, Chl, Ms and oxides</li> <li>• patches of sutured polycrystalline Qtz</li> <li>• Plag with albite twins</li> </ul>

**Table C-1:** Summary of mineralogy and petrography of thin sections. Not all samples are included here.

10AL046	Qtz (50%), Kfs+Plag (31%), Ms (5%), Bt (2%), Chl (8%), Ap (3%), Oxides (1%), Zrc (<1%)	Fine to Medium/Coarse Kfs/Plag (<0.1-5mm), Qtz (<0.1-2mm), Ms (<0.1-3mm), Bt/Chl (<1mm), Oxides/Ap (<0.5mm), Zrc (<0.1mm)	Kfs/Plag/Qtz/Oxides (anhedral), Ms/Bt/Chl (anhedral), Zrc/Ap (euhedral)	<ul style="list-style-type: none"> <li>• Kfs with inclusions of Bt, Chl, Ms and Qtz</li> <li>• recrystallized, polycrystalline layers and lenses of Qtz</li> <li>• late veining offset by micro-shear zones</li> <li>• myrmekite present</li> <li>• alternating mica (&lt;1mm) and Qtz (1-2mm) layers and lenses</li> <li>• significant chloritization of Bt</li> </ul>
10AL047	Qtz (40%), Kfs+Plag (40%), Chl (13%), Ms (1%), Ep (1%), Oxides (1%), Ap (4%), Zrc/Rt (<1%)	Fine - Medium Qtz (<0.1-1mm), Kfs/Plag (0.1-4mm), Ap/Oxides (<0.2mm), Chl (<0.5mm), Zrc/Ep (<0.1mm)	Kfs/Plag/Qtz/Oxides (anhedral), Ms/Chl (an-subhedral), Ap (euhedral), Zrc (subhedral)	<ul style="list-style-type: none"> <li>• majority of Fsp strongly seritized</li> <li>• foliation defined by thin (&lt;0.5mm), discontinuous, wavy mica-rich layers</li> <li>• augen-shaped Fsp</li> <li>• Fsp with inclusions of Ap, Chl and Ms, cut by late veining</li> <li>• few lenses of recrystallized Qtz</li> <li>• lamellar twinning of Plag</li> <li>• majority of Qtz fg in ground mass</li> </ul>
10AL051	Qtz (40%), Ksp+Plag (35%), Bt (18%), Chl (<1%), Ms (1%), Oxides (1%), Ep (1%), Ap (4%), Zrc/Rt (<1%)	Fine - Medium Qtz (<0.1-2mm), Kfs/Plag (<0.1-5mm), Bt (<0.1-1mm), Chl/Ms (<0.1mm), Zrc (<0.1mm), Ap (<0.2mm)	Qtz/Kfs/Plag/Chl (anhedral), Bt/Ms (an-subhedral), Zrc/Ap (euhedral)	<ul style="list-style-type: none"> <li>• minor chloritization of Bt</li> <li>• Qtz and lath-shaped Bt inclusions in Fsp</li> <li>• patchy seritization of Fsp</li> <li>• minor myrmekite</li> <li>• lenses of recrystallized Qtz</li> <li>• pleochroic haloes on Bt</li> </ul>
10AL087	Qtz (48%), Plag (15%), Kfs (18%), Bt (10%), Ms (2%), Oxides (1%), Ep (1%), Ap (2%), Mnz/Zrc (<1%)	Fine - Coarse Qtz (<0.1-2mm), Kfs/Plag (<0.5-10mm), Bt (<0.1-1.5mm), Ms/Oxides/Ap (<0.5mm), Zrc/Mnz (<0.1mm)	Kfs/Plag/Qtz/Oxides (anhedral), Bt/Ms (an-euhedral), Ap/Zrc/Mnz (sub-euhedral)	<ul style="list-style-type: none"> <li>• Bt with pleochroic haloes</li> <li>• patches and lenses of recrystallized Qtz</li> <li>• Kfs with inclusions of Bt, Ms and Qtz</li> <li>• myrmekite present</li> <li>• moderate chloritization of Bt</li> <li>• exsolution features in Kfs</li> </ul>

**Table C-1:** Summary of mineralogy and petrography of thin sections. Not all samples are included here.

10AL040 (Mylonitic)	Qtz (30%), Kfs+Plag (30%), Bt (23%), Amph (10%), Ep (5%), Chl (2%), Oxides (<1%), Ttn (<1%)	Qtz (0.1-0.5mm), Kfs/Plag (0.5-2mm), Bt/Chl- 0.1-0.25mm, Amph- 0.5-1mm, Ep- 0.1-1mm	Qtz/Kfs/Plag/Bt/Chl/Ep (anhedral), Amph (an-subhedral)	<ul style="list-style-type: none"> <li>strongly seritized Fsp</li> <li>Fsp megacrysts with inclusions of Bt, Chl and Qtz</li> <li>few patches of recrystallized Qtz</li> <li>Ep occurs along grain boundaries and is coarser than seen elsewhere (up to 1mm)</li> <li>mica defines foliation</li> </ul>
10AL054	Qtz (45%), Kfs (44%), Ms+Chl (6%), Plag (5%), Ep/Oxides (<1%)	Fine - Medium Qtz (0.1-3mm), Fsp (0.1-20mm), Ms (0.1-1mm), Ep (<0.1mm), Oxides (up to 1mm)	Kfs/Plag/Ms (an-subhedral), Qtz/Ep (anhedral), Oxides (subhedral)	<ul style="list-style-type: none"> <li>strongly seritized Fsp</li> <li>Fsp megacrysts with inclusions of Bt, Chl and Qtz</li> <li>Oxides along cleavage planes and as coarser prismatic grains</li> <li>Qtz filled micro-fractures</li> <li>mica defines foliation</li> </ul>
10AL080	Qtz (50%), Kfs (22%), Plag (15%), Bt+Chl (10%), Ep (1%), Ap (1%), Oxides (1%), Rt (<1%)	Fine - Medium	N/A	<ul style="list-style-type: none"> <li>Kfs with exsolution and microcline features</li> <li>Fsp with significant seritization</li> <li>minor Rt occurring with Oxides</li> <li>mica defines foliation</li> </ul>
10AL082	Qtz (60%), Kfs+Plag(28%), Bt+Chl (7%), Ms(3%), Ep (2%), Ap/Oxides (<1%)	Fine - Medium	N/A	<ul style="list-style-type: none"> <li>Kfs with exsolution and microcline features</li> <li>Ep occurs in fg pods</li> <li>minor myrmekite</li> <li>late Qtz in filled fractures cut Fsp grains</li> </ul>
11AL003	Qtz (50%), Kfs+Plag(30%), Bt+Chl (15%), Ms(3%), Ep (2%), Ap/Oxides (<1%)	Fine - Medium	N/A	<ul style="list-style-type: none"> <li>strongly seritized Fsp</li> <li>few patches of recrystallized Qtz</li> <li>mica defines foliation</li> </ul>
<b><i>Foliated Granodiorite</i></b>				
10AL034	Qtz (50%), Plag (30%), Kfs (5%), Chl (13%), Bt (1%), Ttn (1%), Ep/Ap/Oxides/Rt (<1%)	Fine - Medium Qtz (0.1-0.5mm), Kfs/Plag (0.1-2mm), Bt/Chl (<0.2mm), Ttn (0.4mm)	Qtz (equant- anhedral), Kfs/Plag (anhedral), Chl/Bt (anhedral), Ttn (an-subhedral)	<ul style="list-style-type: none"> <li>strong seritization of Fsp</li> <li>Coarse Fsp up to 2mm</li> <li>fg equant Qtz grains with well-defined boundaries</li> <li>Chl and Bt creates an irregular network and defines the overall foliation</li> </ul>
10AL035(layer)	Qtz (54%), Kfs (30%), Plag (10%), Chl/Bt (5%), Ap (1%), Oxides (<1%)	Medium - Coarse Kfs/Plag (0.1-10mm), Qtz (0.1-2mm), Chl/Bt (<0.1mm), Ap (0.2mm)	Kfs/Plag/Qtz/Chl/Bt (anhedral), Ap (euohedral)	<ul style="list-style-type: none"> <li>overall grain size is mg-cg but fg matrix is present</li> <li>patches of recrystallized Qtz and Kfs megacrysts up to 1cm</li> <li>Fsp with inclusions of Chl and Qtz</li> <li>thin (&lt;0.1mm), wavy network of fg Chl wraps around Fsp</li> <li>mild to moderate seritization of Fsp</li> </ul>

**Table C-1:** Summary of mineralogy and petrography of thin sections. Not all samples are included here.

10AL036	Qtz (40%), Plag (25%), Kfs (15%), Bt (18%), Oxides (1%), Ap (1%), Chl (<1%)	Fine - Medium Kfs/Plag (0.1-2mm), Qtz (0.1-0.5mm), Chl/Bt (<0.1-0.5mm), Ap (0.1mm)	Kfs/Plag (anhedral), Qtz (anhedral-equant), Chl/Bt (an-subhedral), Ap (euhedral)	<ul style="list-style-type: none"> <li>• Bt is strongly pleochroic with few haloes</li> <li>• Fsp megacrysts with seritized cores and unaltered rims</li> <li>• Plag with lamellar and carlsbad twins</li> <li>• well-defined Qtz boundaries</li> <li>• intricate network of fg Bt creates foliation</li> </ul>
10AL088	Qtz (52%), Plag (30%), Kfs (2%), Chl (14%), Bt (1%), Ttn (1%), Ap/Ep/Oxides/Rt (<1%)	Fine - Medium Kfs/Plag (0.1-2mm), Qtz (0.1-0.5mm), Bt/Chl (<0.1mm), Ttn (up to 0.5mm)	Plag/Kfs/Bt/Chl (anhedral), Qtz (equant-anhedral), Ttn (an-subhedral)	<ul style="list-style-type: none"> <li>• strong seritization of Fsp</li> <li>• almost all Bt altered to Chl</li> <li>• micro-fractures offset late Qtz veins</li> <li>• Fsp with inclusions of Qtz, Bt and Chl</li> <li>• remnant twinning only occasionally visible through alteration in Fsp</li> <li>• fg equant Qtz with well-defined boundaries</li> <li>• mica defines wavy foliation</li> </ul>
<b>Intermediate Dyke</b>				
10AL042	Qtz (40%), Plag (40%), Kfs (4%), Chl (14%), Oxides (1%), Ttn (1%), Ap/Rt (<1%)	Fine - Medium Qtz (0.1-0.5mm), Plag/Kfs (0.1-2mm), Chl/Bt (<0.1mm), Ap (<0.1mm)	Qtz (anhedral-equant), Kfs/Plag/Bt/Chl (anhedral), oxides (an-euhedral), Ap (euhedral)	<ul style="list-style-type: none"> <li>• very similar in composition and fabric to the granodiorite unit</li> <li>• Ttn prisms with oxides along grain boundaries</li> <li>• fg Qtz and Chl in matrix with strongly seritized coarser Fsp</li> <li>• Bt/Chl thin bands create augen shaped patterns</li> </ul>
<b>Late Pegmatite/Aplite Intrusions/Veins</b>				
10AL022	Kfs (50%), Qtz (42%), Plag (5%), Ms (3%), Grt (<1%), Oxides (<1%)	Coarse w/ fg shear zones Kfs/Plag (1-10mm), Qtz/Ms (<0.1-2mm), Grt (<0.2mm), Oxides (<1mm)	Kfs/Plag/Qtz (anhedral), Ms (an-subhedral), Grt (subhedral)	<ul style="list-style-type: none"> <li>• Kfs with microcline and exsolution features</li> <li>• Kfs with inclusions of Qtz, Ms and Plag</li> <li>• Qtz filled fractures cut across slide and fracture Fsp</li> <li>• fg Qtz and Ms rich shear zones</li> <li>• abundance of patchy recrystallized Qtz</li> <li>• tiny pinhead Grt in Qtz patches</li> <li>• minor seritization of Fsp</li> </ul>
10AL027	Qtz (50%), Kfs (30%), Ms (8%), Plag (5%), Chl (5%), Grt (2%), Tourm/Ap/Zrc/Oxides (<1%)	Kfs (0.5-10mm), Qtz (0.1-5mm), Plag (0.5-3mm), Ms (0.1-3mm), Grt (0.2mm), Tourm/Ap/Zrc/Oxides (<0.3mm)	Kfs/Plag/Qtz (anhedral), Ms (an-subhedral), Grt (subhedral), Tourm (subhedral), Ap/Zrc (euhedral)	<ul style="list-style-type: none"> <li>• late fluid or Fsp veins with turbid appearance</li> <li>• Kfs with exsolution and microcline</li> <li>• late Qtz fractures cutting Fsp grains</li> <li>• Tourm grains with Chl along boundary</li> <li>• Grt occurring in aligned clusters</li> <li>• banding defined by mica and aligned lenses and layers of recrystallized Qtz</li> </ul>

**Table C-1:** Summary of mineralogy and petrography of thin sections. Not all samples are included here.

10AL033	Qtz (40%), Kfs (30%), Plag (20%), Ms (9%), Grt (1%)	Coarse Kfs (0.1-12mm), Qtz (1-2mm), Plag (0.1-10mm), Grt (<2mm), Ms (0.1-15mm)	Qtz/Kfs/Plag (anhedral), Ms (an-euhedral), Grt (euhedral)	<ul style="list-style-type: none"> <li>abundance of micro-fractures cutting across slide</li> <li>patches of recrystallized Qtz</li> <li>euhedral plucked sites (Grt?)</li> <li>large euhedral flakes of Ms as well as fg Ms in shear zones along grain boundaries</li> <li>Kfs with inclusions of Ms and Qtz</li> <li>minor seritization of Fsp</li> </ul>
10AL043	Qtz- 40%, Plag- 30%, Kfs- 20%, Ms- 6%, Grt- 4%	Coarse Kfs- 0.5-20mm, Qtz/Plag- 0.1-10mm, Ms- 0.1-2mm, Grt- <1mm	Qtz/Kfs/Plag/Ms- anhedral, Grt- sub-euhedral	<ul style="list-style-type: none"> <li>plagioclase with lamellar and carlsbad twins</li> <li>Ms as large flakes and fg in Qtz layers or along grain boundaries</li> <li>mica defines foliation</li> <li>micro-shear-zones cut slide</li> <li>prominent exsolution and microcline in Kfs</li> <li>fg matrix between grains with Qtz, Ms and Grt</li> </ul>
10AL049	Qtz- 40%, Kfs- 30%, Plag- 19%, Ms- 10%, Grt- 1%	Medium Qtz/Ms- <0.1-1mm, Plag/Kfs- 0.2-3mm, Grt- <0.5mm	Qtz/Kfs/Plag/Ms- anhedral, Grt- euhedral	<ul style="list-style-type: none"> <li>moderate seritization of Fsp</li> <li>Kfs with microcline and exsolution</li> <li>fg Qtz and Ms rich matrix with some Grt throughout</li> <li>foliation defined by mica</li> <li>patches of mg recrystallized Qtz aligned with foliation</li> <li>lamellar twinning in Plag</li> </ul>
10AL089	Kfs (50%), Qtz (39%), Plag (10%), Ms (1%), Grt (<1%)	Kfs (1-20mm), Qtz/Plag (0.1-3mm), Ms (<0.2mm), Grt (<0.5mm)	Kfs/Plag/Qtz/Ms (anhedral), Grt (subhedral)	<ul style="list-style-type: none"> <li>Kfs with exsolution and microcline</li> <li>late Qtz veins and an abundance of turbid veining</li> <li>fg Ms along grain boundaries</li> <li>large Fsp grains highly fractured</li> <li>mg patches of recrystallized Qtz</li> <li>micro-shear-zones with fg Qtz and Ms</li> </ul>
<i>Interlayered Mylonite</i>				
10AL053	Qtz, Fsp, Bt/Chl, Ms, Oxides	Fine (<0.5mm) with coarser Ms up to 1mm	dominantly anhedral	<ul style="list-style-type: none"> <li>augen-shaped Ms grains</li> <li>several micro-fractures run parallel w/ foliation</li> <li>foliation defined by mica</li> <li>few lenses of recrystallized Qtz</li> <li>strongly seritized Fsp</li> <li>crenulation cleavage present</li> </ul>
10AL081	Qtz (30%), Fsp (30%), Bt (25%), Chl (10%), Ep (3%), Oxides (2%), Zrc (<1%)	Fine - Medium Qtz/Fsp (up to 2mm), Bt/Chl (<0.5), Ep/Oxides (<0.2mm)	dominantly anhedral	<ul style="list-style-type: none"> <li>strongly seritized Fsp</li> <li>layers (up to 2mm thick) of recrystallized Qtz</li> <li>minor Chl alteration of Bt</li> </ul>
11AL002	Qtz, Plag, Bt/Chl, Ep, Zrc, Ap	Fine	dominantly anhedral, Zrc/Ap (euhedral)	<ul style="list-style-type: none"> <li>little seritization of Fsp</li> <li>fine scale web like network defined by mica</li> <li>majority of grains have irregular grain boundaries</li> </ul>

**Table C-1:** Summary of mineralogy and petrography of thin sections. Not all samples are included here.

10AL084 (some FG in slide)	Qtz (50%), Ms (20%), Bt (15%), Kfs (10%), Plag (5%), Chl/Ep/Oxides/Ap (<1%)	Fine - Medium	Qtz/Fsp/Bt/Ep/Oxides (anhedral), Ms (anhedral)	<ul style="list-style-type: none"> <li>• mica defines foliation</li> <li>• recrystallized Qtz</li> <li>• Chl minor along mica grain boundaries</li> <li>• Bt with radiation haloes</li> </ul>
11AL001	Qtz (45%), Fsp (10%), Bt (30%), Ms (10%), Oxides (2%), Chl (2%), Grt/Zrc/Rt (<1%)	Fine - Medium Qtz/Fsp/Ms/Bt (0.1-1mm), Grt (~1mm), Oxides/Zrc/Rt (<0.1mm)	Qtz/Fsp/Bt (anhedral), Ms (anhedral), Grt/Zrc (euhedral)	<ul style="list-style-type: none"> <li>• mica defines a wavy foliation</li> <li>• recrystallized Qtz</li> <li>• Ms breaking down along grain boundaries</li> <li>• remnant twinning in some Fsp</li> </ul>
<b><i>Act-Bt Mafic Unit</i></b>				
10AL085	Bt, Act, Qtz, Fsp, Ttn, Ap, Ep, Rt	Fine w/ coarser Fsp (up to 1mm)	N/A	<ul style="list-style-type: none"> <li>• recrystallized Qtz with sutured boundaries</li> <li>• Ttn associated with mafic minerals</li> <li>• Elongate Bt and Act define strong fabric</li> <li>• Fsp strongly seritized</li> </ul>
<b><i>Bt-Carb Mafic Unit</i></b>				
10AL086	Bt (65%), Carb (15%), Qtz (10%), Ep (5%), Fsp (3%), Chl (2%), Ttn (<1%)	Very Fine	dominantly anhedral, Carb (elongate grains)	<ul style="list-style-type: none"> <li>• Qtz/Fsp layers (0.1-1mm thick)</li> <li>• Carb occurs in clusters and as elongate grains throughout</li> <li>• Fsp strongly seritized</li> <li>• late Qtz veins</li> <li>• high relief blue mineral in Qtz vein (spinel?)</li> </ul>
11AL004	Bt (68%), Carb (15%), Qtz (8%), Ep (5%), Fsp (3%), Chl (2%), Ap/Ttn (<1%)	Very Fine	dominantly anhedral, Carb (elongate grains)	<ul style="list-style-type: none"> <li>• Qtz/Fsp layers (0.1-1mm thick)</li> <li>• Carb elongate grains cut principle fabric</li> <li>• Fsp strongly seritized</li> <li>• late Qtz veins</li> <li>• Ep mantling (pumpellyite)</li> </ul>
<b><i>Layered Quartz Unit</i></b>				
11AL005	Qtz, Grt, Chl, Ap, And, Oxides	Fine - Medium	dominantly anhedral, Grt/Ap (euhedral)	<ul style="list-style-type: none"> <li>• Grt-rich with inclusions</li> <li>• Al-rich horizons</li> <li>• And minor occurring in Qtz layers</li> <li>• dominantly consists of recrystallized Qtz</li> <li>• planar fabric defined by elongate Qtz, and Al horizons</li> </ul>
<b><i>Contacts (10AL021, 10AL050, 10AL052) No formal description</i></b>				

**Table C-1:** Summary of mineralogy and petrography of thin sections. Not all samples are included here.

<b>Greenspond Road Section</b>				
<b>Unit/Sample No.</b>	<b>Mineralogy</b>	<b>Grain Size</b>	<b>Crystal Habit</b>	<b>Additional Notes (Textures, fabrics, etc.)</b>
<i>Al-Silicate bearing Orthogneiss</i>				
10AL003	Qtz, Plag, Kfs, Bt, Ms, Sil, And, Crd, Chl, Oxides, Zrc, Ap, Mnz	Medium - Coarse Qtz (0.5-4mm), Plag/Kfs (2-4mm), Bt (0.1-1mm), Ms (0.1-1mm), Oxides (<0.5mm), Sil (vfg needles), And (<0.5-3mm)	Qtz (anhedral), Plag/Kfs (an-subhedral), Bt/Ms (an-subhedral), Sil (acicular), And (anhedral)	<ul style="list-style-type: none"> <li>• Bt with inclusion of both Zrc and Mnz (radiation haloes)</li> <li>• Bt and Ms intergrowth (peraluminous melt)</li> <li>• Al-rich minerals (Bt, Ms, Sil, And) occur in clusters. Possible grain replacement (?)</li> <li>• Sil bundles of aligned needles cut across clusters</li> <li>• large Fsp grains w/ corroded edges</li> <li>• thin, discontinuous, mica-rich network, thinning and thickening defining a subtle foliation.</li> </ul>
10AL068	Qtz, Plag Kfs, Bt, Ms, Chl, Sil, And, Crd, Mnz, Zrc, Oxides	Kfs/Plag (0.5-5mm), Qtz (<0.1-3mm), Bt/Ms (<0.1-2mm), Sil (<0.1-1mm), Chl (<0.5mm), And (~2mm), Mnz/Zrc (<0.1mm)	Kfs/Plag/Bt/Ms (an-subhedral), Qtz/And/Crd/Oxides (anhedral), Sil (acicular), Mnz/Zrc (euhedral)	<ul style="list-style-type: none"> <li>• clusters of Al-rich minerals ~5mm diameter</li> <li>• Kfs has irregular grain boundaries</li> <li>• mica unstable and becomes skeletal along grain boundaries</li> <li>• mymekite present in minor amounts</li> <li>• foliation defined by discontinuous alignment of mica</li> <li>• And and Kfs/Plag are both poikilitic with inclusions of Bt, Ms and Qtz</li> </ul>
10AL071	Qtz, Plag, Kfs, Bt, Ms, Sil, Crd, Chl, Zrc, Oxides	Qtz/Plag/Kfs (0.5-4mm), Bt (0.1-4mm), Ms (<0.1-2mm), Sil (<0.2mm), Zrc (<0.1mm)	Qtz (anhedral), Plag/Kfs/Bt/Ms (an-subhedral), Sil (acicular), Crd (anhedral), Oxides (an-euhedral)	<ul style="list-style-type: none"> <li>• large wispy lens of fg Sil (0.5x10mm)</li> <li>• minor myrmekite present</li> <li>• Bt and Ms breakdown, Bt occurs as blebs</li> <li>• Bt and Ms laths cutting through Crd grains</li> <li>• Al-rich clusters w/ weakly defined orientation</li> <li>• minor chloritization of Bt</li> </ul>
10AL073	Qtz, Kfs, Plag, Bt, Ms, Sil, Crd, Zrc, Oxides	Qtz (0.1-3mm), Plag/Kfs (0.5-3mm), Bt/Ms (0.1-1mm), Sil (<0.5mm), Crd (<1mm)	Qtz/Kfs/Plag/Crd (anhedral), Bt/Ms (an-subhedral), Sil (acicular)	<ul style="list-style-type: none"> <li>• lens shaped aggregate of Al-rich minerals (dominantly Crd) w/ blebs of Bt and oxides throughout</li> <li>• myrmekite present</li> <li>• wormy/skeletal breakdown of Bt and Ms</li> <li>• significant amounts of recrystallized Qtz</li> <li>• bundles of Sil needles</li> <li>• Al-rich patches, more irregular than clusters seen in other sections</li> </ul>
10AL075	Qtz, Plag, Kfs, Bt, Ms, Chl, Sil, Crd, And (very minor), oxides, Zrc, Ap	Qtz (0.1-6mm), Plag/Kfs (0.5-5mm), Bt/Ms (0.1-3mm), Sil (<0.2mm), And (~2mm), Crd (~2mm)	Plag/Kfs/Qtz/And/Crd (anhedral), Bt/Ms (an-subhedral), Sil (acicular), Zrc/Ap (euhedral)	<ul style="list-style-type: none"> <li>• minor myrmekite</li> <li>• chloritization of Ms occurs along cleavage planes</li> <li>• Ms unstable breaking down (perhaps to Sil?)</li> <li>• Al-rich discontinuous layers pinch and swell across TS</li> <li>• Kfs with microcline and exsolution features</li> </ul>

**Table C-1:** Summary of mineralogy and petrography of thin sections. Not all samples are included here.

<b><i>Bt-Ms-Sil bearing Granitic Orthogneiss</i></b>				
10AL074	Qtz, Kfs, Plag, Bt, Ms, Sil, oxides	Kfs/Plag (0.5-5mm), Qtz/Bt/Ms (0.1-3mm), Sil (<0.2mm)	Kfs/Plag/Bt/Ms (an-subhedral), Qtz (anhedral), Sil (acicular)	<ul style="list-style-type: none"> <li>• coarse Kfs grains breaking down along edges</li> <li>• less mafic component than other orthogneiss in road cut</li> <li>• Bt being digested</li> <li>• Sil is very minor</li> <li>• significant seritization of Fsp</li> <li>• foliation not apparent in TS</li> </ul>
<b><i>Foliated Two-mica Leucogranite</i></b>				
10AL005	Qtz (50%), Kfs (30%), Plag (10%), Bt (6%), Ms (3%), Chl (1%), Zrc (<1%)	Qtz (0.1-3mm), Plag (0.5-3mm), Kfs (0.5-3mm), Bt (0.1-3mm), Ms (0.1-2mm)	Qtz (anhedral), Plag/Kfs (an-subhedral), Bt/Ms (subhedral), Zrc (euhedral)	<ul style="list-style-type: none"> <li>• Kfs shows microcline and exsolution features</li> <li>• minor chloritization of Bt and Ms</li> <li>• minor seritization of Fsp</li> <li>• Plag exhibits albite twinning.</li> <li>• Bt and Ms intergrown (peraluminous melt)</li> <li>• mica defines foliation.</li> </ul>
10AL072	Qtz (32%), Kfs (30%), Plag (22%), Bt (10%), Ms (3%), Chl (2%), Ep (1%)	Qtz (<0.1-4mm), Plag/Kfs (0.5-3mm), Bt/Ms (0.1-2mm), Ep (<0.2mm), Zrc (<0.2mm)	Qtz/Plag/Kfs/Ep (anhedral), Bt/Ms (an-subhedral), Zrc (euhedral)	<ul style="list-style-type: none"> <li>• significant seritization of Fsp</li> <li>• Kfs with microcline and exsolution features</li> <li>• micro-fractures cut across grains</li> <li>• Plag exhibits lamellar twinning</li> <li>• Coarser Fsp grains with irregular boundaries</li> <li>• irregular shaped patches of recrystallized Qtz</li> </ul>
10AL078	Qtz (35%), Kfs (30%), Plag (25%), Bt (5%), Ms (3%), Chl (2%), Oxides/Mnz/Ap (<1%)	Qtz (<0.1-4mm), Plag/Kfs (0.5-3mm), Bt/Ms (0.1-2mm), Ap/Mnz (<0.2mm)	Qtz/Plag/Kfs (anhedral), Bt/Ms (an-subhedral), Ap/Mnz (euhedral)	<ul style="list-style-type: none"> <li>• pleochroic haloes in Bt</li> <li>• faint alignment of micas</li> <li>• Kfs with microcline and exsolution features</li> <li>• Plag exhibits lamellar twinning</li> <li>• large feldspar grains with irregular boundaries</li> </ul>
<b><i>Enclave-bearing Orthogneiss</i></b>				
10AL004 (Enclave)	Qtz (60%), Plag (20%), Bt (20%), Oxides (<1%)	Medium equigranular Qtz (0.5mm), Plag (0.5-1mm), Bt (1-2mm length, ~0.5mm wide), Oxides (<0.5mm)	Plag/Bt (sub-euhedral), Qtz (anhedral), Oxides (an-euhedral)	<ul style="list-style-type: none"> <li>• Bt defines foliation.</li> <li>• Plag has albite twinning.</li> <li>• fine scale banding created by Bt as well as a larger scale banding created by sections more rich in Bt.</li> </ul>
10AL069 (Enclave)	Qtz (40%), Plag (30%), Kfs (10%), Bt (15%), Ms (3%), Chl (2%), Zrc/Oxides/Ap (<1%)	Medium equigranular Qtz/Plag/Kfs/Bt (0.5-1mm), Ms (<1mm), Oxides (<0.5mm), Zrc/Ap (<0.1mm)	Qtz/Plag/Kfs/Oxides (anhedral), Bt (sub-euhedral), Ms (subhedral), Zrc/Ap (euhedral)	<ul style="list-style-type: none"> <li>• triple junctions btwn many Qtz and Felds grains</li> <li>• even distribution of predominant minerals</li> <li>• elongated Bt defines a foliation</li> <li>• minor seritization of Fsp</li> </ul>

**Table C-1:** Summary of mineralogy and petrography of thin sections. Not all samples are included here.

10AL070 (Enclave)	Qtz (45%), Plag (25%), Bt (27%), Kfs (1%), Ms (1%), Ap (<1%), Oxides (<1%)	Medium Qtz/Bt (0.5-2mm), Plag/Kfs (0.5-1mm), Ms (<0.5mm), Ap (<0.1mm)	Qtz/Plag/Kfs (anhedral), Bt (sub-euhedral), Ms (an-subhedral), Ap (euhedral)	<ul style="list-style-type: none"> <li>• Bt-rich bands about 2mm thick</li> <li>• Qtz has sutured boundaries unlike previous sample</li> <li>• Plag exhibits albite twinning</li> <li>• Bt with pleochroic haloes</li> </ul>
<b>Late Undeformed Granitic Intrusion</b>				
10AL067	Kfs (34%), Plag (30%), Qtz (30%), Bt (2%), Ms (1%), Chl (2%), Oxides (1%)	Kfs (0.5-20mm), Plag (0.5-10mm), Qtz (0.1-5mm), Bt/Ms (0.1-3mm), Oxides (<0.5mm)	Kfs (an-subhedral), Plag (an-euhedral), Qtz (anhedral), Bt/Ms/Oxides (subhedral)	<ul style="list-style-type: none"> <li>• equant quartz grains</li> <li>• Kfs is poikilitic with inclusions of Qtz, Plag, Bt and Ms</li> <li>• oscillatory zoning of feldspar</li> <li>• zonal seritization of feldspar</li> <li>• blebs of Qtz concentrated along Kfs boundaries</li> <li>• Kfs with exsolution and microcline features</li> </ul>

**Table C-1:** Summary of mineralogy and petrography of thin sections. Not all samples are included here.

<b>Trinity Road Section</b>				
<b>Unit/Sample No.</b>	<b>Mineralogy</b>	<b>Grain Size</b>	<b>Crystal Habit</b>	<b>Additional Notes (Textures, fabrics, etc.)</b>
<b><i>Two-mica Granitic Orthogneiss</i></b>				
10AL012	Plag+Kfs (45%), Qtz (20%), Bt (20%), Ms (6%), Oxides (2%), Zrc (<1%)	Plag/Kfs (0.5-8mm), Qtz (<0.1-6mm), Bt (<1-3mm), Ms (0.5-2mm), Oxides (<1mm), Zrc (<0.1mm)	Plag/Kfs/Qtz/Oxides (anhedral), Ms/Bt (an-subhedral), Zrc (subhedral)	<ul style="list-style-type: none"> <li>Moderate- significant seritization of Fsp</li> <li>Kfs exhibits microcline and exsolution features</li> <li>minor chloritization of micas</li> <li>Bt and Ms intergrown.</li> <li>mica defines foliation but also occurs in randomly oriented clusters.</li> <li>patches of recrystallized Qtz with sutured grain boundaries</li> <li>oxides predominantly occur along mica cleavage planes</li> </ul>
10AL098	Qtz+Kfs+Plag (85%), Ms (10%), Bt (5%), Chl/Ap (<1%)	Qtz/Ms (0.1-3mm), Kfs/Plag (0.1-4mm), Bt (0.1-1mm), Ap (<0.1mm)	Qtz/Kfs/Plag (anhedral), Ms/Bt (an-euhedral), Ap (euhedral)	<ul style="list-style-type: none"> <li>primary and secondary Ms present</li> <li>Ms-Bt rich, thin, wavy layers</li> <li>Kfs w/ inclusions of Qtz, Ms and Bt</li> <li>irregular patches of recrystallized Qtz</li> <li>well preserved microcline and exsolution features in Kfs</li> <li>Fsp breakdown and show minor seritization</li> </ul>
10AL101	Qtz (30%), Kfs (30%), Plag (28%), Bt (8%), Ms (3%), Chl (1%)	Qtz/Kfs/Plag (0.1-4mm), Ms/Bt (0.1-3mm), Chl (<0.5mm)	Qtz/Kfs/Plag/Chl (anhedral), Ms/Bt (an-subhedral)	<ul style="list-style-type: none"> <li>myrmekite present</li> <li>moderate seritization of Fsp</li> <li>recrystallized Qtz with sutured boundaries</li> <li>Ms and Bt defines foliation through the presence of scarce, thin, wavy bands</li> </ul>
<b><i>Bt-Ms-Grt bearing Leucogranite</i></b>				
10AL100	Qtz (30%), Plag (30%), Kfs (30%), Ms (7%), Bt (2%), Grt (1%)	Qtz/Plag/Kfs (0.1-3mm), Bt (0.1-1mm), Ms (0.1-2mm), Grt (~0.1mm)	Qtz/Plag/Kfs/Bt (anhedral), Ms (an-euhedral), Grt (euhedral)	<ul style="list-style-type: none"> <li>irregular sutured boundaries btwn Qtz and Fsp</li> <li>Ms defines weak foliation</li> <li>Kfs has well developed microcline twins</li> <li>patches of finer grained recrystallized Qtz</li> <li>micro-shear-zones along some grain boundaries with ground Qtz and mica</li> </ul>
<b><i>Bt-Hbl Intermediate Blocks</i></b>				
10AL099	Amph (30%), Bt (30%), Fsp (15%), Qtz (20%), Oxides (5%) Ap/Zrc (<1%)	Amph (0.5mm), Qtz/Fsp (0.1-0.5mm), Bt (0.1-2mm), Oxides (<0.5mm)	Amph (subhedral), Qtz/Fsp (anhedral), Bt (an-euhedral), Oxides (an-subhedral)	<ul style="list-style-type: none"> <li>pale green, short, subrounded Amph</li> <li>strong foliation defined by Bt alignment and Amph lens-shaped aggregates</li> <li>Bt very orange in color</li> <li>Bt, Qtz, Fsp rich layers with polycrystalline Amph lenses (~0.5x1.5cm)</li> </ul>

**Table C-1:** Summary of mineralogy and petrography of thin sections. Not all samples are included here.

<b>I Love You Road Section</b>				
<b>Unit/Sample No.</b>	<b>Mineralogy</b>	<b>Grain Size</b>	<b>Crystal Habit</b>	<b>Additional Notes (Textures, fabrics, etc.)</b>
<b><i>Tonalitic Orthogneiss</i></b>				
10AL010	Qtz (35%), Plag (35%), Bt (15%), Ms (10%), Chl (2%), Oxides (3%), Mnz/Rt (<1%)	Qtz (<2mm, but few grains up to 1cm). Plag (~2-3mm), Ms (<0.1-2mm), Bt (0.1-2mm), Oxides (<0.1mm)	Qtz (anhedral), Plag/Bt/Ms (an-subhedral), Oxides/Rt (anhedral), Mnz (euhedral)	<ul style="list-style-type: none"> <li>oxides predominantly along mica cleavage planes</li> <li>Bt has pleochroic haloes</li> <li>myrmekite present in minor amounts</li> <li>intergrowths of Bt and Ms</li> <li>minor seritization of Fsp</li> <li>Bt and Ms form wavy, discontinuous bands (&lt;2mm), and Qtz and Plag lack preferred orientation.</li> </ul>
10AL097	Qtz, Plag, Kfs (minor), Bt, Ms, Chl (minor), Ap, Zrc, Mnz, Rt, Oxides	Qtz (0.1-4mm), Bt (0.1-3mm), Plag (0.5-4mm), Kfs (0.5mm), Ms (<0.1-2mm), Mnz/Zrc (<0.1mm), Ap (~0.2mm)	Qtz/Plag/Kfs/Ms (anhedral), Bt/Oxides (an-subhedral), Mnz/Zrc/Ap (euhedral)	<ul style="list-style-type: none"> <li>oxides along mica cleavage planes</li> <li>mica ground in fig Al-rich layers but also as larger flakes in Qtz/Plag layers</li> <li>myrmekite present</li> <li>wavy network of semi continuous Bt-Ms layers (~0.5mm thick) and layers of cg Qtz-Plag rich layers with sutured grain boundaries (~1cm thick)</li> </ul>
<b><i>Tonalite</i></b>				
10AL011	Plag (40%), Qtz (25%), Bt (20%), Amph (5%), Ep (5%), Ap (2%), Ttn (2%), Oxides (1%), Rt (<1%)	Plag (0.5-2mm), Qtz (0.1-2mm), Bt (0.1-2mm), Ttn (1mm), Ep (<0.2mm), Oxides (<0.5mm)	Plag/Bt (subhedral), Qtz (anhedral), Ttn (sub-euhedral), Ep (anhedral), Oxides (an-subhedral)	<ul style="list-style-type: none"> <li>Bt with Ep along grain boundaries</li> <li>Ttn with Plag coronas (Plag coronas ~1-3cm diameter) and Ttn grain is host oikocryst to several Plag laths</li> <li>long Ap prisms abundant throughout.</li> <li>lacks foliation.</li> </ul>
10AL096	Plag (35%), Qtz (30%), Bt (20%), Fe-poor Amph (5%), Ep (3%), Ap (3%), Ttn (2%), Oxides (2%), Rt (<1%)	Qtz/Plag/Bt/Amph (0.1-0.5mm), Oxides/Ap (<0.1mm), Ttn (1mm), Ep (0.1-0.5mm)	Qtz/Plag- anhedral, Bt-an-subhedral, Amph-an-subhedral, Ep-anhedral, Ap/oxides-euhedral	<ul style="list-style-type: none"> <li>Ttn with subophitic Plag laths and surrounded by Plag (feature is ~0.5cm)</li> <li>minus coronas minerals are evenly distributed</li> <li>Plag with lamellar twins</li> <li>abundance of fine grained Ap rectangular prisms</li> <li>Bt altering to Amph (?)</li> </ul>
<b><i>Leucogranite</i></b>				
10AL095	Kfs (40%), Plag (22%), Qtz (20%), Ms (8%), Bt (6%), Chl (2%), Ap (1%), Oxides (1%), Ep (<1%)	Qtz (0.1-1mm), Kfs/Plag (0.1-2mm), Bt/Ms (<0.1-1mm), Ap (0.2mm), Ep (<0.5mm), Oxides (<0.1mm)	Qtz/Kfs/Plag/Ep/Oxides (anhedral), Bt/Ms (an-euhedral), Ap (euhedral)	<ul style="list-style-type: none"> <li>intergrowths of Bt and Ms</li> <li>some seritization restricted to cores of feldspars</li> <li>myrmekite present</li> <li>microcline twinning and some exsolution in Kfs</li> <li>no apparent foliation</li> <li>Fsp has irregular boundaries w/ inclusions of Qtz and Ms</li> </ul>
<b><i>Aplite Vein</i></b>				
11AL006	Two units: Aplite and tonalite	N/A	N/A	Outer boundary of aplite vein in contact with the tonalite consists entirely of orthoclase

**Table C-1:** Summary of mineralogy and petrography of thin sections. Not all samples are included here.

<b>North of Cape Freels</b>				
<b>Unit/Sample No.</b>	<b>Mineralogy</b>	<b>Grain Size</b>	<b>Crystal Habit</b>	<b>Additional Notes (Textures, fabrics, etc.)</b>
<i>Cape Freels Gneiss</i>				
10AL001	Ms (42%), Qtz (32%), Chl (12%), Bt (6%), Oxides (5%), Ep (3%), Mnz/Ttn/Rt (<1%), Sil (<1%)	Chl (long thin sheets ~0.5 x 1mm), Bt (<0.5mm), Ms (<1mm), Qtz (<0.5mm), Oxides (<0.5 mm)	Ms/Chl (sub-euhedral sheets), Qtz/Ep (anhedral), Bt (subhedral), Oxides (euhedral)	<ul style="list-style-type: none"> <li>• distinct banding of Qtz-rich layers/lenses and Chl-Ms rich layers.</li> <li>• Qtz layers &lt;1mm thick and mica layers generally &lt;0.5mm but up to 2mm thick.</li> <li>• mica are aligned parallel with layering, although some isolated grains and clusters have random orientation</li> </ul>
10AL002	Qtz, Plag, Ms, Bt, Chl, Sil (?), Rt, Ap, Oxides	Fine- medium Qtz (<1mm), Plag (<2mm), Ms (<1mm), Chl (<0.2mm), Oxides (<0.5mm), Ap/Rt (<0.1mm)	Plag (subhedral), Qtz (anhedral), Ms (an-subhedral), Chl (anhedral)	<ul style="list-style-type: none"> <li>• seritization of Plag</li> <li>• alternating Qtz/Plag layers (&lt;4mm thick) and mica-rich layers (&lt;1mm)</li> <li>• fg mica strung out parallel to layering, also patches of randomly oriented mica, randomly distributed throughout</li> </ul>
10AL093	Qtz, Ms, Bt, Fsp, Chl, Ep, Oxides, Zrc, Sil	Fine to Medium	Qtz/Fsp/ Ep/ Chl/ Oxides (anhedral), Ms/Bt (an-subhedral), Zrc (sub-euhedral), Sil (acicular)	<ul style="list-style-type: none"> <li>• skeletal oxides</li> <li>• layers of recrystallized Qtz and Fsp (~0.5mm thick)</li> <li>• layers consisting of Qtz, Fsp and micas up to 1cm thick</li> <li>• micas are aligned and form wispy thin layers</li> <li>• turbid patches</li> </ul>
<i>Diabase Dyke</i>				
10AL057 (Not described in txt)	Plag, Bt, Amph, Oxides, Ep	N/A	N/A	<ul style="list-style-type: none"> <li>• dominated by Plag laths with random orientation (cumulate)</li> <li>• highly altered</li> </ul>

**Table C-1:** Summary of mineralogy and petrography of thin sections. Not all samples are included here.

<b>Valleyfield Road</b>				
<b>Unit/Sample No.</b>	<b>Mineralogy</b>	<b>Grain Size</b>	<b>Crystal Habit</b>	<b>Additional Notes (Textures, fabrics, etc.)</b>
<i>Valleyfield Orthogneiss</i>				
10AL006	Qtz (37%), Plag (30%), Kfs (10%), Bt+Chl (10%), Ms (5%), Oxides (2%), Ep (1%), Zrc (<1%)	Qtz (0.1-0.5mm), Kfs/Plag (0.3-3mm), Bt (<0.2mm), Chl (<0.2mm), Ms (<0.5mm), Ap/Zrc/Rt/Oxides (<0.1mm)	Qtz/Chl/Ep (anhedral), Kfs/Plag (subhedral), Bt/Ms (an-subhedral), Ap/Zrc (euhedral)	<ul style="list-style-type: none"> <li>• significant seritization of Fsp</li> <li>• significant chloritization of Bt</li> <li>• Plag exhibits albite twinning</li> <li>• Thin bands (&lt;1mm) of Bt, Ms and Chl wrapping around larger Qtz and Fsp crystals</li> <li>• micas also form randomly oriented clusters throughout slide</li> <li>• Qtz occurs as recrystallized lenses and equant grains</li> </ul>
10AL077	Kfs (30%), Plag (30%), Qtz (20%), Bt (17%), Ms (3%), Chl/Oxides/Zrc/Ap (<1%)	Qtz (0.1-0.5mm), Kfs/Plag (0.2-1mm), Bt/Ms (<0.2-0.5mm), Chl (<0.2mm), Ap/Zrc/Oxides (<0.1mm)	Qtz/Chl/Ep (anhedral), Kfs/Plag (subhedral), Bt/Ms (an-subhedral), Ap/Zrc (euhedral)	<ul style="list-style-type: none"> <li>• Bt rich discontinuous layers (&lt;0.2mm thick) wrap around Qtz and Fsp-rich pockets (0.5mm thick)</li> <li>• Oxides occur along mica cleavage planes</li> <li>• significant seritization of Fsp</li> </ul>
<i>Valleyfield Paragneiss</i>				
10AL007	Qtz (50%), Plag+Kfs (30%), Bt (10%), Ms (8%), Sil (2%), Chl (<1%)	Qtz (0.5-1mm), Kfs/Plag (2-4mm), Ms/Bt (<2mm), Sil/Chl (<1mm)	Qtz/Bt (anhedral), Kfs/Plag (subhedral), Ms (some acicular, anhedral)	<ul style="list-style-type: none"> <li>• Bt has pleochroic haloes</li> <li>• moderate-significant seritization of Fsp</li> <li>• Ms occurring as bundles of acicular fibres as well as sheets.</li> <li>• mica defines the foliation occurring as thin (&lt;1mm), discontinuous, wavy bands.</li> </ul>
10AL008	Qtz (60%), Kfs+Plag (25%), Chl (5%), Ms (5%), Bt (3%), Oxides (2%), Ep/Zrc (<1%)	Kfs/Plag (~0.5mm), Qtz (~0.2mm), Ms/Bt (<0.2mm), Ep/Zrc/Oxides (<0.1mm)	Qtz Bt/Ms/Chl/Ep (anhedral), Kfs/Plag/Zrc (subhedral)	<ul style="list-style-type: none"> <li>• moderate chloritization of Bt and Ms</li> <li>• significant seritization of Fsp</li> <li>• foliation is not apparent in thin section</li> <li>• some albite twins in Plag visible despite sericite alteration</li> </ul>
10AL076	Qtz, Ms, Fsp, Bt/Chl, Grt, Sil, Zrc, Oxides	Qtz (0.1-5mm), Ms/Bt/Chl (<2mm), Fsp (<5mm), Grt (<0.5mm), Sil/Oxides (<0.2mm)	Qtz/Fsp/Oxides (anhedral), Ms/Bt/Chl (an-subhedral), Grt (sub-euhedral), Sil (acicular), Zrc (subhedral)	<ul style="list-style-type: none"> <li>• oxides commonly along mica cleavage planes</li> <li>• lens-shaped pockets of recrystallized Qtz</li> <li>• Sil shows wavy orientation</li> <li>• alternating Al-rich and Qtz rich layers</li> <li>• some mica cleavage planes are kinked</li> </ul>
<i>Valleyfield Mylonite</i>				
10AL013	Qtz (35%), Kfs (25%), Plag (25%), Bt (10%), Ms (3%), Chl (2%)	Medium-Coarse Plag/Kfs (0.5mm-1cm), Qtz (~1mm), Bt/Chl (<1mm), Ms (<0.5mm)	Qtz (anhedral/equant), Plag/Kfs (an-subhedral), Bt/Ms/Chl (anhedral)	<ul style="list-style-type: none"> <li>• minor chloritization of Bt</li> <li>• moderate-significant seritization of Fsp</li> <li>• thin (1mm), wavy bands of mica (thickness variable and passes into randomly oriented clusters)</li> <li>• Qtz boundaries are very clearcut</li> <li>• late Qtz veins fracture coarse Fsp grains.</li> </ul>
10AL014	Qtz (45%), Plag (20%), Kfs (18%), Ms (10%), Bt/Chl-4%, Ap (2%), Oxides (1%), Ep (<1%)	Fine-Medium Plag/Kfs (1-6mm), Qtz (<0.1-1mm), Ms (<0.1-2mm), Bt (<0.1-2mm), Oxides (<0.5mm)	Qtz (anhedral/equant), Plag/Kfs (anhedral), Ms (an-euhedral)	<ul style="list-style-type: none"> <li>• moderate-significant seritization of Fsp</li> <li>• relatively undeformed Qtz layers and lenses</li> <li>• Kfs shows microcline and exsolution</li> <li>• minor chloritization of micas</li> <li>• some larger Ms laths amongst finely ground minerals</li> </ul>

**Table C-1:** Summary of mineralogy and petrography of thin sections. Not all samples are included here.

<b>Town of Hare Bay</b>				
<b>Unit/Sample No.</b>	<b>Mineralogy</b>	<b>Grain Size</b>	<b>Crystal Habit</b>	<b>Additional Notes (Textures, fabrics, etc.)</b>
<i>Hare Bay Orthogneiss</i>				
10AL009	Kfs+Plag (50%), Qtz (25%), Bt (15%), Chl (5%), Ms (3%), Oxides (2%), Mnz/Rt/Ep (<1%)	Medium Kfs/Plag (0.5-2mm), Qtz (0.1-2mm), Bt (<0.1-2mm), Ms (<1mm), Oxides (<1mm)	Qtz/Oxides/Ep (anhedral), Kfs/Plag/Bt/Ms (an-subhedral), Zrc/Mnz (euhedral)	<ul style="list-style-type: none"> <li>• significant seritization of Fsp</li> <li>• Plag shows albite twins</li> <li>• pleochroic haloes in Bt</li> <li>• oxides predominantly associated with thin mica layers</li> <li>• mica-rich thin (~1mm), wavy bands</li> <li>• mica also occurs in a lesser amount in Qtz/Fsp-rich layers with a more random orientation</li> </ul>
10AL094	Qtz (30%), Plag (25%), Bt (15%), Kfs (10%), Ms (10%), Chl (5%), Oxides (5%), Ap/Zrc (<1%)	Medium Qtz (0.1-2mm), Kfs/Plag (0.5-2mm), Bt (<0.1-2mm), Ms (<1mm), Chl/Oxides/Zrc/Ap (<0.5mm)	Qtz (equant anhedral), Kfs/Plag/Bt/Ms (an-subhedral), Chl/Oxides (anhedral) Zrc/Mnz/Ap (euhedral)	<ul style="list-style-type: none"> <li>• mica defines the foliation</li> <li>• moderate seritization of Fsp</li> <li>• equant Qtz grains with triple junction grain boundaries</li> <li>• oxides concentrated in Bt rich clusters</li> <li>• mica with kinked cleavage planes</li> </ul>

**Table C-1:** Summary of mineralogy and petrography of thin sections. Not all samples are included here.

## **Appendix D: Lithochemical Data**

### **C-1: Methodology**

Initially a portion of each of the 48 selected samples was removed for geochemical analysis. The size of this portion was directly proportional to grain size; the larger the grain size, the larger the sample to be crushed. Using the water saw, care was taken to remove undesirable features (veining, extreme weathering, etc) that can obviously affect an analysis.

#### ***Crushing***

The selected sample was crushed using a rock hammer to create small chips, less than 2 cm diameter. The sample was loaded into a tungsten-carbide mill machine and crushed into a fine powder. An airgun, ethanol and occasionally silica sand were used to clean equipment in between samples, minimizing the possibility of cross-contamination.

#### ***XRF Analysis***

Powdered samples were initially analyzed by X-ray fluorescence (XRF) analysis for major and trace element chemistry. XRF measures the fluorescence spectra emitted by a material, when it is subjected to high energy X-rays or gamma rays. XRF-pressed pellet results were provided by Memorial University of Newfoundland's laboratory and XRF-fused disc results were provided by Actlabs.

In the pressed pellet technique, 5 grams of rock powder was measured and combined with 0.7 grams of phenolic resin binder. A Herzog Pellet Press then presses this mixed powder for ten seconds, under 20 ton/in<sup>2</sup> of pressure. Next the produced pellet was baked for 15 minutes at 200 °C. Fused pellets were prepared to acquire precise major

element data.

The fusion technique, analyzes a disc made by mixing 0.5g of roasted sample and 6.5g of a combination of lithium metaborate and lithium tetraborate, using lithium bromide as a releasing agent. The powder is fused using a automated crucible fluxer in Pt crucibles, and poured into a Pt mold, creating the disc that was analysed on a Panalytical Axios Advanced wavelength dispersive XRF.

Loss on Ignition (LOI) was carried out on all samples. In this procedure, two grams of rock powder is precisely weighed and baked in a furnace at 1050 °C. This temperature is reached slowly over a two-hour period and then is maintained for an additional seven hours. At the end of this time the furnace temperature is lowered to 110 °C and the samples remain in the oven until they are re-weighed.

#### *ICP-MS Analysis*

Inductively coupled plasma spectroscopy (ICP-MS), completed by Pam King at Memorial University, offers a precise multielemental analysis of a sample. The same 48 samples were analyzed with this method.

The sinter technique was used to collect REE, Th and Y as well as Zr, Nb, Ba, Hf and Ta data. The sinter technique is advantageous for measuring the latter elements as a simple acid digestion technique may result in incomplete digestion of resistant minerals that host these elements. However, comparison to XRF data is still critical for Zr, Nb, Ba, Hf and Ta to cross-check for incomplete digestion, which may produce erroneous results by ICP-MS.

The sinter technique begins with the sintering of 0.2 g of sample with sodium

peroxide. This sinter cake is dissolved and the REE hydroxide-bearing precipitate is separated and undergoes further dissolution. The method of internal standardization corrects matrix and drift effects when using ICP-MS methods.

## **C-2: Reliability of Results**

When interpreting geochemical data it is necessary to consider the reliability of results. Careful sample collection and calculation of accuracy and precision for geochemical data is critical to the viability of results.

Geochemical samples were selected as representative of a specific unit, avoiding significant alteration and weathering when possible. Any weathered surfaces or alteration features that were unavoidable in field collection were removed as much as possible with a rock saw.

The reliability of the acquired geochemical data has been tested through assessing both accuracy and precision. Analytical accuracy determines how close an analysis is to certified or accepted values. To evaluate the accuracy, standards with known certified values are run with the samples. To calculate accuracy as percent relative difference the following equation is used:

$$\% \text{ Relative Difference (RD)} = [(X_{\text{measured}} - X_{\text{certified}}) / X_{\text{certified}}] * 100$$

$X_{\text{measured}}$  = elemental concentration determined for a standard by the lab

$X_{\text{certified}}$  = known elemental concentration of the standard

In general, data which has a relative difference < 10% is considered to be accurate.

Major element analyses were completed using Memorial's pressed pellet XRF

analysis and Actlab's XRF fusion analysis. The values for major elements reported in the geochemical data table and used in the geochemical analysis of this study are those determined using the XRF fusion technique. To evaluate the accuracy of this technique, five samples of standard reference material were run with submitted samples (Table C-2). For most major minerals the % RD is less than 10, however some exceptions do apply. Relative differences above 10% are observed when elemental values are very low, approaching the limit of detection. Such cases are seen for  $\text{Fe}_2\text{O}_3$  in one standard (11%), MgO for one standard (200%), CaO for one standard (27%),  $\text{Na}_2\text{O}$  for two standards (67% and 77%) and  $\text{P}_2\text{O}_5$  for one standard (58%). Table C-1 shows the accuracy of major element analysis at Memorial using the XRF pressed pellet technique, however these values were not used in this study and therefore will not be discussed.

Trace element concentrations of four standard reference materials are reported from XRF (pressed pellet) analysis at Memorial. Trace element values determined using XRF (pressed pellet) were used where inaccurate results were obtained using ICP-MS due to incomplete dissolution, and in cases where values between ICP-MS and XRF showed minor difference an average of both values was used. The majority of calculated relative differences are less than 10%, indicating good overall accuracy (Table C-1 and Table C-3). Exceptions do apply as several elements have a %RD greater than 10. In many cases, the high %RD is observed when trace element values are very low and approach the limit of detection. In all standards As, S, Cr, Zn and Ce gave inaccurate results with significant differences between measured and certified values but these are not used in this study.

Trace element concentrations for two standards from two separate runs (Run 1 and Run 3) are reported from ICP-MS analysis at Memorial (Table C-3). The majority of elemental values show acceptable differences between measured and certified values, with % RD less than 10. Ta and Th values are commonly low, and approach the limit of detection. They have high % RD ranging from 3-32% for Ta and 5-56% for Th, and may have inaccurate results in the dataset. Relative differences for Ba range from 20-22%, showing these values may not be accurate. Zr and Nb also have some high calculated % RD, but in many cases the XRF value or an average of the XRF and ICP-MS values is reported to improve accuracy.

Analytical precision is a measure of the quality of acquired data and displays how well a lab can reproduce measurements. Precision has been assessed using two methods. The first is based on the percent relative standard deviation (%RSD), and the second is based on the percent difference between duplicate samples. The %RSD was presented with other lab data for most elements. The percent difference is calculated using the following formula:

$$\% \text{ RSD} = (s_i / \mu_i) * 100$$

Where  $s_i$  = standard deviation of the mean value for an element ( $i$ ) for duplicate analyses. The %RSD for elemental values calculated using XRF fusion (Table C-5), XRF pressed pellet (Table C-4) and ICP-MS (Table C-5) are reported. For XRF pressed pellet the %RSD from the standards BHVO-1, SY-2 and PACS-1 is provided in table #, where calculations were completed by Memorial's lab, therefore only the %RSD value is shown. Standards reported were chosen based on relevance to rock types of samples submitted in

each run. According to Jenner (1996) %RSD from 0-3% is excellent, 3-7% is very good, 7-10% is good and anything greater than 10% is poor, with respect to precision. The majority of percent relative standard deviations (%RSD) between duplicate analysis in each analytical technique fall between the 0-3% range meaning over all the data collected has excellent precision. Ni in PACS-1 (XRF-pressed pellet) had a %RSD value of 13.1%, and is the only duplicate analysis with poor precision.

Analyte Symbol	Unit of Reporting	Standard	Measured Value	Certified Value	RD (%)	Standard	Measured Value	Certified Value	RD (%)
SiO2	wt%	AGV-1	60.85	58.79	3.50	DNC-1	44.41	47.04	5.59
TiO2	wt%	AGV-1	1.02	1.05	2.86	DNC-1	0.46	0.48	4.17
Al2O3	wt%	AGV-1	16.98	17.14	0.93	DNC-1	19.47	18.3	6.39
Fe2O3(T)	wt%	AGV-1	6.58	6.76	2.66	DNC-1	9.98	9.93	0.50
MnO	wt%	AGV-1	0.09	0.09	0.00	DNC-1	0.15	0.15	0.00
MgO	wt%	AGV-1	1.45	1.53	5.23	DNC-1	10.44	10.05	3.88
CaO	wt%	AGV-1	4.84	4.94	2.02	DNC-1	11.15	11.27	1.06
Na2O	wt%	AGV-1	3.84	4.26	9.86	DNC-1	1.87	1.87	0.00
K2O	wt%	AGV-1	2.77	2.91	4.81	DNC-1	0.26	0.23	13.04
P2O5	wt%	AGV-1	0.45	0.49	8.16	DNC-1	0.11	0.09	22.22
As	ppm	AGV-1	3	1	200.00	DNC-1	-4	0	
S	ppm	AGV-1	949	26	3550.00	DNC-1	1244	392	217.35
Cr	ppm	AGV-1	3	10	70.00	DNC-1	305	285	7.02
Cu	ppm	AGV-1	56	60	6.67	DNC-1	81	96	15.63
Ga	ppm	AGV-1	21	20	5.00	DNC-1	13	15	13.33
Ni	ppm	AGV-1	15	16	6.25	DNC-1	247	247	0.00
Pb	ppm	AGV-1	34	36	5.56	DNC-1	5	6	16.67
Sc	ppm	AGV-1	13	12	8.33	DNC-1	26	31	16.13
V	ppm	AGV-1	113	121	6.61	DNC-1	141	148	4.73
Zn	ppm	AGV-1	70	88	20.45	DNC-1	54	66	18.18
Ba	ppm	AGV-1	1265	1226	3.18	DNC-1	118	114	3.51
Rb	ppm	AGV-1	71	67.3	5.50	DNC-1	3.4	4.5	24.44
Sr	ppm	AGV-1	697.7	662	5.39	DNC-1	142.2	145	1.93
Th	ppm	AGV-1	8	7	14.29	DNC-1	-2	0	
U	ppm	AGV-1	3	2	50.00	DNC-1	0	0	
Nb	ppm	AGV-1	17	15	13.33	DNC-1	2	3	33.33
Zr	ppm	AGV-1	261.7	227	15.29	DNC-1	37.4	41	8.78
Y	ppm	AGV-1	18.2	20	9.00	DNC-1	15.6	18	13.33
Ce	ppm	AGV-1	99	67	47.76	DNC-1	4	11	63.64

**Table C-1:** Major and trace element concentrations of standard reference materials that were run with samples during XRF (pressed pellet) analysis at Memorial University. Where % Relative Difference (RD) =  $[(X_{\text{measured}} - X_{\text{certified}}) / X_{\text{certified}}] * 100$ .

Analyte Symbol	Unit of Reporting	Standard	Measured Value	Certified Value	RD (%)	Standard	Measured Value	Certified Value	RD (%)
SiO2	wt%	JG-2	79.3	76.95	3.05	BCR-2	56.74	54.06	4.96
TiO2	wt%	JG-2	0.05	0.04	25.00	BCR-2	2.33	2.24	4.02
Al2O3	wt%	JG-2	13.71	12.41	10.48	BCR-2	14.71	13.64	7.84
Fe2O3(T)	wt%	JG-2	1.04	0.92	13.04	BCR-2	12.98	13.41	3.21
MnO	wt%	JG-2	0.02	0.02	0.00	BCR-2	0.19	0.18	5.56
MgO	wt%	JG-2	0	0.04	100.00	BCR-2	3.03	3.48	12.93
CaO	wt%	JG-2	0.8	0.8	0.00	BCR-2	6.99	6.95	0.58
Na2O	wt%	JG-2	3.58	3.55	0.85	BCR-2	3.2	3.27	2.14
K2O	wt%	JG-2	4.59	4.72	2.75	BCR-2	1.82	1.69	7.69
P2O5	wt%	JG-2	0.05	0		BCR-2	0.29	0.36	19.44
As	ppm	JG-2	0	1	100.00	BCR-2	12	0	
S	ppm	JG-2	549	9	6000.00	BCR-2	767	410	87.07
Cr	ppm	JG-2	1	8	87.50	BCR-2	12	16	25.00
Cu	ppm	JG-2	-2	0		BCR-2	20	19	5.26
Ga	ppm	JG-2	18	19	5.26	BCR-2	23	22	4.55
Ni	ppm	JG-2	22	2	1000.00	BCR-2	27	13	107.69
Pb	ppm	JG-2	30	33	9.09	BCR-2	9	14	35.71
Sc	ppm	JG-2	3	2	50.00	BCR-2	33	33	0.00
V	ppm	JG-2	-2	3	166.67	BCR-2	416	407	2.21
Zn	ppm	JG-2	27	13	107.69	BCR-2	90	130	30.77
Ba	ppm	JG-2	48	67	28.36	BCR-2	712	681	4.55
Rb	ppm	JG-2	282.2	297	4.98	BCR-2	47.4	47.2	0.42
Sr	ppm	JG-2	16	16	0.00	BCR-2	344.5	330	4.39
Th	ppm	JG-2	28	30	6.67	BCR-2	3	6	50.00
U	ppm	JG-2	15	13	15.38	BCR-2	1	2	50.00
Nb	ppm	JG-2	15.2	15	1.33	BCR-2	15.2	14	8.57
Zr	ppm	JG-2	89.6	97	7.63	BCR-2	201.1	190	5.84
Y	ppm	JG-2	72.7	89	18.31	BCR-2	33.3	38	12.37
Ce	ppm	JG-2	61	46	32.61	BCR-2	75	54	38.89

**Table C-1:** Major and trace element concentrations of standard reference materials that were run with samples during XRF (pressed pellet) analysis at Memorial University. Where % Relative Difference (RD) =  $[(X_{\text{measured}} - X_{\text{certified}}) / X_{\text{certified}}] * 100$ .

XRF-FUSION

Analyte Symbol	SiO2	Al2O3	Fe2O3(T)	MnO	MgO	CaO	Na2O	K2O	TiO2	P2O5
Unit Symbol	%	%	%	%	%	%	%	%	%	%
Analysis Method	FUS-XRF	FUS-XRF	FUS-XRF	FUS-XRF	FUS-XRF	FUS-XRF	FUS-XRF	FUS-XRF	FUS-XRF	FUS-XRF
MICA-FE Meas	34.69	19.54	25.58	0.345	4.65	0.44	0.53	8.83	2.51	0.41
MICA-FE Cert	34.4	19.5	25.6	0.35	4.55	0.43	0.3	8.75	2.5	0.45
% RD	0.843	0.205	0.078	1.429	2.198	2.326	76.667	0.914	0.400	8.889
FK-N Meas	65.09	18.71	0.1	< 0.001	< 0.01	0.08	2.33	12.97	0.02	0.01
FK-N Cert	65	18.6	0.09	0.005	0.01	0.11	2.58	12.8	0.02	0.024
% RD	0.138	0.591	11.111	-	-	27.273	9.690	1.328	0.000	56.333
BE-N Meas	38.79	10.14	-	0.199	13.28	13.98	3.29	1.37	2.72	1.08
BE-N Cert	38.2	10.1	-	0.2	13.1	13.9	3.18	1.39	2.61	1.05
% RD	1.545	0.396	-	0.500	1.374	0.576	3.459	1.439	4.215	2.857
AC-E Meas	70.73	15.29	2.52	0.059	0.09	0.37	6.76	4.51	0.11	-
AC-E Cert	70.35	14.7	2.56	0.058	0.03	0.34	6.54	4.49	0.11	-
% RD	0.540	4.014	1.563	1.724	200.000	8.824	3.364	0.445	0.000	-
MICA-Mg Meas	38.14	15.29	9.4	0.258	20.32	< 0.01	0.04	9.91	1.61	< 0.01
MICA-Mg Cert	38.3	15.2	9.46	0.26	20.4	0.08	0.12	10	1.63	0.01
% RD	0.418	0.592	0.634	0.769	0.392	-	66.667	0.900	1.227	-

**Table C-2:** Major element concentrations of standard reference materials that were run with samples during XRF (fusion) analysis at Actlabs. Where % Relative Difference (RD) =  $[(X_{\text{measured}} - X_{\text{certified}}) / X_{\text{certified}}] * 100$ .

ICP-MS (RUN 3)

Sample/Analyte Symbol	Y	Zr	Nb	Ba	La	Ce	Pr	Nd	Sm	Eu
BR-688 Certified	17.81	59.15	4.87	163.33	4.98	11.55	1.65	8.03	2.3	0.94
BR-688 Measured	17.121	61.587	4.891	207.030	4.940	11.120	1.631	8.087	2.216	0.843
% RD	4.023	3.957	0.429	21.108	0.806	3.866	1.179	0.706	3.797	11.519

MRG-1 Certified	11.5	107	22.3	49.4	8.83	25.8	3.71	17.6	4.34	1.38
MRG-1 Measured	11.451	121.852	25.330	63.178	9.030	25.692	3.739	18.077	4.033	1.283
% RD	0.430	12.189	11.961	21.808	2.212	0.421	0.769	2.638	7.610	7.549

Sample/Analyte Symbol	Gd	Tb	Dy	Ho	Er	Tm	Yb	Lu	Hf	Ta	Th
BR-688 Certified	2.88	0.48	3.21	0.7	2.1	0.3	2	0.3	1.54	0.18	0.33
BR-688 Measured	2.895	0.477	3.341	0.694	2.061	0.290	2.144	0.286	1.442	0.174	0.744
% RD	0.504	0.727	3.922	0.803	1.875	3.442	6.718	4.775	6.831	3.242	55.616

MRG-1 Certified	3.97	0.52	3	0.49	1.16	0.14	0.79	0.11	3.89	0.74	0.82
MRG-1 Measured	4.116	0.544	2.899	0.506	1.164	0.149	0.839	0.109	3.690	0.634	1.065
% RD	3.542	4.382	3.474	3.103	0.372	6.070	5.787	1.233	5.427	16.662	22.971

**Table C-3:** Trace element concentrations of standard reference materials that were run with samples during ICP-MS analysis at Memorial University. Where % Relative Difference (RD) =  $[(X_{\text{measured}} - X_{\text{certified}}) / X_{\text{certified}}] * 100$

ICP-MS (RUN 1)

Sample/Analyte Symbol	Y	Zr	Nb	Ba	La	Ce	Pr	Nd	Sm	Eu
BR-688 Certified	17.81	59.15	4.87	163.33	4.98	11.55	1.65	8.03	2.3	0.94
BR-688 Measured	17.061	70.345	4.312	204.728	5.028	11.338	1.705	8.111	2.406	0.997
% RD	4.390	15.915	12.930	20.221	0.964	1.873	3.202	1.002	4.419	5.692

MRG-1 Certified	11.5	107	22.3	49.4	8.83	25.8	3.71	17.6	4.34	1.38
MRG-1 Measured	11.153	133.431	19.957	63.381	8.754	24.320	3.569	17.905	4.494	1.391
% RD	3.112	19.809	11.741	22.058	0.872	6.088	3.944	1.705	3.429	0.819

Sample/Analyte Symbol	Gd	Tb	Dy	Ho	Er	Tm	Yb	Lu	Hf	Ta	Th
BR-688 Certified	2.88	0.48	3.21	0.7	2.1	0.3	2	0.3	1.54	0.18	0.33
BR-688 Measured	2.637	0.523	3.236	0.689	2.004	0.314	1.961	0.281	1.659	0.208	0.477
% RD	9.195	8.302	0.806	1.584	4.787	4.506	2.005	6.700	7.185	13.301	30.810

MRG-1 Certified	3.97	0.52	3	0.49	1.16	0.14	0.79	0.11	3.89	0.74	0.82
MRG-1 Measured	3.526	0.537	2.958	0.495	1.186	0.145	0.884	0.101	4.444	0.560	0.778
% RD	12.578	3.196	1.409	1.091	2.182	3.442	10.629	9.237	12.472	32.212	5.351

**Table C-3:** Trace element concentrations of standard reference materials that were run with samples during ICP-MS analysis at Memorial University. Where % Relative Difference (RD) =  $[(X_{\text{measured}} - X_{\text{certified}}) / X_{\text{certified}}] * 100$

	Run T110117T			Run T110329T		
	Relative Standard Deviation (RSD %)			Relative Standard Deviation (RSD %)		
	BHVO-1	SY-2	PACS-1	BHVO-1	SY-2	PACS-1
Na2O	0.4	0.1	0.8	1	0.4	0.7
MgO	2.1	0	0.8	2.5	0.2	0.7
Al2O3	0.6	0.8	0.7	1.7	0.5	1.1
SiO2	0.5	0.4	0.3	1.4	0.3	0.5
P2O5	3.2	0.6	0.5	3.6	0.7	1.3
S	1.1	1.1	1.5	2.1	0.7	0.7
Cl	1.1	2.4	1.1	1.3	1.6	1.4
K2O	0.3	0.3	0.3	3.2	0.9	0.3
CaO	0.9	0.1	0.1	1.7	0.4	0.6
TiO2	0.7	0.3	1.4	2.4	2.2	0.4
V	1.6	-	0.9	1.9	-	3.4
Cr	0.7	-	2.8	2.8	-	1.7
MnO	0.2	0.4	0.8	1.6	0.1	1.7
Fe2O3(T)	0.4	0.3	0.1	1	0.1	0.2
Ni	0.5	-	13.1	2.3	-	6.6
Cu	0.5	-	0.6	1.1	-	1.4
Zn	2.5	3.6	1.7	3.7	1.3	1.7
Rb	1.1	0.1	0.3	5.4	0.2	0.7
Sr	0.1	0.3	0.2	0.3	0.5	0.6
Y	1.4	0.4	1.1	1.7	0.4	1.7
Zr	0.2	0.5	0.2	0.8	1.4	0.5
Nb	0.1	1.5	3.6	2.7	1.4	3
Ba	-	0.7	0.6	-	2	3.6
Ce	-	-	-	-	-	-
Pb	-	3.4	0.1	-	0.6	1.2
Th	-	0.3	-	-	0.6	-
U	-	0.7	-	-	0.4	-

**Table C-4:** %RSD provided by Memorial for standards in two runs using XRF (pressed pellet) analysis. Using  $\% \text{RSD} = (s_i / \mu_i) * 100$ , where  $s_i$  = standard deviation of the mean value for an element ( $i$ ) for duplicate analyses.

**XRF-FUSION Actlabs**

Analyte Symbol	SiO2	Al2O3	Fe2O3(T)	MnO	MgO	CaO	Na2O	K2O	TiO2	P2O5
Unit Symbol	%	%	%	%	%	%	%	%	%	%
10AL079	68.31	14.92	4.57	0.13	1.55	1.32	2.65	3.25	0.64	0.16
10AL079 DUP	68.2	14.96	4.54	0.128	1.54	1.32	2.63	3.27	0.64	0.16
Average	68.255	14.940	4.555	0.129	1.545	1.320	2.640	3.260	0.640	0.160
Standard Dev.	0.078	0.028	0.021	0.001	0.007	0.000	0.014	0.014	0.000	0.000
<b>%RSD</b>	<b>0.114</b>	<b>0.189</b>	<b>0.466</b>	<b>1.096</b>	<b>0.458</b>	<b>0.000</b>	<b>0.536</b>	<b>0.434</b>	<b>0.000</b>	<b>0.000</b>

**ICP-MS (MUN lab)**

Analyte Symbol	Y	Zr	Nb	Ba	La	Ce	Pr	Nd	Sm	Eu	Gd
Unit Symbol	ppm										
10AL090	8.658	50.367	4.720	792.323	12.899	24.415	2.712	10.035	1.858	0.540	1.427
10AL090 DUP	8.825	49.777	4.496	745.156	12.993	24.661	2.780	10.216	2.027	0.570	1.446
Average	8.741	50.072	4.608	768.740	12.946	24.538	2.746	10.126	1.943	0.555	1.437
Standard Dev.	0.118	0.417	0.158	33.352	0.066	0.174	0.048	0.128	0.119	0.021	0.013
<b>%RSD</b>	<b>1.355</b>	<b>0.833</b>	<b>3.428</b>	<b>4.339</b>	<b>0.511</b>	<b>0.709</b>	<b>1.752</b>	<b>1.262</b>	<b>6.122</b>	<b>3.838</b>	<b>0.915</b>
11AL003	22.826	298.923	20.608	497.067	39.228	84.431	10.095	39.052	6.789	1.505	5.423
11AL003 DUP	23.240	303.625	20.407	508.175	40.758	87.655	10.364	38.971	7.323	1.540	5.675
Average	23.033	301.274	20.507	502.621	39.993	86.043	10.229	39.012	7.056	1.522	5.549
Standard Dev.	0.293	3.325	0.142	7.855	1.081	2.280	0.191	0.057	0.378	0.025	0.178
<b>%RSD</b>	<b>1.272</b>	<b>1.104</b>	<b>0.694</b>	<b>1.563</b>	<b>2.704</b>	<b>2.649</b>	<b>1.864</b>	<b>0.147</b>	<b>5.353</b>	<b>1.636</b>	<b>3.207</b>

**ICP-MS  
(MUN lab)**

Analyte Symbol	Tb	Dy	Ho	Er	Tm	Yb	Lu	Hf	Ta	Th
Unit Symbol	ppm									
10AL090	0.276	1.856	0.328	0.942	0.137	1.011	0.130	1.460	1.149	2.530
10AL090 DUP	0.266	1.762	0.328	0.914	0.152	0.918	0.124	1.561	1.103	2.543
Average	0.271	1.809	0.328	0.928	0.145	0.964	0.127	1.510	1.126	2.537
Standard Dev.	0.007	0.066	0.001	0.020	0.011	0.066	0.004	0.072	0.032	0.009
<b>%RSD</b>	<b>2.539</b>	<b>3.676</b>	<b>0.163</b>	<b>2.122</b>	<b>7.701</b>	<b>6.810</b>	<b>2.890</b>	<b>4.735</b>	<b>2.872</b>	<b>0.348</b>
11AL003	0.788	4.581	0.886	2.608	0.396	2.856	0.424	6.611	2.084	12.581
11AL003 DUP	0.772	4.686	0.882	2.592	0.407	2.827	0.451	6.984	1.980	12.810
Average	0.780	4.634	0.884	2.600	0.401	2.841	0.438	6.798	2.032	12.695
Standard Dev.	0.011	0.075	0.003	0.012	0.007	0.020	0.019	0.264	0.074	0.162
<b>%RSD</b>	<b>1.444</b>	<b>1.612</b>	<b>0.377</b>	<b>0.443</b>	<b>1.822</b>	<b>0.715</b>	<b>4.407</b>	<b>3.877</b>	<b>3.639</b>	<b>1.277</b>

**Table C-5:** %RSD calculated for XRF and ICP-MS analysis using duplicates. DUP=duplicate sample. Standard Dev.=standard deviation. % RSD =  $(s_i / \mu_i) * 100$ , where  $s_i$  = standard deviation of the mean value for an element ( $i$ ) for duplicate analyses.

**Table C-6 (following pages):** Raw geochemical data table used in geochemical analysis and interpretations.

Analyte Symbol	SiO2	Al2O3	Fe2O3(T)	Feo*	MnO	MgO	CaO	Na2O	K2O	TiO2	P2O5	LOI
Unit Reported	wt %	wt %	wt %	wt %	wt %	wt %	wt %	wt %	wt %	wt %	wt %	
10AL014	73.347	17.025	3.138	2.823	0.103	0.825	1.025	4.138	5.263	0.400	0.188	1.25
10AL016	64.439	36.206	12.449	11.201	0.315	4.469	3.967	6.156	10.374	1.824	0.775	2.28
10AL017	72.197	19.390	2.841	2.556	0.075	0.858	1.300	4.770	5.467	0.375	0.241	1.34
10AL025A	72.498	18.522	1.754	1.578	0.047	0.486	0.678	3.430	7.462	0.230	0.282	1.28
10AL031	74.193	16.411	1.760	1.583	0.047	0.414	0.736	3.255	6.061	0.207	0.299	1.15
10AL036	65.089	14.792	3.711	3.339	0.109	1.424	2.946	3.961	2.278	0.587	0.347	0.89
10AL041	75.386	11.858	0.574	0.517	0.047	0.139	0.287	2.836	4.707	0.052	0.165	0.87
10AL042	66.612	35.949	9.959	8.961	0.324	4.761	3.772	8.142	8.050	1.518	0.391	2.3
10AL043	74.419	9.648	0.516	0.464	0.360	0.060	0.295	3.196	2.405	0.013	0.134	0.67
10AL046	72.995	17.174	3.013	2.711	0.117	1.141	1.389	3.943	5.171	0.459	0.223	1.24
10AL051	63.935	18.619	5.589	5.029	0.177	2.093	2.852	3.853	4.807	0.932	0.403	1.15
10AL054	68.658	26.227	6.903	6.211	0.197	2.526	2.785	5.865	5.605	1.003	0.519	1.73
10AL057	46.344	43.935	43.616	39.246	0.609	15.515	21.286	10.324	4.408	8.207	1.247	2.9
10AL059	73.305	12.195	5.088	4.578	0.099	1.494	1.947	2.451	2.019	0.783	0.144	1.03
10AL060	64.068	39.745	18.012	16.207	1.396	5.285	1.280	3.271	8.888	2.180	0.261	2.37
10AL061	73.478	27.706	8.237	7.411	0.220	2.538	1.498	4.243	5.595	1.290	0.312	2.08
10AL065	71.092	16.380	4.282	3.853	0.161	1.100	1.825	3.428	4.820	0.573	0.281	1.17
10AL066	70.894	21.808	4.928	4.434	0.077	1.232	1.872	5.200	7.168	0.896	0.288	1.6
10AL068	67.044	18.568	5.253	4.727	0.122	1.954	1.884	3.744	4.610	0.714	0.105	1.17
10AL069	64.427	10.920	4.239	3.814	0.108	1.243	2.627	2.478	1.363	0.788	0.241	0.71
10AL070	63.280	17.456	8.389	7.548	0.180	3.545	1.778	3.323	4.703	1.381	0.246	1.17
10AL071	65.333	20.336	8.392	7.551	0.180	2.608	0.995	2.507	5.216	1.121	0.126	1.26
10AL072	74.806	10.676	1.053	0.947	0.031	0.332	0.761	2.406	3.702	0.146	0.105	0.81
10AL073	73.547	11.528	4.195	3.775	0.127	1.233	0.727	1.684	2.558	0.570	0.120	0.92
10AL074	70.653	11.206	3.595	3.235	0.106	1.100	0.781	2.276	3.990	0.504	0.126	0.84
10AL075	70.197	13.272	3.601	3.240	0.101	1.425	1.311	3.107	3.202	0.475	0.152	0.95
10AL076	79.335	16.884	5.428	4.884	0.169	1.787	0.902	2.271	3.741	0.985	0.217	1.67
10AL077	68.342	23.800	9.265	8.337	0.330	2.329	2.737	5.185	5.848	1.275	0.340	1.7
10AL078	75.269	7.808	0.897	0.807	0.024	0.268	0.763	1.983	2.257	0.122	0.067	0.61
10AL079	69.044	17.181	5.233	4.708	0.148	1.771	1.518	3.036	3.749	0.736	0.184	1.15
10AL082	70.414	19.323	3.471	3.123	0.158	1.327	1.528	3.899	6.526	0.590	0.268	1.34
10AL085	54.912	35.351	24.824	22.337	0.786	28.391	13.224	1.566	13.630	4.118	1.102	2.9

Analyte Symbol	Cr	Cu	Ni	Sc	V	Zn	Pb	Ga	Ba	Rb	Sr	Nb
Unit Reported	ppm	ppm	ppm	ppm	ppm	ppm	ppm	ppm	ppm	ppm	ppm	ppm
10AL014	10		5		22	25	28	17	480.0	150.5	118.0	16.0
10AL016	60	39	19	21	132	43	25	19	1595.2	304.2	238.4	23.7
10AL017	15				22	24	27	19	525.0	174.6	109.1	11.9
10AL025A							36	16	615.6	240.7	60.1	15.0
10AL031	33		6				38	17	394.8	215.1	79.0	14.3
10AL036	34		13	15	84	30	17	23	400.3	211.7	221.3	17.7
10AL041							36	13	234.7	167.6	62.2	5.8
10AL042	25		21	13	80	43	7	17	1346.4	267.7	234.6	10.5
10AL043				1			17	17	68.0	164.9	25.8	11.4
10AL046	23		6	10	44	14	30	16	471.3	201.6	152.1	17.1
10AL051	49	22	16	21	127	33	34	20	1024.6	314.9	259.7	21.9
10AL054	54	10	16	10	75	32	24	16	605.7	182.9	164.8	17.5
10AL057	9	32	45	28	291	59		22	414.0	106.4	482.8	16.6
10AL059	74	6	29	22	80	10	14	14	371.3	79.6	150.7	13.3
10AL060	108	43	47	10	118	36	17	23	627.6	154.5	110.1	21.3
10AL061	49	7	16		57		20	12	958.9	105.1	114.2	15.9
10AL065	15		7	9	41	14	30	18	650.1	139.4	179.6	15.0
10AL066	27	5	7	13	54	10	21	18	626.0	183.2	101.5	18.9
10AL068	48		22	10	59	9	27	19	357.5	227.2	135.8	22.8
10AL069		6	4	19	60	16	15	20	117.6	126.0	198.3	19.5
10AL070			8	15	89	40	21	19	199.3	299.5	98.9	31.3
10AL071	93	93	36	17	109	28	24	24	520.5	225.6	102.9	28.4
10AL072					9		32	11	414.9	172.1	130.6	7.5
10AL073	54		23	13	56	11	19	16	349.7	170.0	83.0	21.3
10AL074	36	29	23	10	47	7	35	18	472.6	366.9	105.0	23.9
10AL075	56		21	11	67	7	25	17	470.3	201.2	164.9	13.7
10AL076	38		12	11	49		19	9	521.4	80.5	91.3	12.6
10AL077	30		10	15	68	21	20	19	535.8	161.8	167.5	19.4
10AL078	10				16		30	11	471.5	143.0	136.1	8.3
10AL079	48		22	15	62	8	26	22	384.6	182.5	126.4	21.5
10AL082	18		7		36		32	17	701.5	288.2	179.8	14.7
10AL085	1039	13	294	23	191	39	7	14	828.0	443.3	95.4	26.5

Analyte Symbol	Y	Zr	Th	La	Ce	Pr	Nd	Sm	Eu	Gd	Tb	Dy
Unit Reported	ppm	ppm	ppm	ppm	ppm	ppm	ppm	ppm	ppm	ppm	ppm	ppm
10AL014	21.0	165.7	9.5	24.15	49.06	5.78	22.60	4.41	0.70	4.44	0.68	4.01
10AL016	34.7	343.4	27.3	48.99	100.44	12.07	46.55	9.13	1.94	7.45	1.16	6.98
10AL017	10.4	133.9	13.1	23.42	51.60	6.00	22.79	4.25	0.72	3.20	0.44	2.24
10AL025A	11.5	69.2	4.0	10.76	23.61	2.74	10.32	2.66	0.53	2.58	0.43	2.35
10AL031	12.1	79.5	4.3	11.79	25.38	3.04	11.37	2.94	0.61	3.02	0.48	2.69
10AL036	10.9	176.4	4.7	13.19	28.20	3.33	13.20	2.63	0.86	2.44	0.36	2.05
10AL041	10.9	44.0	1.8	5.76	10.91	1.34	4.81	1.36	0.39	1.42	0.29	1.94
10AL042	15.9	189.8	9.8	20.27	44.60	4.96	18.65	3.64	0.90	2.62	0.49	3.07
10AL043	7.6	35.9	1.0	1.37	3.06	0.39	1.28	0.45	0.05	0.41	0.16	1.18
10AL046	18.1	130.6	14.7	23.81	50.93	6.04	23.10	4.79	0.91	3.96	0.64	3.74
10AL051	20.6	298.7	18.3	42.37	87.95	10.87	42.71	8.13	1.76	5.88	0.79	4.11
10AL054	24.9	253.4	20.1	41.56	89.35	10.57	40.67	8.15	1.39	6.92	1.01	5.52
10AL057	32.7	278.4	2.5	22.25	52.02	7.07	30.27	7.00	2.17	5.82	1.08	6.64
10AL059	21.5	269.8	9.7	28.39	58.68	6.98	26.20	5.14	1.15	4.14	0.73	4.29
10AL060	26.4	227.8	14.2	47.41	101.63	11.09	41.99	8.14	1.40	6.95	0.98	5.59
10AL061	24.5	218.3	9.5	31.42	64.30	7.41	28.63	5.32	1.20	5.30	0.75	4.82
10AL065	21.5	226.7	12.7	34.95	71.71	8.44	31.96	6.35	1.24	4.71	0.79	4.55
10AL066	25.1	343.4	24.1	35.07	71.99	8.57	34.01	6.29	1.28	6.61	0.91	5.38
10AL068	26.1	151.2	9.5	27.02	54.00	6.33	23.76	4.98	1.13	4.08	0.75	4.90
10AL069		166.5										
10AL070	44.4	266.2	8.2	29.88	63.20	7.64	31.55	7.11	1.31	7.49	1.25	8.62
10AL071	27.6	210.5	11.5	35.72	72.01	8.41	32.38	6.46	1.18	5.78	0.90	5.56
10AL072	14.8	66.4	4.3	11.02	22.53	2.69	9.59	2.08	0.52	2.07	0.37	2.51
10AL073	23.0	278.1	12.7	33.49	68.58	8.10	31.10	5.99	1.11	5.33	0.81	4.58
10AL074	29.0	230.4	13.6	35.37	72.58	8.63	32.69	6.81	1.03	5.13	0.97	5.77
10AL075	18.8	130.3	7.5	23.24	45.53	5.47	20.51	4.00	0.99	3.69	0.57	3.41
10AL076	21.2	252.9	8.1	26.95	56.18	6.56	25.63	5.25	1.12	3.96	0.71	4.46
10AL077	30.2	315.6	13.4	39.33	79.48	9.35	37.14	7.30	1.38	5.99	1.01	6.15
10AL078	16.2	101.3	5.7	14.85	29.48	3.45	12.79	2.74	0.66	2.41	0.48	3.13
10AL079	25.4	187.2	9.5	29.02	59.36	6.89	26.30	5.47	1.21	4.49	0.86	5.37
10AL082	9.1	154.2	14.9	28.65	61.04	7.10	26.84	4.82	1.02	3.22	0.40	1.97
10AL085	16.6	446.3	28.0	79.66	167.59	19.42	71.32	10.09	1.84	5.76	0.66	3.51

Analyte Symbol	Ho	Er	Tm	Yb	Lu	Hf	Recalc. Factor
Unit Reported	ppm	ppm	ppm	ppm	ppm	ppm	
10AL014	0.73	2.24	0.35	2.20	0.30	4.07	1.013
10AL016	1.38	3.80	0.53	3.05	0.41	8.10	1.023
10AL017	0.36	0.96	0.11	0.79	0.11	3.05	1.014
10AL025A	0.39	1.02	0.13	0.93	0.12	1.93	1.013
10AL031	0.42	1.06	0.15	0.83	0.12	2.11	1.012
10AL036	0.39	1.13	0.16	1.15	0.16	3.44	1.009
10AL041	0.36	1.08	0.16	1.19	0.16	1.34	1.009
10AL042	0.59	1.54	0.25	1.42	0.21	4.59	1.024
10AL043	0.21	0.59	0.10	0.93	0.11	1.82	1.007
10AL046	0.72	2.15	0.33	2.08	0.30	2.99	1.013
10AL051	0.79	1.98	0.30	1.95	0.28	6.11	1.012
10AL054	0.96	2.56	0.36	2.12	0.32	6.35	1.018
10AL057	1.23	3.56	0.51	3.28	0.46	6.38	1.030
10AL059	0.85	2.54	0.36	2.35	0.35	6.26	1.010
10AL060	1.08	3.20	0.47	3.22	0.45	4.35	1.024
10AL061	0.95	2.78	0.40	2.66	0.38	4.58	1.021
10AL065	0.82	2.33	0.35	2.61	0.37	5.47	1.012
10AL066	1.02	2.85	0.36	2.23	0.31	7.73	1.016
10AL068	1.01	3.06	0.45	3.04	0.46	4.29	1.012
10AL069							1.007
10AL070	1.78	5.36	0.82	5.58	0.80	5.22	1.012
10AL071	1.11	3.27	0.47	3.29	0.48	4.31	1.013
10AL072	0.49	1.52	0.23	1.56	0.22	1.37	1.008
10AL073	0.80	2.28	0.36	2.57	0.36	6.38	1.009
10AL074	1.12	3.19	0.47	2.90	0.44	5.72	1.008
10AL075	0.65	1.76	0.28	1.90	0.27	2.93	1.010
10AL076	0.85	2.46	0.35	2.34	0.32	6.34	1.017
10AL077	1.23	3.50	0.52	3.48	0.51	7.47	1.017
10AL078	0.63	1.79	0.27	2.03	0.29	2.92	1.006
10AL079	1.07	3.15	0.45	3.13	0.43	4.84	1.012
10AL082	0.34	0.87	0.12	0.85	0.15	3.79	1.014
10AL085	0.61	1.67	0.23	1.45	0.21	9.71	1.030

Analyte Symbol	SiO2	Al2O3	Fe2O3(T)	Feo*	MnO	MgO	CaO	Na2O	K2O	TiO2	P2O5	LOI
Unit Reported	wt %	wt %	wt %	wt %	wt %	wt %	wt %	wt %	wt %	wt %	wt %	
10AL086	51.113	70.027	47.131	42.408	1.310	36.232	22.323	3.250	26.768	8.604	1.864	4.78
10AL087	70.433	17.596	3.546	3.191	0.109	1.352	1.872	3.447	6.312	0.583	0.236	1.24
10AL088	66.667	19.580	4.551	4.095	0.122	1.959	3.819	4.588	3.385	0.781	0.211	1.24
10AL089	73.759	12.839	0.475	0.428	0.114	0.097	0.370	3.881	3.854	0.026	0.202	0.88
10AL090	66.818	10.075	0.400	0.360	0.013	0.104	0.145	1.897	5.504	0.058	0.093	0.58
10AL093	72.217	11.302	4.659	4.192	0.075	1.520	1.829	2.275	1.866	0.746	0.091	0.91
10AL094	67.979	31.405	13.074	11.764	0.175	4.993	2.628	6.044	5.869	1.818	0.329	2.19
10AL095	71.979	11.645	1.406	1.265	0.040	0.498	0.932	3.073	3.247	0.198	0.158	0.79
10AL096	64.632	11.790	3.139	2.824	0.050	1.205	2.876	2.767	1.913	0.445	0.343	0.73
10AL097	71.324	16.951	6.995	6.294	0.115	2.384	1.297	2.306	4.402	1.035	0.105	1.31
10AL098	71.633	11.160	1.808	1.627	0.052	0.504	0.712	2.344	4.336	0.224	0.192	0.8
10AL099	52.464	30.084	22.171	19.949	0.525	18.094	13.342	1.417	8.589	3.117	1.243	2.18
10AL100	73.706	7.400	0.275	0.248	0.014	0.071	0.326	1.933	2.683	0.036	0.092	0.51
10AL101	72.601	10.848	2.264	2.037	0.046	0.752	1.056	2.600	3.088	0.280	0.080	0.8
11AL001	68.310	16.080	7.344	6.608	0.252	2.628	0.816	1.788	5.628	1.140	0.084	1.2
11AL003	66.163	21.488	6.782	6.103	0.179	2.693	4.145	5.259	3.032	1.170	0.423	1.41

Analyte Symbol	Cr	Cu	Ni	Sc	V	Zn	Pb	Ga	Ba	Rb	Sr	Nb
Unit Reported	ppm	ppm	ppm	ppm								
10AL086	354	22	193	21	220	69	10	17	112.1	785.6	84.2	9.6
10AL087	21		10	7	48	1	37	16	791.5	223.0	225.0	14.1
10AL088	13	12	11	14	69		15	20	643.3	162.2	235.1	9.7
10AL089							10	14	569.0	199.0	25.4	9.5
10AL090			6		6		36	14	765.9	391.0	58.9	5.3
10AL093	84	46	28	14	91	7	16	15	381.0	104.0	178.0	14.1
10AL094	105		45	16	127	31	10	21	657.9	97.6	452.4	18.3
10AL095		5			21	9	37	21	446.6	247.9	163.2	14.8
10AL096	16	50			67	21	13	23	679.0	78.7	595.8	12.6
10AL097	64	43	21	15	86	5	18	16	518.0	117.7	163.4	12.9
10AL098			5		15		38	16	332.6	236.5	111.6	16.1
10AL099	541	116	99	31	292	47	12	21	1933.0	314.1	137.4	23.0
10AL100	10						43	15	191.2	246.9	74.1	9.0
10AL101	26		10		22	8	30	14	518.7	150.4	180.1	16.0
11AL001	104	6	33		96	29	28	15	970.2	240.6	114.9	26.6
11AL003	38	33	15	18	115	26	20	18	547.0	198.8	257.6	21.8

Analyte Symbol	Y	Zr	Th	La	Ce	Pr	Nd	Sm	Eu	Gd	Tb	Dy
Unit Reported	ppm	ppm	ppm	ppm	ppm	ppm	ppm	ppm	ppm	ppm	ppm	ppm
10AL086	22.0	144.9	2.1	10.76	25.72	3.85	17.88	4.65	1.38	4.94	0.75	4.42
10AL087	16.7	177.0	18.5	33.68	69.52	8.18	31.38	5.89	1.22	3.79	0.62	3.38
10AL088	12.3	183.6	9.5	27.57	57.49	6.43	23.94	3.88	0.93	2.59	0.42	2.45
10AL089	5.5	31.5	1.0	2.26	4.69	0.57	2.11	0.55	0.11	0.43	0.11	0.73
10AL090	8.9	45.9	2.4	12.38	23.44	2.60	9.63	1.78	0.52	1.37	0.26	1.78
10AL093	26.6	312.8	10.7	33.90	70.70	8.10	30.78	5.95	1.31	4.74	0.85	5.22
10AL094	25.8	203.5	9.5	29.35	60.58	7.20	27.86	5.51	1.27	5.07	0.82	5.29
10AL095	11.3	127.3	9.4	23.11	47.47	5.54	20.62	4.45	0.74	3.50	0.45	2.47
10AL096	9.6	259.2	5.7	40.19	81.90	9.27	33.43	5.44	1.17	3.17	0.45	2.27
10AL097	25.3	259.6	11.8	36.18	73.78	8.52	33.54	6.59	1.16	4.90	0.85	5.21
10AL098	14.4	108.0	6.6	17.68	35.86	4.27	16.62	3.49	0.66	3.27	0.50	3.11
10AL099	32.9	317.5	25.4	61.60	131.01	17.24	70.46	13.42	2.73	9.85	1.26	6.70
10AL100	3.0	60.7	3.5	8.53	16.13	1.82	6.33	1.47	0.43	1.15	0.15	0.66
10AL101	6.8	155.3	7.7	21.67	43.79	5.01	18.78	3.54	0.85	2.85	0.38	1.81
11AL001	15.6	300.8	17.3	49.63	103.52	12.05	46.28	8.37	1.23	6.71	0.85	4.09
11AL003	24.7	297.8	13.6	42.27	90.98	10.88	42.08	7.32	1.62	5.84	0.85	4.94

Analyte Symbol	Ho	Er	Tm	Yb	Lu	Hf	Recalc. Factor
Unit Reported	ppm	ppm	ppm	ppm	ppm	ppm	
10AL086	0.85	2.37	0.34	1.98	0.33	2.62	1.050
10AL087	0.61	1.62	0.22	1.29	0.20	4.52	1.013
10AL088	0.47	1.27	0.18	1.08	0.15	4.02	1.013
10AL089	0.14	0.52	0.09	0.79	0.12	1.25	1.009
10AL090	0.31	0.90	0.13	0.97	0.12	1.40	1.006
10AL093	1.03	3.04	0.43	2.83	0.44	7.35	1.009
10AL094	1.00	3.00	0.44	3.08	0.46	4.48	1.022
10AL095	0.40	1.08	0.14	0.89	0.12	3.02	1.008
10AL096	0.36	0.93	0.13	0.78	0.12	5.89	1.007
10AL097	0.99	2.71	0.39	2.52	0.37	6.37	1.013
10AL098	0.55	1.40	0.19	1.20	0.17	2.61	1.008
10AL099	1.24	3.31	0.49	2.98	0.44	7.16	1.022
10AL100	0.11	0.24	0.03	0.28	0.04	1.98	1.005
10AL101	0.27	0.65	0.09	0.53	0.08	3.06	1.008
11AL001	0.69	1.66	0.21	1.34	0.22	7.08	1.012
11AL003	0.95	2.81	0.43	3.08	0.46	7.12	1.014

## **Appendix E: U-Pb Geochronological Analytical Methods**

### **E.1. Crushing and Initial Separation**

A robust series of steps are necessary before analyzing a sample with the thermal ionization mass spectrometer (TIMS). Sample preparation begins with crushing approximately 20kg of sample. A hydraulic splitter (Figure E-1(A)) is first used to break the sample into fist-sized pieces. The sample is then broken into 0.1-5 cm chips using a jaw crusher (Figure E-1 (B)). Finally the sample is crushed into a fine powder through grinding the chips in a disc mill (Figure E-1 (C)). Contamination throughout the crushing procedure is eliminated through grinding crushing plates with a metal brush, thorough alcohol cleaning and removal of dust and fine particles with an air hose multiple times during processing. The heavy minerals are initially separated using a Wifley table (Figure E-1(D)). Here approximately 200ml of heavy minerals are collected, rinsed with alcohol and dried for further separation in the lab. In all of the above procedures cleaning equipment properly before and after every use is crucial in avoiding sample cross-contamination.

The heavy mineral concentrate is sieved to remove coarser-grained material and a hand magnet is used to remove highly magnetic fragments. The sample then is passed through a heavy liquid to separate minerals, including zircon, that are denser than methylene iodide (3.32 g/cm) and therefore sink when submerged (Figure E-1(E)). After heavy liquid mineral separation is complete, the newly collected densest minerals must be



**Figure E-1:** Photos showing equipment used in both crushing and mineral separation procedures: (A) hydraulic splitter (B) jaw crusher (C) disk mill (D) Wifley table (E) heavy liquid separation apparatus (F) FRANZ magnetic separator.

further separated using a Frantz magnetic separator (Figure E-1(F)). The Frantz separates the sample into different groups based on the varying degrees of magnetism of different minerals. The magnetic separates are collected through changing the tilt of the Frantz separator as well as changing the field strength of the magnet.

Under a binocular microscope, the Frantz mineral separates are examined and the clearest, least magnetic, inclusion-and crack-free zircon grains are picked according to criteria of morphology and clarity. Zircon grains are picked for both isotope dilution (ID) TIMS U-Pb analysis and for scanning electron microscope (SEM) back scatter electron and/or cathodoluminescence imaging.

## **E.2. CL and BSE: Looking at internal structures**

Binocular microscopes allow the analysis of the macroscopic characteristics of zircon such as size, color, clarity, and external morphology, and cathodoluminescence (CL) and back-scattered electron (BSE) imaging allow identification of internal complexities. When minerals are bombarded with electrons they emit light in relation to transitions between elemental components. CL emission in minerals is not always well understood however it appears to be linked to trace element constituents. In zircon the dominant element affecting CL is  $\text{Dy}^{3+}$ , however it has been proposed that other elements such as  $\text{Sm}^{3+}$ ,  $\text{Eu}^{2+}$ ,  $\text{Tb}^{3+}$  and  $\text{Y}^{3+}$  are also responsible for CL emission (Ohnenstetter et al., 1991). CL emission may be suppressed due to  $\text{U}^{4+}$  and the radiation damage associated with its decay (Corfu et al., 2003), so uranium-rich zones will appear darker.

BSE reveals contrast in the average atomic number of regions within a mineral. Parts of a crystal that have higher average atomic numbers will “reflect” and appear brighter in images. Hf is the principle elemental component causing BSE variation in zircon, although U also has an effect (Corfu et al., 2003).

When analyzing zircon both of these techniques reveal similar features, although they typically have contrasting areas of brightness and darkness (Hanchar & Miller, 1993). CL images are typically more useful as the contrast in CL emission is more pronounced and CL images show additional variations in colors. Both imaging techniques play a key role in understanding the geologic processes recorded in zircon and play a crucial role in interpreting ages of igneous crystallization and other events. Imaging is valuable when assessing the cause of discordance in ID TIMS calculated ages. Images allow the identification of small-inherited cores, complex or igneous growth histories, as well as mineral and melt inclusions. Both CL and BSE images were collected using the SEM facility at Memorial University.

### **E.3. Pretreatment and Ion Separation Procedures**

After the grains are hand picked they are annealed in high purity alumina crucibles in a furnace at 900°C for 36 hours. Radiation damaged zones that were not annealed are then removed through etching and partial dissolution in concentrated hydrofluoric acid, at 200°C in a TEFLON bomb. Etched zircon is then rinsed with distilled HNO<sub>3</sub>, doubly distilled H<sub>2</sub>O and acetone. Grains are re-examined with a

binocular microscope and the best (clearest, fracture/inclusion-free) grains or grain fragments are selected for complete dissolution with HF in a TEFLON bomb. Since the mass spectrometer is only capable of measuring ratios of the U and Pb isotopes a “spike” or “tracer” of a known concentration must be added to the sample solution prior to ion exchange chemistry. This is known as “isotope dilution”. A spike with a known  $^{205}\text{Pb}/^{235}\text{U}$  ratio was used for all samples. All U and Pb measurements are calibrated against this spike value.

Prior to dissolution the sample, 1.05mg of spike, 15 drops of concentrated HF and a single drop of  $\text{HNO}_3$  are loaded into clean TEFLON mini-bombs (Figure E-4(A)). The bombs are sealed and placed in an oven at  $210^\circ\text{C}$  for 5 days until zircon is completely dissolved.

Standard column ion exchange techniques are used to separate the desired elements U and Pb. The solution of dissolved zircon mixed with 1.05mg of the known spike solution is put in a TEFLON column where it is held with a strong affinity for the resin (Figure E-2). The sample is then “eluted” by washing specific elements through the column using a suitable concentration of HCl. The amount and rate at which the solvent is added will control the removal of specific ions. Ions are extracted based on their affinity to either the solvent or the resin. Ions with a strong affinity to the resin require more solvent to be washed through the column (Potts, 1987). The steps have been calculated so that first steps remove “waste” elements (Zr, Hf, REEs) and last steps will elute Pb and U (Figure C-3). In the case of U and Pb miniature columns (Figure C-4

(B)(C)), scaled down to one-tenth of the volume of the ones originally designed by Krogh (1973), are used due to the small quantity of sample solution and to reduce Pb blanks.

After ion exchange chemistry is complete, the solution of U, Pb, acid and water has been collected in a clean beaker and one drop of ultrapure  $H_3PO_4$  is added. The solution is dried down on a hotplate, leaving the single drop of  $H_3PO_4$  and U and Pb.

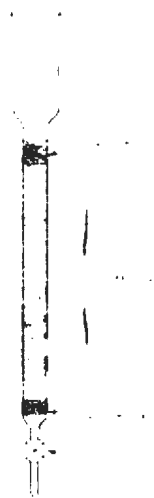


**Figure E-2:** Schematic diagram of ion exchange column (from Potts, 1987).

#### **E.4. Thermal Ionization Mass Spectrometry (TIMS)**

After all required sample preparation has been completed and Pb and U have been chemically separated, analysis with Memorial's MAT 262 thermal ionization mass spectrometer is carried out. The element solution is loaded onto an outgassed metal rhenium filament (Figure E-4(D)) along with silica gel and is evaporated through heating in a clean box, producing an amorphous salt residue for analysis.

<i>Zircon Small Column Chemistry</i>			<i>Prepare 1 set of clean beakers</i>	
<i>Procedure Description</i>	<i>Catch Beaker</i>	<i>Reagent</i>	<i>Quantity</i>	<i>Checklist</i>
1. Column and Resin Cleaning	Spill	12 H <sub>2</sub> O	15 drops	
		6.2N HCl	15 drops	
		12 H <sub>2</sub> O	15 drops	
		6.2N HCl	15 drops	
		12 H <sub>2</sub> O	15 drops	
		6.2N HCl	15 drops	
2. Condition Column	Spill	3.1N HCl	16 drops	
3. Load Sample in Column	Spill	Sample in	Contents of bomb	
		3.1N HCl	(16 drops)	
4. Zircon Wash	Spill	3.1N HCl	2 drops	
		3.1N HCl	2 drops	
		3.1N HCl	2 drops	
		3.1N HCl	10 drops	
5. Elute Pb	Sample	6.2N HCl	10 drops	
			15 drops	
6. Elute U	Sample	12 H <sub>2</sub> O	10 drops	
			20 drops	
7. Add H <sub>3</sub> PO <sub>4</sub>	Sample	H <sub>3</sub> PO <sub>4</sub>	1 drop in beaker	

*(Dry down on hot plate in a small drop (1-2 hours). Make sure sample does not go dry or burn.)*

**Figure E-3:** Standard procedure description for eluting Pb and U from sample solution after Krogh (1973).

First the filament with the sample is mounted on a magazine (Figure E-4(E)) that is then placed in the turret of the mass spectrometer and pumped down to a high vacuum. The filament is then heated to a desired temperature (1400-1600°C) by an electric current and the sample is atomized and ionized. A stable positive ion beam must be maintained throughout analysis. If the sample has a suitable chemical form then this beam will be maintained. Several positive kilovolts are applied to the filament relative to an anode plate, extracting the ions into the mass analyzer (Potts, 1987). It is crucial that the ionization source evaporates the sample at a stable rate throughout the entire analysis (which may take several hours).

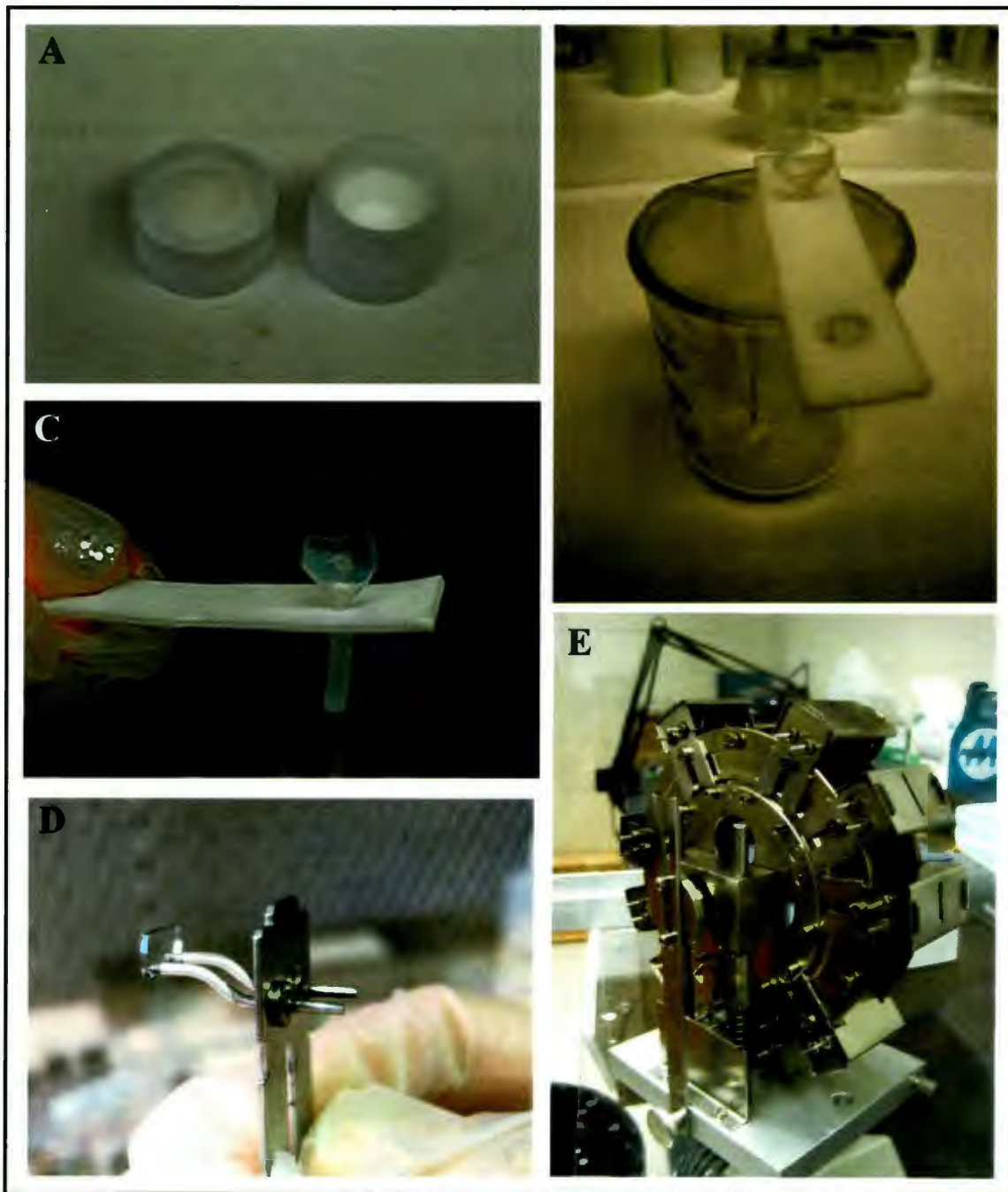


**Figure E-4:** Photos showing equipment used in U-Pb geochronology laboratory procedures. (A) TEFLON mini-bomb (~3 cm diameter) (B) mini-column with resin set up for acid and water cleaning and U-Pb elution (C) mini-column filled with resin (D) rhenium filament (E) magazine with filaments loaded in several positions.

A NBS 981 lead standard is first used to calibrate the faraday cups, and the ion counting SEM is calibrated against the faraday cup through measuring a known Pb isotopic ratio. Signal strength of the Pb and U dictated the method used to collect ratio measurements. For bigger samples the faraday cups were used to determine ratios through simultaneous measurement using 4 Faraday cups, and for smaller samples ratios were measured through peak jumping on the ion counter. Data was collected for Pb between the temperature range of 1400-1500°C and for U between the range of 1550 and 1640°C.

In Figure E-5, a schematic diagram of the TIMS machine, we see the filament and various lenses for collimating and aligning the ion beam in the source area. Once the positive ions are extracted from the filament by accelerating them through the application of typically 10kV they move down a stainless steel flight tube. When they pass through the electromagnetic mass analyzer they are deflected to varying degrees in proportion to their mass. The dispersed ion beams are focused on exit slits and collected and detected in Faraday Cups, or an SEM- ion counter, which is used for lower intensity ion beams. Since it is important to determine isotopic ratios with high precision the electromagnet is programmed to repeatedly scan specific mass peaks and after mass fractionation corrections continually determine and update the precision of the runs. The process is therefore terminated either when desired precision is met or the sample is depleted. The best datasets are used to calculate a mean isotopic ratio.

The correction factors, 0.1% amu and 0.03% amu help compensate for the isotopic fractionation of Pb and U, respectively, and are applied to measured ratios. Laboratory procedure blanks (Pb: 2pg, U: 0.3pg) were also corrected for, and the two-stage model of Stacey and Kramers (1975) was used to calculate the composition of common Pb above the laboratory blank, for use in age calculations. U-Pb decay constants presented in Jaffey et al. (1972) were used in age calculations.

Uncertainties for isotopic ratios are reported at two- sigma (2 $\sigma$ ) and were calculated using an unpublished program. Sources for two sigma uncertainty include uncertainties involving the ratio measured by the mass spectrometer, fractionation of Pb and U, amount of Pb and U blanks and the isotopic composition of Pb used when subtracting excess common Pb in amounts above the laboratory blank. The program, ISOPLOT was used to calculate weighted averages of  $^{206}\text{Pb}/^{238}\text{U}$  ages, reported at the 95% confidence interval.

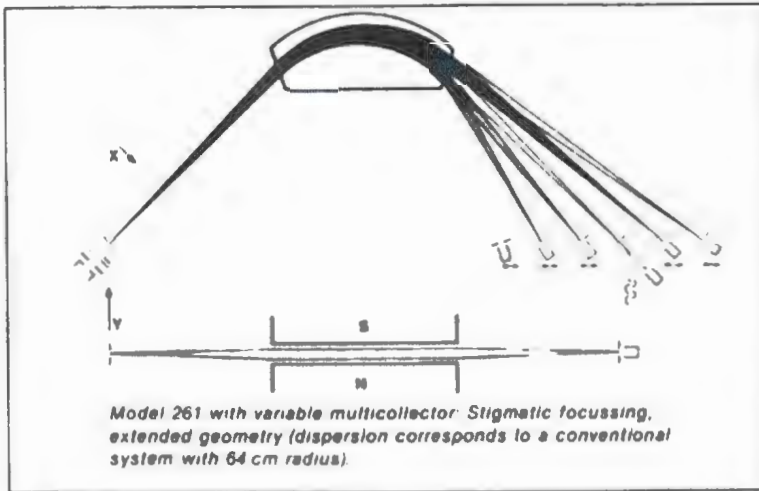


**Figure E-5:** A Schematic Diagram of TIMS.

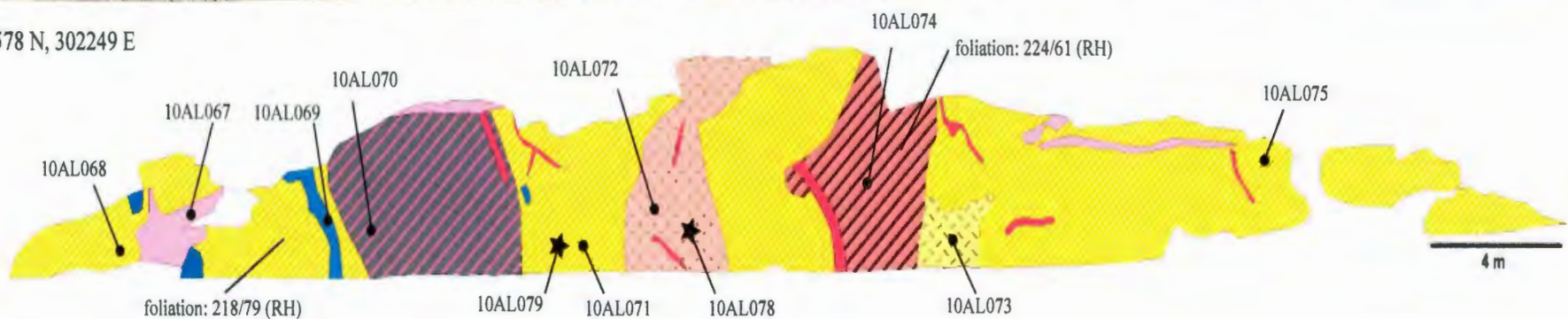
# GREENSPOND ROAD SECTION

## SECTION A-A'

344° ← → 164°



5441578 N, 302249 E



### LEGEND

#### LATE INTRUSIONS

-  Pegmatite  
*Pink to white weathered surface, coarse-grained.*
-  Undeformed Granite  
*Light pink weathering, medium-grained, and lacks foliation.*
-  Foliated, Two-mica Leucogranite  
*Light pink weathering, medium- to coarse-grained, and alignment of mafic minerals defines a foliation.*

#### GNEISSIC UNITS

-  Bt-Ms-Sil bearing Orthogneiss  
*Light grey weathering, medium-grained, with mafic lenses and slivers.*
-  Enclave-bearing Orthogneiss  
*Light to dark grey weathering, medium- to coarse-grained granite with tonalitic enclaves throughout*
-  Intermediate Enclave  
*Dark grey weathering, fine- to medium-grained.*
-  Al-Silicate-Bt-Ms bearing Orthogneiss  
*Grey to pink weathering, medium-grained, with alternating melanosome (<1cm) and leucosome (3-5cm) layers.*
-  Same as unit above but layers are less prominent and with less mafic minerals

#### LINES AND SYMBOLS

-  Contact
-  Sample Number
-  Geochronology Sample

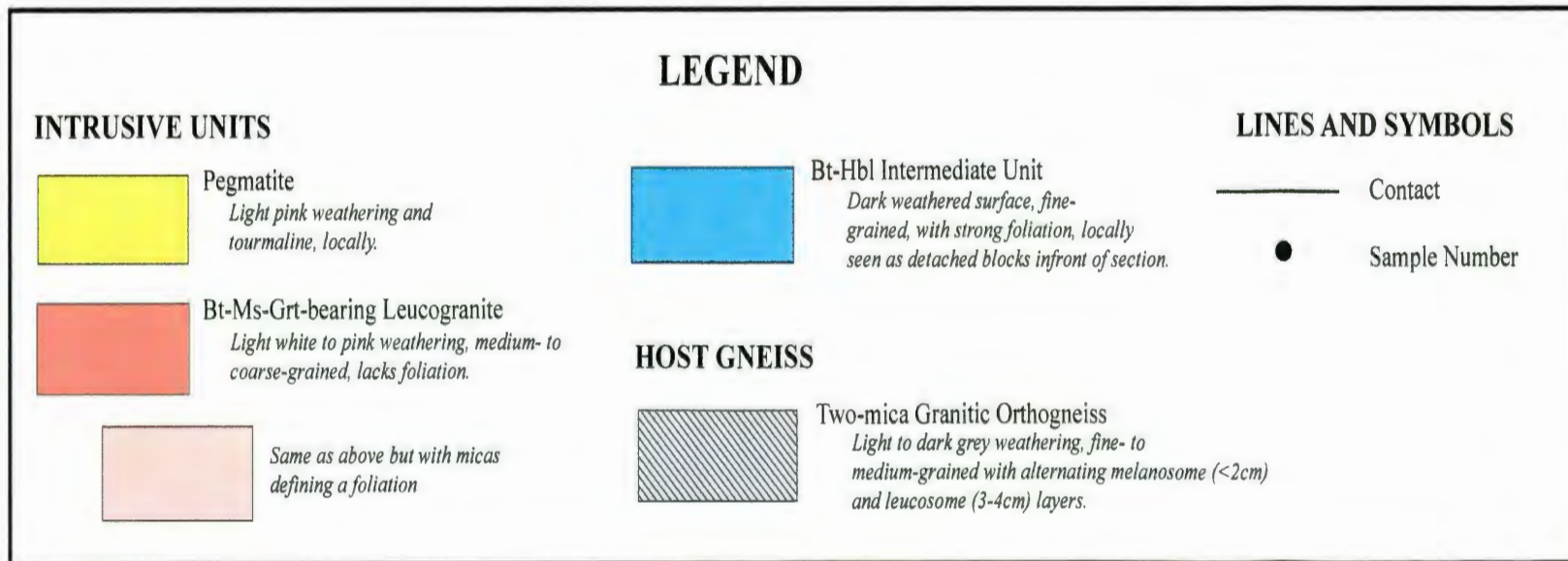
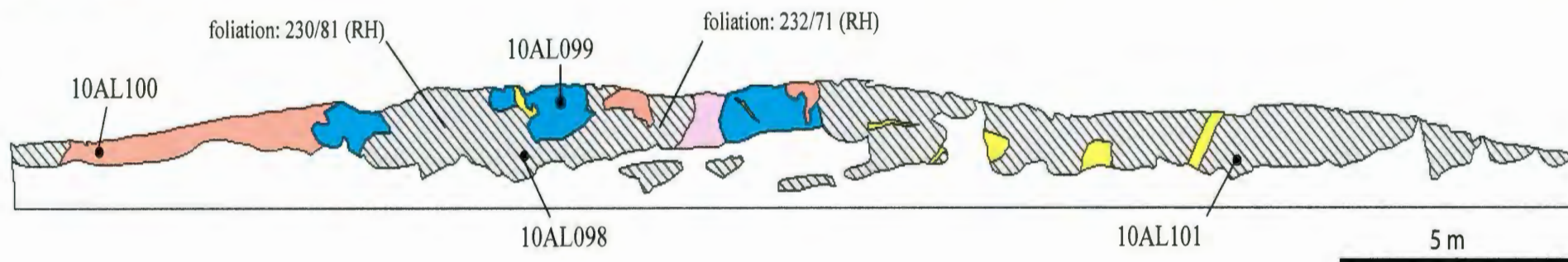
# TRINITY ROAD SECTION

## SECTION B-B'

258° ← → 78°



5429095 N, 286999 E

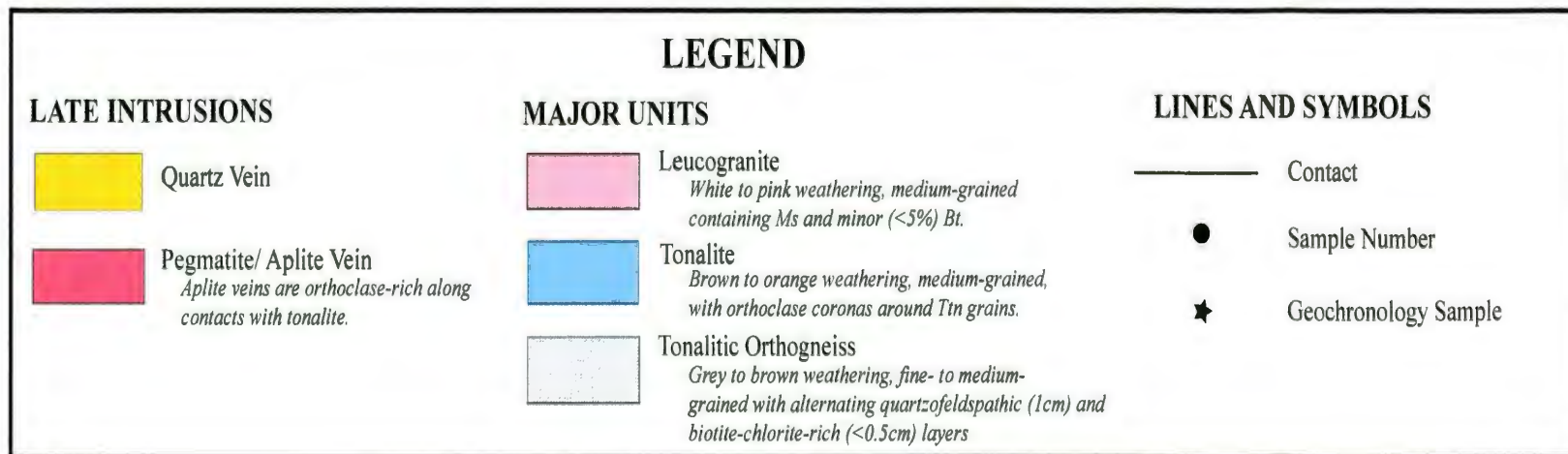
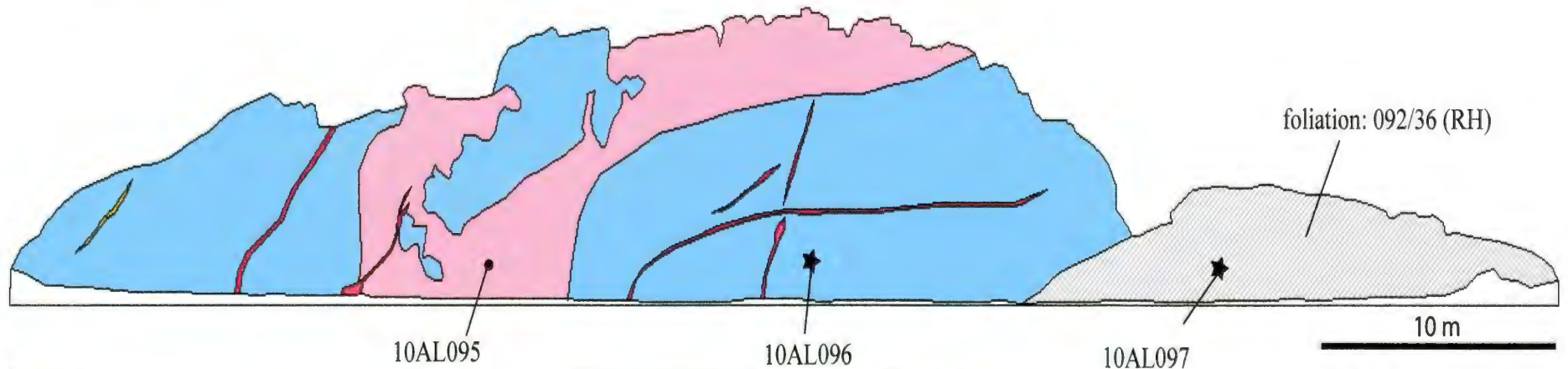


# "I LOVE YOU" ROAD SECTION SECTION C-C'



238° ← → 58°

5426398N, 284449 E

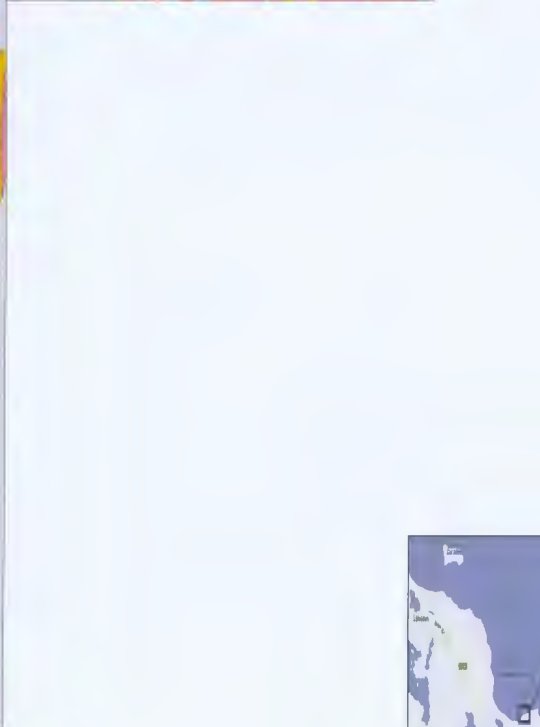
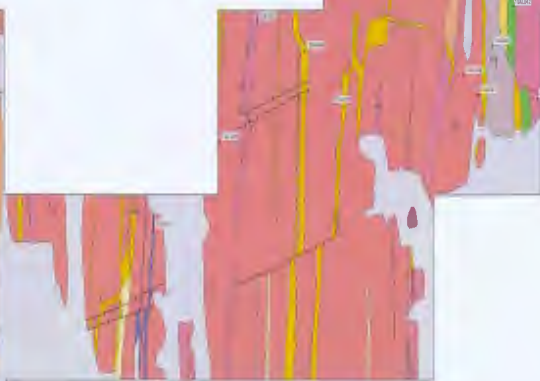


# GEOLOGICAL MAP OF WINDMILL BIGHT HEADLAND

(MAP 1) NAD 27 Z22

Amanda Langille, Memorial University of Newfoundland

SCALE 1:60



## LEGEND Geological Map of Windmill Bight Headland

**Cover**  
Includes tidal pools, grass, boulders, etc.

### LATE INTRUSIONS

- Quartz Vein**  
*Locally containing tourmaline and pyrite.*
- Pegmatite Intrusion or Pegmatite/ Apilite Vein**  
*Medium to coarse-grained, pink to white weathering, locally containing tourmaline, garnet and pyrite.*
- Tonalitic Dyke**  
*Fine-grained, massive with dark brown weathering.*

### MAFIC ROCKS (inferred to be late: uncertain age)

- Actinolite-Biotite bearing Mafic Unit**  
*Fine-grained with feldspar phenocrysts, dark grey to black weathering.*
- Biotite-Carbonate bearing Mafic Unit**  
*Very fine-grained with dull grey to black weathered surface.*

### MAJOR UNITS

- Foliated Gneodiorite**  
*Fine to medium-grained, light grey weathering (orange along fractures) with feldspar phenocrysts and locally containing granitic layers/lenses.*
- Sheared Megacrystic Gneiss**  
*Dark weathered rock with feldspar megacrysts (up to 1cm) in a fine-grained groundmass, and, locally, leucocratic layers and lenses.*
- Highly Sheared Megacrystic Gneiss (Proto-mylonite)**  
*Same as above, with higher degree of shearing and feldspars are smaller (<1cm).*
- Mylonite**  
*Same as above, with higher degree of shearing, only remnants of feldspar megacrysts remain and containing FBH and Ep locally.*
- Leucocratic Layer/Lense**  
*Medium-grained component of unit above with pale pink to white weathering.*
- Foliated Leucogranite**  
*Medium-grained with orange to white weathering, and, locally containing garnet.*
- Foliated Leucogranite with Layers**  
*Same as above, but garnet is absent and contains continuous quartz-rich and feldspar-tourmaline-rich bands.*

### MINOR UNITS OF UNCERTAIN AGE

- Layered Quartzite Unit**  
*Light white to grey weathering, with distinct quartz layers separated by Al-rich layers, and garnet, tourmaline and epidote pods occur locally.*
- Aluminous Mica-rich Intermediate**  
*Fine-grained with black, highly reflective weathered surface, and less deformed, medium-grained discontinuous layers and lenses.*
- Interlayered Mylonite Unit**  
*Fine to medium-grained, dull grey unit, containing layers (<1-2cm thick) of pegmatite, medium-grained gneiss and megacrystic granite.*

### LINES AND SYMBOLS

- Defined Contact**
- Inferred Contact**
- Fault**
- Contact strike and dip**
- Foliation with dip**
- Sample Number**
- Geochronology Sample**

